

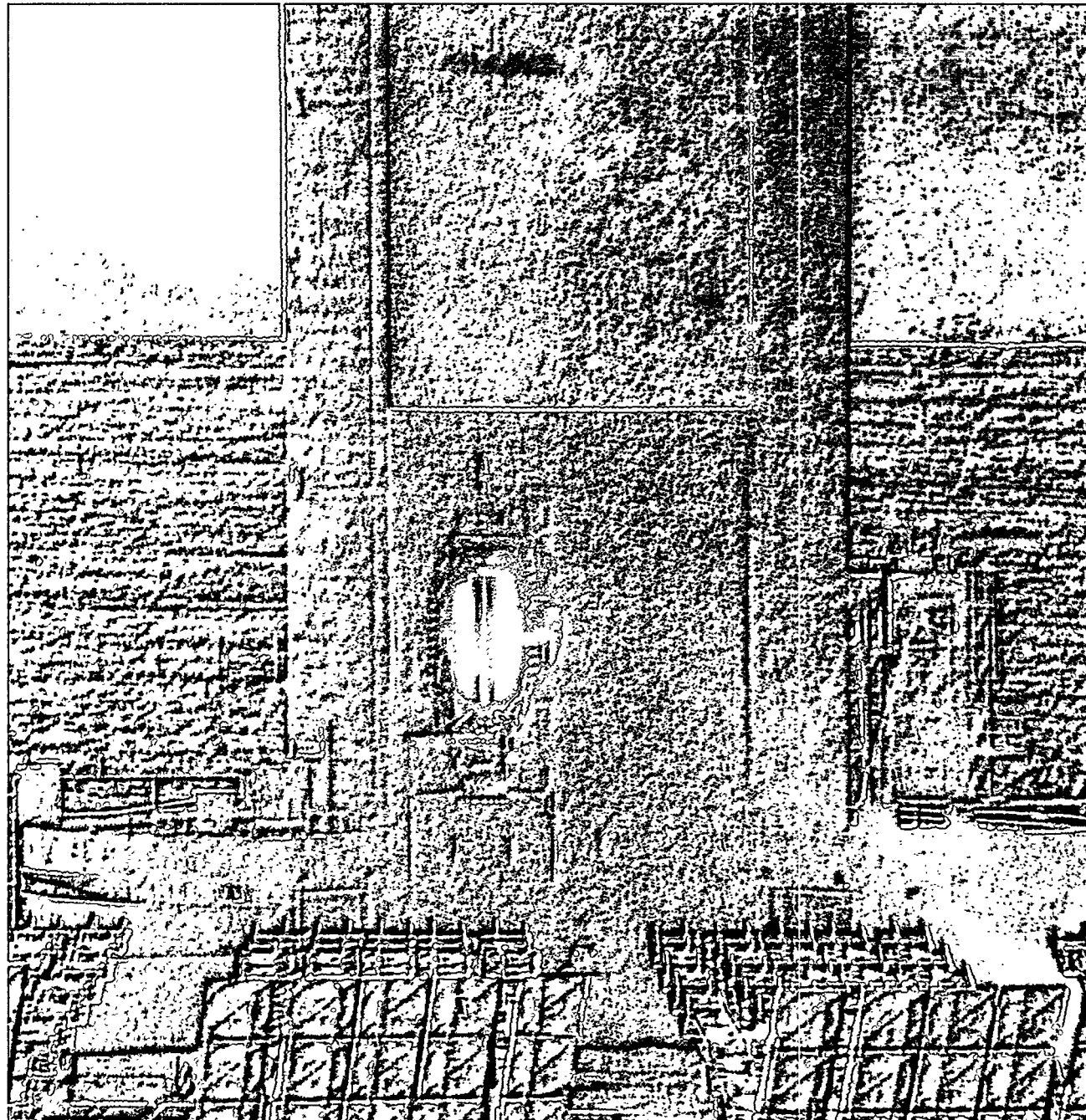
3/23

Results of Molten Salt Panel and Component Experiments for Solar Central Receivers: Cold Fill, Freeze/Thaw, Thermal Cycling and Shock, and Instrumentation Tests

James E. Pacheco, Mark E. Ralph, James M. Chavez,
Sam R. Dunkin, Earl E. Rush, Cheryl M. Ghanbari and Matt W. Matthews
Solar Thermal Technology and Test Departments

SAND94-2525

Printed January 1995



Issued by Sandia National Laboratories, operated for the United States Department of Energy by Sandia Corporation.

NOTICE: This report was prepared as an account of work sponsored by an agency of the United States Government. Neither the United States Government nor any agency thereof, nor any of their employees, nor any of their contractors, subcontractors, or their employees, makes any warranty, express or implied, or assumes any legal liability or responsibility for the accuracy, completeness, or usefulness or any information, apparatus, product, or process disclosed, or represents that its use would not infringe privately owned rights. Reference herein to any specific commercial product, process, or service by trade name, trademark, manufacturer, or otherwise, does not necessarily constitute or imply its endorsement, recommendation, or favoring by the United States Government, any agency thereof, or any of their contractors or subcontractors. The views and opinions expressed herein do not necessarily state or reflect those of the United States Government, any agency thereof, or any of their contractors.

Printed in the United States of America. This report has been reproduced directly from the best available copy.

Available to DOE and DOE contractors from
Office of Scientific and Technical Information
PO Box 62
Oak Ridge, TN 37831

Prices available from (615) 576-8401, FTS 626-8401

Available to the public from
National Technical Information Service
US Department of Commerce
5285 Port Royal Rd
Springfield, VA 22161

NTIS price codes
Printed copy: A16
Microfiche copy: A01

DISCLAIMER

**Portions of this document may be illegible
in electronic image products. Images are
produced from the best available original
document.**

SAND94-2525
Unlimited Release
Printed January 1995

Distribution Category
UC-1301

**RESULTS OF MOLTEN SALT PANEL AND COMPONENT EXPERIMENTS FOR
SOLAR CENTRAL RECEIVERS: COLD FILL, FREEZE/THAW,
THERMAL CYCLING AND SHOCK, AND INSTRUMENTATION TESTS**

James E. Pacheco, Mark E. Ralph, James M. Chavez,
Sam R. Dunkin, Earl E. Rush, Cheryl M. Ghanbari and Matt W. Matthews
Solar Thermal Technology and Test Departments

RECEIVED
APR 03 1995
OSTI

Abstract

Experiments have been conducted with a molten salt loop at Sandia National Laboratories in Albuquerque, NM to resolve issues associated with the operation of the 10MW_c Solar Two Central Receiver Power Plant located near Barstow, CA. The salt loop contained two receiver panels, components such as flanges and a check valve, vortex shedding and ultrasonic flow meters, and an impedance pressure transducer. Tests were conducted on procedures for filling and thawing a panel, and assessing components and instrumentation in a molten salt environment. Four categories of experiments were conducted: 1) cold filling procedures, 2) freeze/thaw procedures, 3) component tests, and 4) instrumentation tests. Cold-panel and -piping fill experiments are described, in which the panels and piping were preheated to temperatures below the salt freezing point prior to initiating flow, to determine the feasibility of cold filling the receiver and piping. The transient thermal response was measured, and heat transfer coefficients and transient stresses were calculated from the data. Analysis is presented which quantifies the thermal stresses in a pipe undergoing thermal shock. In addition, penetration depths were calculated to determine the distances salt could flow in cold pipes prior to freezing shut and validated with panel tests. Freeze/thaw experiments were conducted with the panels, in which the salt was intentionally allowed to freeze in the receiver tubes, then thawed with heliostat beams to assess permanent deformation in the tubes, and to develop procedures to thaw a panel so minimal damage occurs. Slow thermal cycling tests were conducted to measure both how well various designs of flanges (e.g., tapered flanges or clamp type flanges) hold a seal under thermal conditions typical of nightly shut down, and the practicality of using these flanges on high maintenance components. In addition, the flanges were thermally shocked to simulate cold starting the system. Instrumentation such as vortex shedding and ultrasonic flow meters were tested alongside each other, and compared with flow measurements from calibration tanks in the flow loop.

MASTER

DISTRIBUTION OF THIS DOCUMENT IS UNLIMITED *n/w*

ACKNOWLEDGMENT

We would like to acknowledge the following for their contribution to the molten salt panel and component experiments:

Greg Kolb
Scott Rawlinson
Craig Tyner
Roy Tucker
John Kelton
Darrell Johnson
Clifford Hilliard
Albert Mitchusson.

We would also like to thank Ann Van Arsdall for providing helpful suggestions to the report and acknowledge Tech Reps for formatting the manuscript.

Contents

I. BACKGROUND	1
II. SYSTEM DESCRIPTION	3
III. TEST RESULTS	7
COLD FILL TESTS.....	7
Results of Cold Fill Panel, Manifold, and Piping Tests	7
Thermal Analysis During Cold Fill.....	10
Transient Stress Analysis of Piping and Tubes Undergoing Thermal Shock - Nondimensional Analysis	12
Calculations of Penetration Distances - Transient Freezing in Pipes	20
Summary of Cold Fill Tests	22
FREEZE/THAW EXPERIMENTS	23
COMPONENT TESTS	28
Check Valve Cycling	28
Slow Thermal Cycling of Flanges	29
Thermal Shocking of Flanges	33
INSTRUMENTATION TESTS: FLOWMETERS AND PRESSURE TRANSDUCER.....	34
Flowmeters.....	34
Pressure Transducer	40
IV. ONGOING AND FURTHER RESEARCH.....	41
SIMPLE ELEMENT FREEZE/THAW TESTS (ONGOING).....	41
BALL VALVES TEST	41
TRANSIENT FREEZING EXPERIMENTS	41
IMPEDANCE HEATING SYSTEM.....	42
MULTIPORT VALVE.....	42
V. REFERENCES	43
APPENDIX A. FINITE ELEMENT ANALYSIS OF FLANGE UNDERGOING THERMAL SHOCK	45
APPENDIX B. FABRICATION OF HEAT TRACE CIRCUITS.....	81
APPENDIX C. HEAT TRANSFER COEFFICIENT FOR CIRCUMFERENTIALLY VARYING HEAT FLUX	91
APPENDIX D. STRAIN EQUATIONS FOR A RECEIVER TUBE UNDER HIGH FLUX	95
APPENDIX E. MOLTEN AND SOLID NITRATE SALT PROPERTIES	97
Molten Nitrate Salt.....	97
Phase Change Nitrate Salt Properties.....	97
Solid Salt.....	98
APPENDIX F. SELECTED SETS OF DATA AND OTHER INFORMATION.....	99

List of Figures

1.	Flow schematic of the system and the wing panels.....	4
2.	Molten salt panels and flow loop at the base of the Central Receiver Test Facility at Sandia National Laboratories in Albuquerque, NM.....	5
3.	Temperature response of the cold tubes and manifolds as they are filled with 550°F (288°C) salt.....	8
4.	Temperature ramp rates of first, second, third, and fourth pass tubes	9
5.	Outside wall temperature as a function of time of a 2 inch schedule 40 pipe undergoing thermal shock.....	10
6.	Nondimensional circumferential thermal stresses in pipe undergoing thermal shock as function of the nondimensional radius for several times (Fo) using thirty terms in of the nondimensional temperature equation (Eq. 1) for $r_i/r_o=0.8$ and $Bi=100$	14
7.	Nondimensional radial thermal stresses in pipe undergoing thermal shock as function of the nondimensional radius for several times (Fo) using thirty terms in of the nondimensional temperature equation (Eq. 1) for $r_i/r_o=0.8$ and $Bi=100$	14
8.	Nondimensional axial thermal stresses in pipe undergoing thermal shock as function of the nondimensional radius for several times (Fo) using thirty terms in the nondimensional transient temperature equation (Eq. 1) for $r_i/r_o=0.8$ and $Bi=100$	15
9.	Effect of the Biot number on the nondimensional circumferential thermal stress distribution for a specific time ($Fo=0.2$) and $r_i/r_o=0.8$	15
10.	Nondimensional thermal (circumferential or axial) stress at the inner surface of the pipe undergoing thermal shock as a function of time (Fo) for several Biot numbers using 30 terms of the series in the nondimensional transient temperature equation (Eq. 1) for $r_i/r_o=0.8$	16
11.	The maximum nondimensional thermal stress as a function of the Biot number for a pipe undergoing thermal shock for $r_i/r_o=0.8$. These are the maxima of Figure 10	17
12.	The time (Fo) when the maximum thermal stress occurs as a function of the Biot number	17
13.	Maximum stress at the inside wall as a function of velocity for 6 inch piping.....	18
14.	Maximum stress at the inside wall as a function of velocity for 16 inch piping.....	19
15.	The penetration depths for several pipe diameters as a function flow velocity	21
16.	Temperatures receiver panels and header as they cool when filled with molten salt which freezes in the panel at approximately 430°F (221°C)	24
17.	Permanent strain induced in the east panel tubes as a function of the panel height after two freeze/thaw cycles.....	25
18.	Permanent strain induced in the west panel tubes as a function of the panel height after two freeze/thaw cycles.....	25
19.	Permanent strain as a function of the width (tube number) for the east panel.....	26
20.	Permanent strain as a function of the width (tube number) for the west panel.....	26
21.	Photograph of the 3 inch check valve (V-CON model manufactured by Reflange, Inc.) tested in the salt loop	29
22.	Pressure and flow as a function of time during a typical check valve cycle.....	30
23.	Typical slow thermal cycle of flanges simulating nightly cool down of components followed by slow heatup with heat trace.....	31
24.	Schematic of ECON and RCON flanges.....	32
25.	Typical temperature transient of the flanges during a shock	33
26.	Response of vortex and ultrasonic flowmeters during a varying flow condition	36

27.	Comparison of the vortex and ultrasonic flowmeters against the calibration tank flowrate	38
28.	Measured bias errors (relative to the calibration tank flowrate) for each flowmeter as a function of flow.....	38
29.	Measured random errors for each flowmeter as a function of flow.....	39

List of Tables

1.	Components and instrumentation tested in molten salt loop	6
2.	Biot numbers and heat transfer coefficients during cold fill experiments	12
3.	Calculated Maximum Stresses at the Inner Wall of Piping or Tubes Initially at 25°C Undergoing Thermal Shock with Molten Salt at 290°C based on the Biot Numbers from Experiments.....	18
4.	Maximum velocities during cold fill where maximum thermal stresses are below endurance limit of the material for $T_{wall} = 25^{\circ}\text{C}$ and $T_{salt} = 288^{\circ}\text{C}$	19
5.	Penetration depths for molten salt for various pipe diameters, velocities, and salt inlet temperatures for a wall temperature $T_w = 68^{\circ}\text{F}$ (20°C).....	20
6.	Results for cold start experiments with the MSEE external receiver along with the correlation results	22
7.	Estimated penetration depths for Rockwell's Solar Two receiver.....	22
8.	Pre- and Post-Measurements of Tube Diameters in East and West Panel after two Freeze/Thaw Cycles	27
9.	Bias Limit Sources for Calibration Tank Flow Measurements.....	37
10.	Root-sum-square Uncertainty (U_{RSS}) for Each Flowmeter.....	39

Nomenclature

Bi = Biot number
C_{p,s} = specific heat of solid
C_{p,m} = specific heat of liquid
D = diameter of pipe
E = modulus of elasticity
Fo = Fourier number
h = heat transfer coefficient
h_f = heat of fusion
k = thermal conductivity of pipe (Eq. 5)
L = wall thickness
Nu = Nusselt number
Pr = Prandtl number
r = radial coordinate of pipe
r_i = inner radius of pipe
r_o = outer radius of pipe
r^{*} = nondimensional pipe radius
R = radial coordinate of inner radius of pipe
R_o = radial coordinate of frozen layer
Re = Reynolds number
T = temperature
T_f = freezing point
T_i = initial wall temperature
T_o = inlet liquid temperature
T_w = wall temperature
T_∞ = fluid temperature
x^{*} = nondimensional distance from insulated surface
z = distance to freeze closed
 α = thermal diffusivity (Eq. 3) or coefficient of thermal expansion (Eq. 9)
 α_m = thermal diffusivity of liquid
 α_s = thermal diffusivity of solid
 $\delta = 1 - r_i^*$ = nondimensional wall thickness
 λ_n = characteristic values of transient conduction equation
 γ = parameter measuring the relative importance of sensible to latent heat, assumed to be
 0.7 (water)
 θ^* = nondimensional temperature
 θ_o^* = nondimensional temperature at the insulated surface
 σ_θ = circumferential stress
 σ_r = radial stress
 σ_z = axial stress
 σ^* = nondimensional thermal stress
 ν = Poisson's ratio

Executive Summary

This report summarizes experiments we conducted with a molten salt flow loop, located at the Central Receiver Test Facility at Sandia National Laboratories in Albuquerque, New Mexico, under the US DOE Central Receiver Development Program. Experiments were conducted to test hardware and instrumentation in a molten salt environment and to develop procedures that support the design and operation Solar Two. Solar Two is a 10 MW_e Solar Central Receiver Pilot plant in Daggett, California, which is undergoing retrofit with a receiver and storage system which use molten salt as the heat transfer fluid. The major conclusions and recommendations from our experiments with the molten salt loop are summarized below.

Cold Fill Tests

We successfully showed that molten salt can flow through ambient temperature piping without freezing shut provided the flow rate is high enough. These results were scaled to the riser and down comer of the Solar Two and a 100 MW_e molten salt power plant using a correlation. These large diameter pipes should not freeze closed during the cold filling procedure (e.g., at morning startup). The thermal stresses during this thermal shock were calculated to be lower than the material's endurance limit for vertical runs of the piping. We recommend testing the cold filling method in the riser and downcomer of Solar Two and if it proves favorable, implemented as a mode of operation in commercial plants to reduced parasitic power consumption and increase availability.

We found every region of the receiver does not have to be above the salt freezing point before flow is initiated. The minimum temperature to avoid freezing during startup for the Solar Two receiver is estimated to be 200°F (93°C). We found the best method for preheating a panel was to use moving heliostats to avoid hot or cold spots.

Freeze/Thaw Tests

A receiver panel which becomes frozen with salt could require hours to thaw and could damage the tubes. We measured permanent strains as high as 4% after two freeze/thaw cycles. Monitoring the temperatures during the thawing process was also difficult with a limited number of thermocouples, but an infrared camera would simplify the monitoring.

Component Tests

We found that check valves work well in a molten salt environment after repeated pressure cycling and recommend their use. Flanges held up well to slow thermal cycling and to thermal shocking without major failures. All the flanges tested, though, began to leak slowly. Flanges should be minimized in a molten salt loop. Hot torquing the flanges, periodically, may help reduce the leaks.

Instrumentation Tests

Vortex shedding flow meters worked exceedingly well with molten salt and are the preferred flow meter for this application. Overall flow rate uncertainties of less than ±5% can be obtained with a proper calibration. The impedance-type pressure transducer we tested was responsive and performed well. It could replace hard to find NaK filled pressure transducers. The impedance type is relatively expensive, though.

I. Background

In a molten salt central receiver power plant, the parasitic electrical power consumption can be a significant percentage of the total power production if it is not properly managed. Good management also involves careful assessment of operating strategies to minimize the parasitics. Since the nitrate salt, which serves as the heat transfer medium between the receiver and the steam generator, has a freezing point of 430°F (221°C), the associated piping, valves, instrumentation, and tanks must be kept above this temperature (typically at 550°F, 288°C) to assure the salt will not freeze. During inclement weather and during the night the plant does not operate, but the heat trace is kept energized to maintain the temperature of the empty lines at 550°F (288°C). This operating strategy is not an economically advantageous method of conditioning a highly cyclic power plant. One strategy of reducing the nightly parasitic power consumption is to turn off the heat trace at night, allowing the piping to cool down to ambient, then fill the piping cold at start up the next morning.

There has been very little data collected on cold starting the receiver and piping at temperatures below the molten salt freezing point. The Molten Salt Electric Experiment receiver in the external configuration was cold started at temperatures below the freezing point. In one of three cases, the receiver partially froze [1]. No detailed analysis was done on the transient freezing phenomenon. In this report we describe experiments where we cold started receiver panels and piping.

Due to the nitrate salt's high freezing point and the fact that the salt expands upon melting, we were concerned with the damage that could occur in receiver tubes if the salt were to freeze in the receiver and then thaw out. This situation could occur during shut down of the receiver. If one of the drain valves failed to open and went undetected during the drain process, molten salt would be trapped in the associated panel, and the salt would subsequently freeze. Upon thawing, the expanding salt could damage the tube. In previous experiments, detailed assessments of the freezing and thawing of the panel tubes were not conducted. The Martin Marietta molten salt receiver became frozen with salt and was successfully thawed, though no data on tube deformation was available.

Three molten salt receivers and large-scale pump and valve loops have been tested at Sandia National Laboratories to determine the viability of molten salt as a heat transport fluid and storage medium for central receiver solar power plants. The Category B receiver was a 5 MWt cavity molten nitrate salt receiver. The testing of this receiver in 1988 [2] showed the feasibility of fabricating and operating a molten salt receiver consisting of serpentine flow panels. However, there are some components and instrumentation that need further evaluation.

Check valves have not previously been used in molten salt. Check valves are required when pumps are connected in series to a common manifold, or to the base of a riser to prevent back spin and damage to a pump during a sudden shut off of one pump while the others are flowing. Experiments with flanges in the Pump and Valve Loop show that they were a significant source of leaks.

The purpose of the current molten salt experiments is to verify the operation and reliability of components, instrumentation, and procedures proposed for implementation in the Solar Two project. Many of the components have been proven in a molten salt environment, but additional information is required. Other components were not tested sufficiently or at all in previous molten

salt experiments. The goal of these tests was to reduce uncertainties concerning the performance of untested components and operating procedures (e.g., cold filling the receiver or piping, and thawing a frozen panel.)

We conducted these tests to address concerns by the Solar Two Technical Advisory Committee - a committee of utilities, industries, the U.S. Department of Energy, and Sandia National Laboratories overseeing the technical issue of the Solar Two Project. The technical needs and concerns were prioritized, and a test program was developed. Consequently, some issues, such as thermal cycling of full scale valves, could not be implemented. However, this test program did address all the high priority issues.

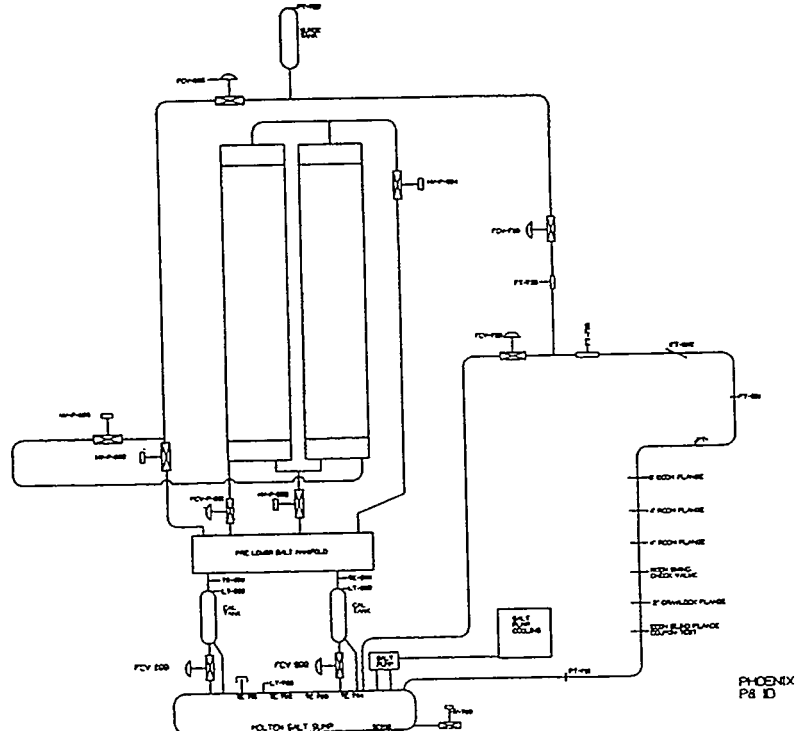
II. System Description

The experiments were conducted with an existing molten salt loop initially built for a direct absorption receiver [3]. It was modified to accommodate two wing panels (fabricated by Foster Wheeler Corporation) removed from a salt-in-tube receiver (the Category B receiver) to evaluate a cold receiver startup procedure and conduct freeze/thaw experiments. Each panel consists of two serpentine flow passes which have six 1 inch (2.5 cm) OD 304 stainless steel tubes with 0.065 inch (1.65 mm) thick walls. The two passes are connected to a common 6 inch (15 cm) diameter manifold (schedule 80 piping) at the top of the panel. Each panel vent connects to a common 1 inch vent line, in which a hand valve is located to vary the venting flow rate. The experiment was located at the base of the Solar Tower at the National Solar Thermal Test Facility in Albuquerque, NM. Figure 1 is a schematic of the system and the wing panels. Figure 2 is a photograph of the panels and flow loop.

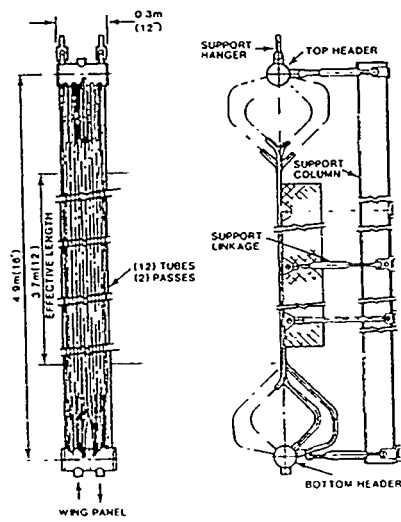
In this flow loop, salt is pumped from the salt sump, through the components, then either returned to the sump or diverted up the riser. At the top of the riser is the pressurized accumulator (surge) tank. The flow goes through the down comer, and can either be diverted to the panel or a manifold. The outlet of the panel flows into the manifold. The manifold drains into two calibration tanks. Flow from the calibration tanks returns to the sump. The pump can flow salt at 100 gallons per minute (380 liters/min) through the 2 inch (5.1 cm) piping.

We added flanges, a check valve, flow meters, and pressure transducers to test their performance. Three types of flanges were tested: 1) clamped, compressive metal-seal type flanges made by Reflange (R-CON) and by Grayloc, 2) bolted, compressive metal-seal flanges (E-CON) also made by Reflange, and 3) a standard ANSI ring-joint flange. The check valve, manufactured by Reflange (V-CON), was a spring-loaded, swing-type check valve. Two types of flow meters were tested: 1) vortex shedding flow meters made by Engineering Measurements Company, and 2) ultrasonic flow meters (wetted type and clamp on type transducers) manufactured by Panametrics. In addition, we installed pieces of performed fiberglass insulation to determine their viability as another insulation material. This insulation is easier to install than the wool blanket or calcium silicate insulation previously used. Its upper temperature limit is approximately 850°F. Table 1 lists the components we tested.

Although we were not able operate the flow loop at the pressures expected to be encountered in the cold side of a typical molten salt system, we were able to simulate operational and thermal cycling expected on the cold side of the system where the thermal ramp rates and stresses are typical of nightly conditioning. The ramp rates on the hot side of a molten salt system (down stream of a receiver) are very difficult to simulate with the existing loop, and therefore were not simulated with this test setup.



a)



b)



Figure 1. Flow schematic of the system (a) and a wing panel front (b) and side view (c).

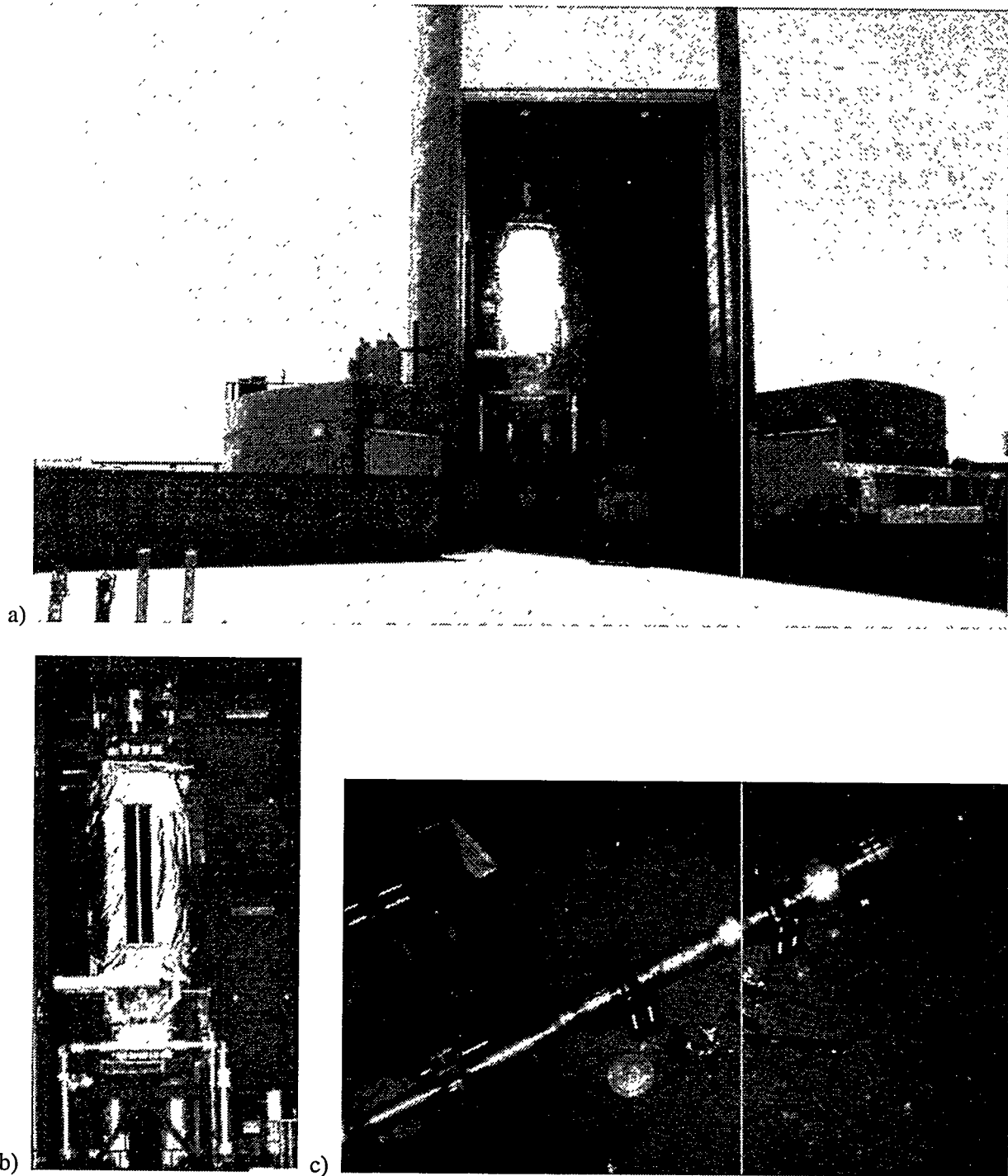


Figure 2. Photographs of molten salt panels (a and b) and flow loop test section (c) at the base of the Central Receiver Test Facility at Sandia National Laboratories.

Table 1. Components and instrumentation tested in molten salt loop.

Component or instrumentation	Type	Size	Manufacturer
Flange	Clamped, compressive metal seal type	2 inch and two 4 inch	Reflange (R-CON) and Grayloc (2 inch)
Flange	Bolted, compressive metal seal type	6 inch	Reflange (R-CON)
Flange	ANSI ring type flange	4 inch	standard
Check valve	Spring loaded swing	3 inch	Reflange (V-CON)
Flow meter	Vortex shedding	2 inch	Engineering Measurements Co.
Flow meter	Ultrasonic - wetted transducer	2 inch	Panametrics
Flow meter	Ultrasonic - clamp on transducer	any sized pipe up to 10 feet dia.	Panametrics
Pressure transducer	High temperature Impedance	0-250 psi range	Kaman

III. Test Results

Cold Fill Tests

Cold filling involves flowing molten salt through piping or the receiver when all or part is below the salt freezing point. Cold filling has several advantages in the operation of a plant that experiences cyclic operation. If the molten salt can flow through parts of the system which are below the freezing point, parasitics could be reduced, since the heat trace would not have to be used on those lines. In addition, the operation of the plant could be more flexible if the plant could be brought on line faster by not having to wait for the heat trace to heat the lines to operating temperatures resulting in increased availability. Also, during morning startup, it is difficult to uniformly preheat the entire receiver. Some spots will experience much more heating than others due to non-uniform flux profiles from heliostats. This is a particular concern for the east side of a cylindrical receiver during morning start up. Localized convection will add to the problem. A roving aiming strategy, where the heliostat aim points are periodically changed, could provide more uniform heating of the receiver panels, thus avoiding severe hot or cold spots. Also, if the receiver can be filled with molten salt when areas of the receiver are below the salt freezing point, the receiver start up procedure would be much simpler, and could occur sooner. These strategies will boost performance and reduce operating expenses, resulting in lower energy costs. There are two major concerns with cold filling components and piping: freezing of the flowing salt, and transient thermal stresses.

We conducted cold fill experiments on the panels and on a section of piping. We measured the thermal response as the panel or piping underwent the rapid change in temperature, and estimated the heat transfer coefficients during this transition. We also derived expressions describing the transient stresses a pipe or tube will experience during a thermal shock. Using a correlation which describes the penetration distance of a liquid as a function of the fluid properties and flow conditions, we estimated the distance salt could flow through cold piping before freezing shut.

Results of Cold Fill Panel, Manifold, and Piping Tests. We conducted tests varying the initial panel temperature to determine whether salt could flow through all four passes of the panel before freezing shut. The flow velocity was approximately the same for each test, 2 ft/s (0.6 m/s). The purposes of these tests were to 1) determine if salt flow could be established in "cold" manifolds, panels, and piping, 2) measure the thermal responses of the tubes and manifolds undergoing thermal shock, and 3) estimate the corresponding stresses in the materials.

We conducted a series of tests trying lower and lower panel preheat temperatures ranging from 550 °F (288°C) to ambient before initiating salt flow. Next, we tried flowing salt through cold (near ambient) manifolds (heat trace off) with the panels preheated to 550°F. Then we tried flowing through cold manifolds and cold panels. Each scenario was repeated several times.

We found we were able to consistently flow through ambient temperature manifolds and panels without freezing salt or blocking tubes. In our test loop, we were able to fill the panels only in a serpentine fashion. To prevent entrapment of air, we had to fill the panel slowly (~2 ft/s, 0.6 m/s). Figure 3 shows the temperature response of the tubes and upper manifold as they are filled with 550°F (288°C) salt. The receiver tubes were initially at 50°F (10°C). The header was

Temperatures During Cold Fill

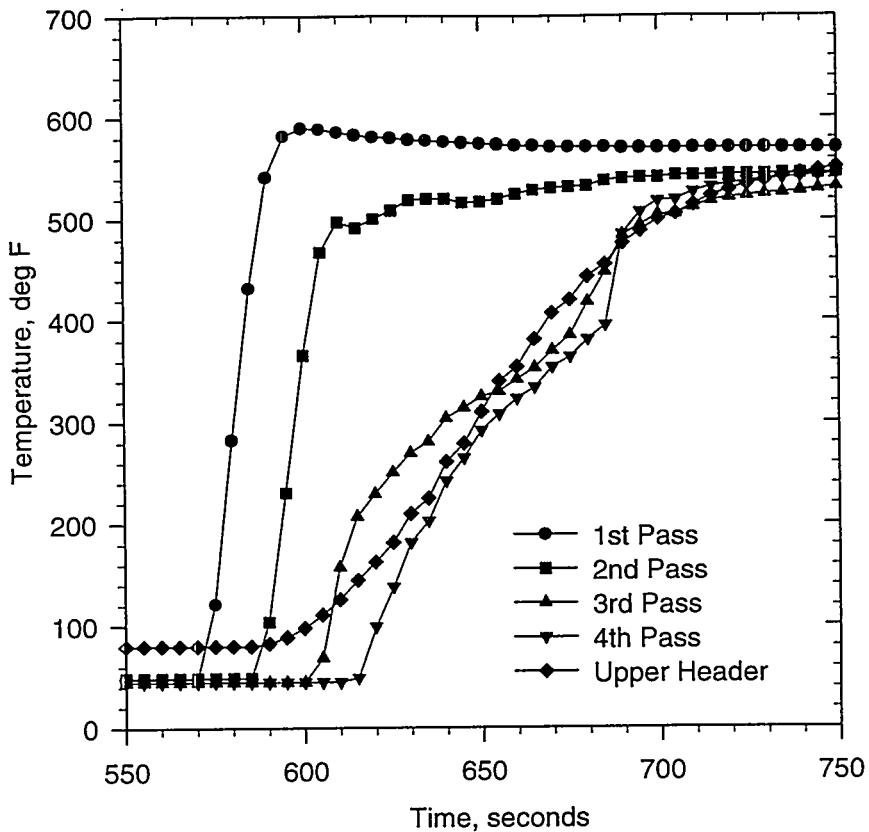


Figure 3. Temperature response of the cold receiver tubes and upper header as they are filled with 550°F (288°C) salt.

initially hotter than the panels, since an adjacent heat trace zone conducted heat to the header. The header and first pass receiver tubes experienced the greatest thermal shock. As the salt continued through the other passes, the temperature of the initial slug of salt decreased, resulting in the deposition of a frozen layer of salt on the tube wall, which reduced the shock, then melted away. This can be inferred from the change in slope of the fourth pass tube temperature and the upper header temperature. Figure 4 shows the temperature ramp rates of first, second, third, and fourth pass tubes. Note how the third and fourth passes show lower peak ramp rates. A frozen layer of salt is likely responsible for the reduced peak ramp rates, since as the initial slug of salt comes in contact with the cold tube surface, a frozen layer develops which limits the rate at which the temperature can rise, and provides some thermal capacitance. The outside tube temperature corresponding to the peak ramp rate in the fourth pass is approximately 395°F (202°C).

A thermal analysis was conducted on a receiver tube and header during this thermal shock, and is described in the Thermal Analysis section. The estimated heat transfer coefficients were calculated. In addition, calculations on the penetration depths—the distance a fluid flows through cold piping before freezing shut—are also discussed in the Calculation of Penetration Distances section.

Ramp Rates

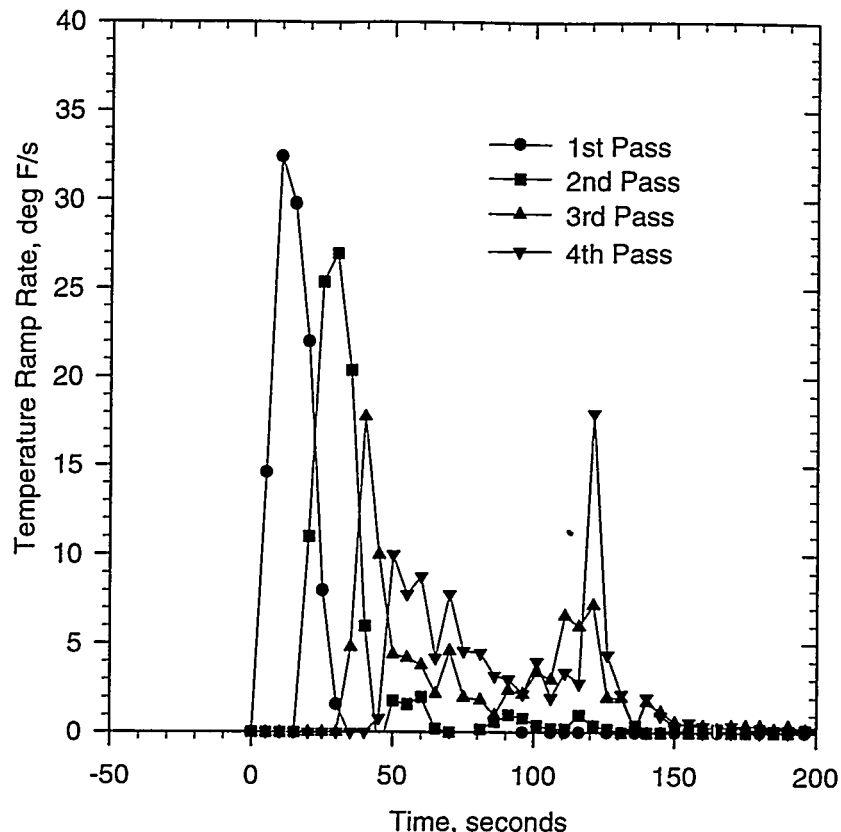


Figure 4. Temperature ramp rates of first, second, third, and fourth pass tubes.

The stresses in the receiver tube were calculated using the heat transfer coefficients obtained from the experiment. A stress model is described in the Transient Stress Analysis section. Stresses in the tube-to-header junction are more complicated, and are dictated by the temperature gradients at the transition.

In addition to cold filling the panels and manifolds, we conducted similar tests on a section of piping. We turned off the heat trace to a section of piping and let it cool to ambient, then initiated salt flow to determine its thermal response and estimate heat transfer coefficients and stresses. We measured the thermal response of an insulated 40 foot (12 m) long, 2 inch (5.1 cm) diameter 316 SS, schedule 40 pipe undergoing thermal shock. The piping was part of the riser. We turned off the heat trace, and allowed it to cool to ambient. When the piping was cold (at ambient), we pumped salt through it at approximately 9.5 ft/s (2.9 m/s) and measured the temperature outside of the pipe. Figure 5 is a plot of the outside wall temperature as a function of time. With this data, we calculated the heat transfer coefficient at the inner wall using a first eigenvalue approximation to an analytical solution of plane wall conduction. These procedures are discussed in the next section.

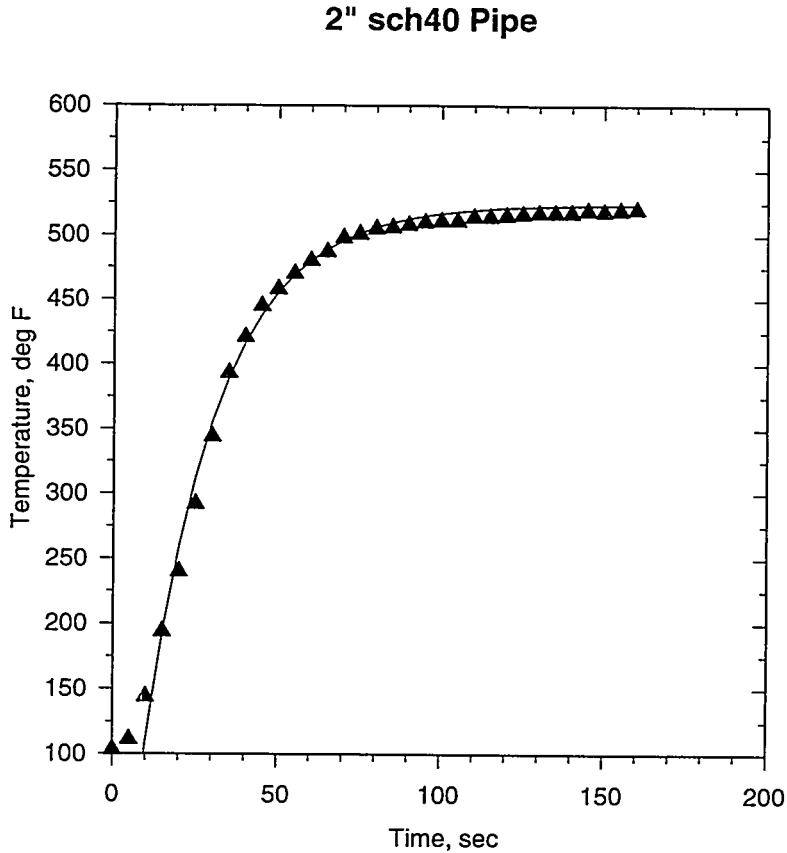


Figure 5. Outside wall temperature as a function of time of a 2 inch schedule 40 pipe undergoing thermal shock. The symbols are actual data points. The solid line is a fit of the data using the thermal model for $Bi = 0.444$.

Thermal Analysis During Cold Fill. In the cold-fill experiment on the panel, manifolds, and piping, we measured the outside wall temperatures as they are thermally shocked. From that data we wanted to obtain the inside wall temperature and the average heat transfer coefficient. The heat transfer coefficient allowed us to calculate the stresses developing in the wall of the pipe or tube as it rapidly heats up.

Assuming that the tube or pipe wall can be approximated as a plane wall, we can use an analytical solution to estimate the inside wall temperature and heat transfer coefficient. Since the receiver tube and piping have relatively thin walls, the plane wall assumption is a good approximation. In our tests, the outside of the pipe, manifolds, and the receiver tubes were insulated. (In actuality, only half of the receiver tube is insulated and the other side is exposed, but this should have minor bearing on the result, since initially the outside natural convective heat transfer to the air is relatively small, and the time scales are short for thermal shock.)

The solution to the energy equation for a plane wall suddenly subjected to a convection boundary condition describes the temperature distribution in the wall as a function of time [4]. Its form is:

$$\theta^*(x^*, t^*) = \frac{T(x, t) - T_\infty}{T_i - T_\infty} = \sum_{n=1}^{\infty} C_n \exp(-\lambda_n Fo) \cos(\lambda_n x^*) \quad (1)$$

where the coefficient C_n :

$$C_n = \frac{4 \sin(\lambda_n)}{2\lambda_n + \sin(2\lambda_n)}, \quad (2)$$

Fo (the Fourier number) is the nondimensional time and x^* is referenced from the insulated surface:

$$Fo = \frac{\alpha t}{L^2}, \quad x^* = \frac{x}{L}. \quad (3, 4)$$

The discrete characteristic values (eigenvalues) of λ_n are the positive roots of the transcendental equation:

$$\lambda_n \tan(\lambda_n) = Bi = \frac{hL}{k}. \quad (5)$$

The length, L , is half the thickness of the plane wall since convection occurs on both faces, but in the case of a pipe or tube wall it is equal to the wall thickness, since one face has convection and the other is insulated. Note the midplane of a plane wall behaves like an insulated surface. The infinite series solution can be approximated by the first term in the series for values of $Fo \geq 0.2$. The solution becomes:

$$\theta^* = C_1 \exp(-\lambda_1^2 Fo) \cos(\lambda_1 x^*) \quad (6)$$

or

$$\theta^* = \theta_o^* \cos(\lambda_1 x^*) \quad (7)$$

where θ_o^* is the temperature at the midplane, $x^*=0$ (the insulated boundary, in our case the outside tube wall). The coefficients C_1 and λ_1 are determined from the equations 2 and 5. Since we measured the outside wall temperature (insulated surface) as a function of time and we knew the approximate salt bulk-fluid-temperature (initial salt temperature), we calculated measured values for θ_o^* and Fo . By iterating on λ_1 until the calculated value of θ_o^* converged on the measured value of θ_o^* , we obtained the Biot number, Bi . From the Biot number we obtained the heat transfer coefficient.

The average heat transfer coefficients determined during the thermal shock for each pass, for the upper header, and for a 2 inch pipe are shown in Table 2. The solid line in Figure 5 is a fit of the data to the model for a constant heat transfer coefficient. Note that initially the temperature changes gradually (the first three data points). In order to get a good fit of the data with the model, the initial starting time of the model had to be adjusted, since the actual heat transfer coefficient is not constant with time. Assuming a constant heat transfer coefficient will yield higher stresses than one which gradually increases to its final value, and thus will be conservative. Stress analyses for an insulated circular pipe undergoing thermal shock are discussed in the next section.

For heat transfer in fully developed pipe flow when applied to freezing with turbulent flow, the following correlation has been suggested to estimate heat transfer coefficients between the fluid and the frozen layer [5]:

$$Nu = 0.0155 Re^{0.83} Pr^{0.5} (R_o/R)^{0.83} \quad (8)$$

Table 2. Biot numbers and heat transfer coefficients during cold fill experiments.

Location	Approx. Velocity m/s	Bi (from data using the model)	h (from Bi) W/m ² K
2" sch40 Pipe	2.9	0.444	1700
6" sch80 Header	0.11	0.881	1200
First Pass Tube	0.67	0.296	2700
Second Pass Tube	0.67	0.243	2200
Third Pass Tube	0.67	0.124	1100
Fourth Pass Tube	0.67	0.114	1000

where R_o is the inner pipe radius and R is the radial coordinate of the frozen layer. This correlation is applicable beyond the thermal entrance length (approximately 10 tube diameters), and provides a conservative estimate of the heat transfer to the pipe, since the frozen layer will act as an insulator.

It should be noted that the heat transfer that occurs when the receiver is under high flux is quite different for a cold start scenario. A description of the heat transfer under high flux is presented in Appendix C.

Transient Stress Analysis of Piping and Tubes Undergoing Thermal Shock - Nondimensional Analysis. The stress calculations are important in determining the material behavior in a severe transient condition. For an insulated pipe, we can use the temperature distribution from the thermal analysis to calculate the circumferential, radial, and axial stresses. These thermal stresses should be superimposed on existing pipe loads due to structural factors. If the temperature is a function of the radial component only, then each component of stress is [6,11]:

$$\sigma_\theta(r) = \frac{E\alpha}{(1-\nu)r^2} \left(\frac{r^2 + r_i^2}{r_o^2 - r_i^2} \int_{r_i}^{r_o} T(r) r dr + \int_{r_i}^r T(r) r dr - T(r) r^2 \right) \quad (9)$$

$$\sigma_r(r) = \frac{E\alpha}{(1-\nu)r^2} \left(\frac{r^2 - r_i^2}{r_o^2 - r_i^2} \int_{r_i}^{r_o} T(r) r dr - \int_{r_i}^r T(r) r dr \right) \quad (10)$$

$$\sigma_z(r) = \frac{E\alpha}{(1-\nu)} \left(\frac{2}{r_o^2 - r_i^2} \int_{r_i}^{r_o} T(r) r dr - T(r) \right) \quad (11)$$

The temperature profile at a given time, Fo , can be found from Equation 7:

$$T(r) = \theta^* \circ (T_i - T_\infty) \cos(\lambda_i x^*) + T_\infty \quad (12)$$

The nondimensional length x^* is referenced from the insulated surface (the outside radius) and can be transformed into the nondimensional radial coordinates, $r^* = r/r_o$ and $r_i^* = r_i/r_o$, from:

$$x^* = (1 - r^*) / (1 - r_i^*) = (1 - r^*) / \delta.$$

In carrying out the integration, the stress components can be expressed in a nondimensional thermal stress format:

$$\sigma^*(r^*) = \frac{\sigma(r)(1-\nu)}{E\alpha(T_i - T_\infty)} \quad (13)$$

Which for the three stress components are:

$$\begin{aligned} \sigma_\theta^*(r^*) &= \frac{r^{*2} + r_i^{*2}}{1 - r_i^{*2}} \frac{\theta_o^*}{r^{*2}} \left\{ \frac{\delta^2}{\lambda_1^2} [1 - \cos(\lambda_1)] + \frac{\delta r_i^*}{\lambda_1} \sin(\lambda_1) \right\} \\ &\quad + \frac{\delta^2 \theta_o^*}{\lambda_1^2 r^{*2}} \{ \cos(A) - \cos(\lambda_1) \} \end{aligned} \quad (14)$$

$$\begin{aligned} \sigma_r^*(r^*) &= \frac{r^{*2} - r_i^{*2}}{1 - r_i^{*2}} \frac{\theta_o^*}{r^{*2}} \left\{ \frac{\delta^2}{\lambda_1^2} [1 - \cos(\lambda_1)] + \frac{\delta r_i^*}{\lambda_1} \sin(\lambda_1) \right\} \\ &\quad - \frac{\delta^2 \theta_o^*}{\lambda_1^2 r^{*2}} \{ \cos(A) - \cos(\lambda_1) \} \\ &\quad + \frac{\delta \theta_o^*}{\lambda_1 r^{*2}} \{ r^* \sin(A) - r_i^* \sin(\lambda_1) \} \end{aligned} \quad (15)$$

$$\begin{aligned} \sigma_z^*(r^*) &= \frac{2\theta_o^*}{1 - r_i^{*2}} \left\{ \frac{\delta^2}{\lambda_1^2} [1 - \cos(\lambda_1)] + \frac{\delta r_i^*}{\lambda_1} \sin(\lambda_1) \right\} \\ &\quad - \theta_o^* \cos(A) \end{aligned} \quad (16)$$

$$A = \frac{\lambda_1}{\delta} (1 - r^*) \quad (17)$$

The characteristic value, λ_1 , is found from the solution to Equation 5 and is a function of the Biot number, Bi , which indicates the relative importance of surface heat transfer to conduction. Equations 14 to 16 are valid for $Fo \geq 0.2$. For smaller times ($Fo < 0.2$), several terms in the series in Equation 1 must be used to calculate the temperature distribution. The temperature distribution is then used in Equations 9-11 to calculate the stresses. These equations can be used to calculate the transient stresses as a function of the Biot number and the pipe geometry. Figures 6, 7, and 8 show the nondimensional circumferential, radial, and axial thermal stresses as function of the nondimensional radius for several times (Fo) for a specific geometry. Note that in Figure 6 a skin stress develops at the inner surface. When the pipe is cold relative to the fluid—"up shock"—the stresses at the inner surface are compressive and tensile on the outer surface during the thermal shock. When it is hot relative to the fluid—"down shock"—the stresses are tensile on the inner surface. Figure 9 shows the effect of the Biot number on the stress distribution for a specific time. Figure 10 shows the nondimensional thermal (circumferential or axial) stress at the inner surface of the pipe as a function of time (Fo) for several Biot numbers using 30 terms of the series in Equation 1. When the heat transfer coefficient is large relative to the pipe thermal conductivity (large Bi numbers), there will be significant temperature gradients across the pipe wall and larger thermal stresses will develop during a thermal shock. At small Biot numbers, conductivity dominates relative to surface heat transfer and there are small thermal gradients across the wall

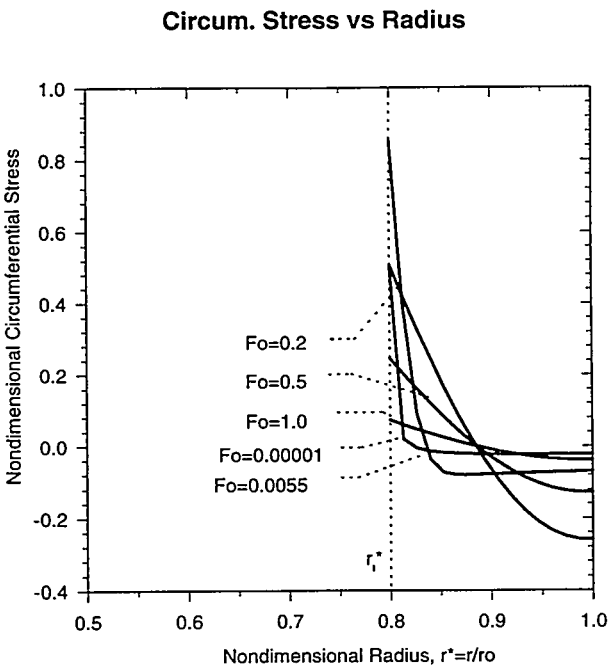


Figure 6 . Nondimensional circumferential thermal stresses in pipe undergoing thermal shock as function of the nondimensional radius for several times (Fo) using thirty terms in of the nondimensional temperature equation (Eq. 1) for $r_i/r_o=0.8$ and $Bi=100$.

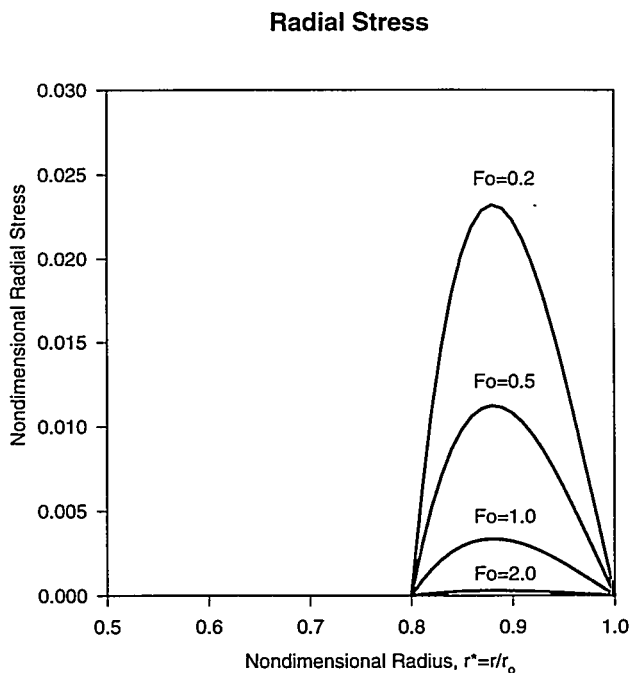


Figure 7. Nondimensional radial thermal stresses in pipe undergoing thermal shock as function of the nondimensional radius for several times (Fo) using thirty terms in of the nondimensional temperature equation (Eq. 1) for $r_i/r_o=0.8$ and $Bi=100$.

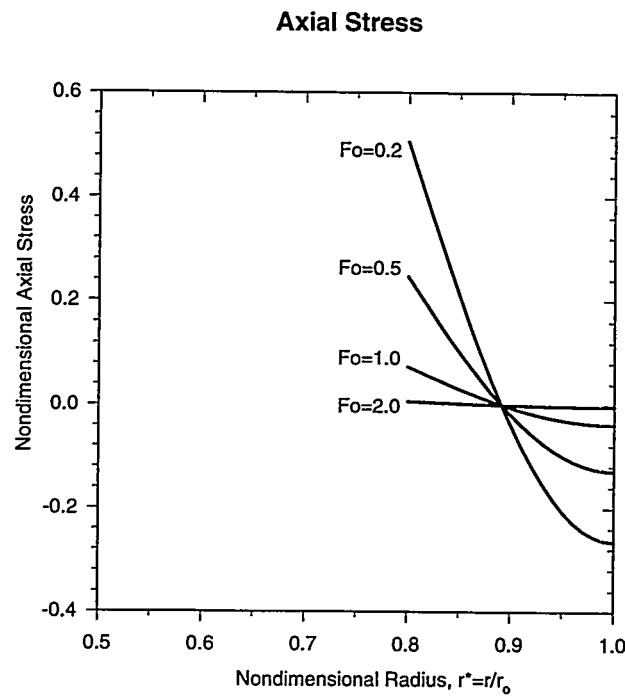


Figure 8. Nondimensional axial thermal stresses in pipe undergoing thermal shock as function of the nondimensional radius for several times (Fo) using thirty terms in the nondimensional transient temperature equation (Eq. 1) for $r_i/r_o = 0.8$ and $Bi=100$.

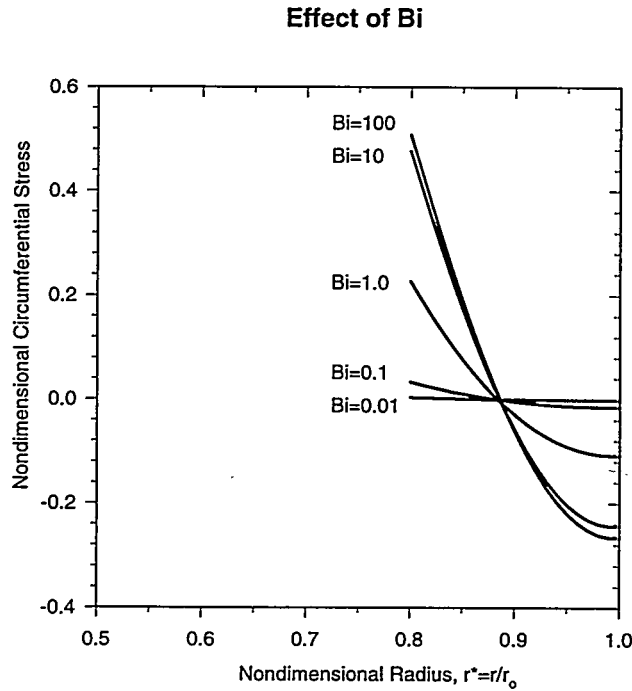


Figure 9. Effect of the Biot number on the nondimensional circumferential thermal stress distribution for a specific time ($Fo=0.2$) and $r_i/r_o = 0.8$.

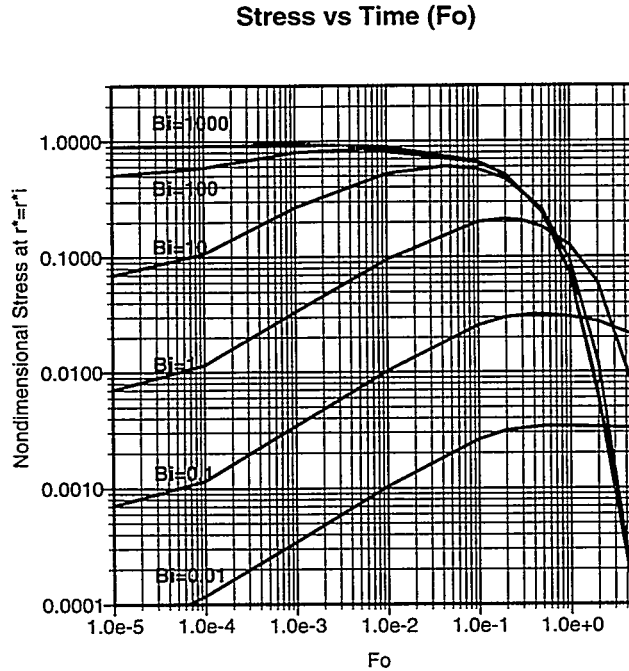


Figure 10. Nondimensional thermal (circumferential or axial) stress at the inner surface of the pipe undergoing thermal shock as a function of time (Fo) for several Biot numbers using 30 terms of the series in the nondimensional transient temperature equation (Eq. 1) for $r_i/r_o=0.8$.

resulting in small thermal stresses. The stresses build with time, reaching a peak, then finally drop as the wall reaches a uniform temperature. Each curve has a maximum thermal stress. These maximum stresses are shown in Figure 11 as a function of the Biot number. Figure 12 shows the time (Fo) when the maximum stress occurs as a function of Biot number.

From the data we gathered during the shock tests, we determined the Biot numbers are relatively small. We used these Biot numbers to calculate the stresses in piping or tubes we thermally shocked: a 2-inch schedule 40 316SS pipe, a 6-in schedule 40 304SS header and a 1-inch 0.065 inch wall 304SS receiver tube. Table 3 shows the maximum equivalent stress based on the maximum energy distortion theory of failure [7], sometimes referred to as the von Mises stress, for each case. In each case the stresses were calculated to be lower than the endurance limit of the material ($\sigma_e \approx 270$ MPa for stainless steel [8]) for these tests indicating that for the test conditions the piping itself can handle these stresses over the life of the system. It is likely these stresses are conservative, since the heat transfer coefficients are not constant, but gradually increase to the equilibrium value.

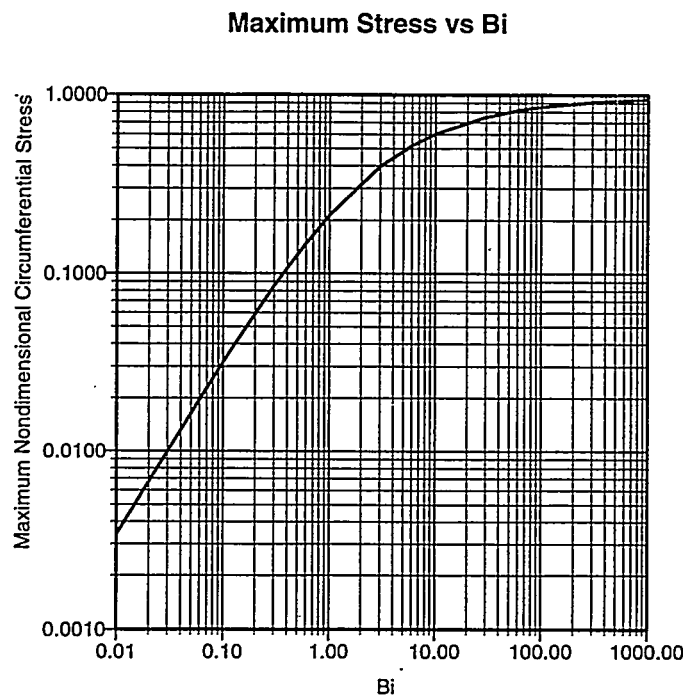


Figure 11. The maximum nondimensional thermal stress as a function of the Biot number for a pipe undergoing thermal shock for $r_i/r_o = 0.8$. These are the maxima of Figure 10.

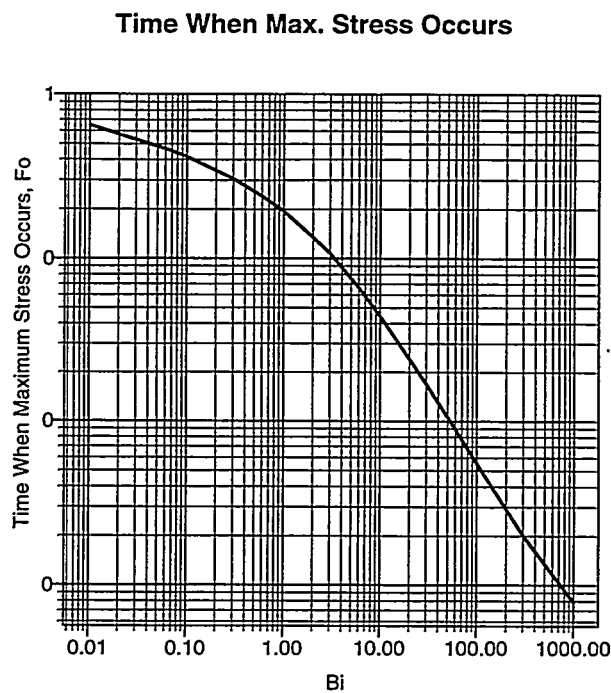


Figure 12. The time (Fo) when the maximum thermal stress occurs as a function of the Biot number.

Table 3. Calculated Maximum Stresses at the Inner Wall of Piping or Tubes Initially at 25°C Undergoing Thermal Shock with Molten Salt at 290°C based on the Biot Numbers from Experiments.

Pipe or Tube Size	$\sigma_{\text{Equivalent}}$, MPa
1 inch receiver tube, 0.065 inch wall, 304 SS	-100
2 inch schedule 40, 316 SS	-140
6 inch schedule 80 header, 304 SS	-240

Using Equation 9, a conservative estimate of the peak circumferential stresses at the inner surface of a pipe or tube can be calculated as a function of salt velocity. Plots of these relations are shown in Figures 13 and 14 for 6 inch and 16 inch piping proposed for handling molten salt in the Solar Two and Commercial scale systems, respectively. There is a critical velocity at which the stresses exceed the endurance limit of the material. These velocities are listed in Table 4 for several pipe schedules and materials proposed for handling molten salt. Carbon steel is able to handle thermal stresses better than stainless steel, because carbon steel has a much lower coefficient of thermal expansion, even though its endurance limit is lower.

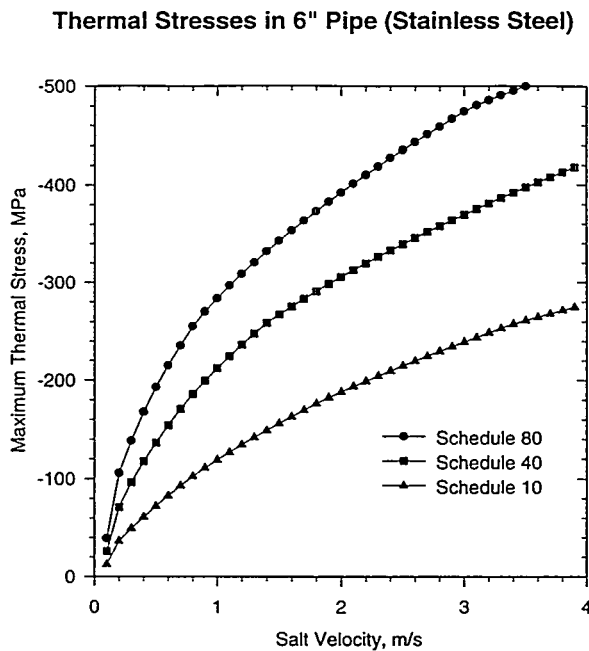


Figure 13. Maximum stress at the inside wall as a function of velocity for 6 inch piping.

Thermal Stresses in Stainless Steel 16 inch Pipe

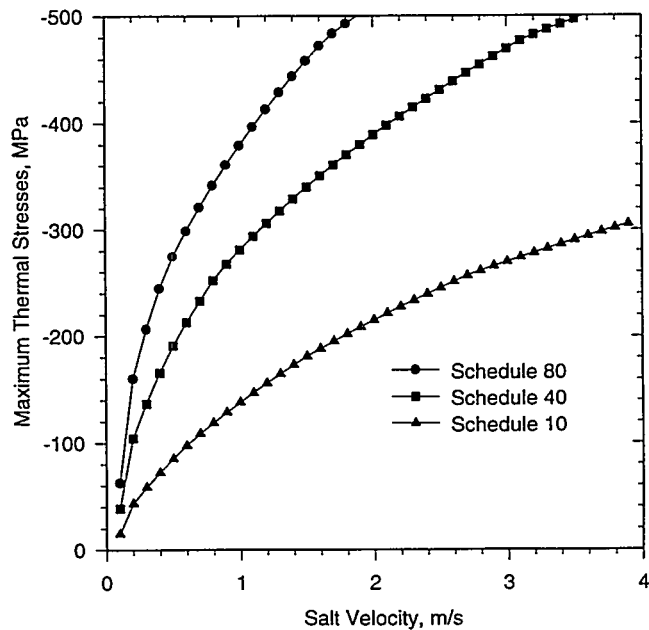


Figure 14. Maximum stress at the inside wall as a function of velocity for 16 inch piping.

Table 4. Maximum Velocities During Cold Fill Where Maximum Thermal Stresses are Below Endurance Limit of the Material for $T_{\text{wall}} = 25^{\circ}\text{C}$ and $T_{\text{salt}} = 288^{\circ}\text{C}$.

Pipe Size	Schedule	Material	Maximum Velocity, m/s
6 inch	80	Stainless 316	0.9
6 inch	80	Carbon	3.7
6 inch	40	Stainless 316	1.5
6 inch	40	Carbon	6.3
6 inch	10	Stainless 316	3.8
16 inch	80	Carbon	1.9
16 inch	40	Carbon	3.7
16 inch	10	Carbon	12.2
16 inch	10	Stainless 316	5.7

Even though the stresses in the walls of piping or tubes were low when thermally shocked in our tests, high stresses could develop where there are large loads already existing in the piping due to structural considerations, where there is a sudden change in wall thickness, or where there is abrupt changes in contour resulting stress concentrations. It should be noted this analysis applies only to vertical runs of piping or tubes where the temperature gradient is a function of the radial coordinate. In horizontal pipes, the leading edge of the fluid could have a sloped profile resulting in circumferential temperature gradient, in addition to the radial gradient. This would result in stress condition. Most of the piping in the risers and downcomers of molten-salt central-receiver solar power plants is in vertical runs.

For a receiver illuminated with high flux, the stresses are quite different from the stresses during thermal shock. In addition to a through-wall stress, there is a front-to-back tube stress. Appendix D shows the strain equations applicable to receiver tubes under high flux.

Calculations of Penetration Distances - Transient Freezing in Pipes. Another issue pertaining to cold starting piping is how far the molten salt can flow through a cold pipe before freezing shut. This length is known as the penetration distance. There are several models which describe transient freezing in pipes, but one model correlates data from several experiments and a variety of fluids into a single equation that describes the penetration depth as a function of the fluid properties, the Reynolds number, the wall temperature, and fluid temperature [9]. The correlation, Equation 18, describes the axial distance a fluid will flow through a cold pipe whose temperature is held below the fluid's freezing point before the pipe freezes shut. The wall temperature is held constant.

$$\frac{z}{D} = 0.23 \text{ Pr}^{1/2} \text{ Re}^{3/4} (\alpha_m / \alpha_s)^{1/9} [h_f / (Cp_s(T_f - T_w))]^{1/3} [1 + \gamma Cp_m(T_o - T_f) / h_f] \quad (18)$$

The penetration depths were calculated for molten salt properties at several pipe diameters and flow velocities. These results are shown in Table 5 and in Figure 15. For large diameter piping, such as used with the riser or downcomer in the Solar Two central receiver power plant, we could theoretically flow through hundreds or thousands of feet of piping. In a commercial scale plant, we may be able to flow through *miles* of cold piping. We expect these values to be conservative, since the correlation was developed for a constant wall temperature.

Table 5. Penetration depths for molten salt for various pipe diameters, velocities, and salt inlet temperatures for a wall temperature $T_w = 68^\circ\text{F}$ (20°C).

Diameter	Flow Velocity	Salt Inlet Temperature	Penetration Depth
0.75 in	3 m/s (9.8 ft/s)	288°C (550°F)	39 m (129 ft)
0.75	1 m/s (3.3 ft/s)	288°C (550°F)	17 m (57 ft)
0.75	1 m/s	371°C (700°F)	27 m (87 ft)
1.5 in	3 m/s	288°C (550°F)	132 m (435 ft)
1.5	1 m/s	288°C (550°F)	58 m (191 ft)
1.5	1 m/s	371°C (700°F)	90 m (294 ft)
6 in	3 m/s	288°C (550°F)	1498 m (4920 ft)
6	1 m/s	288°C (550°F)	657 m (2160 ft)
16 in	3 m/s	288°C (550°F)	8340 m (27400 ft)
16	1 m/s	288°C (550°F)	3660 m (12000 ft)

For the panel experiments described previously, we were able to flow through four passes and the associated headers and jumper tubes all at ambient temperature with a salt velocity of 2 ft/s (0.6 m/s). The total length of tubing is about 60 feet (18 m). The correlation predicts the fluid should freeze in about 50 feet (15 m). This means we were probably on the border of freezing.

Penetration Depths vs Salt Flow Rate

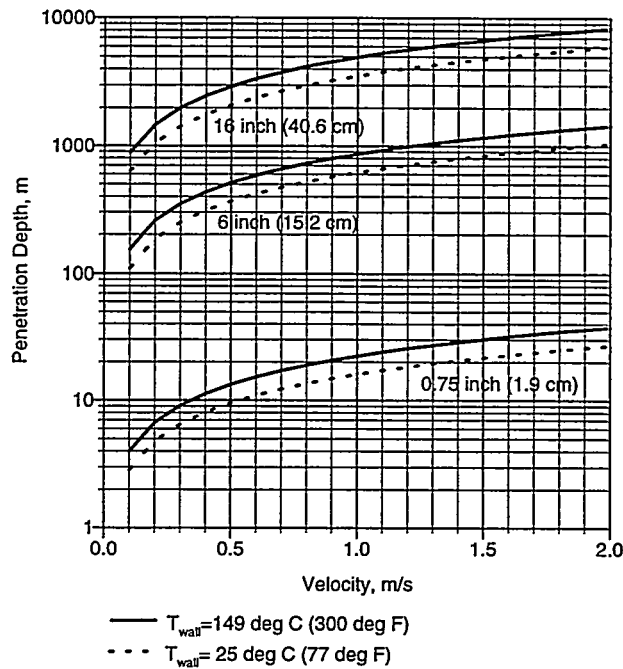


Figure 15. The penetration depths for several pipe diameters as a function flow velocity.

In addition, we were able to flow through over 155 feet (47 m) of ambient temperature ($<100^{\circ}\text{F}$) 2 in piping without freezing the pipe shut. The correlation predicted we would be able to flow at least twice that distance. It should be noted that the correlation was developed for piping that was submerged in a bath of fluid to hold the pipe outer surface at a constant temperature. In the cold fill tests described in the previous section, the piping or receiver tubing was not held at a constant temperature, but allowed to heat up. The correlation may be conservative, because an insulated pipe has a finite heat capacitance.

When tried filling the panels at lower velocities (0.4 m/s), we were not able to flow through all the passes. We detected salt in the second and part of the third pass, but it is unclear whether the flow stopped in third pass due to freezing, or a systematic problem. The correlation predicted we should have frozen in the third pass. Unfortunately, we could not verify the accuracy of the correlation very well with the panels, because they are connected with a common vent line which allows the flow to bypass the second and third pass and enter the fourth pass. We postulate that when the flow through the tubes in the second and third pass becomes restricted due to a buildup of a frozen layer of salt, the preferential path of least resistance is the bypass line. This could effectively cut off the venting of air through the second and third passes, resulting the panel becoming air bound.

In a report on the Molten Salt Electric Experiment of a receiver in the external configuration [1], experiments are described in which the receiver was started cold in a flood fill mode (all the panels in a receiver are filled from the bottom up). In two cases they succeeded in filling the panel, but in one case they froze part of it. For this case, the correlation predicts that salt would have barely made it through the 11.5 foot (3.5 m) high panel, which is consistent with the results.

The data are summarized in Table 6. (The flow rate was not given in the report, but was calculated from information about the system. The fact that third test in the series has a higher penetration distance than the second one may be attributed the uncertainty in the flow assumption and average panel temperature measurement.)

Table 6. Results for cold start experiments with the MSEE external receiver along with the correlation results. The panel height is 11.5 feet (3.5 m), tube diameter 0.62 inches (1.6 cm), salt flow rate approximately 0.4 ft/s (0.1 m/s).

Wall Temp	Salt Temp	Penetration Distance	MSEE Result
325°F (163°C)	700°F (371°C)	19.0 ft (5.8 m)	Fill OK
240°F (116°C)	650°F (343°C)	13.6 ft (4.2 m)	Fill OK
210°F (99°C)	700°F (371°C)	14.7 ft (4.5 m)	Partially frozen panel

For the Solar Two receiver designed by Rockwell, in order to prevent freezing, the receiver panels should be heated (with heliostats) to temperatures above 200°F (93°C) with headers and jumper tubes preheated with heat trace to the salt temperature, assuming the panels are flood filled at the design flow rate. The panels should be heated to at least 390°F (199°C) with jumper tubes initially at ambient temperature. These results are shown in Table 7.

Table 7. Estimated penetration depths for Rockwell's Solar Two receiver. Panel height is approximately 21 feet (6.4 m), jumper tube length: approximately 10 ft (3.0 m), tube inside diameter: 0.7145 inches (1.81 cm), salt velocity during flood fill: 0.87 ft/s (0.27 m/s).

Tube Temp	Penetration depth
10°F (-12°C)	18.35 ft (5.6 m)
100°F (38°C)	19.9 ft (6.1 m)
200°F (93°C)	22.4 ft (6.8 m)
400°F (204°C)	44.3 ft (13.5 m)

Summary of Cold Fill Tests

The following conclusions can be made about the cold fill tests:

- Cold filling the panel and/or manifolds is feasible. In normal operation it would not be necessary to cold fill the panel. As a minimum, our results show that the entire panel does not have to be above the salt freezing temperature before salt flow is established.
- Results from the stress analysis show that the stresses in the header and receiver tubes were below the endurance limit during a thermal shock. Analysis should be done for a particular design of the tube-to-header junction and transitions in piping cross section to make sure there are not any localized stress concentrations, and to estimate the life based on fatigue of these areas.
- The best combination of reduced parasitics and increased availability might be partial preheating (e.g., preheating to 300°F).

- We recommend that even if the piping is cold started, valves, flanges, and instrumentation should be kept near the salt temperature to minimize reliability issues that could arise if these components were thermally stressed.
- Our experience has shown that the most successful method for uniformly preheating the panels is to use a roving aiming pattern where the heliostat aim points change every few seconds to avoid localized under- and overheating.
- Although our results show that we can successfully flow through cold piping and tubes, care must be taken to avoid freezing of salt past slow leaking valves in unheated piping.

Freeze/Thaw Experiments

In a molten salt receiver, there are multiple drain valves. During the nightly shut down of the receiver, a drain valve might fail to actuate. If a valve fails to actuate once in a thousand times, a receiver—which has 14 drain valves—will fail to drain approximately once every two and a half months. That does not necessarily mean a panel will freeze that often. Only if this failure is not detected in time and corrective action (such as manually opening the valve) is not taken will the salt trapped in the associated panels freeze. Since the volume of salt increase when it goes from the solid to the liquid state for a fixed mass, damage can occur to the panel if the salt is thawed in a section of tubing or piping which is constrained at both ends.

The objectives of these tests were to determine the procedure required to thaw a receiver panel if it became frozen with salt, and to determine what amount of damage were done to the receiver tubes during the thawing process. A total of five freeze/thaw cycles were conducted. Prior to installation of the panels, all the tubes' outside diameters were measured at various locations along its length, so we could determine the permanent strain induced during the freeze/thaw tests. The freeze/thaw test procedures we used are described below.

First, we established flow in all tubes of the panels to allow the panels to reach thermal equilibrium. After flowing salt through the panels for several minutes, we shut off all drain and outlet valves to prevent salt from draining out of the panel. We then allowed the panels to cool so their temperatures dropped below salt the freezing point. Figure 16 shows panel and header temperatures as they cool. Note how the slopes of the curves change at the salt freezing temperature, 430°F (221°C). When the salt becomes solid, the slopes change again. The header temperature is maintained above 460°F (238°C) by heat trace. The panels cooled to the salt's freezing point only 25 minutes after the pump stopped in the shielded environment of the solar tower. An exposed external central receiver (e.g., the Solar Two receiver) will cool much faster.

After the average panel temperature was less than 280°F (138°C), we opened the drain and panel outlet valves to empty the lower header of salt. Heat trace was kept on in the headers and on the jumper tubes to maintain the temperature above the freezing point. Once the headers had drained, we initiated thawing with heliostats. The only way for salt to leave the panel as it thaws is through the drain. Therefore, we started thawing from the bottom by putting on one heliostat and allowing it to heat that area of the panel to > 500°F (260°C). We continued to add heliostats, one at a time above the previous one, raising the panel temperature. One test was interrupted by weather and had to be continued the next sunny day. Once all thermocouple readings on the panel were above the salt freezing point, we tried to establish flow through the panel. On the first attempt, we were

Panel Freeze Test: 01/04/94

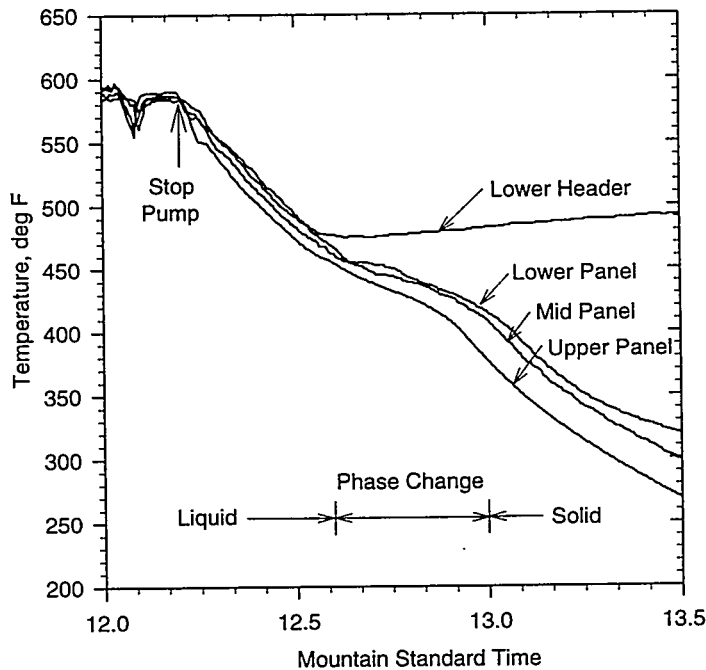


Figure 16. Temperatures receiver panels and header as they cool when filled with molten salt which freezes in the panel at approximately 430°F (221°C).

unable to flow though the majority of the panel because there were sections of tubes under the insulation where the heat trace could not heat it up enough, and we could not heat it with solar. In these regions we had to rely on conduction to melt the salt. Once we achieved flow through part of the panel we continued to flow salt, which helped thaw the frozen areas. After several hours we were able clear all tubes.

After two freeze/thaw cycles we measured the tube diameters. Plots of the permanent (plastic) strain as a function of the panel height are shown in Figure 17 for the east panel and 18 for the west panel. There did not seem to be any pattern to the damage. The maximum permanent strain induced in the tubes was over 4%. Figures 19 and 20 show the plastic permanent strain as a function of the horizontal location (tube number). The values of tube deformations are also shown in Table 8. Tubes 3, 4, and 5 in the east panel have much lower permanent strains than the other tubes in the panel. The west panel does not show this behavior. These results indicate the freezing phenomenon is complex, and requires further study.

Some observations and conclusions can be made regarding these tests:

- Thawing a frozen panel can require several hours, and could result in significant down time.
- The major problem with thawing the panel was a lack of sufficient heat under the insulation, particularly in the upper header where beneficial natural convection within the header oven cavity is not significant. It may be necessary to install additional heat trace in the regions where the insulation meets the panel to assure those areas can heat up to above the salt melting point.

East Panel Deformation

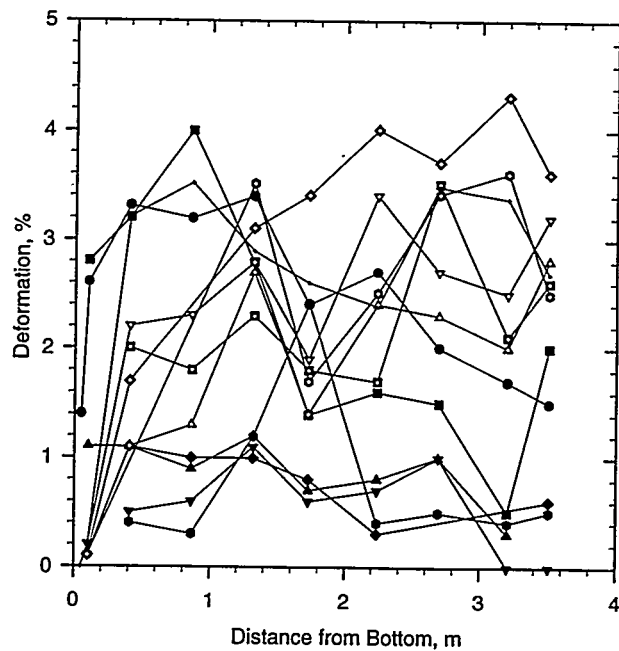


Figure 17. Permanent strain induced in the east panel tubes as a function of the panel height after two freeze/thaw cycles.

West Panel Deformation

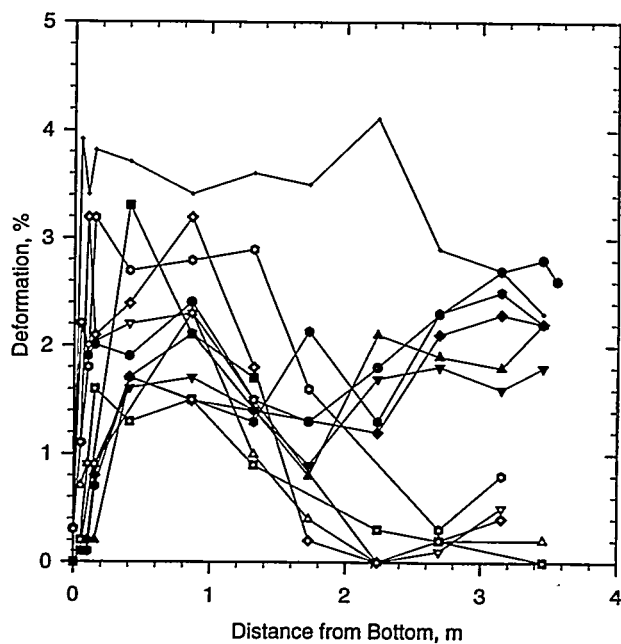


Figure 18. Permanent strain induced in the west panel tubes as a function of the panel height after two freeze/thaw cycles.

Side View: East Panel Deform.

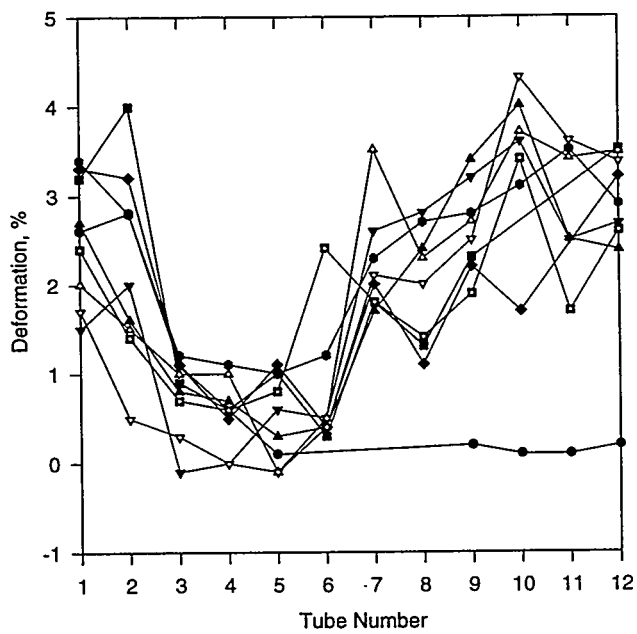


Figure 19. Permanent strain as a function of the width (tube number) for the east panel.

Side View: West Panel Deformation

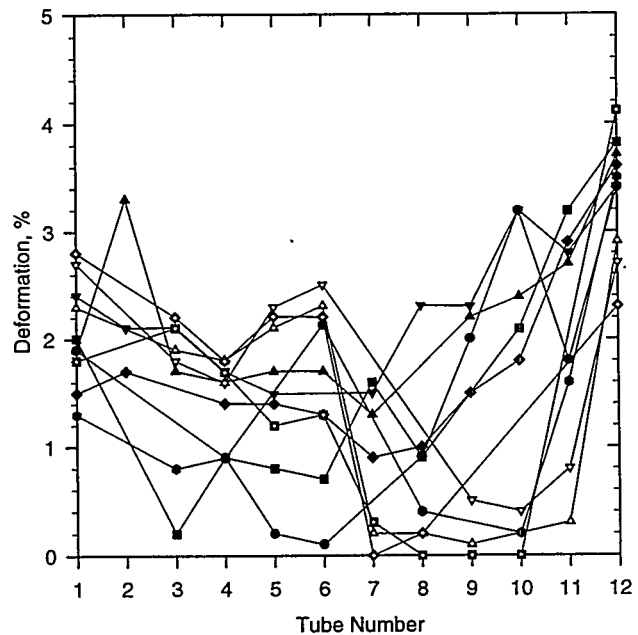


Figure 20. Permanent strain as a function of the width (tube number) for the west panel.

Table 8. Pre- and Post-Measurements of Tube Diameters in East and West Panel after 2 Freeze/Thaw Cycles.

Molten Salt Panel Deformation Measurements

- Although we had over 41 thermocouples on the 24 receiver tubes and 4 headers, we were unable to determine where the blockages were. Even when all the thermocouples indicated that the temperatures were above the salt melting point, we still had plugs of salt. In the Solar Two and commercial receivers there will be even less instrumentation. If a panel becomes frozen, temporary thermocouples should be installed to monitor the panel temperatures more thoroughly. They could be mounted on the outside of the tubes. Another option is to monitor the temperatures with an IR camera.
- The heat trace should be designed to heat the headers and jumper tubes above 500°F within 10 hours when they are *full* of salt.

Component Tests

The main objectives of the component tests were to test unproven hardware and determine how well they perform in a molten salt environment, and to reduce uncertainties of the performance of untested components and operating procedures. Many of the flanges were tested in a molten salt environment, but additional information is required. Check valves were not tested previously in molten salt. The component tests were broken down into three areas: 1) check valve cycling, 2) slow thermal cycling of flanges, and 3) thermal shocking of flanges.

Check valves are needed at the pump outlet to prevent damage to the pump from the static "head" of salt when the pump stops, or to prevent pressure surges caused by redundant pumps on a common header when one pump stops. Serious damage to the pump can result if it is not protected from the strong inertial forces of the salt coming from the other pump and from the salt head in the riser.

It is desirable to use flanges that facilitate service of certain high maintenance components in molten salt loops. The flanges used in the molten salt pump and valve test loops were a constant source of salt leaks. The purpose of these tests was to test various other designs of flanges (e.g., tapered flanges or clamp type flanges) to measure how well they held a seal under thermal cycling, and to determine if it is practical to use flanges around the high maintenance components. We tested five flanges: a 2 inch Grayloc, two 4 inch R-CONs, a 6 inch E-CON, and a 4 inch ANSI ring type.

Check Valve Cycling. The purpose of the experiments with the check valve were to test their operation in a molten salt environment and to determine how to drain the salt from the check valve. A 3 inch spring loaded swing check valve was tested in a section of piping between flanges in the loop. Although we could not simulate the pressures expected to be encountered in cold side of a molten salt loop, we did simulate the flow velocities and the temperature cycles on the cold loop.

Figure 21 is a photograph of the check valve we tested (V-CON model manufactured by Reflange, Inc.). A drain hole was drilled in the flapper to allow a short section of piping downstream of the check valve to drain.

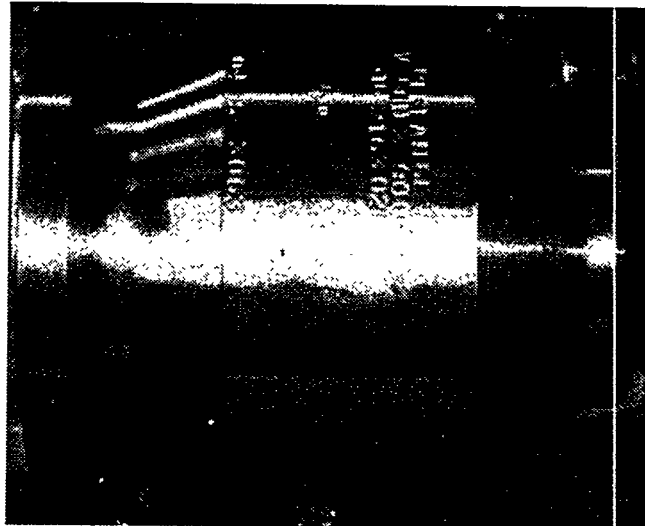


Figure 21. Photograph of the 3 inch check valve (V-CON model manufactured by Reflange, Inc.) tested in the salt loop.

In these tests we pressure cycled the check valve by flowing salt at the maximum flow rate - approximately 100 gallons/min (380 l/min) and establishing pressure in the accumulator to 30 psi, then shutting a bypass valve (FCV 720) and turning off the pump. Shutting the valve before turning off the pump caused a momentary spike in the pressure, but assured the check valve would receive positive pressure on the downstream side of the flapper. We monitored the pressure decay in the accumulator tank. After waiting approximately 30 minutes to allow the pump motor to cool, we repeated the cycling. Figure 22 shows the pressure and flow as a function of time for several cycles. There were no problems with its operation after over 300 cycles (approximately 1 year of operation). The flapper was inspected after the 300 cycles, and found to be in good condition with no signs of wear.

Slow Thermal Cycling of Flanges. Flanges in a molten salt environment have been known to leak significantly after being thermally cycled [12]. It is desirable to use flanges to facilitate service of high maintenance components, such as the pumps, in molten salt loops. The flanges used in the molten salt pump and valve experiments were a constant source of salt leaks. We tested various flanges to determine how well they hold a seal under the slow thermal cycling expected during nightly shut down of the plant followed by morning preheat with heat trace. We slow cycled four flanges: a Grayloc 2 inch with clamp type connectors, two 4 inch R-CON flanges with clamp type connectors manufactured by Reflange, and one 6 inch E-CON bolted flange also manufactured by Reflange. The Reflange flanges have a unique metal gasket that is radially compressed (elastically) when the two faces are brought together, providing a tight seal.

Checkvalve Cycling

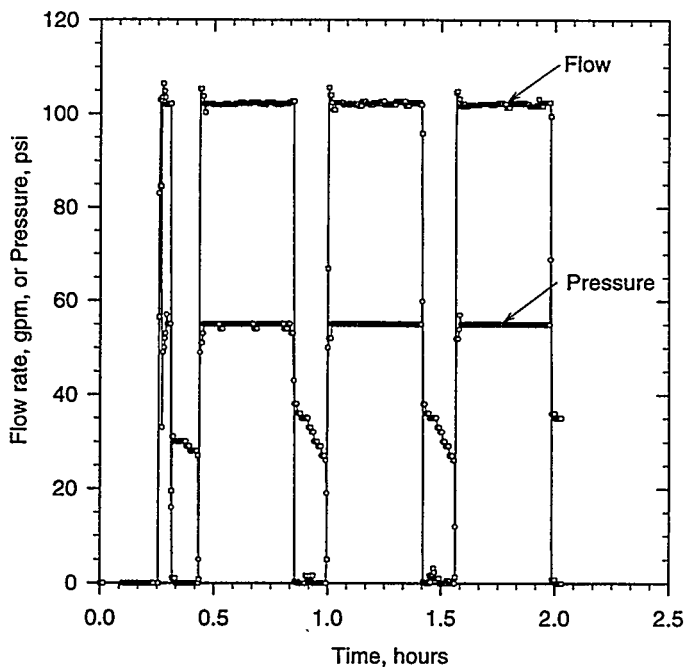
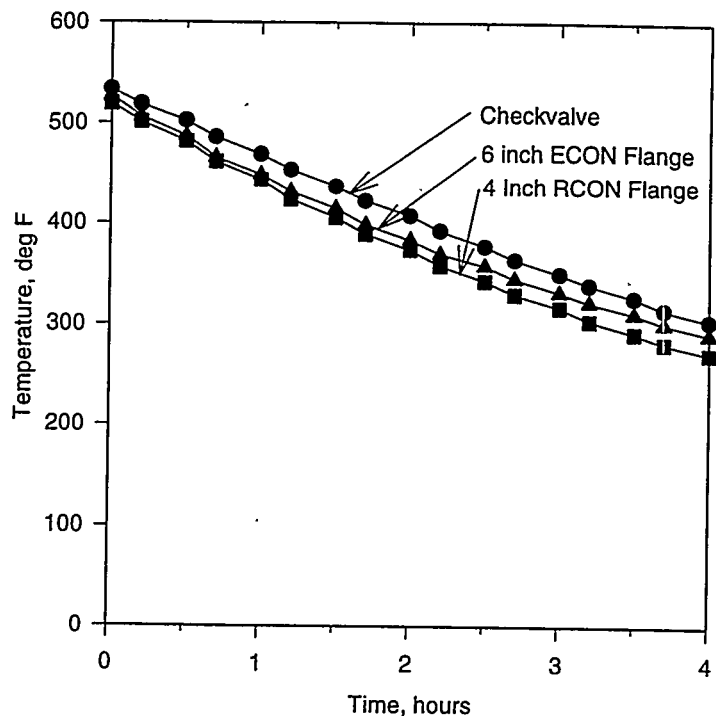


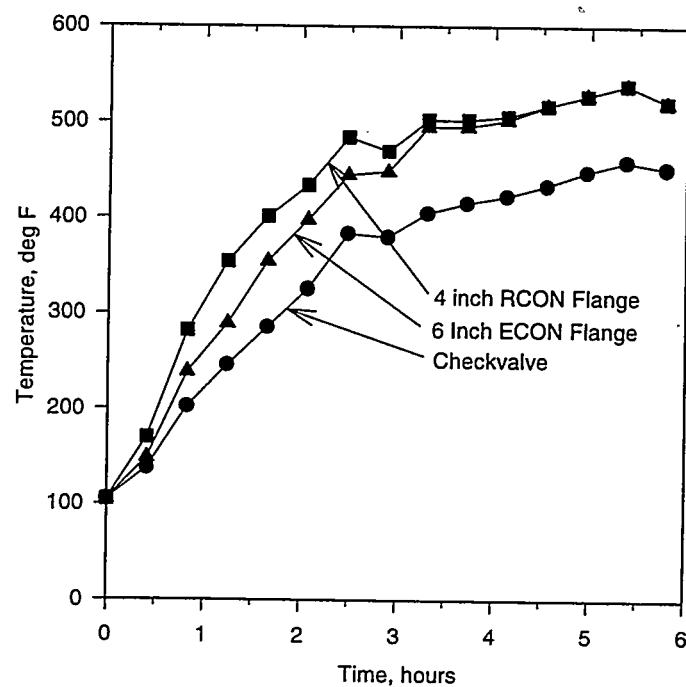
Figure 22. Pressure and flow as a function of time during a typical check valve cycle.

In these tests we simulated the nightly shut down and cooling of the components (assuming the heat trace were turned off) by using a fan and removing some of the insulation to enhance the cooling and match the temperature profiles we had expected to see in service at Solar Two. We cycled between 200 and 500°F. Each cycle took between six and eight hours. Figure 23 shows a typical slow thermal cycle. After approximately 180 slow thermal cycles, one of the 4 inch flanges started leaking very slightly. (We realized the torque on the bolts for the first 180 cycles was lower than the recommended value for the size of bolts we were using, and may have resulted in a less than optimum compression on the gasket.) We inspected all the flanges (we disassembled the two 4 inch flanges) and noticed they had all leaked to some extent, except the bolted 6 inch E-CON which showed no visible signs of salt. The bolted flange may provide a more uniform compression on the faces of the flange and gasket as compared to the clamp type flanges. See Figure 24. Since the salt is very wetting, it tends to get into cracks and seeps past gaskets, soaking and degrading the insulation. The continuous thermal cycling adds to its migration. Even though the flanges leaked a small amount (approximately 1 drop per hour), they would not likely fail catastrophically, since the gaskets are metal.

We retorqued the bolts to their recommended torque and continued the slow thermal cycling for an additional 120 cycles (a total of 300 cycles -- approximately one year of service) without any failures.

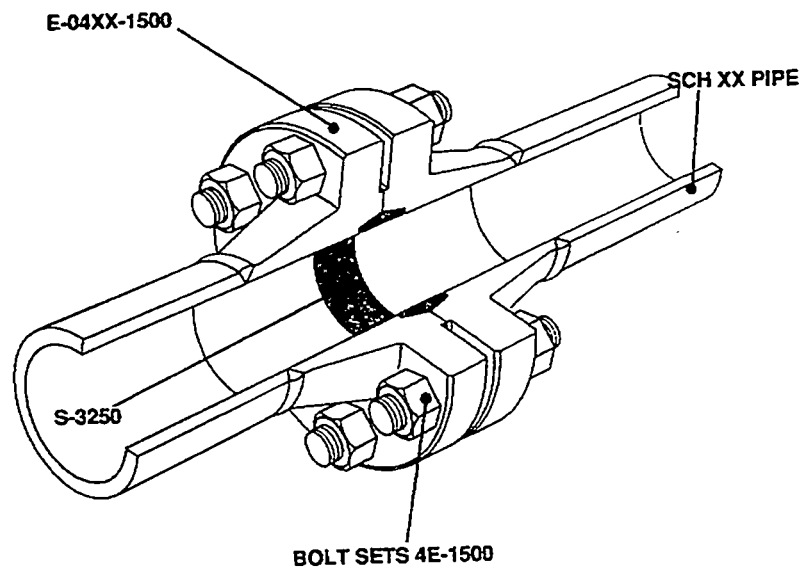


a)

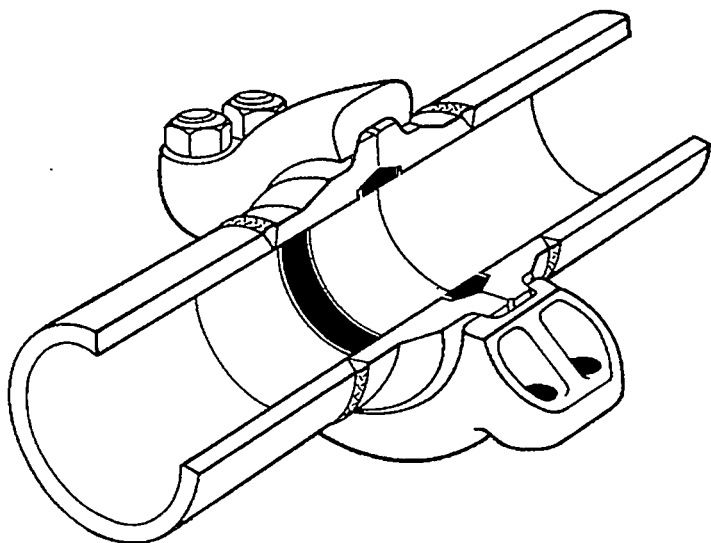


b)

Figure 23. Typical slow thermal cycle of flanges simulating nightly cool down of components followed by slow heatup with heat trace.



a)



b)

Figure 24. Schematic of a) ECON and b) RCON flanges.

Thermal Shocking of Flanges. The most severe thermal cycling a flange could experience in a molten salt system would be a thermal shock where the flange is at one temperature and it is suddenly subjected to salt at a different temperature. This situation could occur in one of two ways: 1) when the salt temperature at the outlet of the receiver suddenly drops due to a cloud transient, or 2) at startup if the flanges were at a temperature below the salt temperature. In the first case, the salt temperature transient could be from 1050 to 550°F (566 to 288°C) in approximately five minutes. In the second case, the flange could be as cold as ambient with the salt at approximately 550°F (288°C). This situation could arise if the parasitic power consumption were being minimized at nightly shut down by turning off the heat trace followed by cold filling of the piping. In our test loop we only simulated the second thermal shock case, since it would be very difficult to simulate the transient salt temperature at the receiver outlet. We conducted these tests at two initial flange temperatures either: 300°F or ambient (~100°F) with the salt at 550°F.

Prior to the start of the thermal shock tests we installed a 4 inch ring-type flange to test alongside the other flanges. In these tests we allowed the flanges to cool for several hours or overnight by lowering set point temperature of the heat trace or by turning off the heat trace completely. After the flanges had cooled to the desired temperature, we shock them by pumping 550°F salt through them. Figure 25 shows a typical temperature profile of the flanges and check valve during a shock.

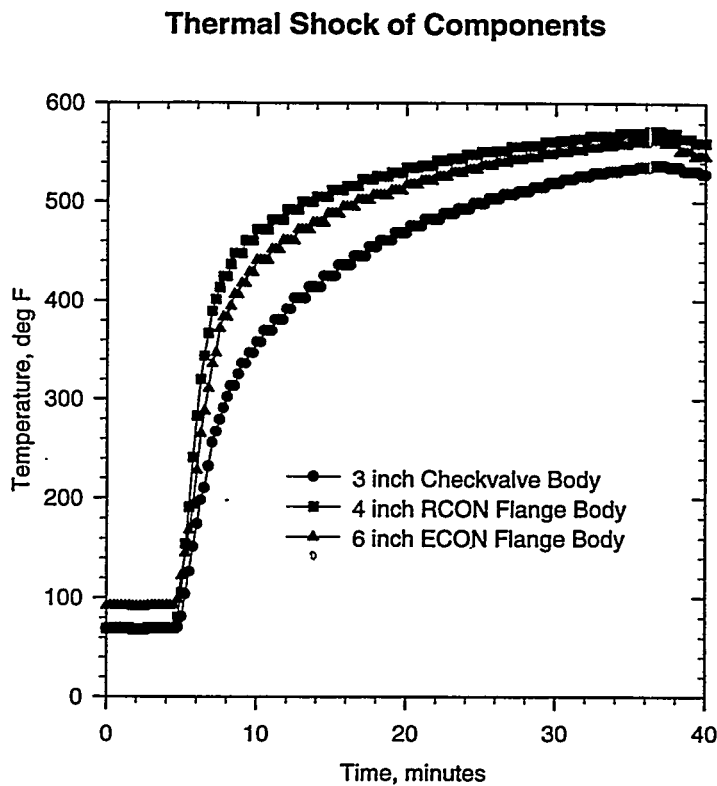


Figure 25. Typical temperature transient of the flanges during a shock.

After 25 cycles at 300°F, we inspected the flanges. There did not appear to be any visible breaches of integrity. We continued the thermal shocks with the flanges at ambient temperature. The flanges experienced 146 shocks without failure, although the flanges continued to leak at a very slight rate. After all these thermal shocks, none of the flanges failed catastrophically. With continuous operation and exposure to pressurized salt, all except one of the flanges showed only minor leaking (wetting between the interfaces of the flange faces or actually dripping of salt at a rate of approximately one drop per hour). The exception is the Grayloc flange which leaked significantly, enough to form a stalagmite of salt on the floor. Leaks over a long period of time can soak the insulation and increase the thermal losses. Exposure of salt to heat trace can also cause an electrical short in the heat trace.

A finite element analysis was done on the 6 inch E-CON flange to determine the stresses that developed in this flange undergoing thermal shock with salt at 550°F and the flange either initially at 77°F (25°C) or at 300°F (149°C). The details of this analysis are included in the appendix. There were two areas of concern in the flange where the stresses reached a maximum: 1) at the interface of the two flange faces at the outer most radius, and 2) on the inner surface of the flange adjacent to the gasket. The stresses developed at the interface between the two flange faces during either initial condition (77 or 300°F) were highly localized and were in excess of the yield for the material, but a chamfer exists at this location. The actual stress should be much lower with the chamfer, so that region is not a concern. On the other hand, the stresses in second region are in excess of the yield when the flange is shocked from an initial temperature of 77°F (25°C) but not in excess when shocked at 300°F (149°C). Based on this analysis, we recommend that flanges are preheated at least to 300°F (149°C) prior to initiating salt flow.

These flanges are an improvement over the flanges used in the pump and valve test loops which were raised-faced flanges with a Flexitalic type gasket. Those flanges tended to leak severely under cyclic conditions.

Our observations and recommendations regarding these flanges are:

- The flanges held up remarkably well to the conditions to which we subjected them. There were no severe failures. The majority of the salt leaks were very slight.
- Flanges should be minimized in a salt system. They should be used only for removal of high maintenance equipment such as the pumps, if at all. All welded construction is preferred, especially on hot loops.
- If the piping is cold started, the flanges should be preheated to at least 300°F (149°C) prior to flowing salt through them.
- The flanges tend to seal better if they are not thermally cycled.
- Hot retorquing the bolts periodically may reduce the leaks.
- Heat trace zones should be designed so that flanges and valves are not part of the same heat trace circuit as the rest of the riser or down comer, so that cold starting the rest of the piping can be done.

Instrumentation Tests: Flowmeters and Pressure Transducer

Flowmeters. Flowmeters were a considerable source of problems in previous molten salt experiments [2]. For example, the Category B receiver used venturi type flowmeters with differential pressure transducers using silicone oil as an intermediate fluid to measure flow. The

pressure transducers had problems with silicone oil volatilizing at the cold salt temperature. In addition, venturi flowmeters only have a range of about 4:1. Because of the limited range and silicone oil problems, we investigated other designs of flow meters that could be more reliable, provide higher accuracy, and have a greater range.

We chose to test two types of flowmeters: vortex shedding and ultrasonic. These flowmeters were selected because they are common, commercially available products which can withstand the temperatures we expected to encounter in the cold side of a salt system. The vortex shedding flowmeter has wedge in the flow field and senses oscillations of the vortices which are shed from the wedge. The frequency of the oscillations is proportional to the flow rate. The ultrasonic flowmeter sends a sound wave through the moving fluid from one transducer to the other, with and against the flow. It measures the time difference between the traverses. We tested two types of ultrasonic flowmeters: a wetted type where the transducers actually send the sound wave directly into the fluid, and a clamp-on type where the transducers simply mount on the outside of the pipe and propagate the sound wave through the pipe wall. The vortex shedding flowmeter we tested was manufactured by Engineering Measurement Company, and the ultrasonics by Panametrics. Both have temperature limitations and are only rated for the cold side of a molten salt system. The ultrasonic flowmeters were calibrated with water at the factory prior to installation in the salt loop. The vortex shedding flowmeters had been calibrated under the Direct Absorption Receiver Program.

We have operated the flowmeters since the beginning of this test program. The first clamp-on transducers were not made for the cold salt temperatures and their bodies (made of a "high" temperature phenolic material) melted. The manufacturer replaced them with all metal transducers. We also experienced some problems with the cables to the wetted transducers. Once we worked through the bugs in the hardware and programming, the ultrasonic flow meters worked reasonably well. The clamp-on flowmeter uses a petroleum couplant between the transducer and the pipe wall which allows the sound wave to penetrate through the pipe and into the fluid. After approximately a week or two of intermittent service at the cold salt temperatures (above 500°F), the couplant dried out and caused inaccuracies in its readings. A new application of couplant restored the contact between the transducer and the pipe wall.

A comparison between the flowmeters is shown in Figure 26 during a varying flow condition. The vortex shedding responds much faster and stabilizes better to changes in flow rate. For control purposes, the vortex shedding would be the preferred flowmeter. The ultrasonic flowmeter took some time to tune and to get operating properly, partly due to the faulty cable. By changing the parameters (such as the number of samples it averages for a reading) in the software of the electronics for the ultrasonic flowmeters, we were able to change its response.

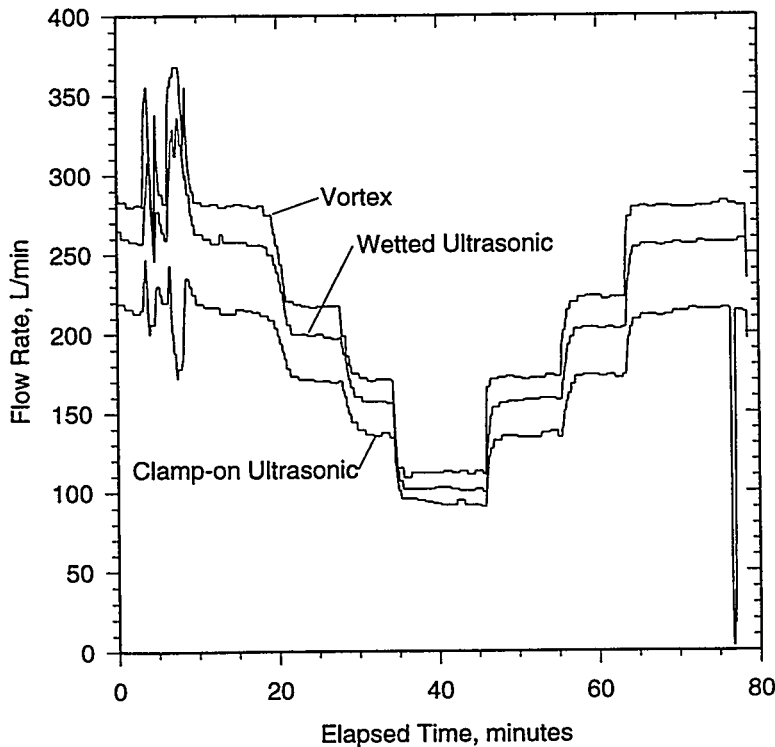


Figure 26. Response of vortex and ultrasonic flowmeters during a varying flow condition.

The flowmeters were compared with calibration tanks in the salt loop. Since the volumes of the calibration tanks are essentially constant with time, and the accuracy of the bubbler level measurement devices is good ($\pm 3.8\%$), we chose to compare the flowmeters with the calibration tank flow.

The uncertainty of the flow measurement has two components: the bias (also called systematic) errors and the random errors [10]. The bias errors affect each measurement the same amount (at a given condition) and represent the offset from the “true” value. Random errors are the errors that change in a random fashion with repeated measurement. The random errors are not correlated with each other, and their limit can be measured if several data points are taken. Since the true bias and random errors are not known, their estimates are approximated by limits of each. The bias limit equals the square root of the sum of squares of each elemental bias limit (b_i):

$$B = [\sum b_i^2]^{1/2} \quad (19)$$

The random limit equals:

$$S = \left(\frac{t_{95} S_x}{\sqrt{N}} \right) \quad (20)$$

where t_{95} is the Student’s t statistic at 95% confidence, S_x is the standard deviation of the data set, and N is the number of data points [10]. For the root-sum-square uncertainty model, the uncertainty is found by combining the bias and random limits as follows:

$$U_{RSS} = \pm [B^2 + S^2]^{1/2} \quad (21)$$

This model provides an interval around the test average that will contain the true value $\approx 95\%$ of the time. In the flow tests, the flowmeter readings were compared with a reference—the calibration tanks. The bias errors relative to the reference can be measured. However, the reference (the calibration tanks) also has bias errors which we could not measure.

Table 9 lists each bias error source and estimated magnitude for the calibration tank flow measurement. The calibration tanks use bubblers to sense level. The amount of time to fill between two levels in each tank is measured and the flow rate calculated. Since the volumes of calibration tanks were not measured when the Panel Research Experiment was fabricated, exact volumes are not known. However, the dimensions were determined from drawings of the tanks. The volume was calculated, accounting for an overflow standpipe. Even if the tanks have significant amounts of eccentricity (5% change in the diameter) causing the tank to become elliptical, the volume of each is not significantly affected (it changes by less than 0.5%). Other bias sources of errors are thermal expansion of the tank volume between ambient and 550°F, salt density variations due to temperature, and the bubbler calibration.

Table 9. Bias Limit Sources for Calibration Tank Flow Measurement.

Error Source	Magnitude
1. Tank Eccentricity (tank cross section is elliptical: minor axis is 95% tank radius, major axis 105% radius).	0.5%
2. Tank Thermal Expansion (change in tank volume from ambient to 550°F).	1.5%
3. Salt Property Variations (change in density and thus level between 550 and 650°F).	1.8%
4. Bubbler Calibration (approximately 0.5 inch in 18 inches).	<u>3.0%</u>
Total Bias Limit Calibration Tank Flow (Root Sum Square)	3.8%

The flowmeters were compared with the calibration tanks at several flow rates. Starting at 100% flow, we allowed the flow to stabilize, then closed the drain valves to the calibration tanks. The bubblers measured the level in each tank as a function of time. The elapsed time for the salt to fill the tank between the lower and upper level settings is measured in each tank to calculate the flowrate. The total flowrate is the sum of the two calibration tank flows.

Figure 27 shows the results of the comparison of the flowmeters against the calibration tank flowrate. Each data point represents the average of several readings during the calibration run. Figure 28 shows the measured bias errors (relative to the calibration tank flowrate) for each flowmeter as a function of flow. The bias errors represent the systematic errors in the measurements. Note how the bias errors are a function of the flow rate. The implication of this dependency is that calibration constant for each flow meter is off by a fixed percentage. The random errors are shown in Figure 29. The random errors were calculated from the data using Equation 20. The random errors are quite small, indicating the flowmeters give consistent readings over the range of the flows tested. The root-sum-square uncertainties, U_{RSS} , for each flow meter as a function of flow rate are shown in Table 10. The U_{RSS} accounts for the bias errors of the reference source—the calibration tanks.

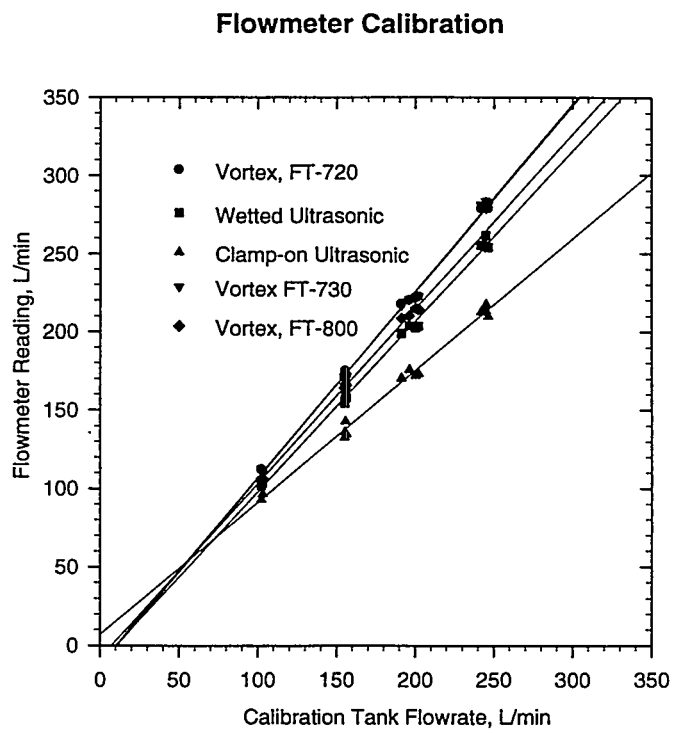


Figure 27. Comparison of the vortex and ultrasonic flowmeters against the calibration tank flowrate.

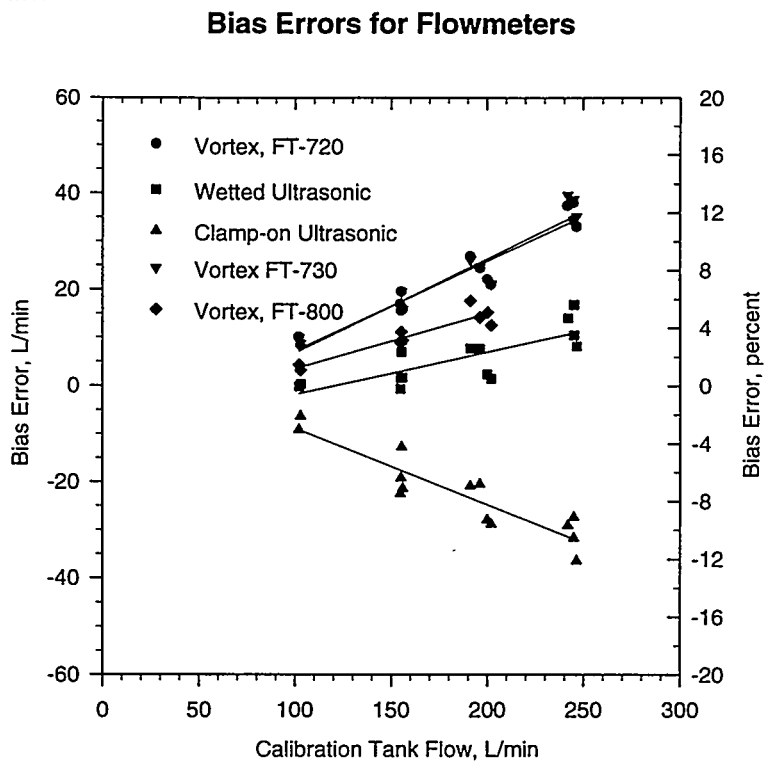


Figure 28. Measured bias errors (relative to the calibration tank flowrate) for each flowmeter as a function of flow.

Random Errors for Flowmeters

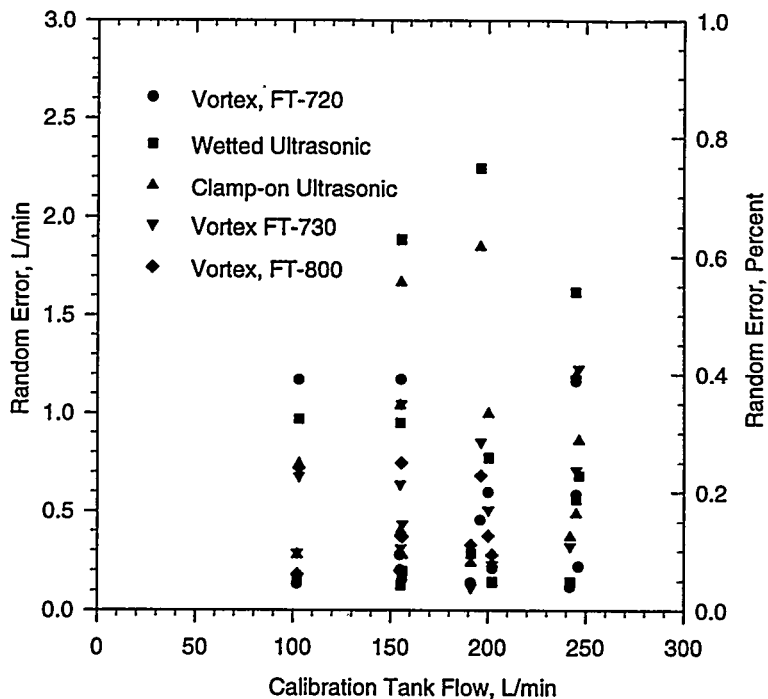


Figure 29. Measured random errors for each flowmeter as a function of flow.

Table 10. Root-sum-square Uncertainty (U_{RSS}) for Each Flowmeter.

Flowrate, L/min	Vortex, FT-720	Wetted Ultrasonic, PF-001	Clamp-on Ultrasonic, PF-002	Vortex, FT-730	Vortex, FT-800
102.6	$\pm 9.8\%$	$\pm 3.9\%$	$\pm 8.5\%$	$\pm 9.9\%$	$\pm 5.3\%$
155.4	11.6	4.2	12.8	11.6	7.3
197.4	12.6	4.6	13.0	12.5	8.5
244.6	15.1	6.4	13.3	15.6	--

The large uncertainties observed are primarily due to the large bias errors. By periodically calibrating the flowmeters against a calibrated reference (such as calibration tanks or the cold surge tank of receiver with a *calibrated* bubbler - this is important), the majority of bias error limits can be calibrated out resulting in a root-sum-square uncertainty with a magnitude of the uncertainty equal to the calibrated reference. Overall uncertainties (U_{RSS}) of less than $\pm 5\%$ can be obtained with these flowmeters. The random error limits were much smaller and did not contribute significantly to the overall uncertainty under steady conditions.

Other observations and recommendations regarding flowmeters:

- The vortex shedding flowmeter worked exceedingly well (very reliable) in the molten salt environment and should be used whenever possible. The ultrasonic flowmeters were less reliable.

- It is essential that provisions to calibrate the flowmeters in situ are designed into a molten salt system (e.g., calibrated level indicators in the cold tanks).
- For calibration purposes, the tank volume should be measured before installation and the bubbler must be calibrated.
- The clamp-on ultrasonic flowmeters are useful for temporarily (< 1 week) measuring flow in areas where there is no flow measurement or to verify flow measurement of an existing flowmeter and where the effort or expense and down time does not justify installation of a welded in flowmeter. During the check out phase of the receiver and salt system or during performance monitoring may be the time when clamp-on ultrasonic flowmeters could be useful on a very temporary basis or as a temporary backup if one of the permanent flowmeters were to fail and the plant was ready to run.
- The flow rate only needs to be measured on the cold side. There should be no need to measure flow on the hot side.

Pressure Transducer. We have tested an impedance-type pressure transducer and a NaK-filled pressure transducer in the salt loop to determine how well they work in molten salt. The silicone oil used in pressure transducers in previous molten salt tests tended to volatilize. The NaK-filled pressure transducers made by Taylor worked well in the pump and valve loop once snubbers were used to eliminate pressure pulsations which fatigued the membrane. Unfortunately, NaK-filled pressure transducers are difficult to find anymore. The impedance-type pressure transducer we tested in our loop is made by Kaman, and is good for temperatures up to 1200°F. It senses small displacements in its membrane and correlates them to pressure. It is self temperature compensating. Although we don't have any method to calibrate the pressure transducers in our system, the impedance-type pressure transducer was calibrated at the factory at 550, 750, and 1050°F. The impedance-type pressure transducer in our loop experienced the same thermal cycling and shock as the flanges, and did not fail or give erroneous readings. The pressure measurement in Figure 22 was from the impedance-type pressure transducer.

Comments regarding pressure transducers:

- The impedance-type pressure transducers work well but are expensive (~\$5k each).
- NaK-filled pressure transducers are hard to find.
- To keep instrumentation costs down, minimize the number of salt pressure measurements needed.
- The pressure transducers should be oriented so the salt can drain from them. Experience from previous molten salt experiments has shown, that if salt is allowed to freeze on the membrane, then thawed, the thawing process causes the membrane to rupture.

IV. Ongoing and Further Research

The work conducted so far has answered many of the questions regarding how far salt can flow through cold pipes during a cold fill scenario and the thermal stresses that develop when components and piping are thermally shocked, and some of the effects of freezing and thawing. We have also tested instrumentation that are an improvement over previous instruments. Ongoing and further research is directed towards understanding the freeze/thaw phenomenon, validating transient freezing models, and testing improved components and instrumentation. A description of each of these follows.

Simple Element Freeze/Thaw Tests (Ongoing)

A two-chamber oven was built to investigate the salt freeze/thaw phenomenon in typical receiver tubes. The purpose of the simple-element freeze/thaw experiments is to quantitatively measure in a controlled setup the permanent deformation inflicted to samples of receiver tubes undergoing freezing and thawing. When nitrate salt changes from the solid to the liquid phase the volume increases, causing an expansion of a given mass of salt. During the expansion process, the tube material can yield resulting in a plastic deformation of the tube material. In these tests, several receiver tubes of various diameters and wall thicknesses filled with nitrate salt undergo several freeze/thaw cycles to measure the deformation of tubes. Preliminary results indicate under the most severe case (freezing the lower half of a tube, then freezing the upper half, followed by thawing the lower part with a stop in the upper half to prevent sliding of the solid salt) the tubes will rupture after 12 cycles.

Ball Valves Test

Ball valves are desirable for use as drain and fill valves because they are relatively compact and in the fully opened position the flow restriction is small relative to other types of valves, such as globe valves. We have pressure cycled a 2 inch Mogas ball valve to assess its functionality and leak rate in a molten salt environment. The valve was closed and pressurized to 60 psi (410 kPa) for five minutes followed by flow for five minutes. After each 50 cycles, the leak rate was measured with the valve in the closed position and pressure on the valve. The amount of salt that leaks by was measured every 0.5 hour. After 300 cycles the leak rate was measured to be approximately 15 grams of salt per half hour.

Transient Freezing Experiments

The correlation for transient freezing in pipes used to calculate penetration depths is based on experiments where the pipe wall is cooled externally to maintain a constant wall temperature. In reality, pipes have a finite heat capacitance. The effects of the pipe heat capacitance on the penetration depths for molten salt penetration depths is an area that could be investigated further.

Impedance Heating System

For long runs of piping, impedance heating could have advantages over mineral insulated (MI) cable. With impedance heating, the pipe wall becomes the heater by passing a low A-C voltage (<80 volts) through it. One lead of the electrical cables is connected to the electrical midpoint of the pipe, and the other is divided in two, with each of these connected to an end of the pipe that is to be heated. The cables run on the outside of the pipe and are easy to access. We plan to test an impedance heating system in our salt loop.

Multiport Valve

A multiport valve allows flow from one line to be distributed to several lines. It has a single actuator to control the valve. A multiport valve could be used in place of several drain and fill valves, thus reducing the complexity associated with controlling and maintaining several valves. Although this valve is not a commercial product, a small company in Colorado (TedCo) has designed such a valve for molten salt applications. This type of valve should be investigated further.

V. References

1. N. E. Bergan, *Testing of the Molten Salt Electric Experiment Solar Central Receiver in an External Configuration*, Sandia National Laboratories, SAND86-8010, October 1986.
2. D. C. Smith and J. M. Chavez, *A Final Report on the Phase I Testing of a Molten Salt Cavity Receiver*, Volume II - The Main Report, Sandia National Laboratories, SAND87-2290, May 1992.
3. C. E. Tyner, *Status of the Direct Absorption Receiver Panel Research Experiment: Salt Flow and Solar Test Requirements and Plans*, Sandia National Laboratories, SAND88-2455, March 1989.
4. F. P. Incopera, D. P. De Witt, *Fundamentals of Heat and Mass Transfer*, second edition, John Wiley & Sons, pp. 181-191, 1985.
5. A. S. Mujumdar, R. A. Mashelkar, *Advances in Transport Processes*, John Wiley & Sons, Vol. III, pp. 35-117, 1984.
6. J. N. Goodier, "Thermal Stress," ASME *J. Appl. Mech.*, Vol. 4, no. 1, March 1937.
7. A. H. Burr, *Mechanical Analysis and Design*, Elsevier Science Publishing Co., Inc., 1982.
8. H. E. Boyer and T. L. Gail, editors, *Metals Handbook Desk Edition*, American Society for Metals, 1985.
9. F. B. Cheung and L. Baker, Jr., "Transient Freezing of Liquids in Tube Flow," *Nuclear Science and Engineering*, Vol. 60, pp. 1-9, 1976.
10. R. H. Dieck, *Measurement Uncertainty Methods and Applications*, Instrument Society of America, 1992.
11. W. C. Young, *Roark's Formulas for Stress and Strain*, sixth edition, McGraw-Hill, pp. 722-724, 1989.
12. E. E. Rush, J. M. Chavez, C. W. Matthews, P. Bator, *An Interim Report on Testing the Molten Salt Pump and Valve Loops*, Sandia National Laboratories, SAND89-2964, April

Appendix A. Finite Element Analysis of Flange Undergoing Thermal Shock

The following is memo written by Scott Rawlinson describing a finite element analysis of an ECON type 6 inch flange undergoing thermal shock at two different initial conditions: 25 and 149°C.

Sandia National Laboratories

Albuquerque, New Mexico 87185-1127

date: July 27, 1994

to: Jim Pacheco, MS-0703
Org. 6216

SC RT R
from: Scott Rawlinson, MS-1127
Org. 6215 5-3137

subject: Finite Element Results for Salt Flange

To ensure the reliability of some aspects of Solar Two, you are concerned about stresses in several critical components, one of which is the flange coupling. As an alternate method of thermal conditioning at night, some of the salt line may be drained and allowed to cool. At startup these lines will be at ambient temperature or they will be preheated to a temperature below the salt freezing point and will undergo a significant thermal shock. The purpose of this memo is to document the finite element analysis (FEA) results on the flanges undergoing thermal shock that will be used in these molten salt loops.

I used the COSMOS/M finite element program to model the pipe flange. This program can be used on a PC and according to a survey done by our analysis group about three years ago, is one of the better FEA programs. The program has been continuously updated and improved since that time. I used the latest version, 1.70. The developers of this code, Structural Research and Analysis Corporation (SRAC), verify its results using numerous test case models.

The system being modeled is two E-CON flanges that are bolted together at 45 degree intervals. A step is machined into each of the mating flanges. A gasket is placed in this notch that is formed from these steps. The model was developed to determine: (1) stresses at steady-state conditions; (2) stresses that would occur if 290 °C salt suddenly flowed through this pipe connection without any heat trace (at ambient temperature); and (3) stresses that would occur if 290 °C salt suddenly flowed through this pipe connection after the flanges are preheated to 149 °C (300 °F). Therefore a transient solution is required for (2) and (3).

The envelope of the FEA model was developed from the sketch you supplied, using data from Reflange. Several iterations of the model were developed. The first model was developed in an older version, 1.65A. Then the newer version arrived, and although it did not contain any changes that should affect this particular model, I developed the model in the newer version. In addition, after knowing what loading would occur, I decided that gap elements should be placed between the flange and the gasket. Otherwise, the gasket would appear to be part of the flange, adding to its strength -- this would not be realistic. Only the results using the gap elements, separating the gasket from the flanges, will be presented.

A summary of the parameters in the FEA model is given below:

- Element type (for flanges and gasket): 4-node planar, "PLANE2D", axisymmetric
- Average element size: 2-mm
- Element type (gap between flange and gasket): 2-node "GAP"
- Force/pressure boundary conditions: 28,300 N at bolt hole location
- Flux/Temperature boundary conditions:
 - Convection along entire length of inner pipe
 - Convection coeff = 550 W/m²-K
 - Bulk fluid temp: 290 °C
- Displacement boundary conditions: Zero displacement in y direction at midpoint of gasket
- Flange material properties (SS316) [1,2]:
 - Modulus of elasticity: 193 GPa
 - Poisson's ratio: 0.3
 - Coefficient of thermal expansion: 17.5×10^{-6} m/m-K
 - Density: 8000 kg/m³
 - Specific Heat at Constant Pressure: 505 J/kg-K
 - Thermal conductivity: 15.6 W/m-K
- Gasket material properties (17-4PH) [3]:
 - Modulus of elasticity: 193 GPa
 - Poisson's ratio: 0.3
 - Coefficient of thermal expansion: 12.1×10^{-6} m/m-K
 - Density: 7832 kg/m³
 - Specific Heat at Constant Pressure: 505 J/kg-K
 - Thermal conductivity: 12.1 W/m-K

Note: Material properties were taken as constant and were calculated at the average between an ambient temperature of 25 °C and the operating temperature of 290 °C.

The boundary conditions stated above require some explanation. Since the pipe flange is modeled axisymmetrically, the proper bolt load must be calculated. COSMOS/M assumes axisymmetric problems are based on one radian. Therefore the proper bolt load is:

$$F = F_b \frac{\# bolts}{2\pi}$$

The force in the bolt was given as 4000-5000 lb. from Bob Lathan at Reflange, Inc.. I used 5000 lb. = 22,242N, or an equivalent load of about 28,300N, using the above equation.

When I first developed the thermal model, I placed 290 °C boundary conditions (salt temperature) along the inside of the pipe. The resultant stresses were extremely high in this region. However, I realized that was not the proper boundary condition. The inside of the pipe will not instantaneously reach 290 °C -- it will reach that temperature much more slowly through the boundary layer. Therefore I re-analyzed the problem using convective boundary conditions.

The correlation I used to determine the convection coefficient is based on turbulent flow in circular tubes and is given as [4]:

$$\bar{h} = .023 \frac{k}{D} Re_D^{4/5} Pr^{0.3}$$

for

$$0.7 \leq Pr \leq 160$$

$$Re_D \geq 10,000$$

$$L/D \geq 60$$

where k = thermal conductivity

D = pipe diameter

L = pipe length

Re_D = Reynolds number

Pr = Prandtl number

Using your stated flowrate of 100 gpm and using the properties of salt at 290 °C from [5], I calculated a convection coefficient of $552 \text{ W/m}^2\text{-K} \cong 550 \text{ W/m}^2\text{-K}$ (the above assumptions were met). This number is very close to your calculated value based on experimental results from the smaller pipe flange at time ≥ 90 seconds.

Since the problem is transient in nature, a timestep is needed. The critical timestep is calculated as (information supplied by SRAC):

$$\Delta t_{cr} \leq \frac{2}{1-2\theta} \frac{\Delta x^2 \rho c_p}{k}$$

where Δx = smallest mesh size

ρ = density

c_p = specific heat at constant pressure

θ = stability parameter

Using the values of material properties and stability factor to give the smallest possible stable timestep, I calculated a critical timestep of 0.86 seconds. I used a 0.5 second timestep in the analysis.

My assumptions in the analysis were as follows:

- (1) Constant material properties (linear problem)
- (2) Constant convection coefficient
- (3) No external thermal losses (insulated)
- (4) Bolt load does not change with time or temperature
- (5) No friction at gasket/flange interface (it will become apparent later that this value is irrelevant)
- (6) Flowrate = 100 gpm

Steady-State Results (Ambient Temperature):

The results of the steady-state analysis for 25 °C are shown in Figures 1a through 1d. All stresses discussed below are Von-Mises stresses, a common stress criterion used to predict failure. Figure 1a illustrates the model's element mesh, force, and displacement boundary conditions. Two areas, regions A and B are also illustrated -- these will be referred to later. Figures 1b and 1c are exaggerated displacement plots. The pipe flanges tend to be clamped together due to the bolt loads. This plot appears to show that the gasket is separating from the lower pipe flange. However, remember that this is an exaggerated plot on a scale on the order of several hundred. I was concerned that the apparent non-symmetry indicated a problem, so I consulted personnel at SRAC -- they said that sometimes this happens in a deformed plot when the displacements are very small, resulting in a very distorted plot with the huge scale factor. This is what happened in this case. In fact, he checked the entire model and found no problems. Figure 1d is a Von-Mises stress plot of the center of the bolted connection. The maximum stress is 175 MPa, and occurs where the two flange bodies contact due to the bolt forces (region A). This stress is well below the yield point of SS316 at ambient temperature.

Transient Results for No Preheat:

Next, the convective boundary condition was applied along the inside of the pipe wall. Since the temperature distribution changes with time, the resultant stresses will also change. I examined the results at $t = 0.5, 1, 5, 10, 20, 30, 60, 120, 180$, and 240 seconds. To observe how the stress patterns develop with time, I included the results at $t = 0.5, 5, 10, 30, 60, 120$, and 240 seconds in Figures 2 through 8.

The maximum stress occurs at the same location as the steady-state results, but is higher due to the additive effect of the temperature or convective boundary conditions. Because the pipe is being heated from the inside of the pipe, this inner region expands faster than the outer region, which tends to compress the contact line even greater than with only bolt loads.

The following table summarizes the stresses in the two areas of concern:

Table I - FEA Results for Case Without Preheat

Time (seconds)	Von-Mises Stress, Region A (MPa)	Corresponding Temperature, Region A (°C)	Yield Strength, Region A (MPa)	Von-Mises Stress, Region B (MPa)	Corresponding Temperature, Region B (°C)	Yield Strength, Region B (MPa)
0.0	175	25	240	35	25	240
0.5	180	25	240	90	37	240
1.0	171	25	240	90	44	240
5.0	178	25	240	142	69	240
10.0	214	25	240	172	81	240
20.0	279	25	240	196	98	240
30.0	341	25	240	239	107	240
60.0	527	25	240	265	128	240
120.0	537	50	240	323	161	240
180.0	542	58	240	325	178	240
240.0	547	67	240	328	187	240

These results at the contact point (region A) indicate that the yield strength is easily exceeded. However, I asked if this was actually chamfered at this point. It turns out that it is, which would eliminate this high stress point. More of a concern is the stresses along the inner pipe adjacent to the gasket. For times > 30 seconds, stresses exceed the yield point in this region (the yield point is constant from 25-200 °C). Based on this, it is apparent that local yielding may occur if you thermally shock this bolted connection.

Notice that maximum stresses are nearly level at 240 seconds. As the temperature distribution evens out, the stresses will decrease and eventually return to the stresses with bolt loading only (since the expansion will be equal throughout the flange assembly). Therefore, the stresses at $t=240$ seconds are about as high as can be expected.

Finally, I looked at any gap that may occur between the flange and gasket surfaces. There is a slight gap at $t=240$ seconds but is nearly undetectable -- less than ≤ 0.1 -mm. Because of the effect of the bolt force and thermal loading, the gasket is never compressed. Any stresses in the gasket are only due to the thermal gradient. Because the gasket is never constrained, the coefficient of friction used is not relevant.

Transient Results with Preheat:

I re-ran the model assuming the entire flange was preheated to a uniform temperature of 149 °C (300 °F). I examined the results at $t = 0.5, 30, 60, 120, 180$, and 240 seconds. The results are displayed in Figures 9 through 14. The following table summarizes the Von-Mises stresses in regions A and B.

Table I - FEA Results for Case Without Preheat to 149 °C

Time (seconds)	Von-Mises Stress, Region A (MPa)	Corresponding Temperature, Region A (°C)	Yield Strength, Region A (MPa)	Von-Mises Stress, Region B (MPa)	Corresponding Temperature, Region B (°C)	Yield Strength, Region B (MPa)
0.5	177	150	240	18	150	240
30.0	266	150	240	133	193	240
60.0	361	150	240	145	204	240
120.0	454	162	240	182	221	≥ 240
180.0	495	170	240	198	230	≥ 240
240.0	504	180	240	202	235	≥ 240

As with the case with no preheat, the highest stresses occurred at the point of contact between the two flange bodies. Again, this point was ignored because there is actually a chamfer at this location. The other area of concern, region B, has much more acceptable stresses. A maximum Von-Mises stress of 202 MPa occurs at $t=240$ seconds. The corresponding temperature at that point and time is approximately 235 °C. The yield strength of SS316 at this temperature point is nearly 240 MPa, therefore the stress level is acceptable. Note that as with the case with no preheat, the stresses have very nearly peaked and would begin to decrease with time to the levels of that in the steady-state condition.

Conclusions:

Based on these results of this model, it appears that local yielding may occur (without preheat) along the inner pipe adjacent to the gasket. It is possible that a full 3-D model may indicate otherwise, but it is not likely since the region in question is far from the bolts. Therefore, it is not recommended that this flange connection be thermally shocked from ambient conditions. However if heat trace is used to preheat the flanges to 149 °C (300 °F), the stresses would remain below the yield point of the material..

References:

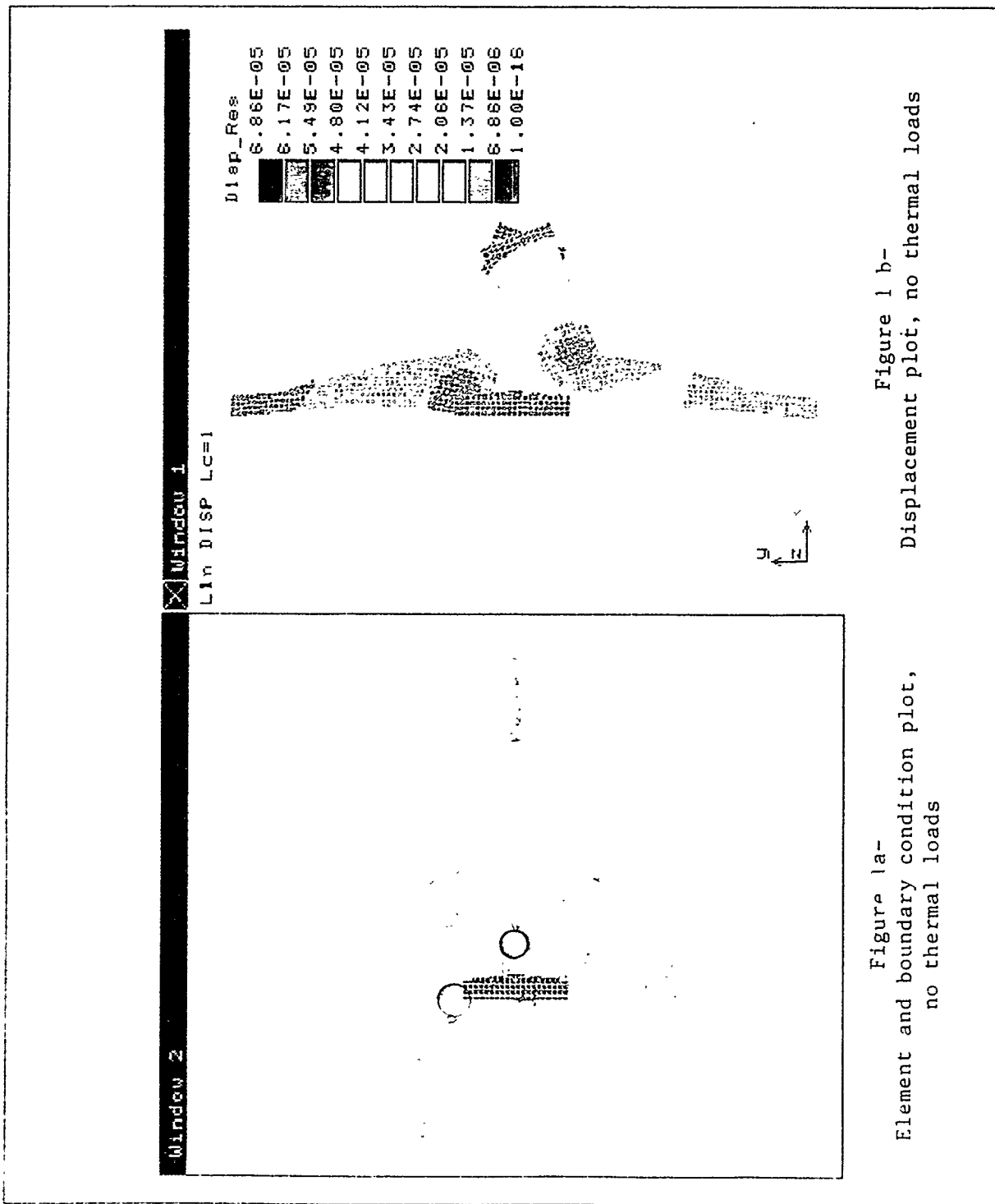
1. American Society for Metals, Engineering Properties of Steel, pp. 292-296, ASM, 1982.
2. Incropera, F. P., and DeWitt, D.P., Fundamentals of Heat Transfer, p765, Wiley, New York, 1981.
3. Kattus, J.R., Aerospace Structural Metals Handbook, code 1501, March, 1978.
4. Incropera, F. P., and DeWitt, D.P., Fundamentals of Heat Transfer, p406-407, Wiley, New York, 1981.
5. Smith, David C., Chavez, James M., Final Report on Phase I Testing of a Molten Salt Cavity Receiver, Vol II - The Main Report, Table 2-II, p 2-4, SAND 87-2290, May 1992.

Attachments with all copies: Figures 1 through 14

Copy to:

Chuck Lopez, SCE
Bill Gould, Bechtel
Alex Zavoico, Bechtel
Dick Holl, Jenna Baskets
Bob Lathan, Reflange
Mark Marko, Rockwell
Tom Tracey, Ted Co.

MS-0703 Jim Chavez, 6216
MS-0703 Craig Tyner, 6216
MS-0703 Greg Kolb, 6216
MS-0704 Paul Klimas, 6201
MS-1127 Chris Cameron, 6215
MS-1127 Scott Rawlinson, 6215 (2)
File K.3, 6215



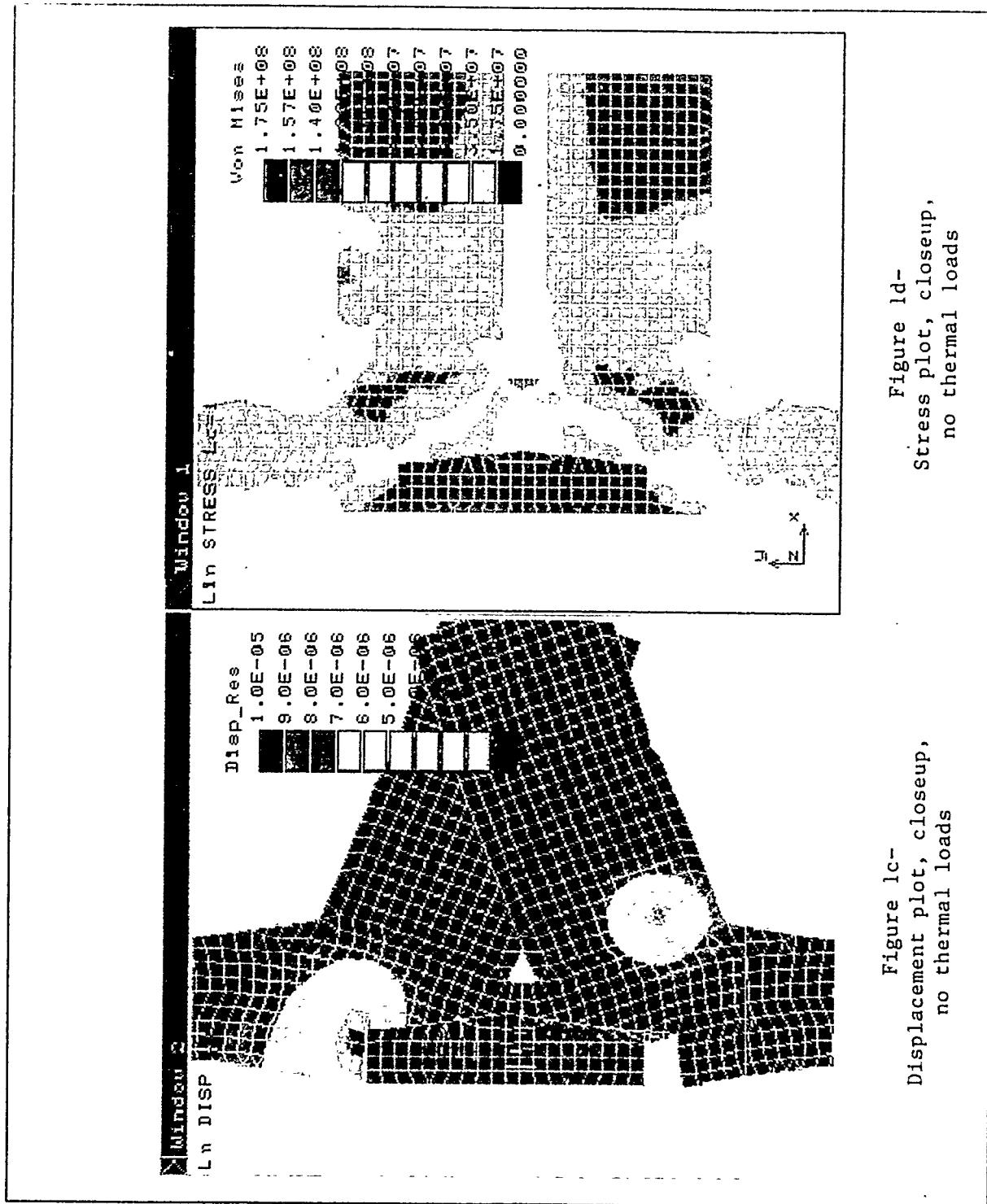


Figure 1c-
Displacement plot, closeup,
no thermal loads

Figure 1d-
Stress plot, closeup,
no thermal loads

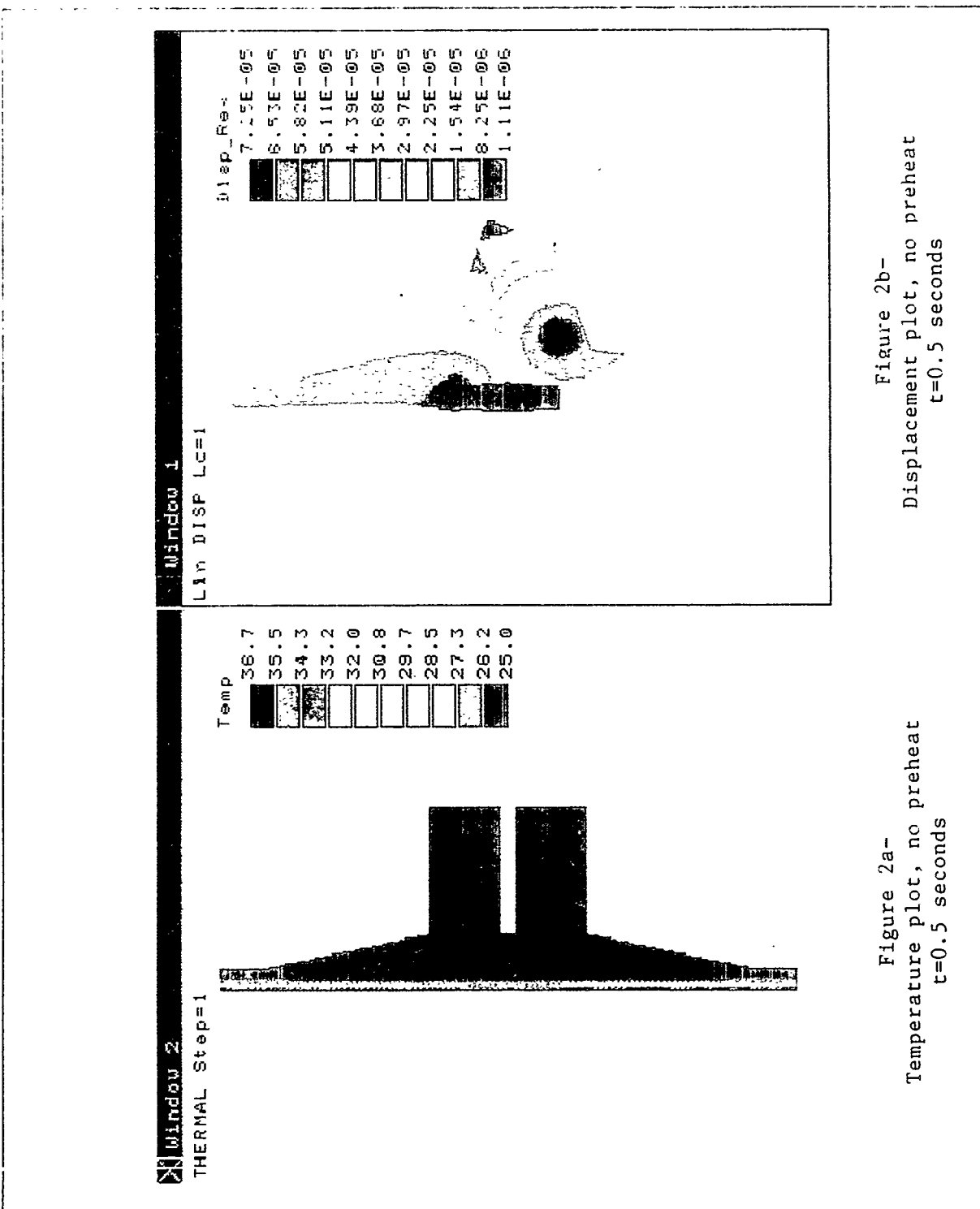


Figure 2a-
Temperature plot, no preheat
 $t=0.5$ seconds

Figure 2b-
Displacement plot, no preheat
 $t=0.5$ seconds

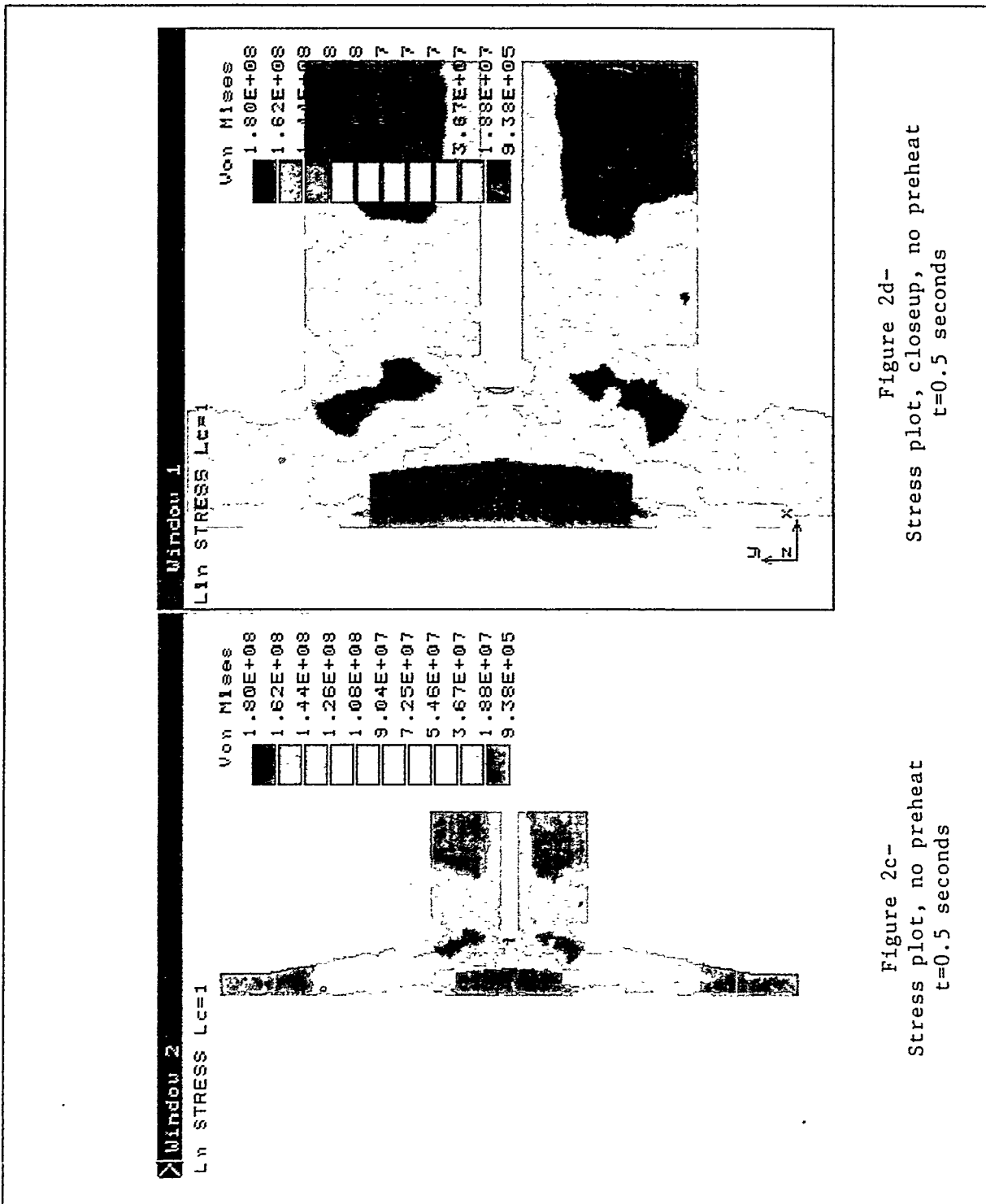


Figure 2c-
Stress plot, no preheat
 $t=0.5$ seconds

Figure 2d-
Stress plot, closeup, no preheat
 $t=0.5$ seconds

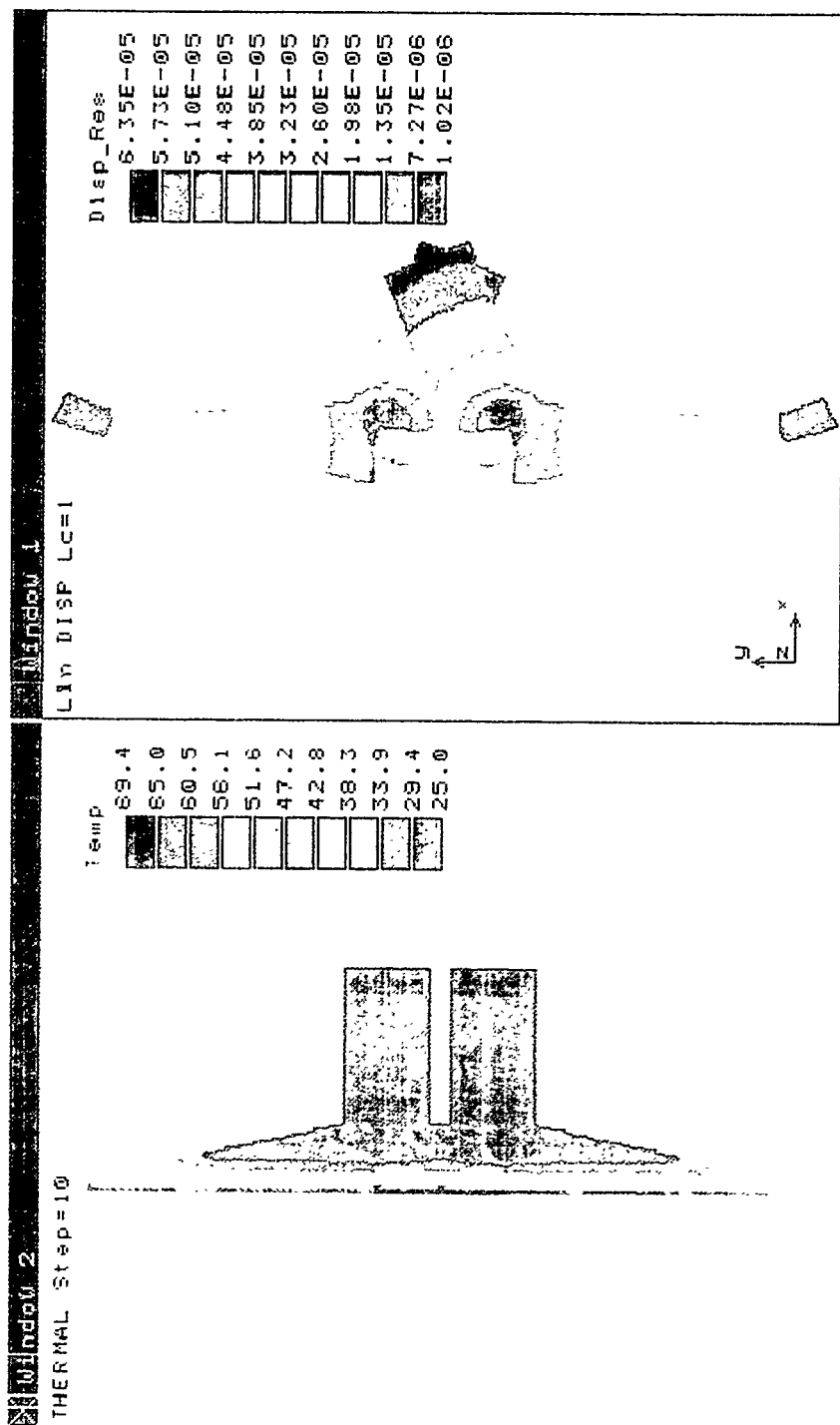


Figure 3a-
Temperature plot, no preheat
 $t=5$ seconds

Figure 3b-
Displacement plot, no preheat
 $t=5$ seconds

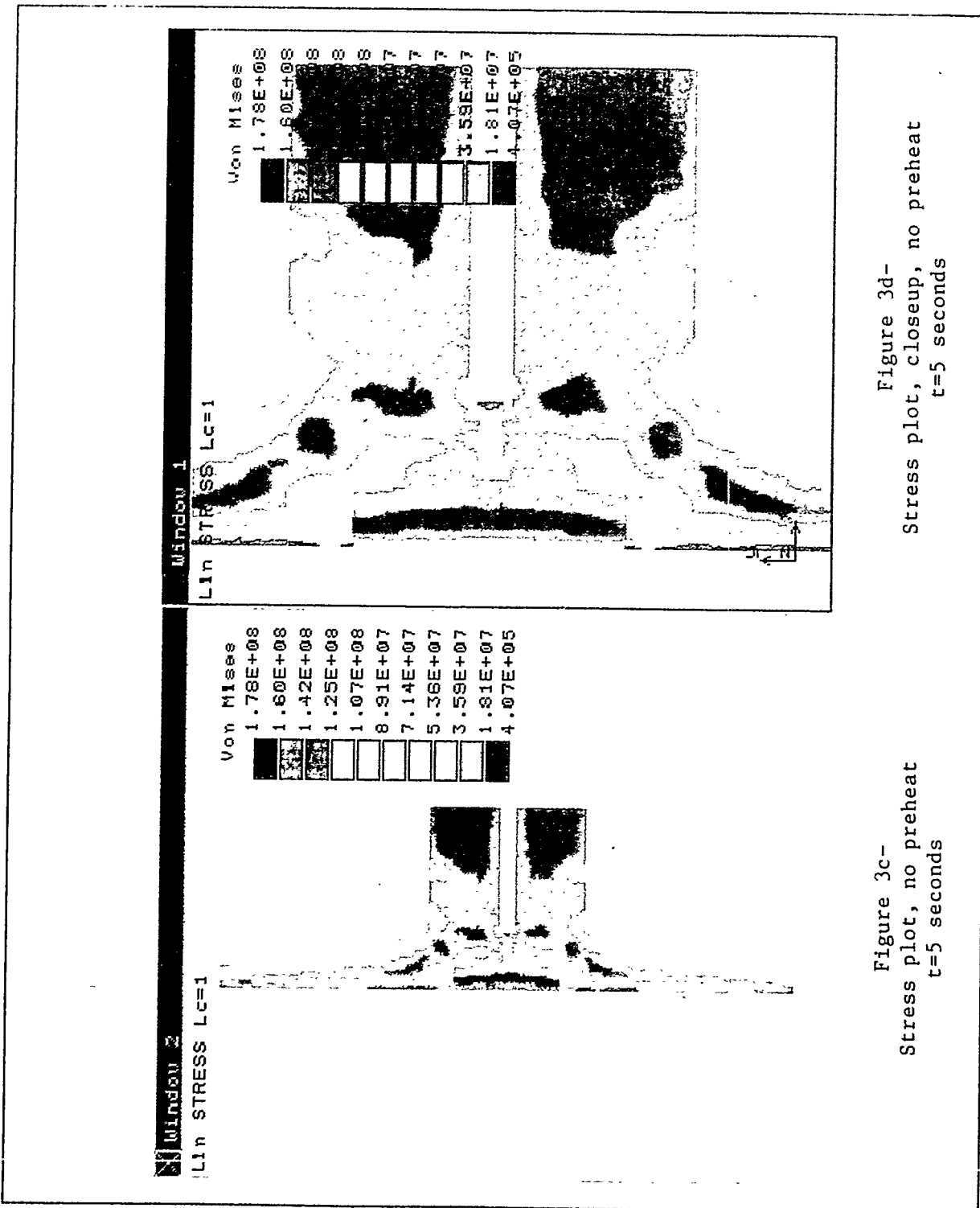


Figure 3c-
Stress plot, no preheat
 $t=5$ seconds

Figure 3d-
Stress plot, closeup, no preheat
 $t=5$ seconds

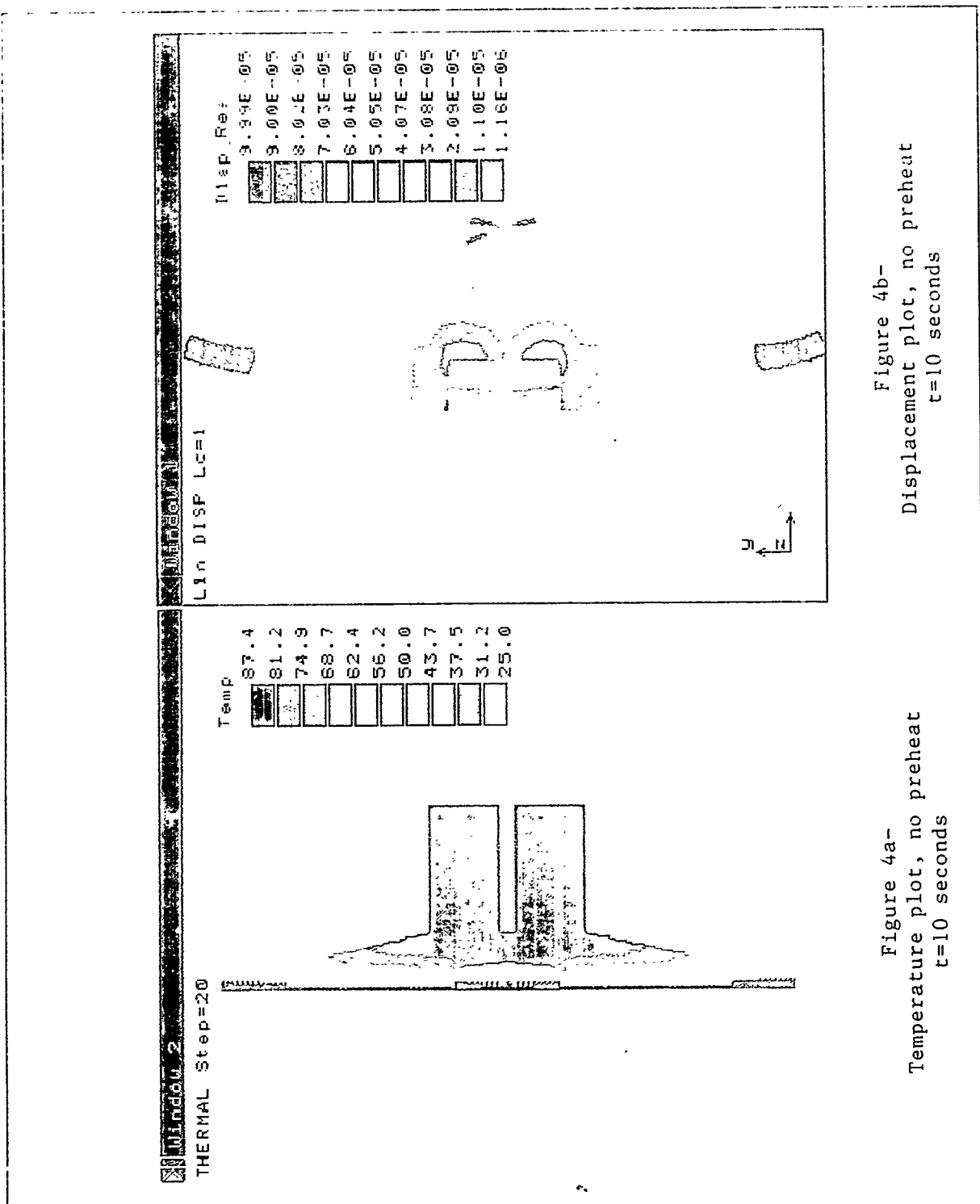


Figure 4a-
Temperature plot, no preheat
 $t=10$ seconds

Figure 4b-
Displacement plot, no preheat
 $t=10$ seconds

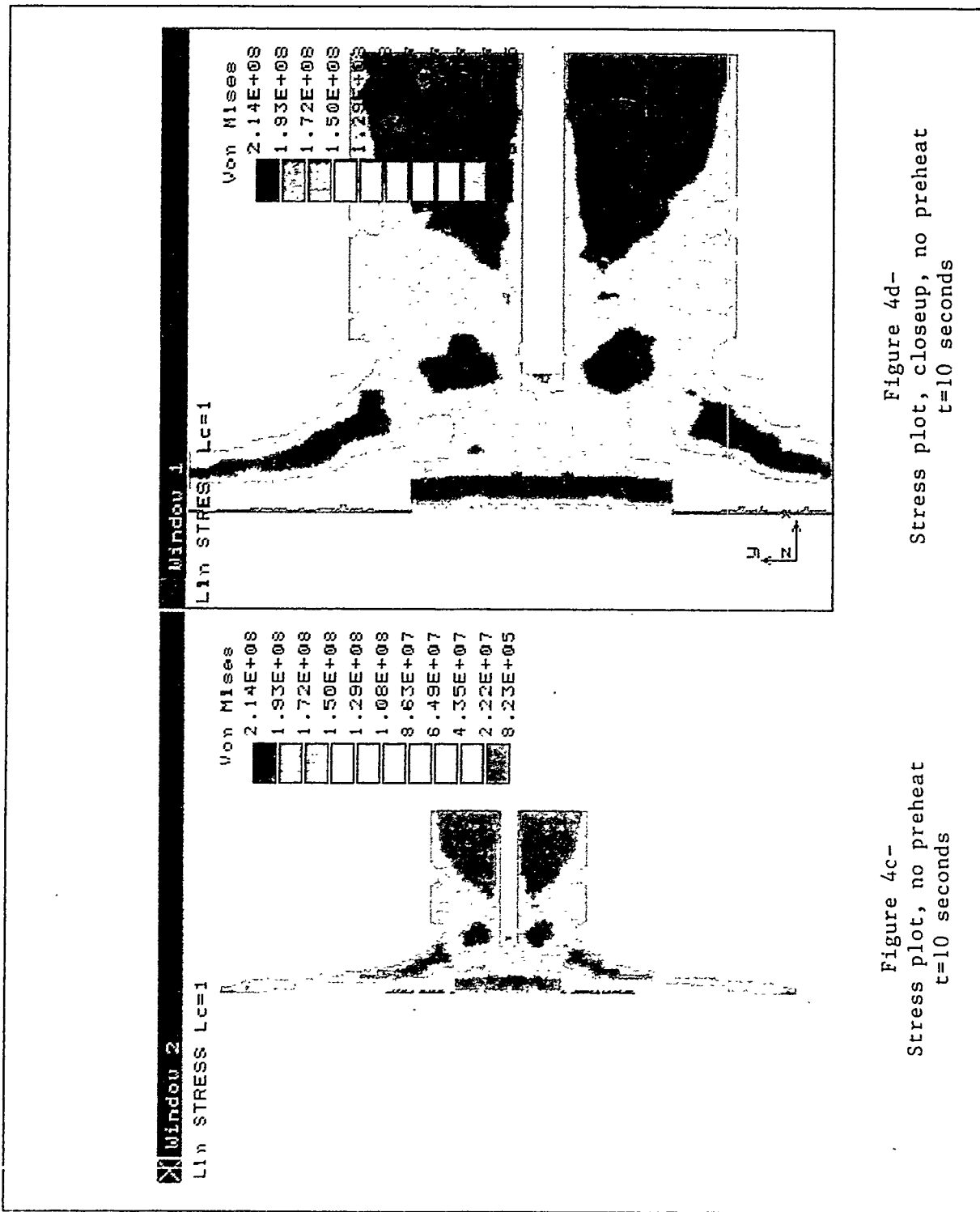


Figure 4c-
Stress Plot, no preheat
 $t=10$ seconds

Figure 4d-
Stress plot, cleanup, no preheat
 $t=10$ seconds

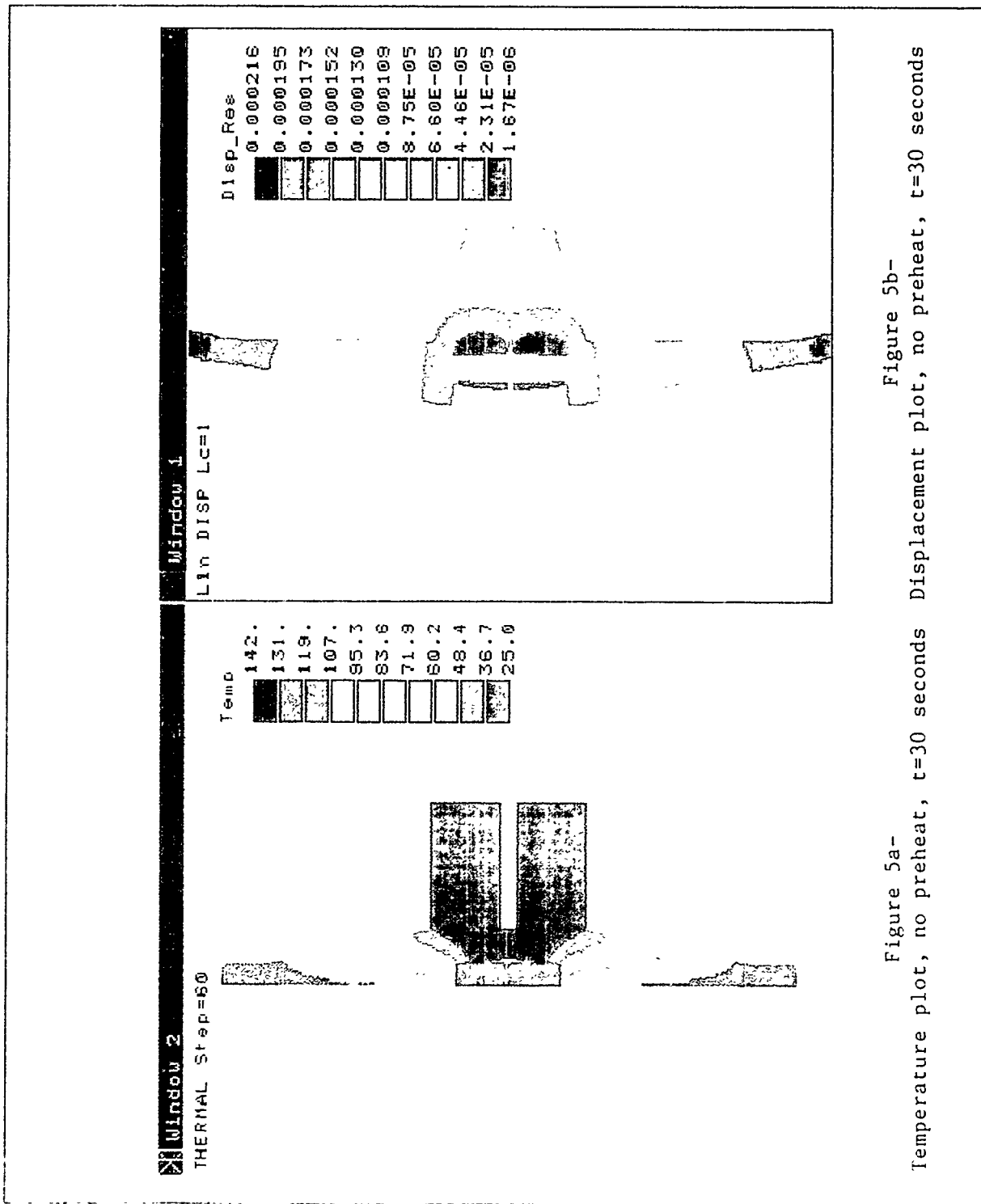


Figure 5a-
Temperature plot, no preheat, $t=30$ seconds
Figure 5b-
Displacement plot, no preheat, $t=30$ seconds

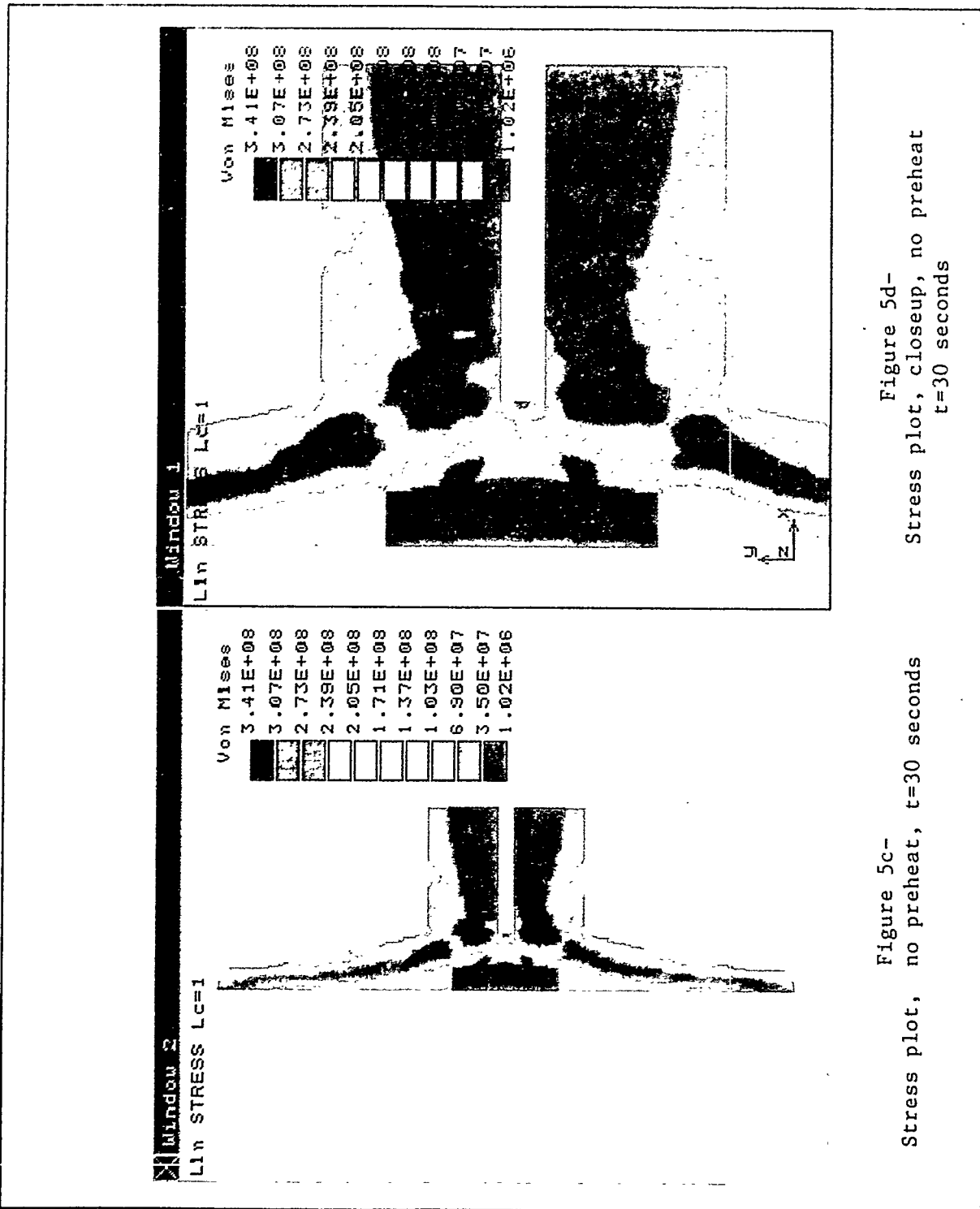


Figure 5c-
Stress plot, no preheat, $t=30$ seconds

Figure 5d-
Stress plot, closeup, no preheat
 $t=30$ seconds

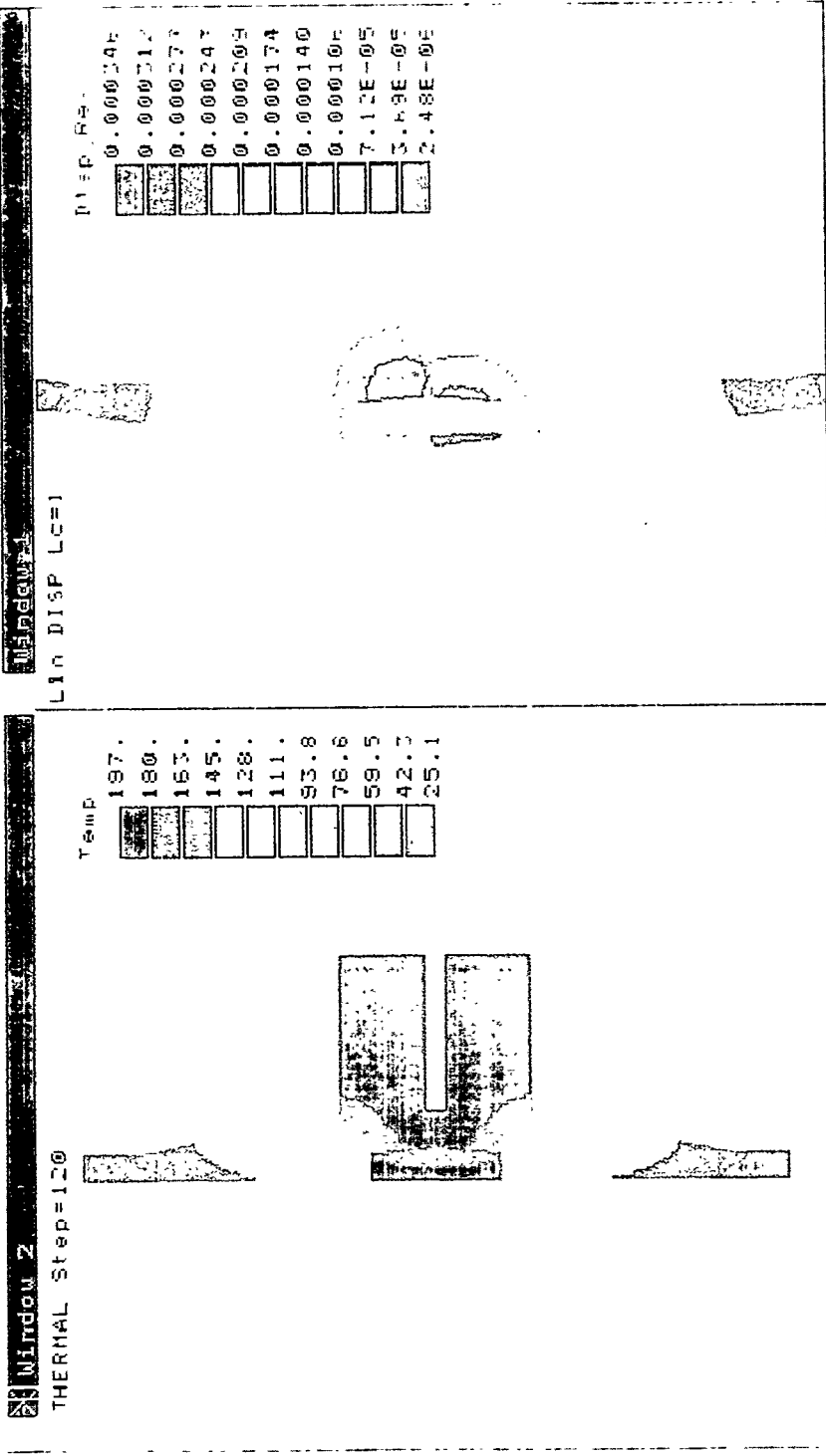
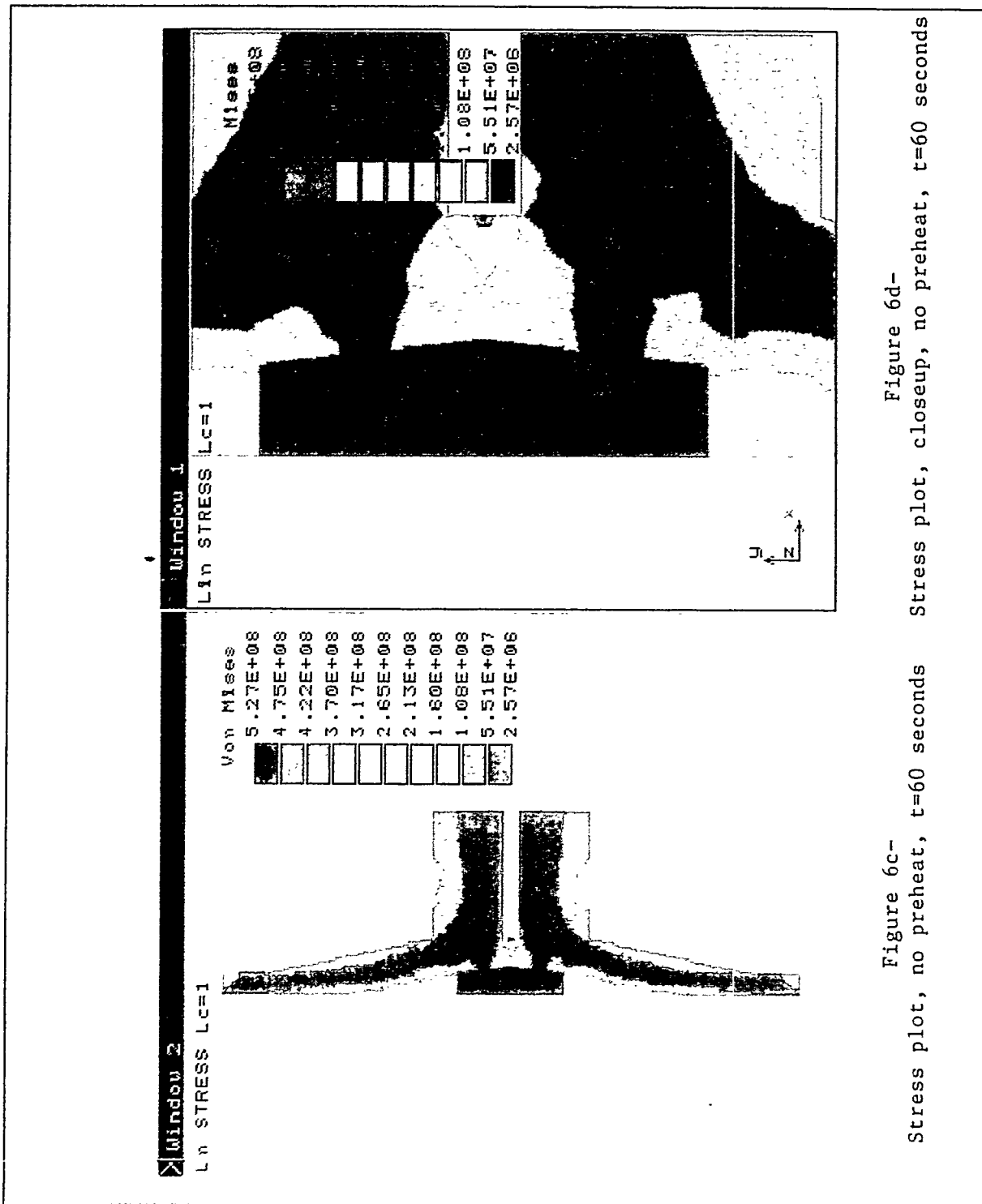


Figure 6a-
Temperature plot, no preheat
 $t=60$ seconds

Figure 6b-
Displacement plot, no preheat
 $t=60$ seconds



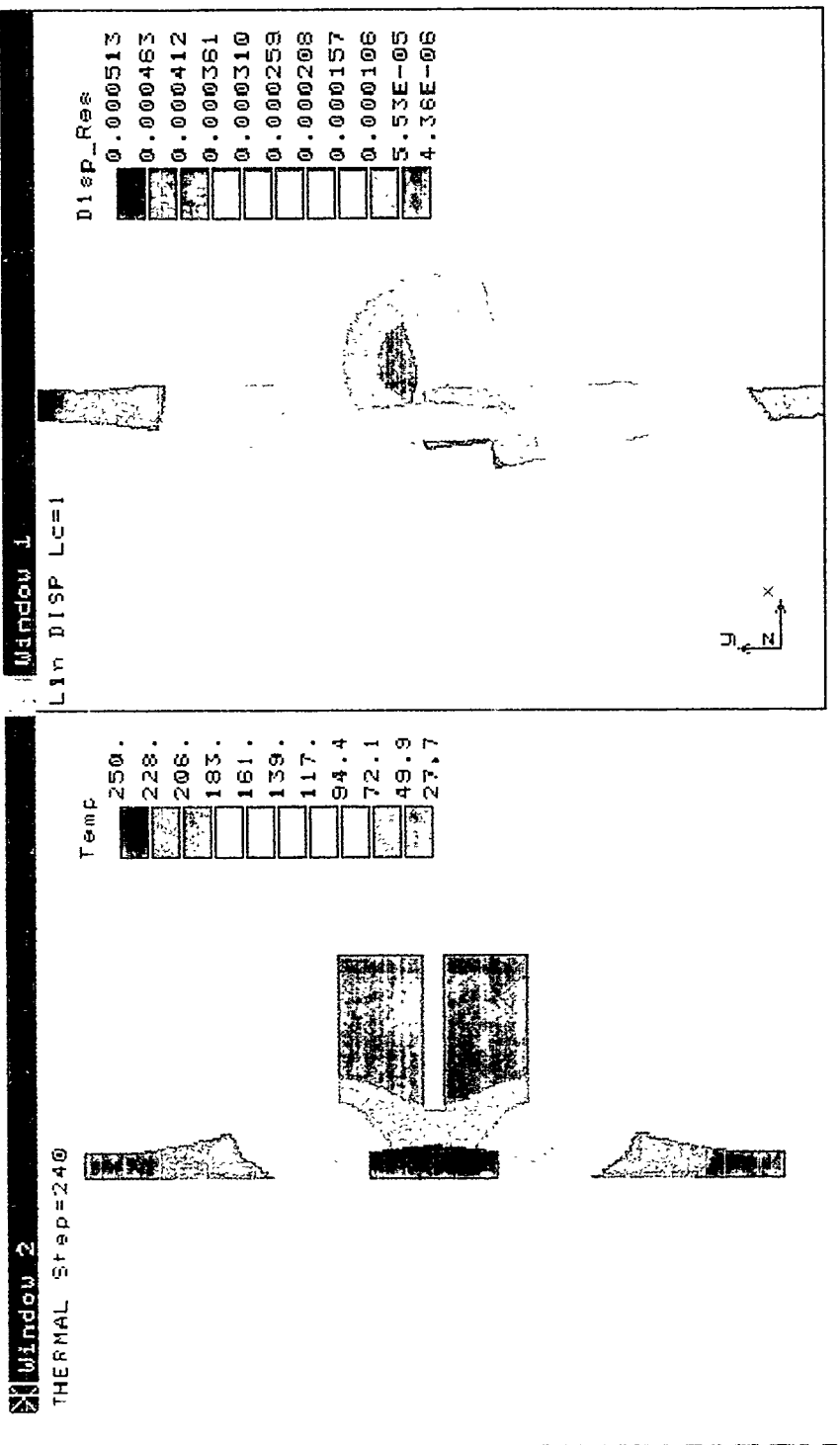
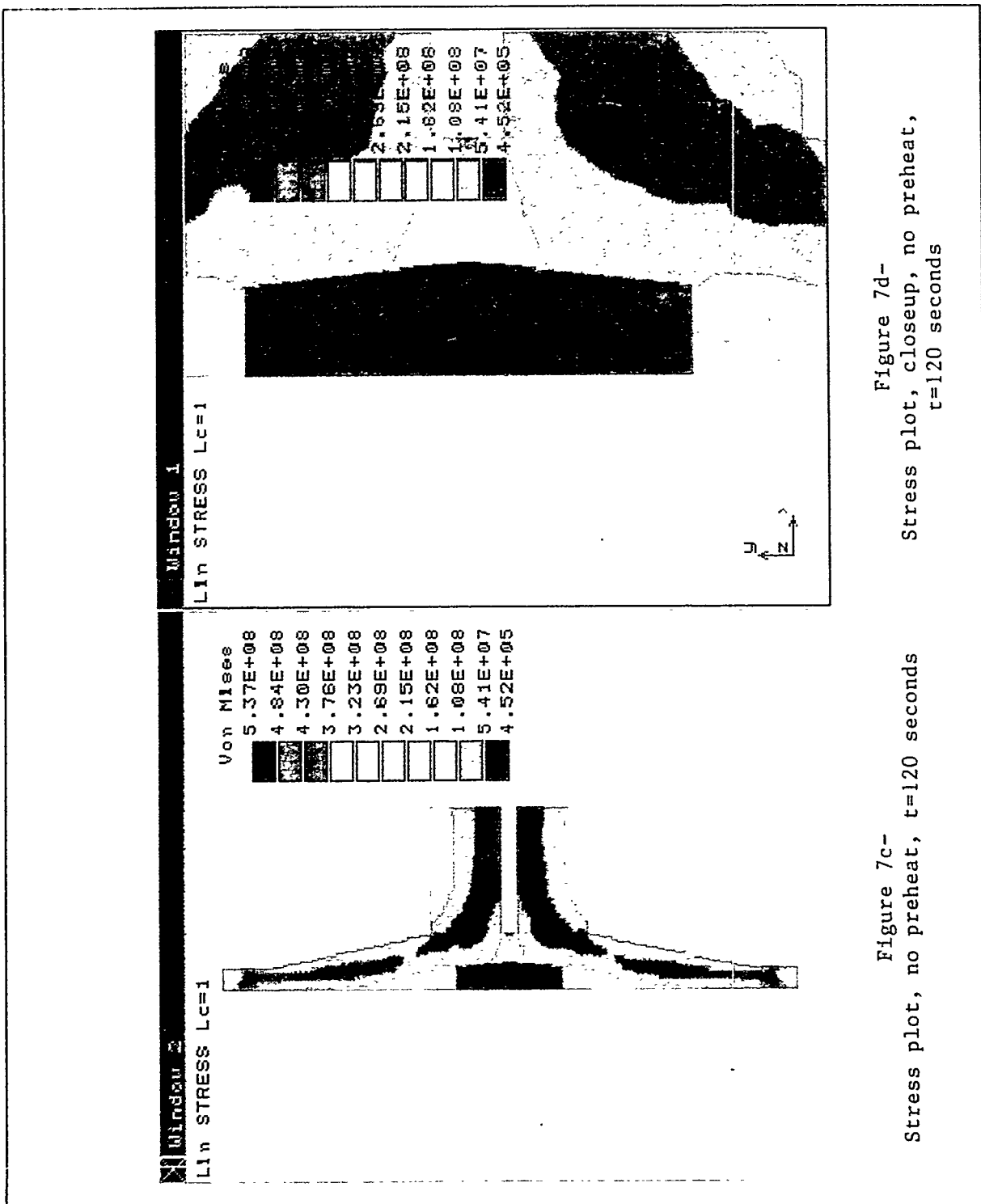
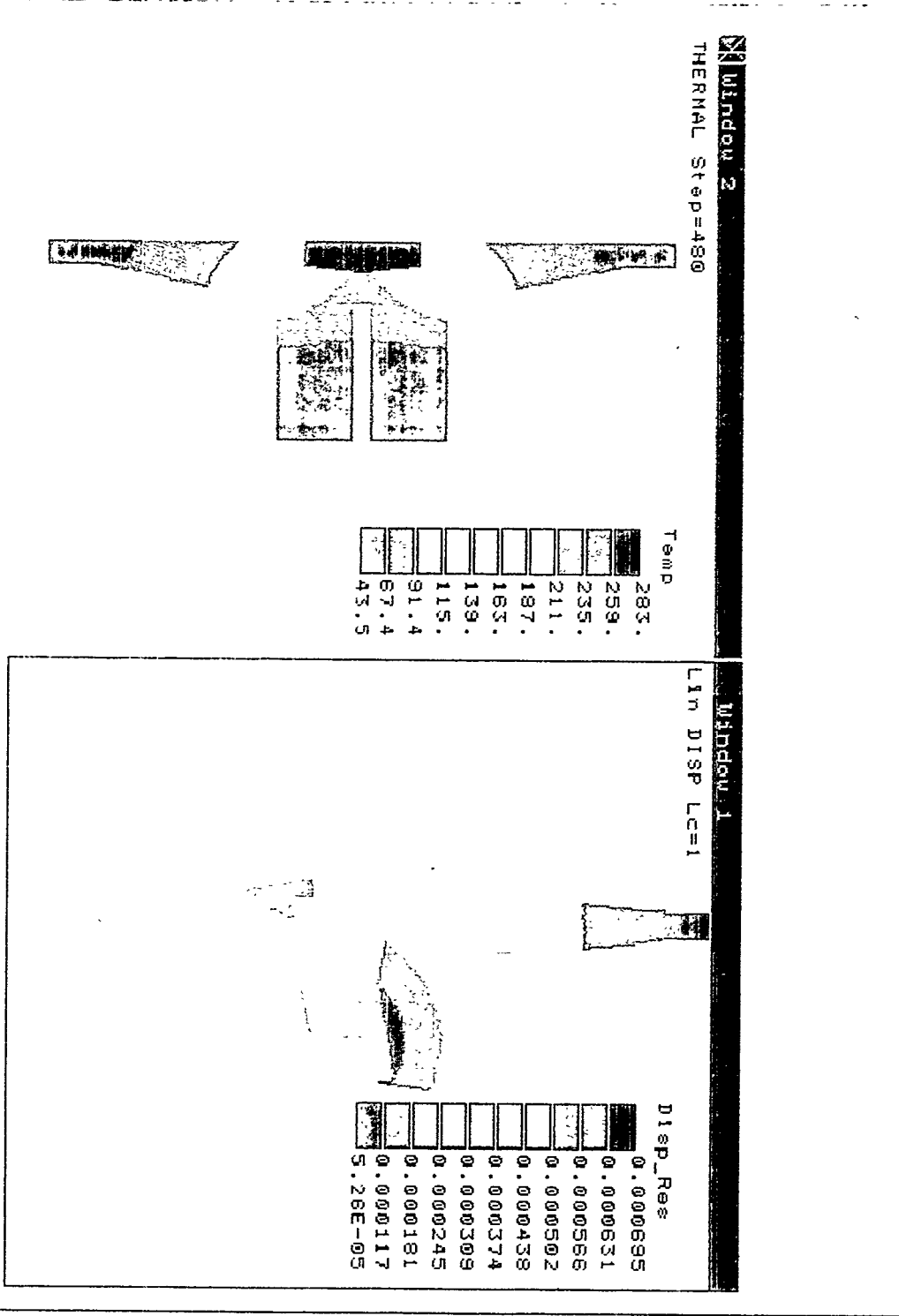
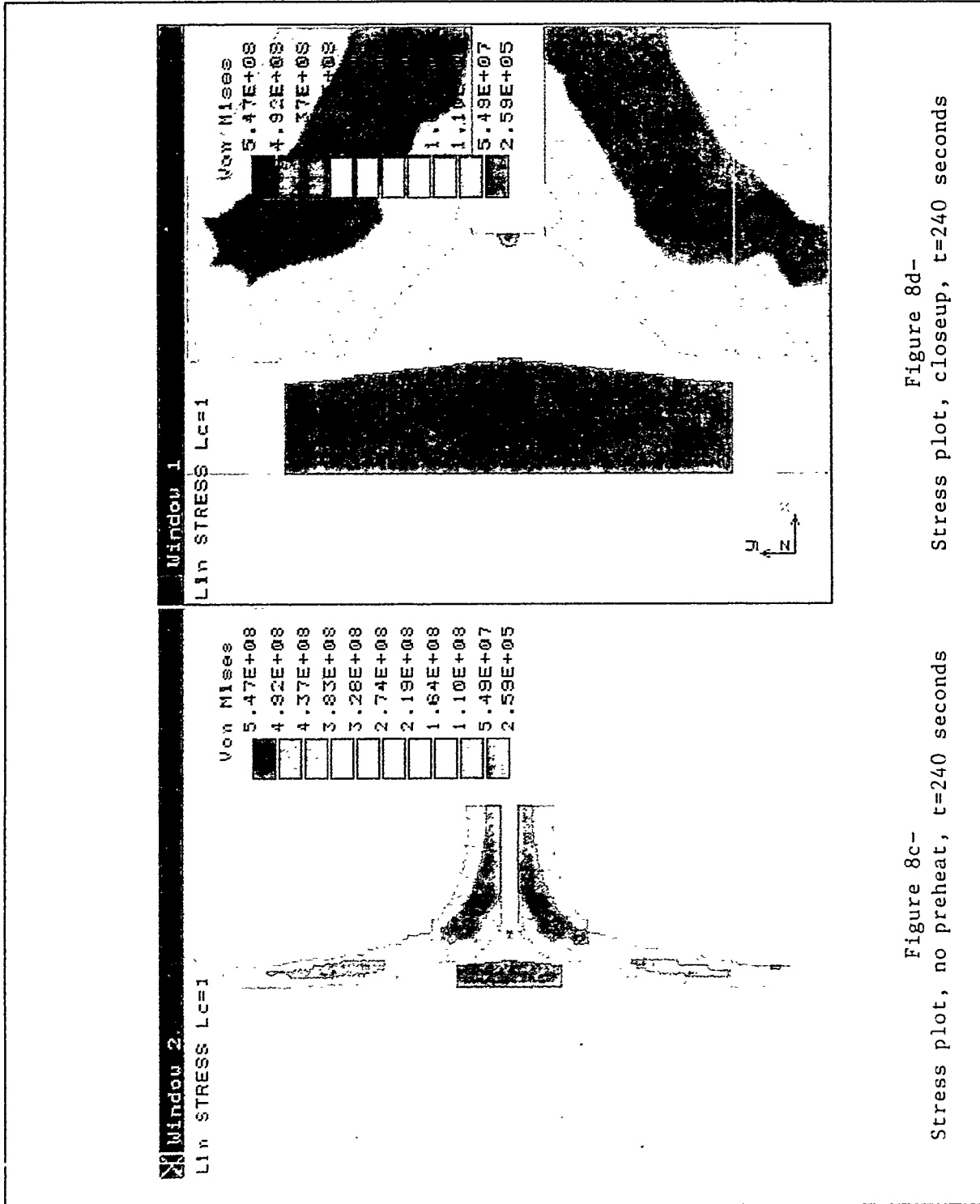


Figure 7a-
Temperature plot, no preheat, $t = 120$ seconds

Figure 7b-
Displacement plot, no preheat
 $t = 120$ seconds







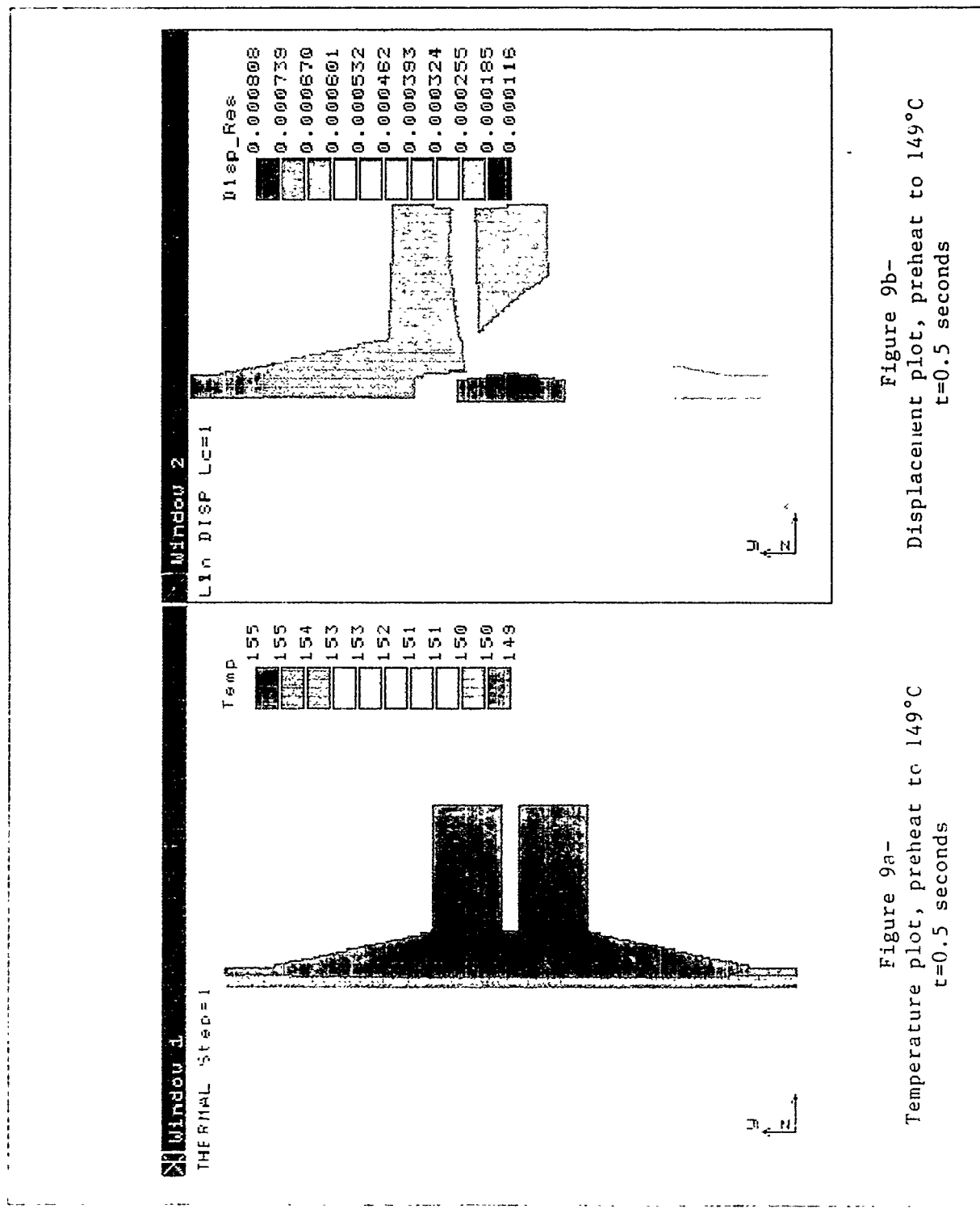


Figure 9a-
Temperature plot, preheat to 149°C
 $t=0.5$ seconds

Figure 9b-
Displacement plot, preheat to 149°C
 $t=0.5$ seconds

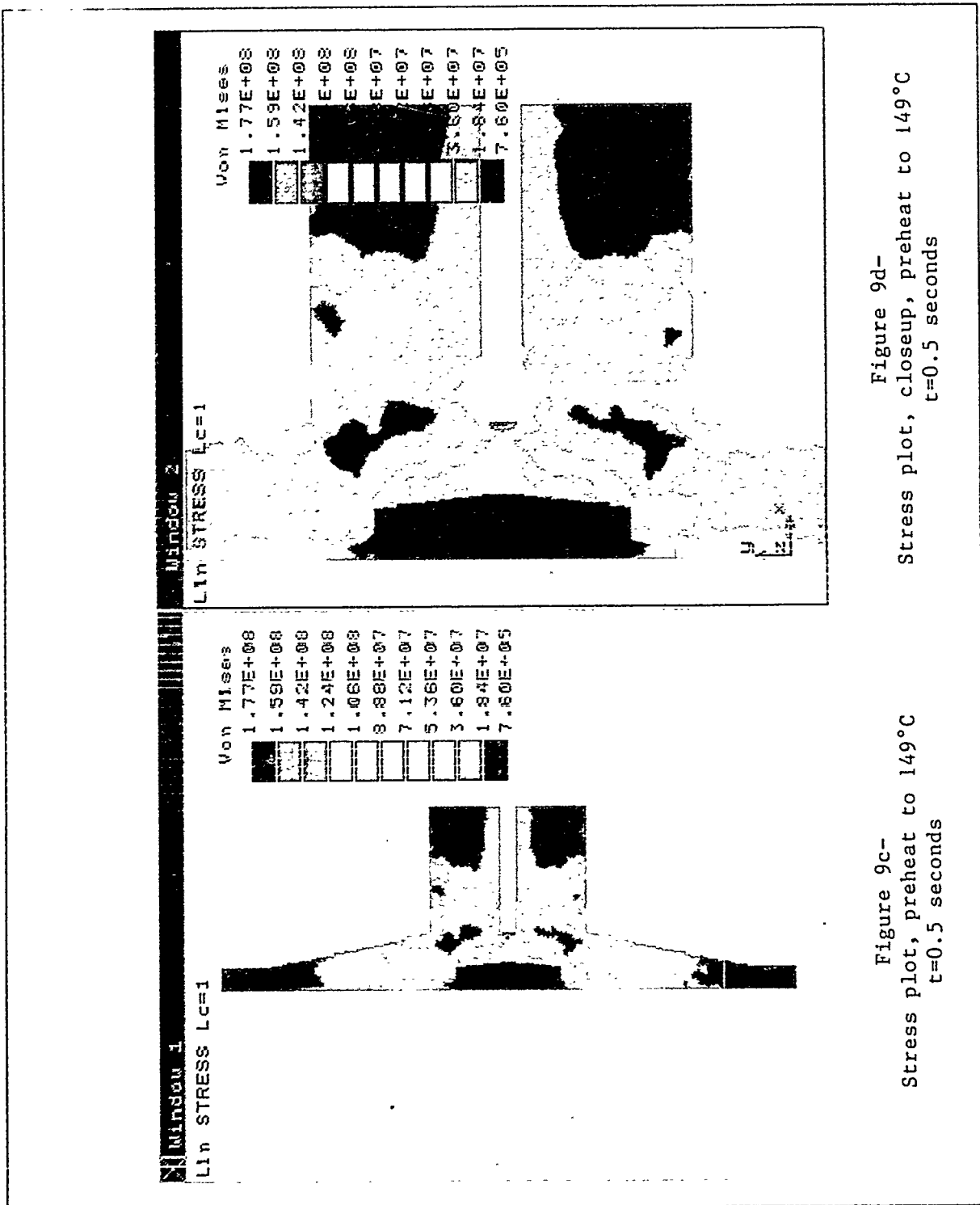
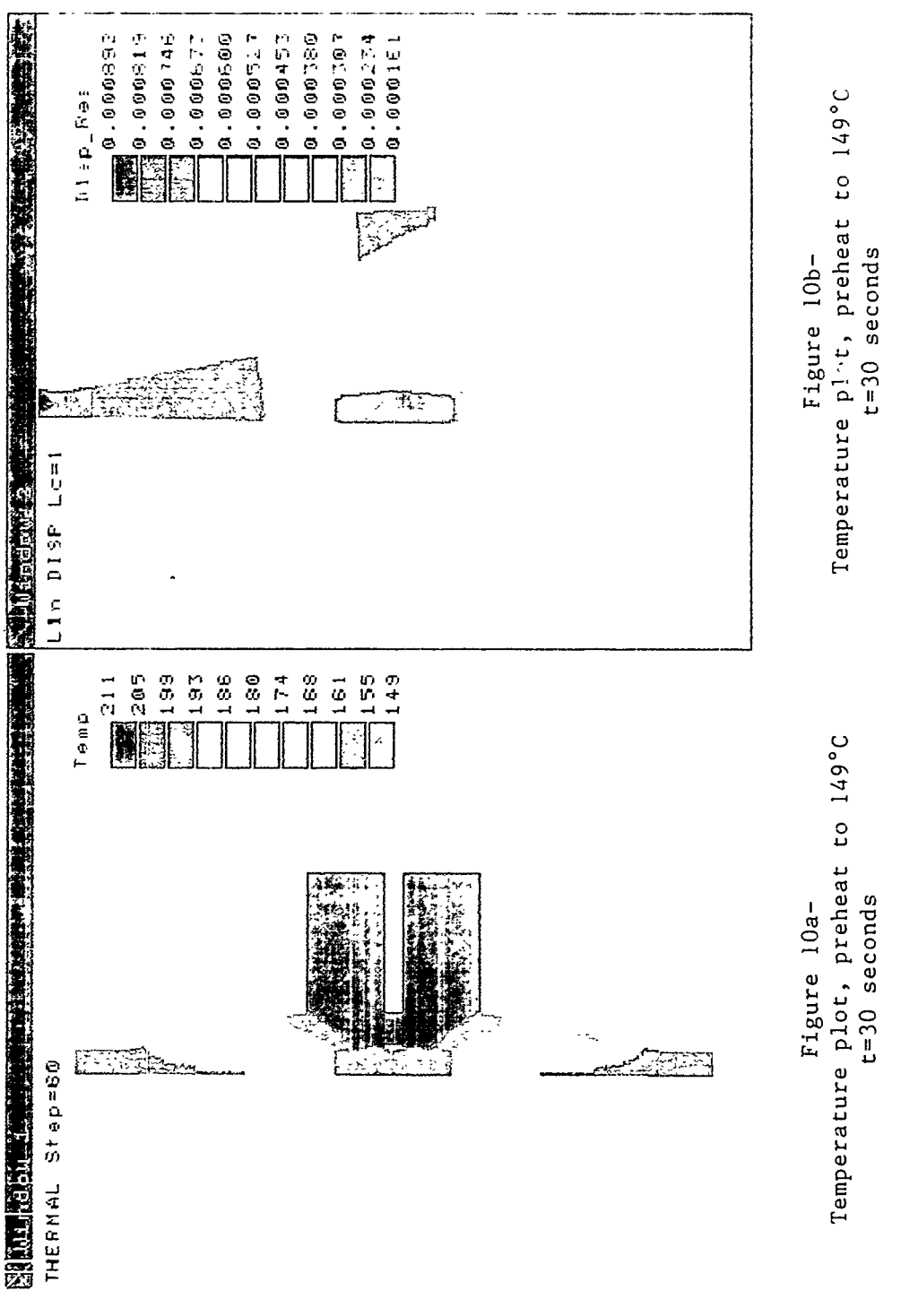


Figure 9c-
Stress plot, preheat to 149°C
 $t=0.5$ seconds

Figure 9d-
Stress plot, closeup, preheat to 149°C
 $t=0.5$ seconds



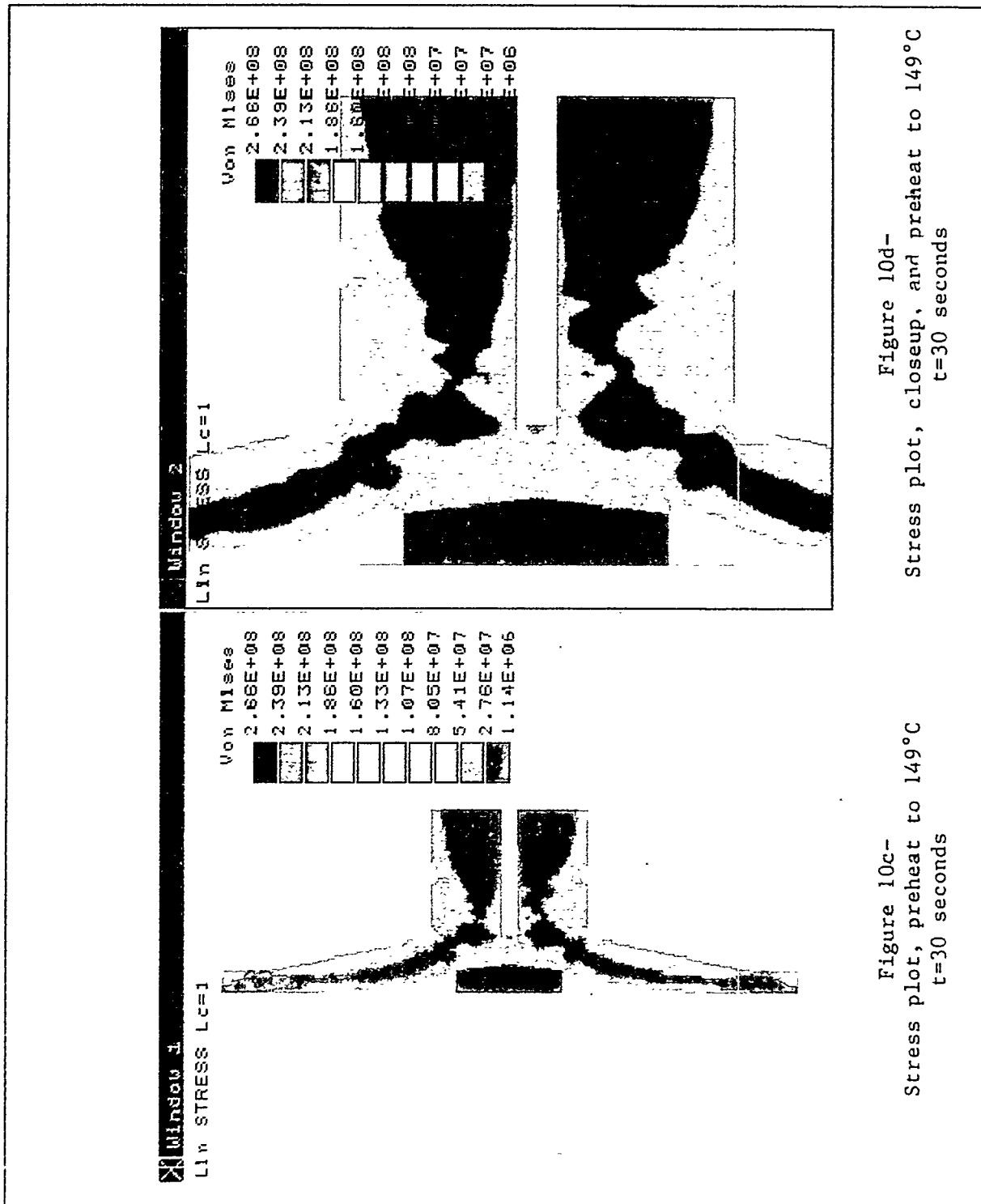


Figure 10c-
Stress plot, preheat to 149°C
t=30 seconds

Figure 10d-
Stress plot, closeup, and preheat to 149°C
t=30 seconds

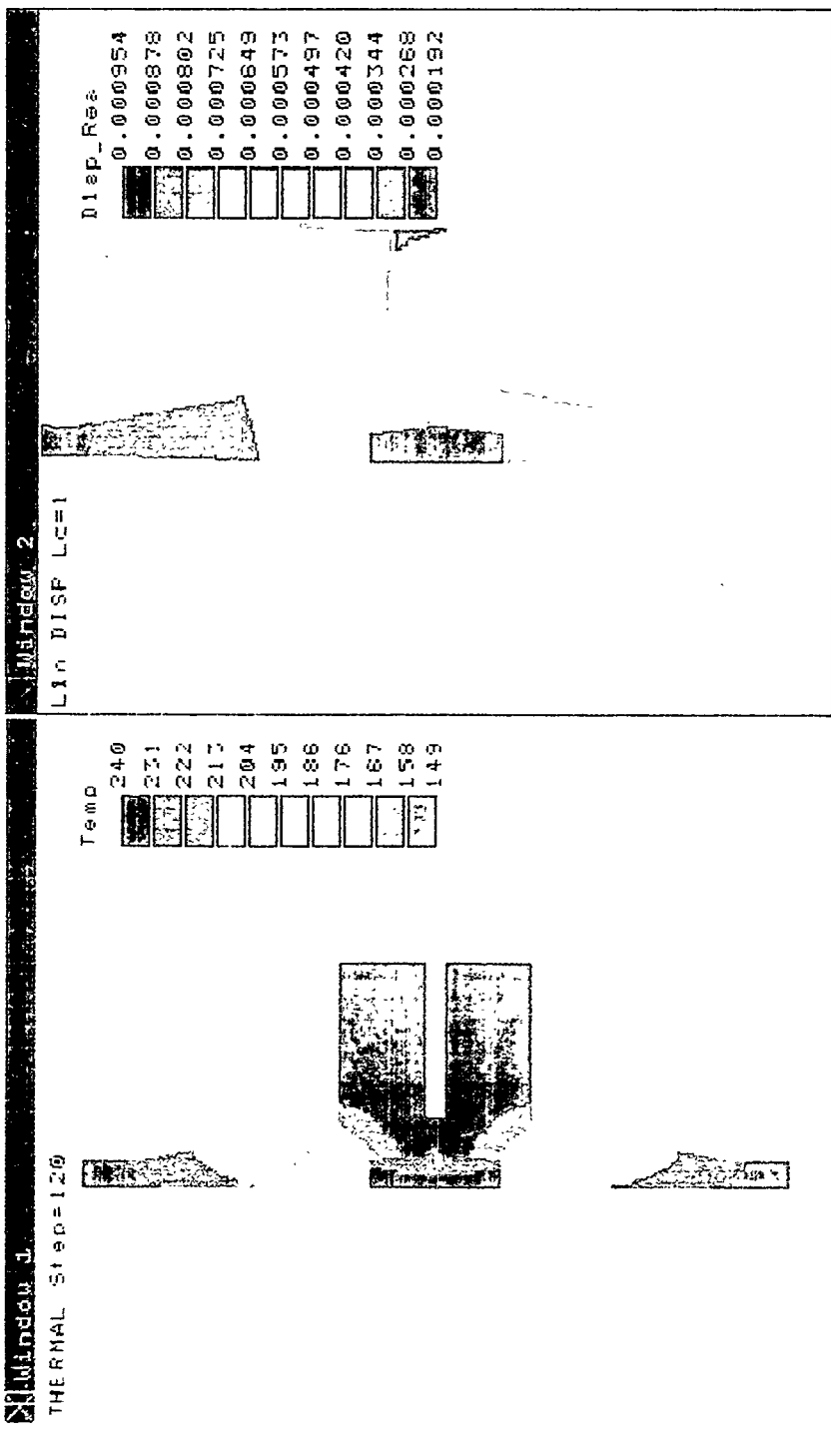
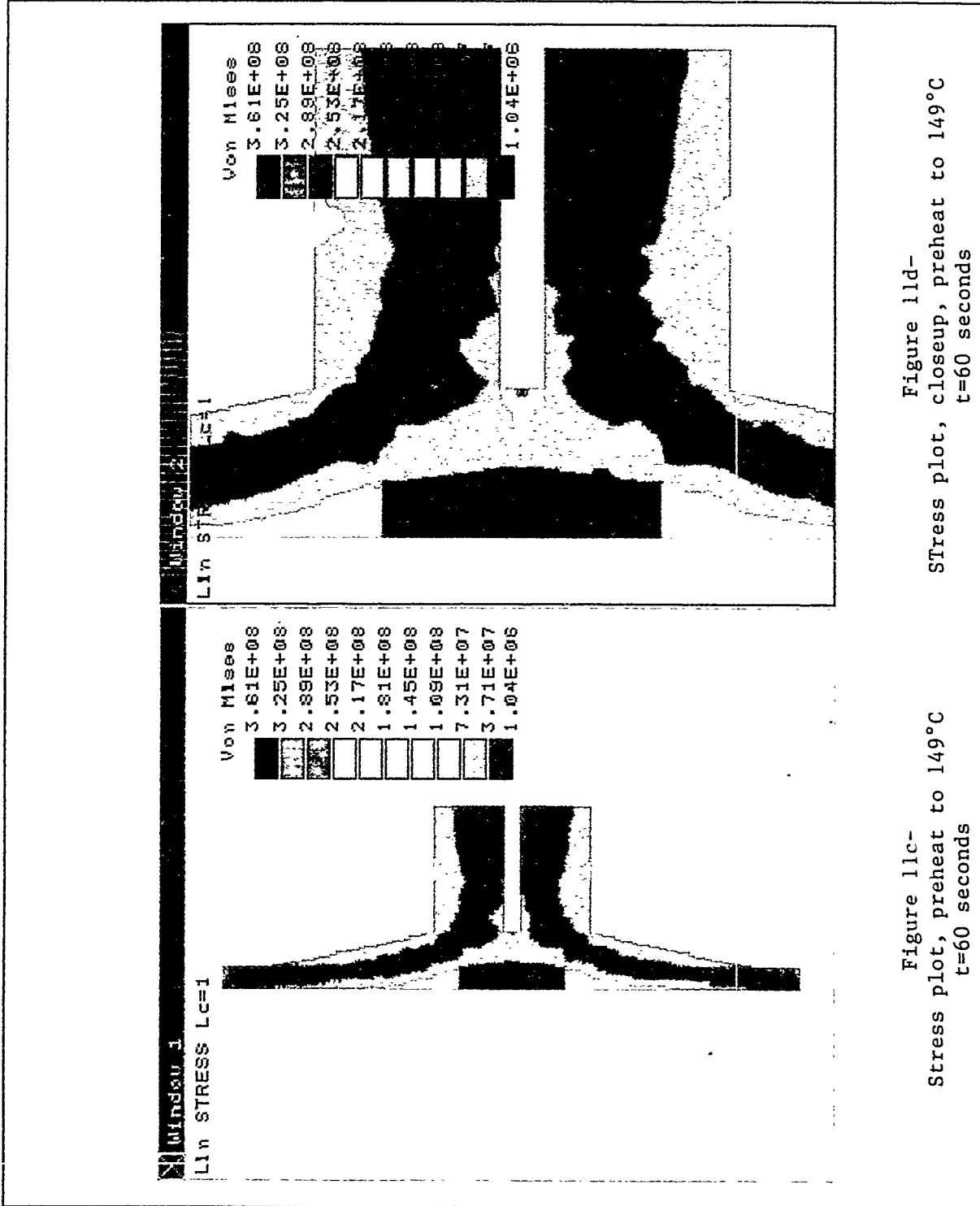


Figure 11a-
Temperature plot, preheat to 149°C
 $t=60$ seconds

Figure 11b-
Displacement Plot, preheat to 149°C
 $t=60$ seconds



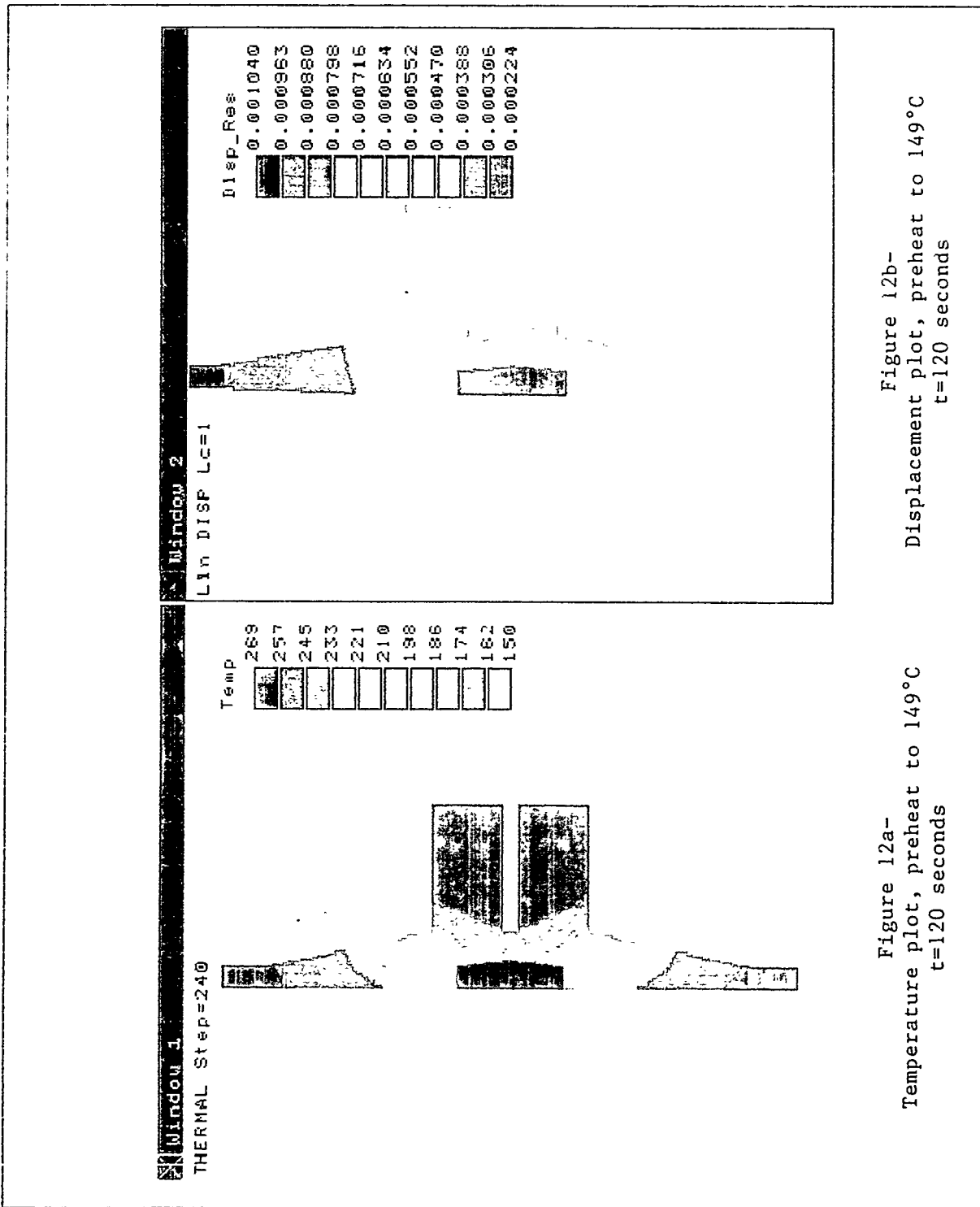
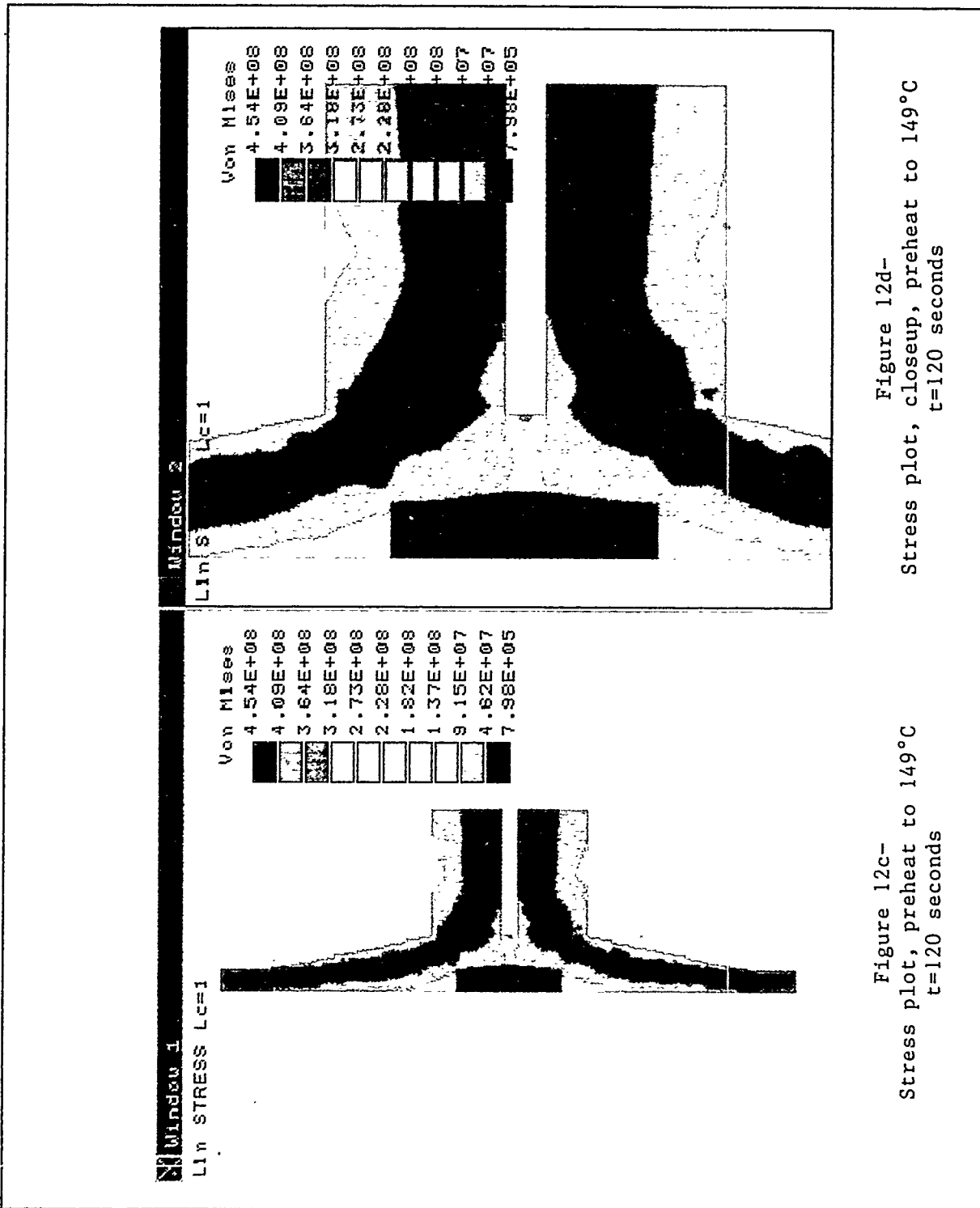


Figure 12a-
Temperature plot, preheat to 149°C
t=120 seconds

Figure 12b-
Displacement Plot, preheat to 149°C
t=120 seconds



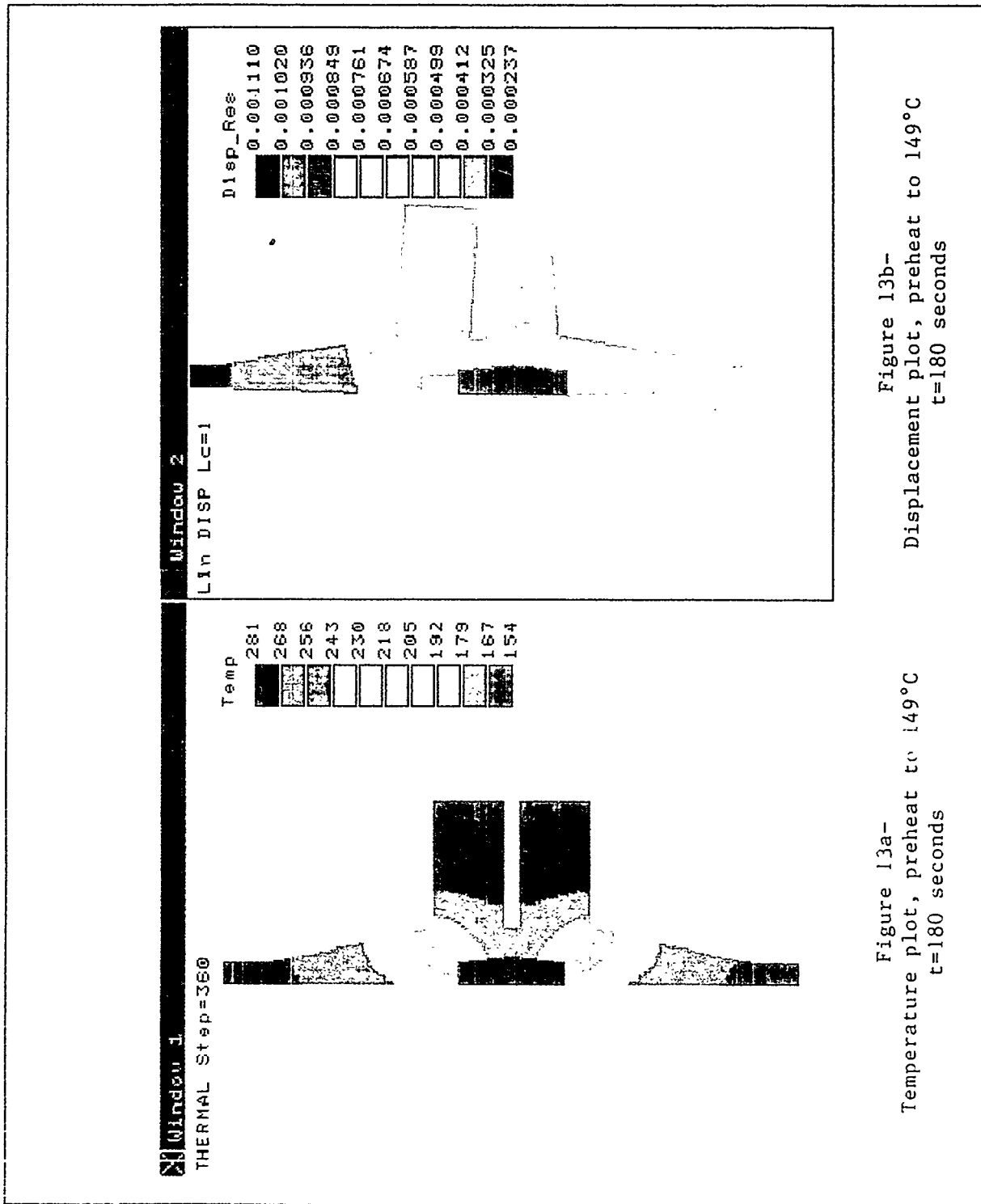


Figure 13a-
Temperature plot, preheat to 149°C
t=180 seconds

Figure 13b-
Displacement plot, preheat to 149°C
t=180 seconds

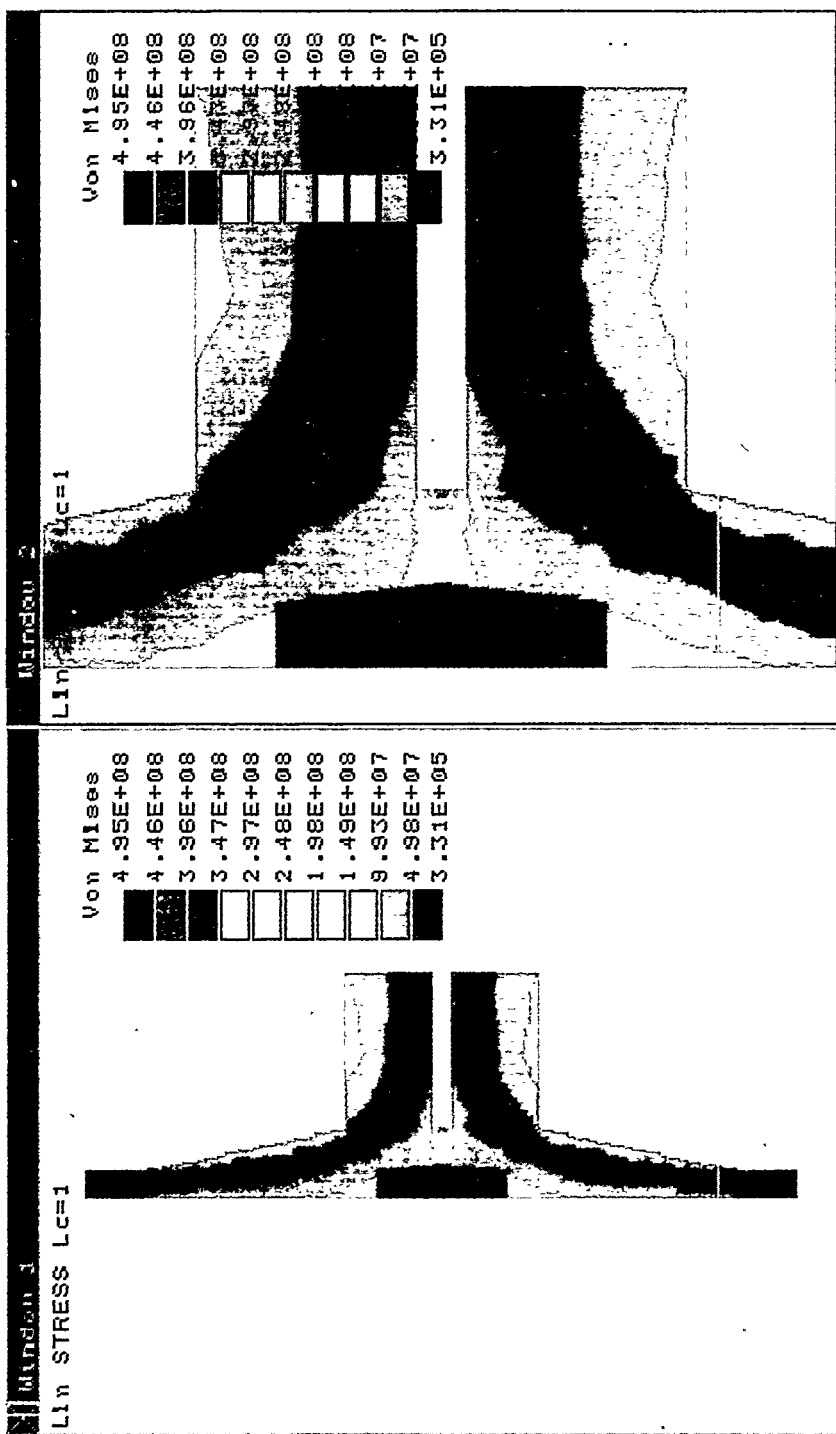


Figure 13c-
Stress plot, preheat to 149°C
 $t=180$ seconds

Figure 13d-
Stress plot, closeup, preheat to 149°C
 $t=180$ seconds

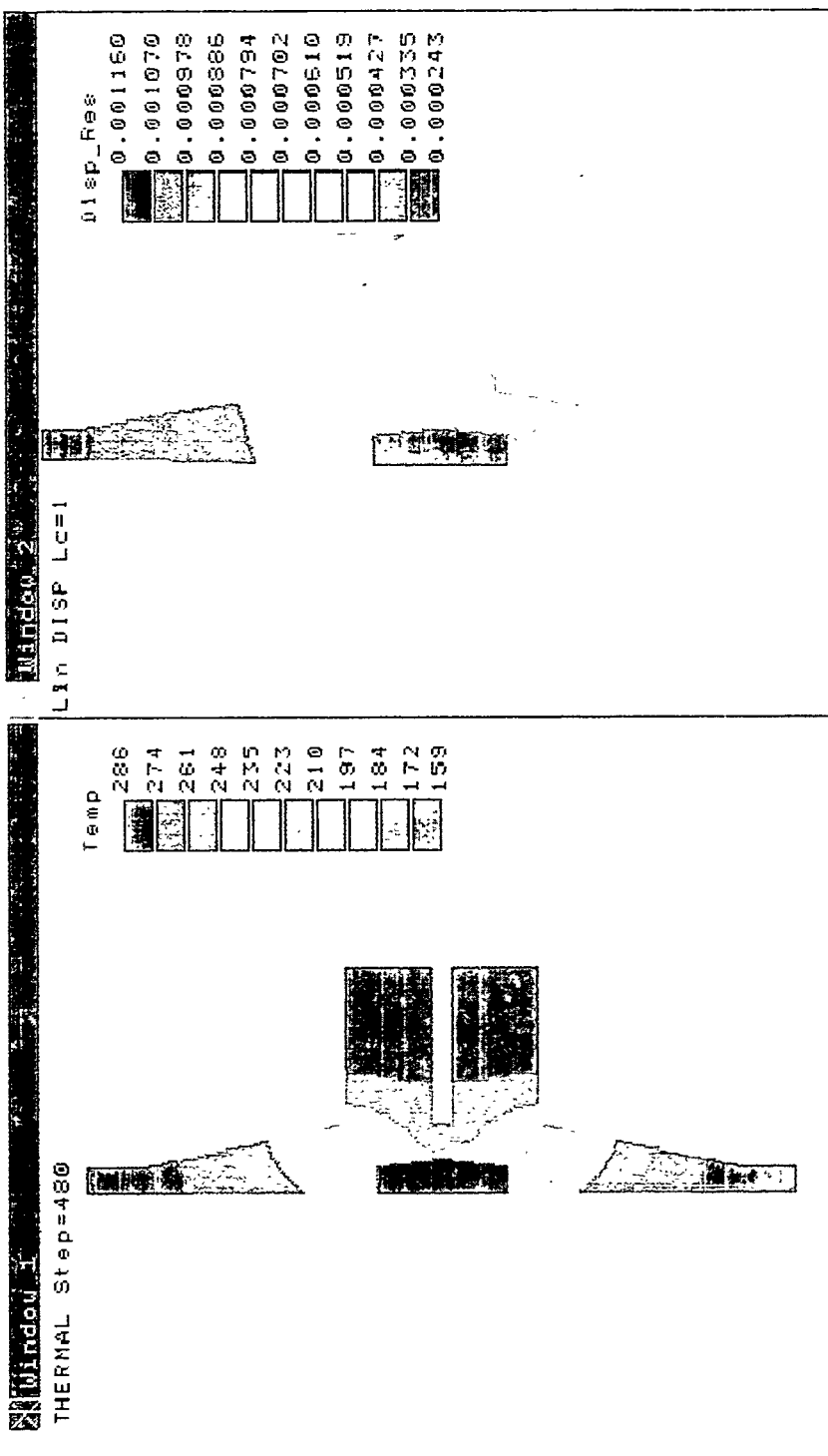
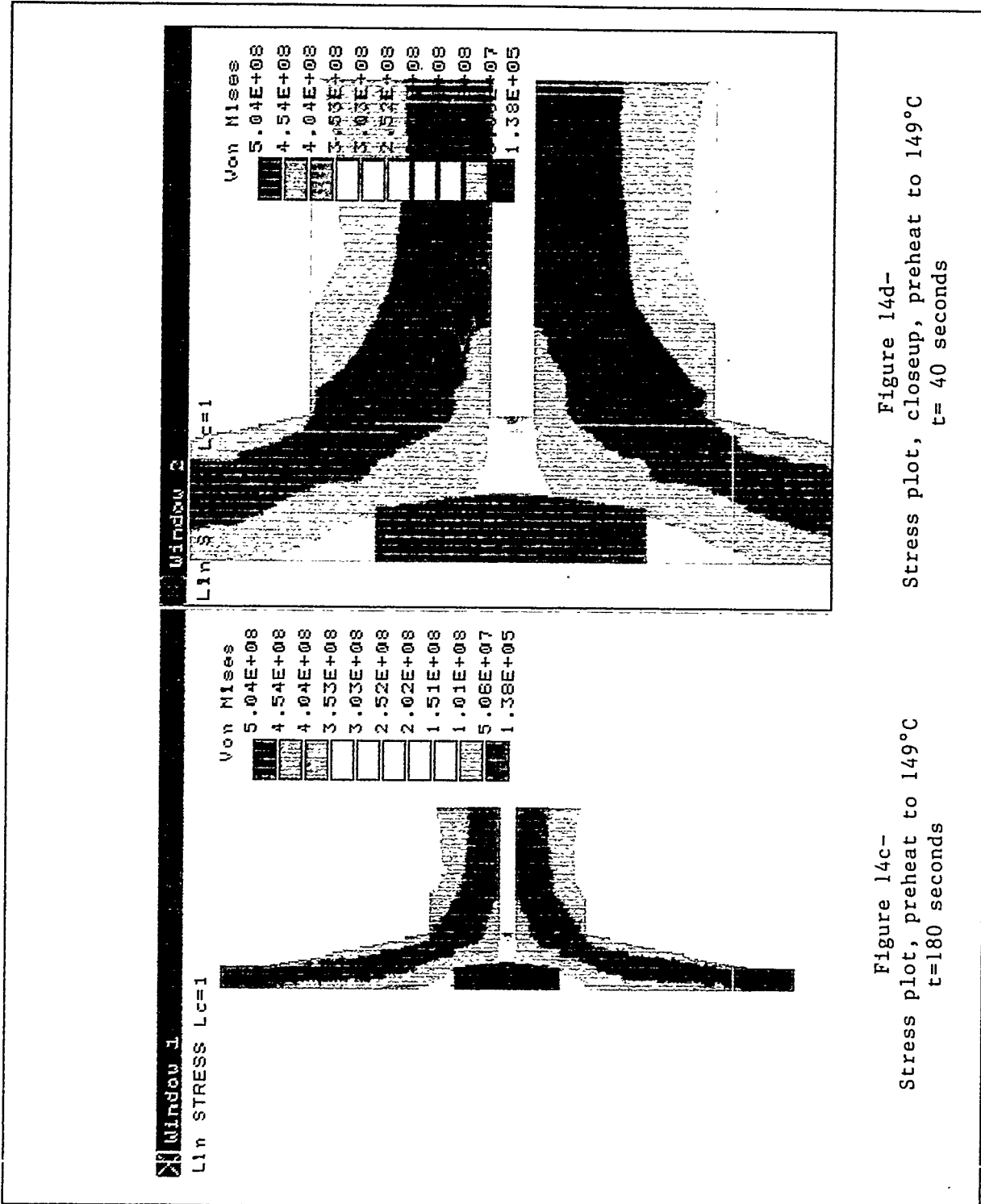


Figure 14a-
Temperature plot, preheat to 149°C
 $t=240$ seconds

Figure 14b
Displacement plot, preheat to 149°C
 $t=240$ seconds



Appendix B. Fabrication of Heat Trace Circuits

The heat trace for large systems is usually designed by the supplier. Each zone is sized based on the heating load and the piping diagrams. The length and power rating of a heat trace cable are sized based on the power required to maintain a pipe at given temperature and the power supply voltage. For a given voltage and heat trace cable length, the MI cable resistance density can be selected to provide the desired power. As a rule of thumb, we try to limit the power wattage density to less than 50 W/ft of MI cable length. Figures B-1 through B-4 are photographs of heat trace installed on a section of piping, a valve body, the header of a receiver panel, and above the jumper tubes in a receiver panel.

To maintain the integrity of the electrical circuit, only, tube benders should be used to bend the heat trace cable. See Figure B-5. After the heat trace is installed, it is covered with metal foil to prevent insulation from getting between the heater and the pipe causing the heater to overheat. The metal foil also helps to direct the radiant heat from the heat trace to the pipe or component. The metal foil can either be wrapped around the pipe and heat trace or tack welded over the heat trace to the pipe.

A critical area in heat trace circuit fabrication is the hot to cold junction. This junction makes a transition from the power lead (copper cable) to the heater (NiCr cable). Most of the failures of heat trace circuits can be attributed to a failure at the hot to cold junction. Below is an outline of the fabrication of hot-to-cold junctions.

1. First, a splice is drilled out to fit over the MI cable. See Figure B-6.
2. Cut the MI cable by scoring it three times, but not cutting it all the way through because it may cause a short of the conductor wire. Snap off the cut piece.
3. Remove 3/8 inch of the sheath to expose the inner wire of the MI cable. Peel the sheath to expose the Magnesium Oxide (MgO) and conductor wire (Figure B-7.)
4. File the inner conductor wire flat. Everything must be kept clean to make sure the silver solder adheres. Clean with emery cloth (Figure B-8).
5. Test (Meger Test) the insulation quality of each MgO MI cable by measuring the resistance between the conductor and the sheath. The resistance should be at least $5\text{ M}\Omega$ preferably $20\text{ M}\Omega$.
6. Clean everything that has to be brazed: the conductors and sheath.
7. Check the splice and stress fitting for fit.
8. Slip the stress fitting and splice over the MI cable.
9. Put flux on the conductor of the cold lead (copper wire) to help the brazing process.
10. Put solder on with a torch.
11. Check the resistance again to make sure there are no shorts.
12. Line up the hot (NiCr) and cold (Cu) leads (Figure B-9).
13. Melt the solder from the cold (Cu) side and let it flow towards the hot (NiCr) side.
14. Remove flux residue with pliers. Check integrity of joint. Buff with emery cloth.
15. Check resistance again for shorts.
16. Clean any outgassing of flux residue on the surface of the MgO by taking out the top surface of the MgO. The MgO is very hydroscopic.
17. Slide the splice over the junction until the junction can be seen through the breather hole.



Figure B-1. Heat trace installed on 2 inch pipe before metal foil was installed. It is snaked to allow for thermal expansion.

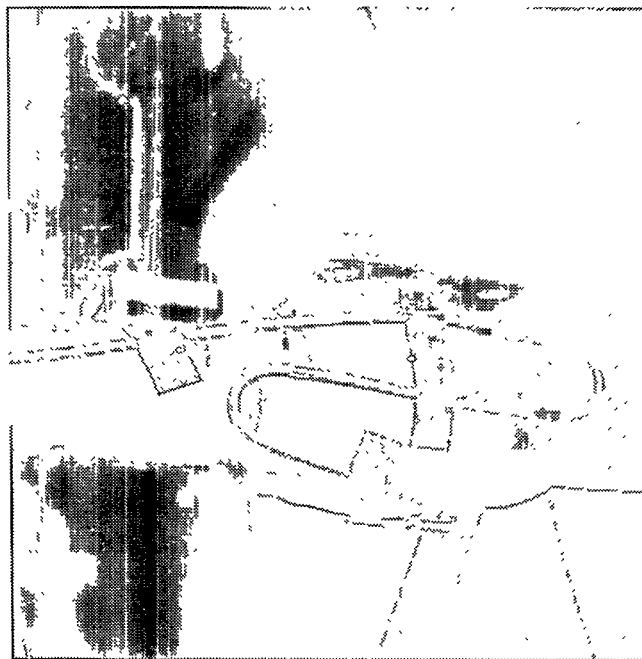


Figure B-2. Heat trace installed on valve body prior to being covered with metal foil.

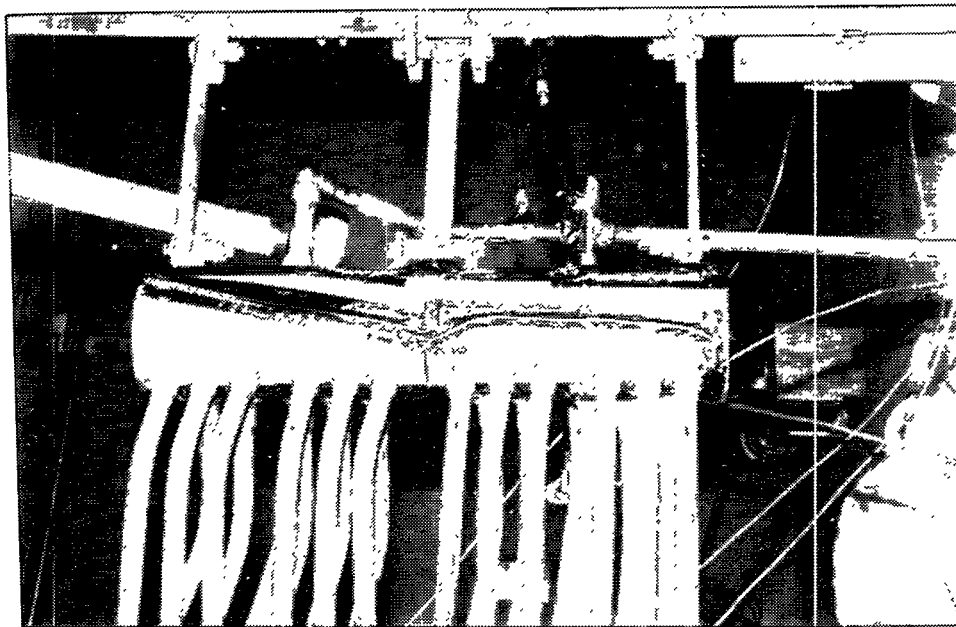


Figure B-3. Heat trace on receiver panel header with metal foil covering the cable.

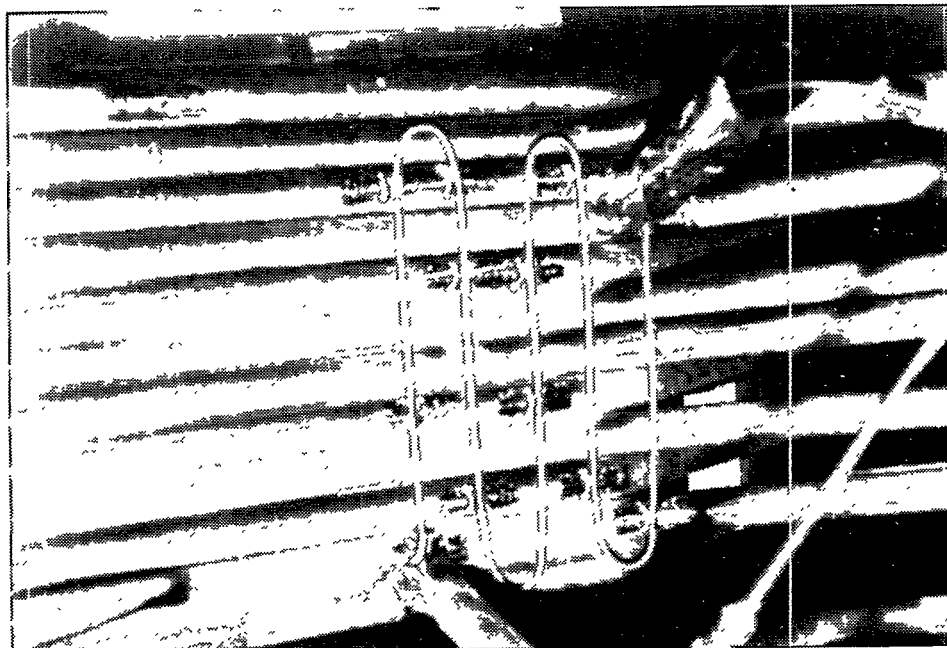


Figure B-4. Heat trace on jumper tubes in receiver panel.

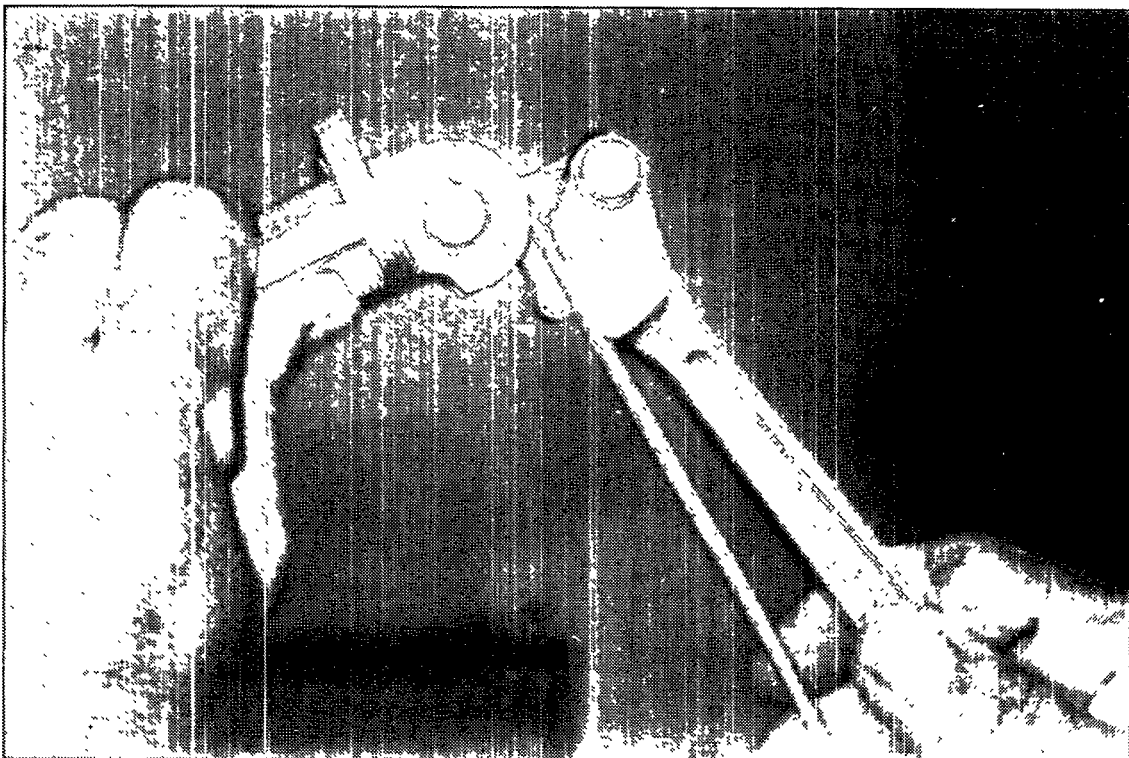


Figure B-5. Tube bender used for bending MI cable.

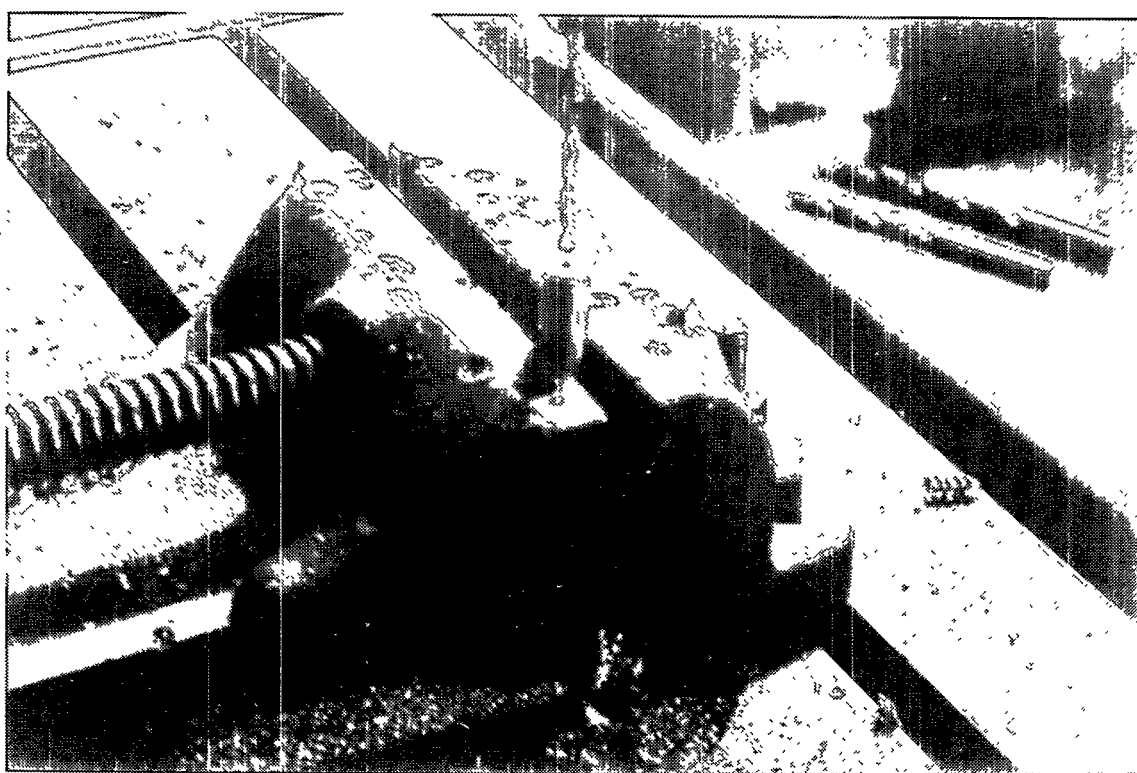


Figure B-6. Splice is drilled to fit over MI cable.

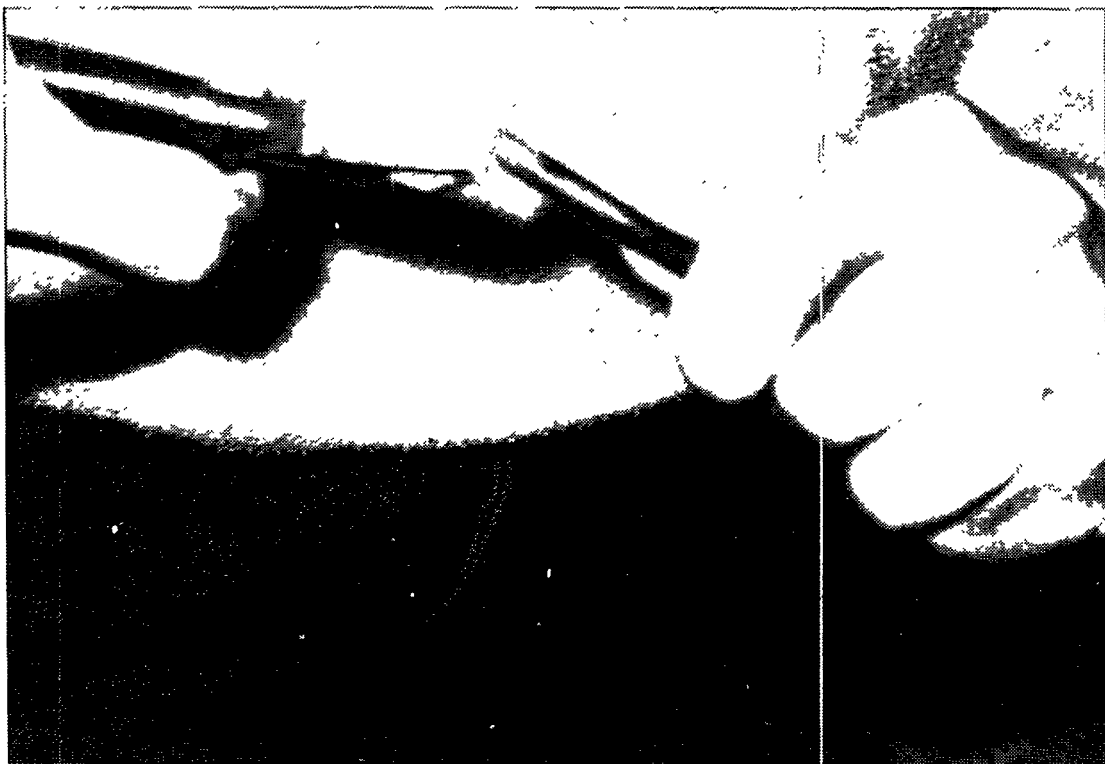


Figure B-7. Sheath is peeled away to expose magnesium oxide (MO) and the conductor wire.

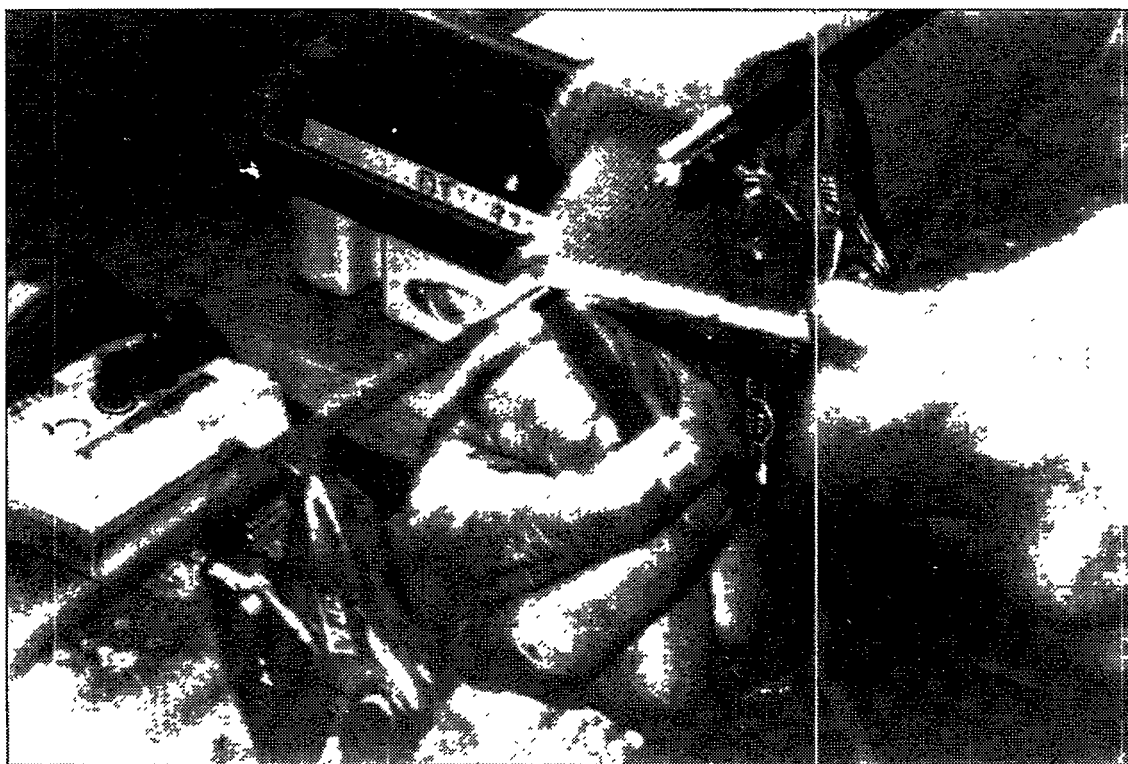


Figure B-8. The conductor wire must be cleaned so the silver solder will adhere.

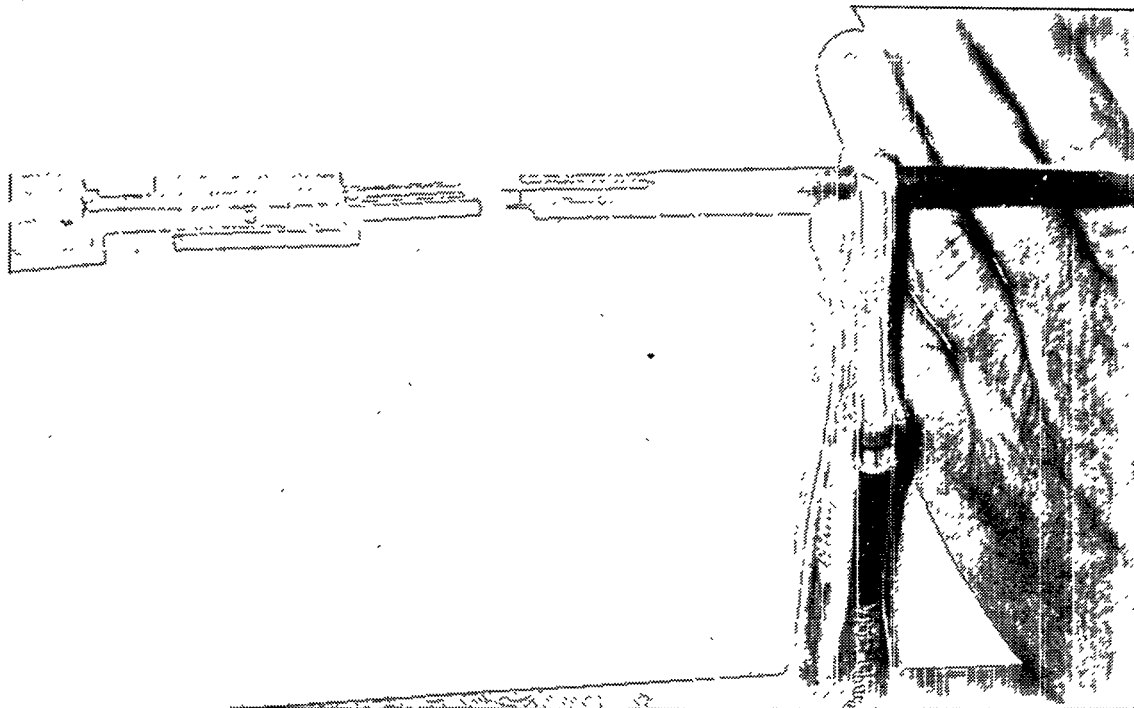


Figure B-9. The heater wire - NiCr, (on the left) and cold lead - Cu (on the right) are lined up.

18. Braze the heater side of the splice to the sheath first. Don't have both sides of the MI cable clamped tight otherwise stress will build in the joint. Allow the junction to grow. Braze the hot side by first heating the splice because it has more thermal mass than the sheath, then heating the surrounding cable to bring all parts to temperature at once. Flow solder around the splice. Repeat for cold side (Figure B-10).
19. Check resistance again.
20. Use a screw to cap off the breather hole in the slice by first putting a kink in the threads two or three threads up to prevent the screw from going in too far and screwing it in the breather hole. Clip off the screw flush with the surface of the splice. File it down. Use a round tail file to make grooves in splice for solder to adhere.
22. Flux area. Seal vent hole with solder.
22. Use a wet rag (Figure B-11) to determine if junction is sealed by measuring resistance. If water penetrated the seal, the resistance would decrease.

Don'ts with Heat Trace:

1. Don't weld near heat trace. Weld splatter could burn a hole in the sheath.
2. Don't hammer heat trace to fit it in tight spots (Figure B-12).
3. Don't use pliers or files to bend the MI cable (Figures B-13 and B-14). Use a tube bender (Figure B-5).



Figure B-10. The splice is brazed to the cable sheath.



Figure B-11. Use a wet rag to determine if the junction is sealed.

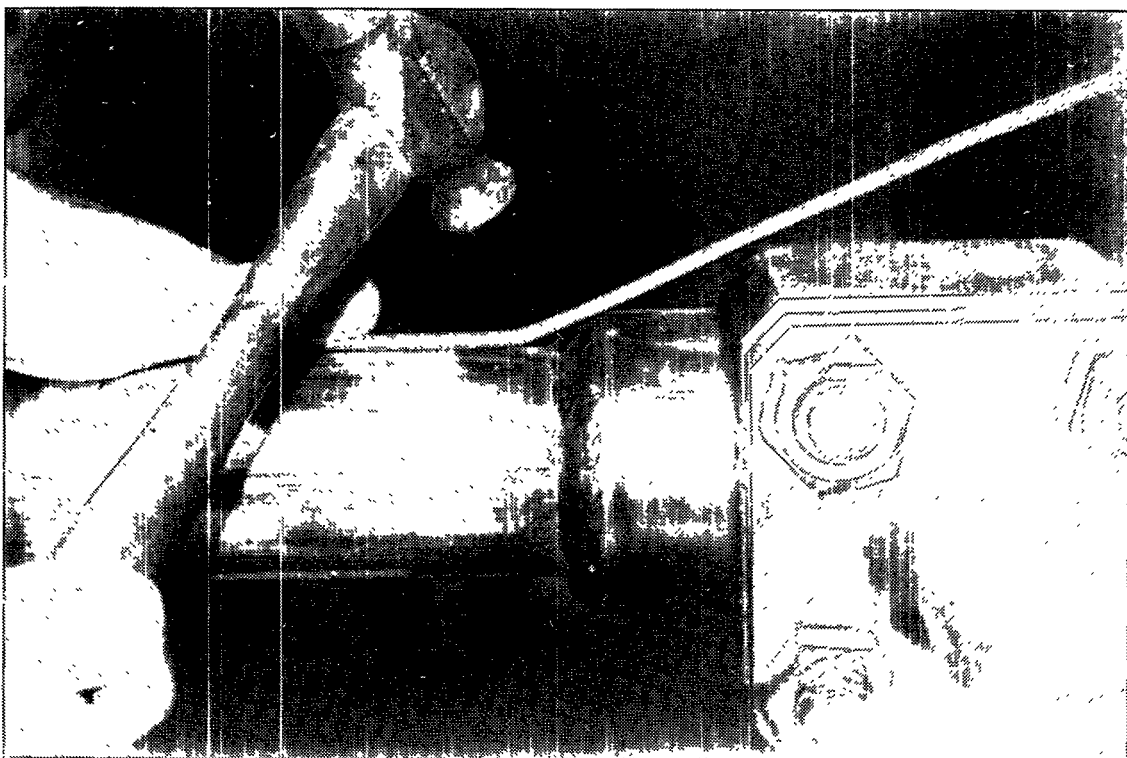


Figure B-12. Do not hammer heat trace.

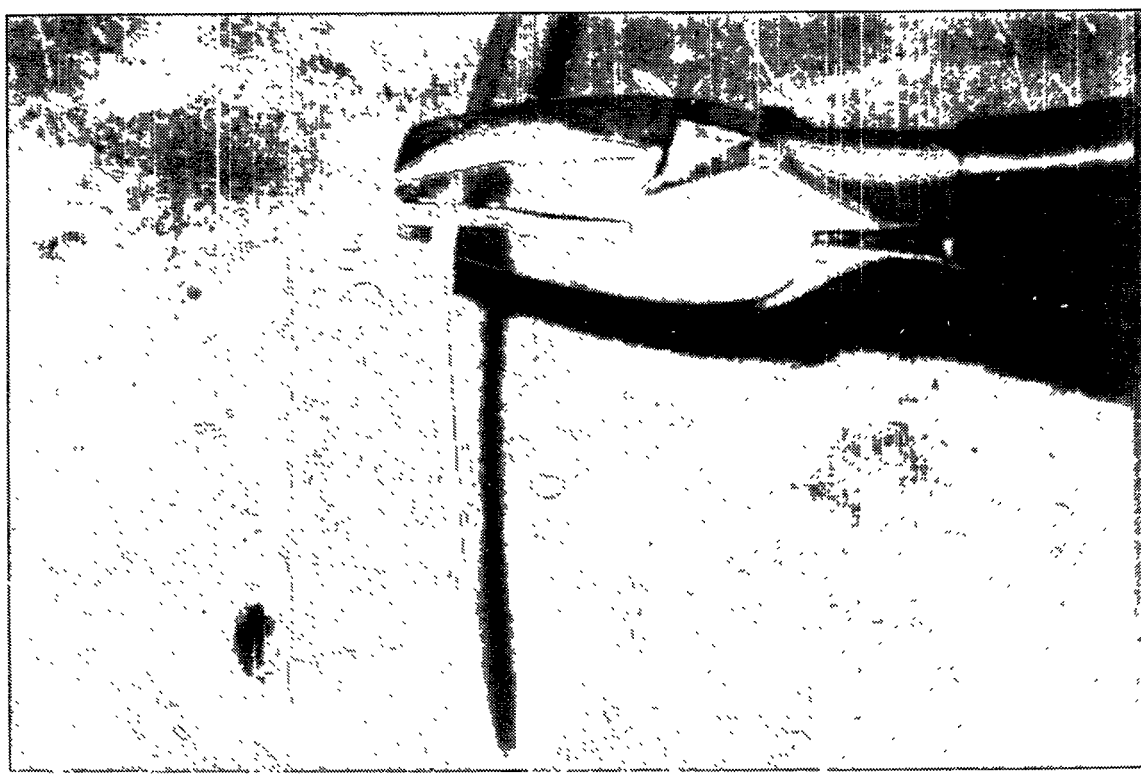


Figure B-13. Do not use pliers to bend heat trace.

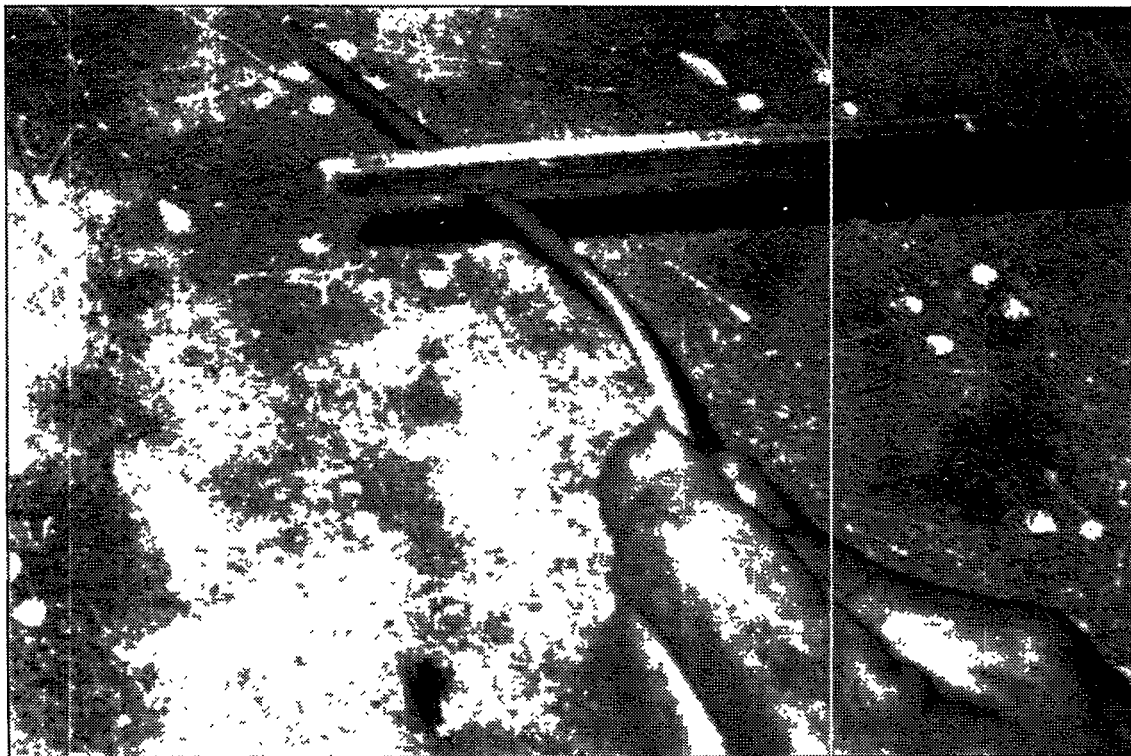


Figure B-14. Do not use a file on the heat trace sheath.

Appendix C. Heat Transfer Coefficient for Circumferentially Varying Heat Flux

The impetus behind establishing a method to estimate accurately heat transfer coefficients is so that the flux limitations on receiver tubes can be set using thermal fatigue data based on the maximum temperature the tube material will experience during normal operation. Since the receiver tubes in a central receiver are heated on one side and insulated on the other, asymmetric heating will affect the heat transfer and thus the tube-temperature distribution. In the *Handbook of Heat Transfer Fundamentals* there is a description of the effects of circumferentially varying heat flux distribution on the Nusselt number (the nondimensional heat transfer coefficient, $Nu=hD/k$) for a specific flux distribution, but not a general case. In the journal article referenced by the handbook¹, the methodology to estimate the Nusselt number for an arbitrarily varying flux distribution is described. Basically, the authors describe an analytical derivation where they solve the energy equation by breaking the arbitrary flux distribution into the average flux around the tube plus the variation from the average. The authors claim the theoretical results are within 10% of experimental data for $0.7 \leq Pr \leq 75$. The model accounts for variations in the radial and circumferential thermal eddy diffusivities for turbulent flow ($\varepsilon_{H\rho}$ and $\varepsilon_{H\theta}$) which are based on experimental data. The local Nusselt number, $Nu(\theta)$, can be calculated if the flux variation can be expressed in terms of a Fourier series.

In the case of a receiver tube, the flux distribution varies approximately with cosine of the angle from the tube crown assuming the flux is specular (parallel rays). See Figure C-1a). Normalizing the flux distribution by the average flux, $q''_o = q''_{net}/\pi$, the distribution can be represented as $q''(\theta)/q''_o = 1 + F(\theta)$ where:

$$F(\theta) = \begin{cases} \pi \cos(\theta) & 0^\circ \leq \theta \leq 90^\circ \\ 0 & 90^\circ \leq \theta \leq 270^\circ \\ \pi \cos(\theta) & 270^\circ \leq \theta \leq 360^\circ. \end{cases}$$

$F(\theta)$ is represented by the Fourier series:

$$F(\theta) = \sum_{n=1}^{\infty} F_n(\theta) = \sum_{n=1}^{\infty} a_n \cos(n\theta)$$

where

$$a_1 = \pi/2$$

$$a_n = \frac{\sin((1-n)\pi/2)}{1-n} + \frac{\sin((1+n)\pi/2)}{1+n}.$$

Figure C-1b) shows the comparison of the flux distribution to Fourier series representation ($n=0$ to 6). Once the Fourier series representation is known, the fully developed, local Nusselt number is calculated from:

$$Nu_{\infty}(\theta) = \frac{2(q''(\theta)/q''_o)}{G_o + \sum_{n=1}^{\infty} G_n F_n(\theta)} = h(\theta)D/k$$

¹"Turbulent Heat Transfer in a Circular Tube with Circumferentially varying Thermal Boundary Conditions," *J. Heat. Mass. Transfer*, Vol. 17, pp 1003-1018, (1974).

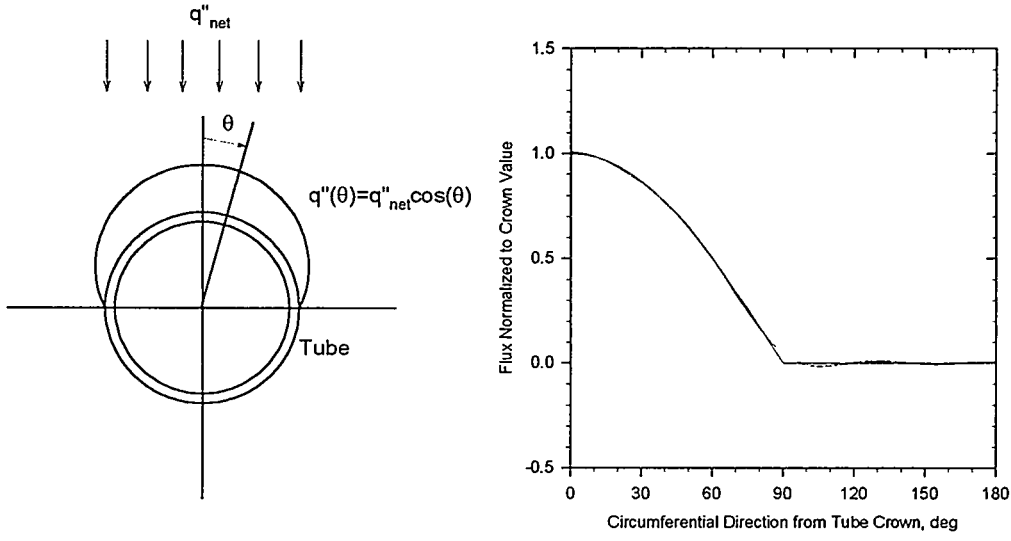


Figure C-1. a) Flux distribution around an asymmetrically heated tube with insulation on the unilluminated side, and b) comparison of flux distribution to Fourier series representation (six terms).

where G_O and G_h are found from solutions to the energy equation and are functions of the Prandtl, Pr , and Reynolds, Re , numbers. They are tabulated in the referenced article.

Figure C-2 shows a comparison of the Nusselt number computed by the above method to that computed by the Dittus Boelter equation - a commonly used correlation for uniformly heat tubes ($Nu=0.023Re^{0.8}Pr^{0.4}$). As can be seen, the analytical estimate of the heat transfer coefficient is greater in value. The authors also state for $Pr=8$, the dependence of the Nusselt number upon Reynolds number exceeds the power of 0.8 and thus the Dittus-Boelter equation tends to give more conservative results the higher the Reynolds number. This has been cited by other researchers. According to the referenced article, the deviations between the derivation and experimental data do not exceed 10% and are generally much less. Note, the Pr and Re number for nitrate salts vary from approximately 3.2 and 100,000, respectively, at 1050°F to 10.2 and 30,000, respectively, at 550°F.

This method will give an accurate estimate of localized heat transfer coefficients for a non-uniformly heated tube.

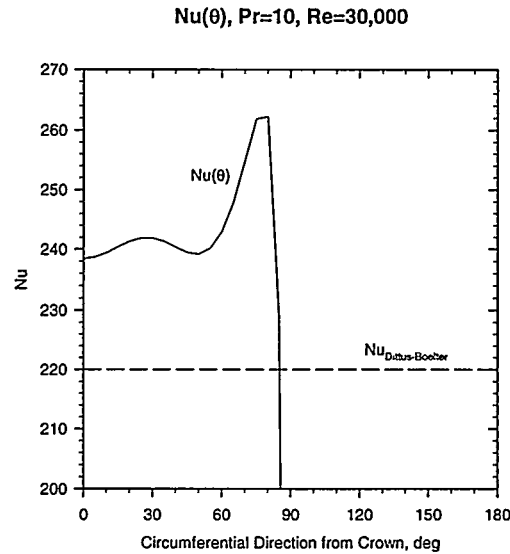


Figure C-2. Comparison of analytical calculation of Nusselt number which accounts for variations in flux to that determined by the Dittus-Boelter equation for $\text{Pr}=10$ and $\text{Re}=30,000$. $\text{Nu}(\theta)$ drops to zero between 90° to 180° .

Appendix D. Strain Equations for a Receiver Tube Under High Flux

Assuming a flux profile on the tube that follows a cosine function (Eq. D-1), a relation can be found between the tube strain and flux, tube material properties, and heat transfer coefficient. The plane strain in the tube is the sum of the strain in the tube wall due to the temperature difference across the wall and the strain due to the tube front-to-back temperature difference (Eq. D-2). The flux profile, strain equation, ϵ , and the tube inside and outside crown temperatures are defined below (assuming thin walled tubes):

$$q''(\theta) = q''_{net} \cos(\theta) \quad (D-1)$$

$$\epsilon = \alpha \left[\left(\frac{T_{o,c} - T_{i,c}}{2(1-\nu)} \right) + \left(\frac{T_{o,c} + T_{i,c}}{2} - T_{avg} \right) \right] \quad (D-2)$$

$$T_{o,c} = \frac{q''_{net} t_{wall}}{k} + T_{i,c} \quad (D-3)$$

$$T_{i,c} = T_s + \frac{q''_{net}}{h_c} \quad (D-4)$$

The average tube temperature can be approximated by:

$$T_{avg} = \frac{q''_{net}}{\pi h_c} + \frac{q''_{net} t_{wall}}{2\pi k} + T_s \quad (D-5)$$

Substituting these into the strain equation yields:

$$\epsilon = \frac{\alpha q''_{net}}{\pi} \left[\frac{t_{wall}}{2k} \left(\frac{\pi(2-\nu) - (1-\nu)}{(1-\nu)} \right) + \frac{(\pi+1)}{h_c} \right] \quad (D-6)$$

Eq. D-6 shows how the flux, tube thickness, material properties and heat transfer coefficient at the crown affect the strain. Also note that the heat transfer coefficient is a function of the salt velocity and temperature. Assuming the control system has anticipatory capabilities, the flow rate and thus the heat transfer coefficient will be tied to the incident flux. At nominal operating conditions, a deviation in the heat transfer coefficient of 10% will only result in a 5% change in strain.

Appendix E. Molten and Solid Nitrate Salt Properties

The following properties are for molten and solid nitrate salt. Table E-1 shows the density, heat capacity, thermal conductivity, absolute and kinematic viscosities, Prandtl number, and thermal diffusivity as a function of temperature for molten salt. These data were compiled from various sources. Many properties were obtained for an equimolar ratio of sodium nitrate (46% by weight) and potassium nitrate (54% by weight). We have assumed the difference is not significant. For further details on salt properties please refer to *A Review of the Chemical and Physical Properties of Molten Alkali Nitrate Salts and Their Effect on Materials Used for Solar Central Receivers*, R.W. Bradshaw and R.W. Carling, SAND87-8005, printed April 1987.

Molten Nitrate Salt

Composition:

Sodium Nitrate	NaNO ₃	60% by weight
Potassium Nitrate	KNO ₃	40% by weight

Physical Properties (300-600°C, T is in °C):

Density (kg/m³):

$$\rho = 2090 - 0.636 T$$

Heat Capacity (J/kg•K):

$$C_p = 1443 + 0.172 T$$

Thermal Conductivity (W/m•K):

$$k = 0.443 + 1.9 \times 10^{-4} T$$

Absolute Viscosity (mPa•s):

$$\mu = 22.714 - 0.120 T + 2.281 \times 10^{-4} T^2 - 1.474 \times 10^{-7} T^3$$

Other Molten Salt Properties:

Isotropic Compressibility (NaNO₃) at the melting point:

$$2 \times 10^{-10} \text{ m}^2/\text{N}$$

Speed of Sound:

NaNO ₃ :	1763.3 m/s (5785.1 ft/s) at 336°C (637°F)
KNO ₃ :	1740.1 m/s (5709 ft/s) at 352°C (666°F)

Change in Sound Speed with Temperature:

NaNO ₃ :	0.74 m/s•K
KNO ₃ :	1.1 m/s•K

Phase Change Nitrate Salt Properties

Freezing Point:

Solidifies at 221°C (430°F)

Start to crystallize at 238°C (460°F)

Heat of Fusion - (based on molecular average of heat of fusion of each component):
 $h_{\text{fus}} = 161 \text{ kJ/kg}$

Change in Density Upon Melting:

$$\Delta V/V_{\text{solid}} = 4.6\% \Rightarrow V_{\text{liquid}} = 1.046 V_{\text{solid}}$$

Solid Salt

Density, ρ :

NaNO_3 : 2260 kg/m^3 at room temperature

KNO_3 : 2190 kg/m^3 at room temperature

Heat Capacitance, C_p :

NaNO_3 : $37.0 \text{ cal/K}\cdot\text{mol} = 1820 \text{ J/kg}\cdot\text{K}$ near melting point

KNO_3 : $28.0 \text{ cal/K}\cdot\text{mol} = 1160 \text{ J/kg}\cdot\text{K}$ near melting point

Thermal Conductivity, k :

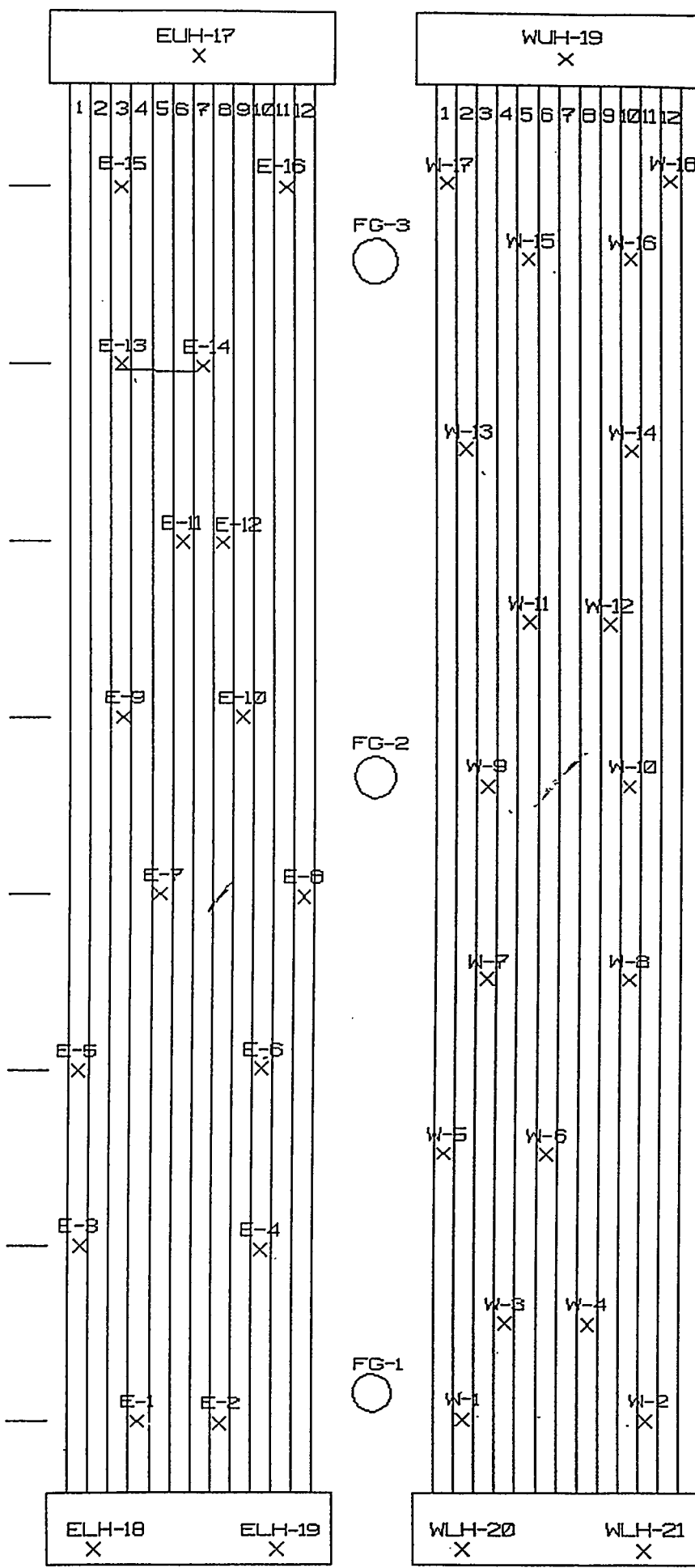
KNO_3 : $2.1 \text{ W/m}\cdot\text{K}$

Table E-1. Molten Nitrate Salt Properties: 60% NaNO₃, 40% KNO₃.

T Temperature C	ρ Density kg/m^3	Cp Heat Capacity J/kg/K	k Thermal Conductivity W/m/K	μ Absolute Viscosity Pas	v Kinematic Viscosity m^2/s	Pr Prandtl m^2/s	α Thermal Diffusivity ft^2/h
270	518	1918	119.8	1489	0.3558	0.493	0.2850
280	536	1912	119.4	1491	0.3562	0.495	0.2861
290	554	1906	119.0	1493	0.3566	0.497	0.2872
300	572	1899	118.6	1495	0.3570	0.499	0.2883
310	590	1893	118.2	1496	0.3574	0.501	0.2894
320	608	1886	117.8	1498	0.3578	0.503	0.2905
330	626	1880	117.4	1500	0.3582	0.505	0.2916
340	644	1874	117.0	1501	0.3586	0.507	0.2927
350	662	1867	116.6	1503	0.3591	0.509	0.2938
360	680	1861	116.2	1505	0.3595	0.510	0.2949
370	698	1855	115.8	1507	0.3599	0.512	0.2960
380	716	1848	115.4	1508	0.3603	0.514	0.2971
390	734	1842	115.0	1510	0.3607	0.516	0.2982
400	752	1836	114.6	1512	0.3611	0.518	0.2993
410	770	1829	114.2	1514	0.3615	0.520	0.3004
420	788	1823	113.8	1515	0.3619	0.522	0.3015
430	806	1817	113.4	1517	0.3623	0.524	0.3026
440	824	1810	113.0	1519	0.3628	0.526	0.3037
450	842	1804	112.6	1520	0.3632	0.528	0.3048
460	860	1797	112.2	1522	0.3636	0.529	0.3059
470	878	1791	111.8	1524	0.3640	0.531	0.3070
480	896	1785	111.4	1526	0.3644	0.533	0.3081
490	914	1778	111.0	1527	0.3648	0.535	0.3092
500	932	1772	110.6	1529	0.3652	0.537	0.3103
510	950	1766	110.2	1531	0.3656	0.539	0.3114
520	968	1759	109.8	1532	0.3660	0.541	0.3125
530	986	1753	109.4	1534	0.3664	0.543	0.3136
540	1004	1747	109.0	1536	0.3669	0.545	0.3147
550	1022	1740	108.6	1538	0.3673	0.547	0.3158
560	1040	1734	108.2	1539	0.3677	0.548	0.3169
570	1058	1727	107.8	1541	0.3681	0.550	0.3180
580	1076	1721	107.4	1543	0.3685	0.552	0.3191
590	1094	1715	107.0	1544	0.3689	0.554	0.3202
600	1112	1708	106.7	1546	0.3693	0.556	0.3213

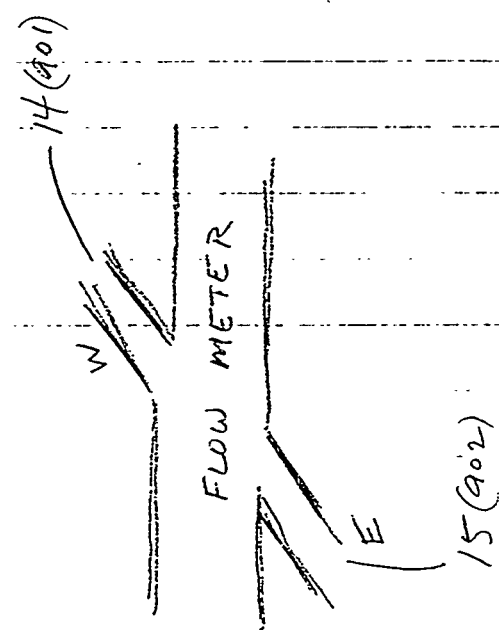
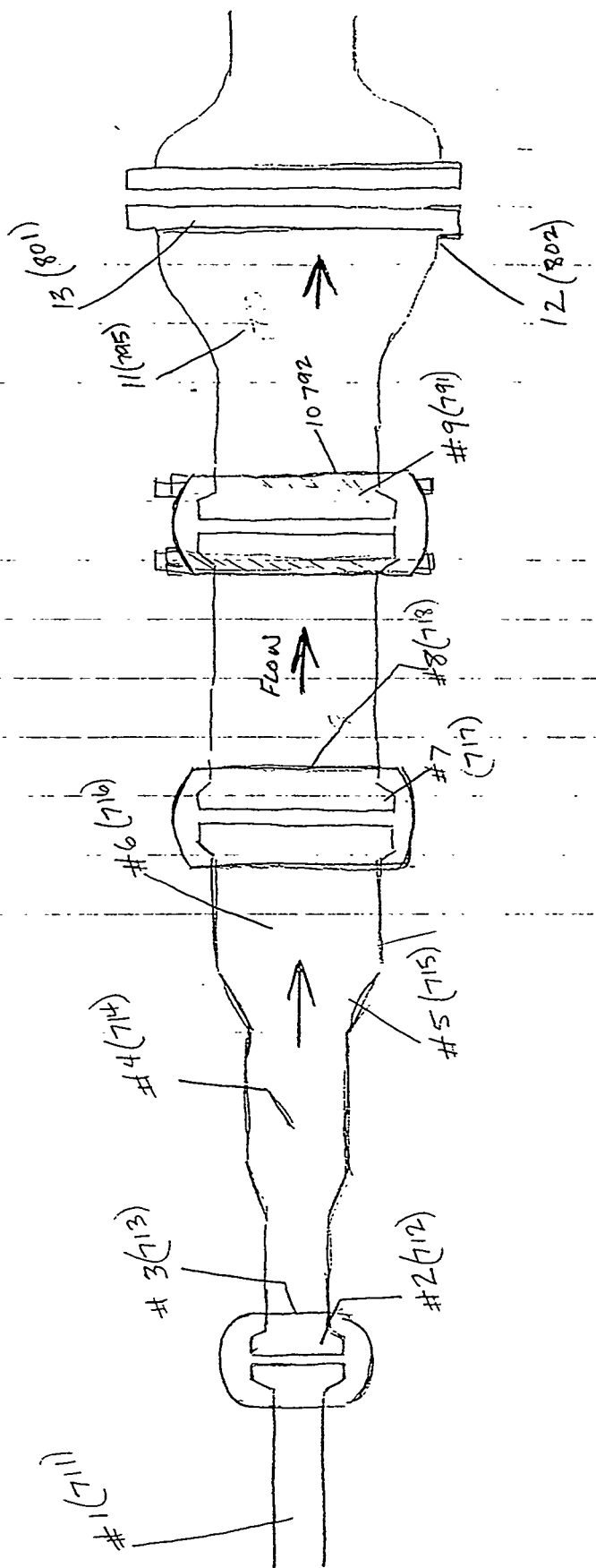
Appendix F. Selected Sets of Data and Other Information

Thermocouple Layout on Panels	101
Thermocouple Layout on Components	102
Ultrasonic Flow Meter Parameters	103
Component Part Numbers and Weights	105
Selected Sets of Data:	
- Panel Cold Fill Test	107
- Cold Fill Test of 2 inch Pipe	112
- Flow Meter Calibration Data Summary	114
- Flow Meter Calibration Data	118
- Panel Temperature Data During Freezing	130
- Checkvalve Cycling Data	142
- Thermal Shock Data for Components	149
- Data for Slow Cool Down of Components with Fan	152
- Data Slow Heat Up of Components with Heat Trace Circuits	153



PANEL TC
LOCATION

Thermocouple Layout on Components



SETUP INFORMATION FOR THE PANAMETRICS ULTRASONIC FLOWMETER

PROMPT	SETTING
System Units	METRIC
Volumetric Units	liters
Time Units	minutes
Decimal Digits	2
Totalizer Units	liters
Decimal Digits	2
Analog Out Units	Volumetric
Analog Out Zero	0.0 liters/min (4 mA)
Full Scale	500.0 liters/min (20 mA)
Error Handling	Force Low
Response Time	30 readings
Fluid Type	Other (for Molten Sodium Nitrate-60% and Potassium Nitrate-40%)
Fluid Sound Speed	1800.0 m/s (nitrate salt, 1812 m/s was measured when clamp on flowmeter was work)
Reynolds Correction	Active
Kin. Viscosity	1.863 E-6 m^2/s @ 288 C (550F) nitrate salt
Meter Factor K	1.000
Transducer #	91 for the wetted flow cell (Channel 1) 116 for the clamp on transducer (Channel 2)

The setup for each type of transducer is different and continues on the next page.

The Following Apply to the CLAMP ON TRANSDUCERS. (Note the clamp on transducer temperature should not exceed 288 C (550 F). It should be removed before operating at higher temperatures.)

Pipe Temperature	93 C (Wedge Temperature - measured half way up wedge)
Wall Thickness	3.91 mm (0.154 in for 2" dia SCH 40 SS piping)
Pipe I.D.	52.50 mm (2.067 in)
# Traverses	2
Pipe Material	Stainless Steel
Pipe Type	Round
Zero Cutoff	0.3 m/s
Xducer Spacing S	58.00 mm (enter actual dimension)

This is the space needed for the clamp on transducers as computed from the parameters entered into the computer. If the actual spacing doesn't match this value, the value can be overwritten to match the actual physical spacing.

The Following Apply to the WETTED TRANSDUCERS. (Note the wetted transducer temperature should be monitored and the sensor itself - which is out of the fluid - should not exceed 288 C (550 F). It should be removed before operating at higher temperatures.)

Path Length P	256.4816 mm (10.0977 in from Panametrics)
Axial Dimension L	157.5054 mm (6.2010 in from Panametrics)
Pipe I.D.	52.50 mm (2.067 in)
Pipe Type	Round
Zero Cutoff	0.3 m/s

Type Parameter 909 to enter parameters for wetted transducer 91:

Transducer Number	91
Transducer type	Wetted
Tranducer Frequency	1.0 MHz
Transducer Tw (delay)	36 μ sec (or 36.7 per Mike Pouglio of Panametrics)
Transducer THETA 1	N/A
Transducer Wedge Soundspeed	N/A m/sec (ft/sec)

Metal Clamp-on Flow transducers Numbers:

CTS-1.0-HT	CTS-1.0-HT
1192256	CTS. 1.0 MHz
1.0 MHz	S/N 693286
XDCR#21	XDCR #21
on elbow: 2R0308	

Part Numbers on Components in Molten Salt Experiments

Tee and cap for Corrosion Experiments:

E-CON E0204-300 S-2063 316 ISZ
E-CON E0204-300 S-2063 316 ISZ

2" Flange:

Clamp: GRAYLOC 2
182F304 GNS0218
CANADA SN48302

Body (2 of these):

PN115405 GRAYLOC® 2GR20 BW
2SCH40 SA182-F316L G1316 S07037700

Checkvalve: REFLANGE V-CON 3-900

316 216302

(Clamp side): F04 S-3063

4" Flange (on checkvalve):

(Clamp): REFLANGE C-04

(Body): R-CON F04-0304 S-3063 316 216302

4" Flange:

(Clamp): REFLANGE C-04

(Body, 2): R-CON S4063 316 91461

6" Flange (8 bolt):

(Body, 2): E-CON E0604-300 S-6065 316 AJM

E-CON E0604-300 S-6065 316 LDI

Panametrics Flow Meter - Electronics

Model 6468-22-1000-0

Serial Number 791

Software Version 4.D

Weight of Components

31 lbs: from elbow to blind flange for corrosion coupons to first half of 2" grayloc flange

14.5 lbs: 2" grayloc clamp

39 lbs: 2nd half of 2" grayloc flange + 2x3 reducer + 3" V-CON checkvalve + half of 3" inner 4" outer R-CON flange

27 lbs: 2nd half of 3" inner, 4" outer R-CON flange to 1st half of 4" R-CON flange

27 lbs: 1st R-CON 4" clamp

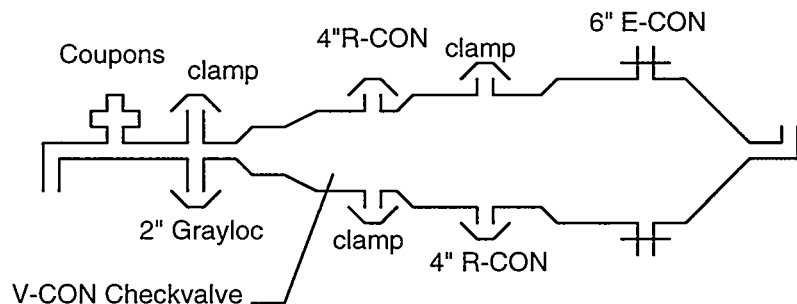
29lbs: 2nd R-CON 4" clamp

42 lbs: 2nd half of 4" R-CON flange + 4x6 reducer + 1st half of 6" E-CON flange.

42 lbs: 2nd half of 6" E-CON flange + 6"x2" reducer + elbow

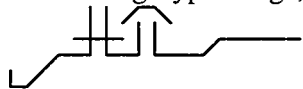
Total weight: 251 lbs

Total length outer edge of elbow to outer edge of elbow: 100"



Added 2-1-94

4" ANSI Ring Type flange, 300#, oval grove, oval ring, stainless steel



Ring Type Flange

added between 4" R-CON Flanges

43.1 lbs: 2nd half of 3" inner, 4" outer R-CON flange to 1st half of 4" Ring-type flange

36.5 lbs: 2nd half of 4" Ring-type flange to 1st half of 4" R-CON flange

New Total Weight: 303.6 lbs

Panel Cold Fill Test: 12/01/93

CRTF	Panel Cold Fill Test, 12/01/93					
TEST		1st pass	2nd pass	3rd pass	4th pass	Upper he
Time		TEW4	TEW17	TEE12	TEE9	TEWUH19
hour	Time	DEG F				
9.4494	475	48	48	46	46	80
9.4508	480	48	48	46	46	80
9.4522	485	48	48	46	46	80
9.4536	490	48	48	46	46	80
9.455	495	48	48	46	46	80
9.4564	500	48	48	46	46	80
9.4581	505	48	48	46	46	80
9.4594	510	48	48	46	46	80
9.4608	515	48	48	45	46	80
9.4622	520	48	48	45	45	80
9.4636	525	48	48	45	45	80
9.465	530	48	48	45	45	80
9.4664	535	48	49	45	45	80
9.4678	540	48	49	45	45	80
9.4692	545	48	49	45	45	80
9.4706	550	48	49	45	45	80
9.4717	555	48	49	45	45	80
9.4731	560	48	49	45	45	80
9.4744	565	48	49	45	45	80
9.4758	570	48	49	45	45	80
9.4772	575	121	49	45	45	80
9.4786	580	283	49	45	45	80
9.48	585	432	49	45	45	80
9.4814	590	542	104	45	45	83
9.4828	595	582	231	45	45	89
9.4842	600	590	366	45	45	98
9.4856	605	589	468	69	45	111
9.4869	610	586	498	158	45	126
9.4883	615	583	492	208	49	145
9.4897	620	581	501	230	99	163
9.4911	625	580	509	251	138	182
9.4925	630	578	519	270	182	210
9.4939	635	577	520	281	203	225
9.4953	640	576	520	304	242	261
9.4967	645	575	516	314	265	279
9.4983	650	574	517	325	292	310
9.4997	655	573	520	330	308	340
9.5011	660	572	525	342	323	354
9.5025	665	572	529	353	334	381
9.5039	670	571	531	370	354	407
9.5053	675	571	532	385	364	420
9.5067	680	571	533	418	381	443
9.5081	685	571	538	448	395	455
9.5094	690	570	540	484	485	476
9.5108	695	570	541	494	507	488

Panel Cold Fill Test: 12/01/93

CRTF	Panel Cold Fill Test, 12/01/93					
TEST		1st pass	2nd pass	3rd pass	4th pass	Upper head
Time		TEW4	TEW17	TEE12	TEE9	TEWUH19
hour	Time	DEG F				
	9.5122	700	570	541	504	518
	9.5136	705	570	543	505	519
	9.5147	710	570	543	512	527
	9.5161	715	570	543	518	532
	9.5175	720	570	544	521	534
	9.5189	725	570	544	523	537
	9.5203	730	570	544	525	539
	9.5217	735	570	545	526	540
	9.5231	740	570	545	528	542
	9.5244	745	570	545	530	543
	9.5258	750	570	546	532	544
	9.5272	755	570	546	533	545
	9.5286	760	570	546	535	546
	9.5303	765	570	547	536	547
	9.5317	770	570	547	537	549
	9.5331	775	569	547	538	550
	9.5344	780	569	547	538	550
	9.5358	785	569	548	539	551
	9.5372	790	569	548	540	551
	9.5386	795	569	548	540	551
	9.54	800	569	548	542	552
	9.5414	805	569	548	542	552
	9.5425	810	569	550	543	553
	9.5439	815	569	550	543	553
	9.5453	820	569	550	543	553
	9.5467	825	569	550	544	553
	9.5481	830	569	550	544	555
	9.5494	835	569	550	544	555
	9.5508	840	569	550	545	555
	9.5522	845	569	550	545	555
	9.5536	850	569	550	545	555
	9.555	855	569	550	545	555
	9.5564	860	569	550	545	556
	9.5581	865	569	550	546	556
	9.5594	870	568	550	546	556
	9.5608	875	568	550	546	556
	9.5622	880	568	550	546	556
	9.5636	885	568	550	546	556
	9.565	890	568	550	546	556
	9.5664	895	567	550	548	556
	9.5678	900	567	550	548	557
	9.5689	905	567	550	548	557
	9.5703	910	567	550	548	557
	9.5717	915	567	550	548	557
	9.5731	920	567	550	548	557

Panel Cold Fill Test: 12/01/93

CRTF	Panel Cold Fill Test, 12/01/93					
TEST	1st pass	2nd pass	3rd pass	4th pass	Upper he	
Time	TEW4	TEW17	TEE12	TEE9	TEWUH19	
hour	Time	DEG F	DEG F	DEG F	DEG F	DEG F
	9.5744	925	567	550	548	557
	9.5758	930	567	550	548	557
	9.5772	935	567	550	548	556
	9.5786	940	567	550	548	554
	9.58	945	567	550	548	552
	9.5814	950	567	550	548	549
	9.5831	955	567	550	548	548
	9.5844	960	567	550	548	547
	9.5858	965	567	550	548	546
	9.5872	970	567	550	548	546
	9.5886	975	567	550	548	545
	9.59	980	566	550	548	545
	9.5914	985	566	550	548	545
	9.5928	990	566	550	550	545
	9.5942	995	565	550	550	543
	9.5953	1000	565	550	550	543
	9.5967	1005	565	550	550	548
	9.5981	1010	565	550	550	555
	9.5994	1015	564	550	550	557
	9.6008	1020	564	550	550	557
	9.6022	1025	564	550	550	557
	9.6036	1030	564	550	550	557
	9.605	1035	564	550	550	557
	9.6064	1040	564	550	550	557
	9.6078	1045	564	550	550	557
	9.6092	1050	564	550	549	557
	9.6106	1055	564	550	549	557
	9.6122	1060	564	550	549	557
	9.6136	1065	564	550	549	557
	9.615	1070	564	550	549	557
	9.6164	1075	564	550	549	557
	9.6178	1080	564	550	549	557
	9.6192	1085	564	550	549	557
	9.6206	1090	564	550	549	557
	9.6219	1095	564	550	549	557
	9.6233	1100	564	550	549	557
	9.6244	1105	564	550	549	557
	9.6258	1110	564	550	550	557
	9.6272	1115	564	549	550	557
	9.6286	1120	564	549	550	557
	9.63	1125	564	549	550	557
	9.6314	1130	564	549	550	557
	9.6328	1135	564	549	550	558
	9.6342	1140	564	549	550	558
	9.6356	1145	564	550	550	566

Panel Cold Fill Test: 12/01/93

CRTF	Panel Cold Fill Test, 12/01/93				
TEST	1st pass	2nd pass	3rd pass	4th pass	Upper head
Time	TEW4	TEW17	TEE12	TEE9	TEWUH19
hour	Time	DEG F	DEG F	DEG F	DEG F
9.6369	1150	564	550	550	558
9.6383	1155	564	550	551	558
9.64	1160	564	550	551	558
9.6414	1165	564	550	551	558
9.6428	1170	564	550	551	558
9.6442	1175	564	550	551	558
9.6456	1180	564	550	551	558
9.6469	1185	564	550	551	558
9.6483	1190	564	550	551	558
9.6497	1195	564	550	551	559
9.6511	1200	564	550	551	559
9.6522	1205	564	550	551	559
9.6536	1210	564	550	551	559
9.6553	1215	564	550	551	559
9.6567	1220	568	550	551	559
9.6578	1225	571	551	551	559
9.6592	1230	574	555	551	559
9.6606	1235	576	557	551	559
9.6619	1240	577	559	551	560
9.6633	1245	578	561	554	561
9.6647	1250	579	562	555	562
9.6661	1255	579	562	558	563
9.6675	1260	580	563	558	566
9.6689	1265	580	563	559	566
9.6703	1270	580	565	560	567
9.6717	1275	580	565	560	568
9.6731	1280	580	565	561	568
9.6744	1285	580	565	561	570
9.6761	1290	580	565	563	570
9.6775	1295	580	565	563	571
9.6789	1300	580	566	563	571
9.6803	1305	580	566	564	571
9.6817	1310	577	566	564	571
9.6831	1315	574	565	564	571
9.6844	1320	570	562	564	571
9.6858	1325	568	560	564	571
9.6872	1330	566	557	564	571
9.6886	1335	565	554	563	571
9.69	1340	565	553	560	570
9.6911	1345	564	552	559	567
9.6925	1350	564	552	556	565
9.6939	1355	564	550	555	563
9.6953	1360	564	550	554	562
9.6967	1365	564	550	554	561
9.6981	1370	564	550	553	560

Panel Cold Fill Test: 12/01/93

CRTF	Panel Cold Fill Test, 12/01/93					
TEST		1st pass	2nd pass	3rd pass	4th pass	Upper he
Time		TEW4	TEW17	TEE12	TEE9	TEWUH19
hour	Time	DEG F				
9.6994	1375	564	550	553	560	570
9.7008	1380	564	550	553	560	569
9.7022	1385	564	550	552	559	569
9.7036	1390	564	550	552	559	568
9.705	1395	564	550	552	559	568
9.7064	1400	564	550	552	559	568

Cold Fill Test of 2 inch Pipe

Cold Pipe Test		Schedule 40, 2in pipe						
Sept. 24, 1993		Salt Temperature, 524 F						
Outside Pipe Temperature, deg F								
Channel		439	440	441	442	443	444	445
Hrs:Min:Sec								
9:16:55		367	262	103	99	96	126	613
9:17:00		363	263	104	99	96	126	613
9:17:05		362	263	103	99	96	125	613
9:17:10		362	263	103	99	96	126	613
9:17:15		362	263	103	98	96	126	613
9:17:20		361	263	104	99	96	125	613
9:17:25		363	263	102	99	96	125	613
9:17:30		363	262	103	99	96	126	613
9:17:35		361	262	103	99	96	125	613
9:17:40		383	268	111	100	95	125	613
9:17:45		415	281	144	122	100	125	613
9:17:50		444	302	194	157	124	141	607
9:17:55		462	320	240	191	152	164	592
9:18:00		475	341	292	230	186	194	572
9:18:05		485	358	344	275	222	227	555
9:18:10		493	377	393	334	277	280	540
9:18:15		496	391	421	377	335	331	532
9:18:20		496	405	445	416	395	384	528
9:18:25		499	415	458	440	431	420	527
9:18:30		500	425	470	460	460	451	527
9:18:35		502	434	480	473	478	469	529
9:18:40		504	441	487	483	490	482	529
9:18:50		507	455	498	498	503	499	531
9:18:55		507	460	501	501	506	503	532
9:19:00		508	465	505	506	509	507	532
9:19:05		509	468	506	508	510	508	532
9:19:10		508	472	508	510	513	510	532
9:19:15		509	475	510	512	514	512	532
9:19:20		509	478	511	513	515	512	532
9:19:25		511	480	511	513	515	512	532
9:19:30		511	483	514	515	517	514	532
9:19:35		511	485	514	517	518	515	532
9:19:40		511	487	515	517	519	516	532
9:19:45		510	488	516	519	519	515	532
9:19:50		513	490	517	519	519	517	532
9:19:55		511	491	517	518	520	516	532
9:20:00		513	493	517	519	520	519	532
9:20:05		513	495	519	520	520	519	532
9:20:10		515	495	518	521	521	519	532
9:20:15		514	497	519	522	523	520	532
9:20:20		514	497	520	521	522	520	533
9:20:25		516	498	519	521	522	520	533
9:20:30		514	499	521	522	522	521	532
9:20:35		515	499	519	521	521	520	532

Cold Fill Test of 2 inch Pipe

Cold Pipe Test		Schedule 40, 2in pipe						
Sept. 24, 1993		Salt Temperature, 524 F						
		Outside Pipe Temperature, deg F						
Channel		439	440	441	442	443	444	445
Hrs:Min:Sec								
9:20:40		516	501	520	522	523	521	532
9:20:45		517	502	520	523	523	522	532
9:20:50		516	503	521	524	523	521	533
9:20:55		516	503	520	524	524	522	533
9:21:00		517	503	521	524	524	523	533
9:21:05		516	504	521	524	524	523	533
9:21:10		519	504	522	525	524	523	533
9:21:15		518	505	522	524	524	522	533
9:21:20		516	505	522	525	524	523	533
9:21:25		517	505	522	525	525	523	533
9:21:30		517	507	523	526	525	523	533
9:21:35		517	507	523	526	525	524	533
9:21:40		518	507	523	525	525	524	533
9:21:45		517	507	523	525	526	524	534
9:21:50		516	507	523	526	525	524	533
9:21:55		518	508	523	526	525	525	533
9:22:00		517	508	523	526	525	524	533
9:22:05		519	508	523	526	526	525	533
9:22:10		518	509	523	527	526	525	533
9:22:15		519	507	523	526	525	523	532
9:22:20		519	509	524	526	527	525	533
9:22:25		518	510	524	527	527	525	533
9:22:30		518	509	523	526	525	524	533

Flow meter calibration data summary.

Total Bias and Random Uncertainty Percents and Urss Uncertainties												
Flow L/min	FT-720 Vortex Flow			PF-001 Wetted Ultra			PF-002 Clamp-on Ultrasonic			FT-730 Vortex		
	Random Bias	Random Biass	t95S/N^5 Bi	Random Bias	Random Biass	t95S/N^5 Bi	Random Bias	Random Biass	t95S/N^5 Bi	Random Bias	Random Biass	t95S/N^5 Bi
Average	%	%	%	%	%	%	%	%	%	%	%	%
Flow, l/min	%	%	%	%	%	%	%	%	%	%	%	%
102.58	9.76	0.63	3.84	0.55	8.47	0.50	9.90	0.47	5.29	0.39	7.29	0.44
155.40	11.58	0.29	4.14	0.51	12.78	0.55	11.55	0.39	0.27	0.22	8.48	0.21
197.41	12.56	0.18	4.56	0.44	12.97	0.42	12.50	0.35	15.62	0.35	—	—
244.65	15.09	0.21	6.35	0.31	13.27	0.30	—	—	—	—	—	—
Flow	Urss	Urss	Urss	Urss	Urss	Urss	Urss	Urss	Urss	Urss	Urss	Urss
102.5759	9.77976	—	3.878089	8.485958	—	9.91473	—	—	—	—	—	5.310453
155.3991	11.58529	—	4.168351	12.79488	—	11.55541	—	—	—	—	—	7.295545
197.4063	12.55799	—	4.581304	12.97705	—	12.49935	—	—	—	—	—	8.48723
244.6471	15.08722	—	6.358041	13.27571	—	15.62751	—	—	—	—	—	—

Flow meter calibration data summary.

Flow L/min	Bias and Random Uncertainty Percents Relative to Bubbler Reference						FT-800 Vortex Random t95S/N ^{1.5} % Bi	
	FT-720 Vortex Flow			PF-001 Wetted Ultra				
	Random Bias t95S/N ^{1.5} %	Random Bias t95S/N ^{1.5} %	Random Bias t95S/N ^{1.5} %	Random Bias t95S/N ^{1.5} %	Random Bias t95S/N ^{1.5} %	Random Bias t95S/N ^{1.5} %		
245.07	15.52159	0.475089	6.862377	0.662462	-11.1397	0.488859	15.82366	
245.07	13.99688	0.239153	4.261886	0.230269	-12.9097	0.200013	14.08849	
196.22	12.42478	0.232202	3.896936	1.145752	-10.4407	0.944796	12.56068	
191.20	13.99572	0.071855	4.027049	0.149455	-10.8986	0.125255	13.66786	
155.47	12.56275	0.753997	4.490394	1.213737	-8.18096	1.074611	12.56275	
155.19	10.07565	0.12859	1.012406	0.081947	-12.3653	0.25961	10.29978	
102.99	8.110337	1.133905	0.300727	0.940323	-6.15803	0.721195	8.490264	
102.16	9.834467	0.130553	-0.22997	0.152059	-8.94488	0.272782	9.767941	
154.91	10.90267	0.179409	-0.45872	0.614047	-14.4883	0.671667	10.51535	
156.03	10.16607	0.099755	1.122052	0.125268	-13.7377	0.177755	10.1898	
200.13	11.02	0.299602	1.208081	0.386784	-13.964	0.498647	10.88372	
202.08	10.38117	0.10355	0.711803	0.070636	-14.2525	0.116727	10.46034	
246.46	13.39638	0.089405	3.323362	0.277316	-14.7587	0.349742	14.27843	
242.00	15.44113	0.048174	5.7871	0.059108	-12.0118	0.152921	16.38737	
							0.134167	

Flow meter calibration data summary.

Flow L/min	Bias and Random Uncertainty Levels Relative to Bubbler Reference						FT-800 Vortex					
	FT-720 Vortex Flow			PF-001 Wetted Ultra			PF-002 Clamp-on Ultrasonic			FT-730 Vortex		
	Random Bias	Random t95S/N ^{0.5}	Bias	Random Bias	Random t95S/N ^{0.5}	Bias	Random Bias	Random t95S/N ^{0.5}	Bias	Random Bias	Random t95S/N ^{0.5}	Bias
	L/min	L/min	L/min	L/min	L/min	L/min	L/min	L/min	L/min	L/min	L/min	L/min
245.07	38.04	1.164281	16.82	1.623467	-27.30	1.198025	38.78	1.180883	34.53	0.711559	24.65	0.85409
245.07	34.30	0.586083	10.44	0.564311	-31.64	0.490163	26.13	0.115611	26.13	0.115611	17.64	0.328358
196.22	24.38	0.455627	7.65	2.248196	-20.49	1.853879	19.53	1.048475	19.53	1.048475	11.13	0.747537
191.20	26.76	0.137384	7.70	0.285752	-20.84	0.239483	15.98	0.312721	15.98	0.312721	8.79	0.375527
155.47	19.53	1.172231	6.98	1.886982	-12.72	1.670686	9.98	0.288162	9.98	0.288162	4.29	0.178255
155.19	15.64	0.199558	1.57	0.127173	-19.19	0.402888	16.29	0.638965	16.29	0.638965	9.19	0.2
102.99	8.35	1.167861	0.31	0.968482	-6.34	0.742792	8.74	0.678615	8.74	0.678615	3.18	0.720163
102.16	10.05	0.133369	-0.23	0.155334	-9.14	0.278667	9.98	0.288162	9.98	0.288162	4.29	0.178255
154.91	16.89	0.277923	-0.71	0.951224	-22.44	1.040483	15.90	0.435503	15.90	0.435503	9.42	0.36883
156.03	15.86	0.155645	1.75	0.195453	-21.43	0.277347	21.78	0.510226	21.78	0.510226	15.21	0.376051
200.13	22.05	0.599587	2.42	0.774063	-27.95	0.997932	21.14	0.230634	21.14	0.230634	12.56	0.278538
202.08	20.98	0.209255	1.44	0.142743	-28.80	0.235883	35.19	1.231332	35.19	1.231332	39.66	0.324677
246.46	33.02	0.220348	8.19	0.683476	-36.37	0.86198	39.07	0.370062	39.07	0.370062	39.66	0.324677
242.00	37.37	0.11658	14.00	0.14304	-29.07	0.370062	39.66	0.324677	39.66	0.324677	39.66	0.324677

Flow meter calibration data summary.

Percent Flow	FT-720 Vortex Flow			PF-001 Wetted Ultra			PF-002 Clamp-on Ultra			FT-730 Vortex			FT-800 Vortex			Num of ptst95 N
	Ave L/min	Std L/min	Ave L/min	Ave L/min	Std L/min	Ave L/min	Ave L/min	Std L/min	Ave L/min	Ave L/min	Std L/min	Ave L/min	Std L/min	Ave L/min	Std L/min	
100	283.10	5.11	261.88	7.12	217.77	5.26	283.84	5.18				103.55	141.51	245.07	77.00	2
100	279.37	2.57	255.51	2.48	213.43	2.15	279.59	3.12				103.55	141.51	245.07	77.00	2
80	220.60	0.83	203.87	4.09	175.73	3.37	220.87	1.55	210.40	1.24	89.88	106.34	196.22	15.00	2.131	
80	217.96	0.56	198.90	1.17	170.36	0.98	217.33	0.47	208.84	1.34	91.55	99.65	191.20	67.00	2	
60	175.00	2.51	162.45	4.05	142.75	3.58	175.00	2.25	166.60	1.60	84.01	71.45	155.47	20.00	2.086	
60	170.83	0.68	156.76	0.43	136.00	1.37	171.17	1.06	163.98	1.27	84.01	71.18	155.19	46.00	2	
40	111.35	2.71	103.30	2.24	96.65	1.72	111.74	1.57	106.17	1.67	77.87	25.12	102.99	23.00	2.069	
40	112.20	0.68	101.92	0.79	93.02	1.41	112.14	1.46	106.45	0.90	77.87	24.28	102.16	103.00	2	
60	171.80	0.76	154.20	2.61	132.47	2.85	171.20	1.75	164.10	0.55	84.29	70.62	154.91	30.00	2	
60	171.89	0.57	157.78	0.72	134.59	1.02	171.93	1.60	165.44	1.36	84.29	71.73	156.03	54.00	2	
80	222.18	1.72	202.55	2.22	172.18	2.87	221.91	1.47	215.33	1.08	90.71	109.41	200.13	33.00	2	
80	223.06	0.74	203.52	0.50	173.28	0.83	223.22	0.82	214.64	0.98	91.27	110.81	202.08	50.00	2	
100	279.48	0.51	254.65	1.58	210.09	2.00	281.65	2.85			104.95	141.51	246.46	23.00	2.069	
100	279.36	0.48	256.00	0.59	212.93	1.54	281.65	1.35			100.48	141.51	242.00	69.00	2	
															Bias Errors:	
															Tank Dim: 0.5	
															Therm. Exp: 1.5	
															Bubble Cal: 3	
															Prop. Vary: 1.8	
															Bias RMS 3.839271	

Flow meter calibration data.

12.07611	12	4	34	171	157	135	172	165	109	0	0	165	22	0
12.0775	12	4	39	171	157	135	172	165	109	0	0	165	22	0
12.07889	12	4	44	171	157	135	172	165	109	0	0	165	22	0
12.08028	12	4	49	171	157	135	172	163	109	0	0	165	22	0
12.08167	12	4	54	171	157	135	172	163	109	0	0	165	21	2
12.08306	12	4	59	171	157	137	172	163	109	0	0	161	21	3
12.08444	12	5	4	171	157	137	172	163	109	0	0	161	21	6
12.08583	12	5	9	171	157	137	170	166	109	0	0	161	21	7
12.08722	12	5	14	171	157	137	170	163	109	0	0	161	21	9
12.08861	12	5	19	171	157	137	170	163	109	0	0	161	20	11
12.09	12	5	24	171	157	137	170	163	109	0	0	161	20	13
12.09139	12	5	29	171	157	137	170	163	109	0	0	161	20	15
12.09278	12	5	34	171	156	137	170	166	109	0	0	161	20	17
12.09417	12	5	39	171	156	137	170	163	109	0	0	161	19	19
12.09556	12	5	44	171	156	137	170	163	109	0	0	161	19	21
12.09694	12	5	49	171	156	137	170	163	109	0	0	161	19	22
12.09833	12	5	54	171	156	137	170	163	109	0	0	161	19	25
12.09972	12	5	59	171	156	134	170	163	109	0	0	165	19	26
12.10083	12	6	3	171	156	134	170	163	109	0	0	165	18	28
12.10222	12	6	8	171	156	134	170	163	109	0	0	165	18	29
12.10361	12	6	13	170	156	134	170	163	109	0	0	165	18	29
12.105	12	6	18	170	156	134	170	166	109	0	0	165	19	25
12.10639	12	6	23	170	156	134	170	159	109	0	0	150	19	20
12.10778	12	6	28	145	156	134	150	124	117	0	0	120	20	14
12.10917	12	6	33	127	145	128	127	118	118	0	0	120	21	10
12.11056	12	6	38	127	137	117	127	118	118	0	0	120	21	3
12.11194	12	6	43	127	130	117	127	118	118	0	0	120	22	0
12.11333	12	6	48	121	125	112	122	111	119	0	0	108	22	0
12.11472	12	6	53	115	119	106	116	108	120	0	0	108	22	0
12.11611	12	6	58	115	113	106	110	108	120	0	0	108	22	0
12.1175	12	7	3	115	113	101	110	105	120	0	0	108	22	0
12.11889	12	7	8	115	107	101	110	105	120	0	0	105	22	0
12.12028	12	7	13	115	107	101	110	107	120	0	0	105	22	0
12.12167	12	7	18	115	107	101	110	107	120	0	0	105	22	0
12.12306	12	7	23	115	107	96	110	107	120	0	0	105	22	0
12.12444	12	7	28	115	107	96	110	107	120	0	0	105	22	0
12.12583	12	7	33	115	107	96	110	104	120	0	0	105	22	0
12.12722	12	7	38	115	102	96	110	104	120	0	0	105	22	0
12.12861	12	7	43	109	102	96	110	104	120	0	0	105	22	0
12.13	12	7	48	109	102	96	110	104	120	0	0	105	22	0
12.13139	12	7	53	109	102	96	110	104	120	0	0	105	22	0
12.13278	12	7	58	109	102	96	113	108	120	0	0	105	22	0
12.13417	12	8	3	109	102	96	113	108	120	0	0	105	22	0
12.13556	12	8	8	109	102	96	113	108	120	0	0	106	22	0
12.13694	12	8	13	109	102	96	113	105	120	0	0	106	22	0
12.13833	12	8	18	109	102	96	113	105	120	0	0	106	22	0
12.13972	12	8	23	109	102	96	113	105	120	0	0	106	22	0
12.14111	12	8	28	109	102	96	113	105	120	0	0	106	22	0
12.1425	12	8	33	109	102	96	113	105	120	0	0	106	22	0
12.14389	12	8	38	109	102	96	113	108	120	0	0	106	22	0
12.14528	12	8	43	112	102	96	113	108	120	0	0	106	22	1
12.14667	12	8	48	112	102	96	113	108	120	0	0	106	22	3
12.14806	12	8	53	112	102	96	113	108	119	0	0	106	22	4
12.14944	12	8	58	112	102	96	114	108	119	0	0	106	21	6
12.15083	12	9	3	112	102	96	114	108	119	0	0	106	21	8
12.15222	12	9	8	112	102	96	114	108	119	0	0	108	21	10
12.15361	12	9	13	112	102	96	114	108	119	0	0	108	21	11
12.155	12	9	18	112	102	96	114	108	119	0	0	108	21	14
12.15639	12	9	23	112	102	95	114	108	119	0	0	108	21	15
12.15778	12	9	28	112	102	95	114	108	119	0	0	108	21	17
12.15917	12	9	33	112	102	95	114	108	119	0	0	108	20	18
12.16056	12	9	38	112	102	95	114	106	119	0	0	108	20	20
12.16778	12	10	4	112	102	95	112	106	119	0	0	108	20	30
12.16917	12	10	9	112	102	95	112	106	119	0	0	108	19	31
12.17056	12	10	14	112	102	95	112	106	119	0	0	108	19	31
12.17194	12	10	19	112	102	95	112	106	119	0	0	108	19	32
12.17333	12	10	24	112	102	94	112	106	119	0	0	108	19	32
12.17444	12	10	28	112	102	94	112	106	119	0	0	108	19	32
12.17583	12	10	33	112	102	94	112	106	119	0	0	108	19	32
12.17722	12	10	38	112	102	94	112	107	119	0	0	108	19	32
12.17861	12	10	43	112	102	94	112	107	119	0	0	108	19	32
12.18	12	10	48	112	102	94	112	107	119	0	0	108	19	32
12.18139	12	10	53	112	102	94	112	107	120	0	0	108	19	32
12.18278	12	10	58	112	102	94	111	107	120	0	0	108	19	32
12.18417	12	11	3	112	102	94	111	107	120	0	0	108	19	32
12.18556	12	11	8	112	102	94	111	107	120	0	0	107	19	32
12.18694	12	11	13	112	102	94	111	107	120	0	0	107	19	32
12.18833	12	11	18	112	102	94	111	107	120	0	0	107	19	32
12.18972	12	11	23	112	102	93	111	107	120	0	0	107	19	32

Flow meter calibration data.

12.19111	12	11	28	112	102	93	111	107	120	0	0	107	19	32
12.1925	12	11	33	112	102	93	111	107	120	0	0	107	19	32
12.19389	12	11	38	112	103	93	111	105	120	0	0	107	19	32
12.19528	12	11	43	112	103	93	111	109	119	0	0	107	19	32
12.19667	12	11	48	112	103	93	111	109	119	0	0	107	19	32
12.19806	12	11	53	112	103	93	111	109	119	0	0	107	19	32
12.19944	12	11	58	112	103	93	113	106	119	0	0	107	19	32
12.20083	12	12	3	112	103	93	113	106	119	0	0	107	19	32
12.20222	12	12	8	112	103	93	113	106	119	0	0	108	19	32
12.20361	12	12	13	112	103	93	113	106	119	0	0	108	19	32
12.205	12	12	18	112	103	93	113	106	119	0	0	108	19	31
12.20639	12	12	23	112	103	92	113	106	119	0	0	108	19	29
12.20778	12	12	28	112	103	92	113	106	119	0	0	108	19	25
12.20917	12	12	33	112	103	92	113	106	119	0	0	108	20	18
12.21056	12	12	38	112	103	92	113	106	119	0	0	108	21	13
12.21194	12	12	43	113	103	92	113	106	120	0	0	108	21	7
12.21333	12	12	48	113	103	92	113	106	120	0	0	108	22	3
12.21472	12	12	53	113	103	92	113	106	120	0	0	108	22	0
12.21611	12	12	58	113	103	92	112	106	120	0	0	108	22	0
12.2175	12	13	3	113	103	92	112	106	120	0	0	108	22	0
12.21889	12	13	8	113	103	92	112	106	120	0	0	107	22	0
12.22028	12	13	13	113	103	92	112	106	120	0	0	107	22	0
12.22167	12	13	18	113	103	92	112	106	120	0	0	107	22	0
12.22306	12	13	23	113	103	92	112	106	120	0	0	107	22	0
12.22444	12	13	28	113	103	92	112	106	120	0	0	107	22	0
12.22583	12	13	33	113	103	92	112	106	120	0	0	107	22	0
12.22722	12	13	38	113	102	92	112	106	120	0	0	107	22	0
12.22861	12	13	43	112	102	92	112	106	120	0	0	107	22	0
12.23	12	13	48	112	102	92	112	106	120	0	0	107	22	0
12.23139	12	13	53	112	102	92	112	106	120	0	0	107	22	1
12.23278	12	13	58	112	102	92	114	107	120	0	0	107	22	2
12.23417	12	14	3	112	102	92	114	107	120	0	0	107	22	4
12.23556	12	14	8	112	102	92	114	107	120	0	0	108	21	6
12.23694	12	14	13	112	102	92	114	107	120	0	0	108	21	8
12.23833	12	14	18	112	102	92	114	107	120	0	0	108	21	9
12.23972	12	14	23	112	102	95	114	107	120	0	0	108	21	11
12.24111	12	14	28	112	102	95	114	107	120	0	0	108	21	13
12.24245	12	14	33	112	102	95	114	107	120	0	0	108	21	15
12.24389	12	14	38	112	101	95	114	107	120	0	0	108	21	16
12.24528	12	14	43	113	101	95	114	107	120	0	0	108	21	18
12.24667	12	14	48	113	101	95	114	107	120	0	0	108	20	20
12.24806	12	14	53	113	101	95	109	107	120	0	0	108	20	22
12.24944	12	14	58	113	101	95	109	106	120	0	0	108	20	23
12.25083	12	15	3	113	101	95	109	106	120	0	0	108	20	25
12.25222	12	15	8	113	101	95	109	106	120	0	0	104	20	27
12.25361	12	15	13	113	101	95	109	106	120	0	0	104	20	29
12.255	12	15	18	113	101	95	109	106	120	0	0	104	20	30
12.25639	12	15	23	113	101	92	109	106	120	0	0	104	19	31
12.25778	12	15	28	113	101	92	109	106	120	0	0	104	19	32
12.25917	12	15	33	113	101	92	109	106	120	0	0	104	19	32
12.26056	12	15	38	113	101	92	109	106	120	0	0	104	19	32
12.26194	12	15	43	111	101	92	109	106	120	0	0	104	19	32
12.26333	12	15	48	111	101	92	109	106	120	0	0	104	19	32
12.26472	12	15	53	111	101	92	112	106	120	0	0	104	19	32
12.26611	12	15	58	111	101	92	112	107	120	0	0	104	19	32
12.2675	12	16	3	111	101	92	112	107	120	0	0	104	19	32
12.26889	12	16	8	111	101	92	112	107	120	0	0	106	19	32
12.27028	12	16	13	111	101	92	112	107	120	0	0	106	19	32
12.27167	12	16	18	111	101	92	112	107	120	0	0	106	19	32
12.27306	12	16	23	111	101	92	112	107	120	0	0	106	19	32
12.27444	12	16	28	111	101	92	112	107	120	0	0	106	19	32
12.27611	12	16	34	111	101	92	112	107	120	0	0	106	19	32
12.2775	12	16	39	113	102	92	112	107	120	0	0	106	19	32
12.27889	12	16	44	113	102	92	112	107	120	0	0	106	19	32
12.28028	12	16	49	113	102	92	112	107	120	0	0	106	19	32
12.28167	12	16	54	113	102	92	113	107	120	0	0	106	19	32
12.28306	12	16	59	113	102	92	113	105	120	0	0	106	19	32
12.28444	12	17	4	113	102	92	113	105	120	0	0	106	19	32
12.28583	12	17	9	113	102	92	113	105	120	0	0	106	19	32
12.28722	12	17	14	113	102	92	113	105	120	0	0	106	19	32
12.28861	12	17	19	113	102	92	113	105	120	0	0	106	19	32
12.29	12	17	24	113	102	91	113	105	120	0	0	106	19	32
12.29139	12	17	29	113	102	91	113	105	120	0	0	106	19	32
12.29278	12	17	34	113	102	91	113	105	120	0	0	106	19	32
12.29417	12	17	39	111	100	91	113	105	120	0	0	106	19	31
12.29556	12	17	44	111	100	91	113	105	120	0	0	106	19	26
12.29694	12	17	49	111	100	91	113	105	120	0	0	106	20	22
12.29833	12	17	54	111	100	91	112	105	120	0	0	104	20	15
12.29972	12	17	59	117	100	91	118	143	118	0	0	129	21	10

Flow meter calibration data.

12.30111	12	18	4	160	105	99	160	160	111	0	0	159	21	4
12.3025	12	18	9	166	123	106	160	160	111	0	0	159	22	1
12.30389	12	18	14	166	131	112	160	160	111	0	0	159	22	1
12.30528	12	18	19	166	136	117	166	160	111	0	0	159	22	1
12.30667	12	18	24	166	136	122	166	160	111	0	0	160	22	1
12.30806	12	18	29	166	142	122	166	164	109	0	0	166	22	1
12.30944	12	18	34	171	148	127	166	164	109	0	0	166	22	1
12.31083	12	18	39	171	148	127	166	164	109	0	0	166	22	1
12.31222	12	18	44	171	148	127	172	164	109	0	0	166	22	1
12.31361	12	18	49	171	153	127	172	164	109	0	0	166	22	1
12.315	12	18	54	171	153	127	172	164	109	0	0	166	22	1
12.31639	12	18	59	171	153	132	172	164	109	0	0	166	22	1
12.31778	12	19	4	171	153	132	172	164	109	0	0	166	22	1
12.31917	12	19	9	171	153	132	172	164	109	0	0	166	22	0
12.32056	12	19	14	171	153	132	172	164	109	0	0	166	22	0
12.32194	12	19	19	171	153	132	172	164	109	0	0	166	22	0
12.32333	12	19	24	171	153	132	172	164	109	0	0	166	22	0
12.32472	12	19	29	171	153	132	172	164	109	0	0	164	22	0
12.32611	12	19	34	172	153	132	172	164	109	0	0	164	22	0
12.3275	12	19	39	172	153	132	172	164	109	0	0	164	22	0
12.32889	12	19	44	172	156	132	172	164	109	0	0	164	22	0
12.33028	12	19	49	172	156	132	172	164	109	0	0	164	22	0
12.33167	12	19	54	172	156	132	172	164	109	0	0	164	22	0
12.33306	12	19	59	172	156	135	172	164	109	0	0	164	22	0
12.33444	12	20	4	172	156	135	172	164	109	0	0	164	22	0
12.33583	12	20	9	172	156	135	172	164	109	0	0	164	22	0
12.33722	12	20	14	172	156	135	172	164	109	0	0	164	22	0
12.33861	12	20	19	172	156	135	172	164	109	0	0	164	21	2
12.34	12	20	24	172	156	135	172	164	109	0	0	164	21	4
12.34139	12	20	29	172	156	135	172	164	109	0	0	164	21	6
12.34278	12	20	34	173	156	135	172	164	109	0	0	164	21	8
12.34417	12	20	39	173	156	135	172	164	109	0	0	164	21	10
12.34556	12	20	44	173	156	135	169	164	109	0	0	164	20	12
12.34694	12	20	49	173	157	135	169	164	109	0	0	164	20	14
12.34833	12	20	54	173	157	135	169	167	108	0	0	164	20	15
12.34972	12	20	59	173	157	135	169	164	108	0	0	164	20	18
12.35111	12	21	4	173	157	135	169	164	108	0	0	164	19	19
12.3525	12	21	9	173	157	135	169	164	108	0	0	164	19	22
12.35389	12	21	14	173	157	135	169	164	108	0	0	164	19	23
12.35528	12	21	19	173	157	135	169	164	108	0	0	164	19	25
12.35667	12	21	24	173	157	135	169	164	108	0	0	164	19	27
12.35806	12	21	29	173	157	135	169	164	108	0	0	164	18	29
12.35944	12	21	34	172	157	135	169	164	108	0	0	164	18	29
12.36083	12	21	39	172	157	135	169	164	108	0	0	164	18	29
12.36222	12	21	44	172	157	135	171	164	108	0	0	164	19	25
12.36361	12	21	49	172	157	135	171	164	108	0	0	164	20	19
12.365	12	21	54	172	157	135	171	164	108	0	0	164	20	15
12.36639	12	21	59	172	157	134	171	165	109	0	0	164	21	9
12.36778	12	22	4	172	157	134	171	165	109	0	0	164	21	6
12.36917	12	22	9	172	157	134	171	165	109	0	0	164	22	1
12.37056	12	22	14	172	157	134	171	165	109	0	0	164	22	1
12.37194	12	22	19	172	157	134	171	165	109	0	0	164	22	1
12.37333	12	22	24	172	157	134	171	165	109	0	0	164	22	1
12.37472	12	22	29	172	157	134	171	165	109	0	0	165	22	1
12.37583	12	22	33	171	157	134	171	165	109	0	0	165	22	1
12.37722	12	22	38	171	157	134	171	165	109	0	0	165	22	1
12.37861	12	22	43	171	157	134	173	165	109	0	0	165	22	1
12.38028	12	22	49	171	158	134	173	165	109	0	0	165	22	1
12.38167	12	22	54	171	158	134	173	165	109	0	0	165	22	1
12.38306	12	22	59	171	158	134	173	167	109	0	0	165	22	1
12.38444	12	23	4	171	158	134	173	167	109	0	0	165	22	1
12.38556	12	23	8	171	158	134	173	167	109	0	0	165	22	1
12.38694	12	23	13	171	158	134	173	167	109	0	0	165	22	0
12.38833	12	23	18	171	158	134	173	167	109	0	0	165	22	0
12.38972	12	23	23	171	158	134	173	167	109	0	0	165	22	0
12.39111	12	23	28	171	158	134	173	167	109	0	0	165	22	0
12.3925	12	23	33	172	158	134	173	167	109	0	0	165	22	0
12.39389	12	23	38	172	158	134	173	167	109	0	0	165	22	0
12.39528	12	23	43	172	158	134	172	164	109	0	0	165	22	0
12.39667	12	23	48	172	158	134	172	164	109	0	0	165	22	0
12.39806	12	23	53	172	158	134	172	164	109	0	0	165	22	0
12.39944	12	23	58	172	158	134	172	164	109	0	0	165	22	0
12.40083	12	24	3	172	158	134	172	164	109	0	0	165	22	0
12.40222	12	24	8	172	158	134	172	164	109	0	0	165	22	0
12.40361	12	24	13	172	158	134	172	164	109	0	0	165	22	0
12.40405	12	24	18	172	158	134	172	164	109	0	0	165	22	0
12.40639	12	24	23	172	158	134	172	164	109	0	0	165	22	0
12.40778	12	24	28	172	158	134	172	167	109	0	0	166	22	0
12.40917	12	24	33	172	158	134	172	167	109	0	0	166	22	0

Flow meter calibration data.

12.41056	12	24	38	172	158	134	172	167	109	0	0	166	22	0
12.41194	12	24	43	172	158	134	174	167	109	0	0	166	22	1
12.41333	12	24	48	172	159	134	174	167	109	0	0	166	21	3
12.41472	12	24	53	172	159	134	174	167	109	0	0	166	21	5
12.41611	12	24	58	172	159	137	174	167	108	0	0	166	21	6
12.4175	12	25	3	172	159	137	174	167	108	0	0	166	21	9
12.41889	12	25	8	172	159	137	174	167	108	0	0	166	20	10
12.42028	12	25	13	172	159	137	174	167	108	0	0	166	20	13
12.42167	12	25	18	172	159	137	174	167	108	0	0	166	20	14
12.42306	12	25	23	172	159	137	174	167	108	0	0	166	20	16
12.42444	12	25	28	172	159	137	174	167	108	0	0	166	20	18
12.42583	12	25	33	174	159	137	174	167	108	0	0	166	19	20
12.42722	12	25	38	174	159	137	174	167	108	0	0	166	19	22
12.42861	12	25	43	174	159	137	173	167	108	0	0	166	19	24
12.43	12	25	48	174	159	137	173	167	108	0	0	166	19	26
12.43139	12	25	53	174	159	137	173	167	108	0	0	166	18	28
12.43278	12	25	58	174	159	137	173	167	108	0	0	166	18	29
12.43417	12	26	3	174	159	138	173	167	108	0	0	166	18	30
12.43556	12	26	8	174	159	138	173	167	108	0	0	166	18	31
12.43694	12	26	13	174	159	138	173	167	108	0	0	166	18	31
12.43833	12	26	18	174	159	138	173	167	108	0	0	166	18	32
12.43972	12	26	23	174	159	138	173	167	108	0	0	166	18	30
12.44111	12	26	28	174	159	138	173	164	108	0	0	166	19	25
12.4425	12	26	33	174	159	138	173	164	108	0	0	164	19	19
12.44389	12	26	38	173	159	138	173	167	108	0	0	164	20	15
12.44528	12	26	43	173	159	138	172	167	108	0	0	164	21	8
12.44667	12	26	48	173	158	138	172	167	108	0	0	164	21	4
12.44806	12	26	53	173	158	138	172	163	108	0	0	164	22	1
12.44944	12	26	58	173	158	138	172	163	109	0	0	164	22	1
12.45083	12	27	3	173	158	134	172	163	109	0	0	164	22	1
12.45222	12	27	8	173	158	134	172	166	109	0	0	164	22	1
12.45361	12	27	13	173	158	134	172	166	109	0	0	164	22	1
12.45528	12	27	19	173	158	134	172	166	109	0	0	164	22	1
12.45667	12	27	24	173	158	134	172	166	109	0	0	169	22	1
12.45806	12	27	29	181	158	134	187	199	103	0	0	199	22	1
12.45944	12	27	34	195	164	140	195	199	100	0	0	199	22	1
12.46083	12	27	39	195	170	140	195	199	99	0	0	199	22	1
12.46222	12	27	44	202	170	146	202	199	98	0	0	199	22	1
12.46361	12	27	49	202	176	151	202	199	98	0	0	199	22	1
12.465	12	27	54	202	176	151	202	199	98	0	0	198	22	0
12.46639	12	27	59	202	181	151	208	211	95	0	0	209	22	0
12.46778	12	28	4	209	181	157	208	211	94	0	0	209	22	0
12.46917	12	28	9	209	188	157	208	211	93	0	0	209	22	0
12.47056	12	28	14	215	188	157	215	211	93	0	0	209	22	0
12.47194	12	28	19	215	193	162	215	211	93	0	0	209	22	0
12.47333	12	28	24	215	193	162	215	211	93	0	0	209	22	0
12.47472	12	28	29	215	193	162	215	208	93	0	0	210	22	0
12.47611	12	28	34	215	193	162	215	216	91	0	0	216	22	0
12.4775	12	28	39	220	198	162	220	216	91	0	0	216	22	0
12.47889	12	28	44	220	198	168	220	216	90	0	0	216	22	0
12.48028	12	28	49	220	198	168	220	216	90	0	0	216	22	0
12.48167	12	28	54	220	198	168	220	216	90	0	0	216	22	0
12.48306	12	28	59	220	198	168	220	216	90	0	0	216	22	0
12.48444	12	29	4	220	198	168	220	216	90	0	0	216	22	0
12.48583	12	29	9	220	203	168	220	216	90	0	0	216	22	0
12.48722	12	29	14	220	203	173	220	216	90	0	0	216	22	0
12.48861	12	29	19	220	203	173	220	216	90	0	0	216	22	0
12.49	12	29	24	220	203	173	220	213	90	0	0	216	22	0
12.49139	12	29	29	220	203	173	220	213	90	0	0	216	22	0
12.49278	12	29	34	220	203	173	220	213	90	0	0	215	22	0
12.49417	12	29	39	223	203	173	223	213	90	0	0	215	22	0
12.49556	12	29	44	223	203	173	223	213	90	0	0	215	22	0
12.49694	12	29	49	223	203	173	223	216	90	0	0	215	22	0
12.49833	12	29	54	223	203	173	223	216	90	0	0	215	22	0
12.49972	12	29	59	223	203	173	223	216	89	0	0	215	22	0
12.50111	12	30	4	223	203	173	223	216	89	0	0	215	22	0
12.5025	12	30	9	223	204	173	223	216	89	0	0	215	22	0
12.50389	12	30	14	223	204	174	223	216	89	0	0	215	22	0
12.50528	12	30	19	223	204	174	223	216	89	0	0	215	22	0
12.50667	12	30	24	223	204	174	223	216	89	0	0	215	22	0
12.50806	12	30	29	223	204	174	223	216	89	0	0	215	22	0
12.50944	12	30	34	223	204	174	223	216	89	0	0	214	22	0
12.51083	12	30	39	224	204	174	223	216	89	0	0	214	22	0
12.51222	12	30	44	224	204	174	223	216	89	0	0	214	22	0
12.51361	12	30	49	224	204	174	223	215	89	0	0	214	22	0
12.515	12	30	54	224	204	174	223	215	89	0	0	214	22	0
12.51639	12	30	59	224	204	174	223	215	89	0	0	214	22	0
12.51778	12	31	4	224	204	174	223	215	89	0	0	214	22	0
12.51917	12	31	9	224	204	174	223	215	89	0	0	214	22	0

Flow meter calibration data.

12.52056	12	31	14	224	204	174	223	215	89	0	0	214	22	0
12.52194	12	31	19	224	204	174	223	215	89	0	0	214	22	0
12.52333	12	31	24	224	204	174	223	215	89	0	0	214	22	0
12.52472	12	31	29	224	204	174	223	215	89	0	0	214	22	0
12.52611	12	31	34	224	204	174	223	215	89	0	0	214	22	0
12.5275	12	31	39	224	204	174	223	215	89	0	0	214	22	0
12.52889	12	31	44	224	204	174	223	215	89	0	0	214	22	1
12.53028	12	31	49	224	204	174	223	215	89	0	0	214	21	3
12.53167	12	31	54	224	204	174	223	215	89	0	0	214	21	5
12.53306	12	31	59	224	204	174	223	215	89	0	0	214	21	7
12.53444	12	32	4	224	204	174	223	215	89	0	0	214	20	9
12.53583	12	32	9	224	203	174	223	215	89	0	0	214	20	11
12.53694	12	32	13	224	203	173	223	215	89	0	0	214	20	13
12.53833	12	32	18	224	203	173	223	215	89	0	0	214	19	15
12.53972	12	32	23	224	203	173	223	215	89	0	0	214	19	17
12.54111	12	32	28	224	203	173	223	215	89	0	0	214	19	19
12.5425	12	32	33	224	203	173	223	215	89	0	0	215	19	22
12.54389	12	32	38	222	203	173	222	215	89	0	0	215	18	23
12.54528	12	32	43	222	203	173	222	215	89	0	0	215	18	26
12.54667	12	32	48	222	203	173	222	215	89	0	0	215	18	27
12.54806	12	32	53	222	203	173	222	215	89	0	0	215	18	26
12.54944	12	32	58	222	203	173	222	212	89	0	0	215	19	23
12.55083	12	33	3	222	203	173	222	212	89	0	0	215	19	19
12.55222	12	33	8	222	204	173	222	212	89	0	0	215	20	14
12.55361	12	33	13	222	204	174	222	212	89	0	0	215	20	11
12.555	12	33	18	222	204	174	222	215	89	0	0	215	20	6
12.55639	12	33	23	222	204	174	222	215	89	0	0	215	21	2
12.55778	12	33	28	222	204	174	222	215	89	0	0	215	21	1
12.55917	12	33	33	222	204	174	222	215	89	0	0	214	21	1
12.56056	12	33	38	223	204	174	224	215	89	0	0	214	22	1
12.56194	12	33	43	223	204	174	224	215	89	0	0	214	22	1
12.56333	12	33	48	223	204	174	224	215	89	0	0	214	22	1
12.56472	12	33	53	223	204	174	224	215	89	0	0	214	22	1
12.56611	12	33	58	223	204	174	224	215	89	0	0	214	22	1
12.5675	12	34	3	223	204	174	224	215	89	0	0	214	22	1
12.56889	12	34	8	223	203	174	224	215	89	0	0	214	22	1
12.57028	12	34	13	223	203	172	224	212	89	0	0	214	22	1
12.57167	12	34	18	223	203	172	224	215	89	0	0	214	21	1
12.57306	12	34	23	223	203	172	224	215	89	0	0	214	21	3
12.57444	12	34	28	223	203	172	224	215	89	0	0	214	21	5
12.57583	12	34	33	223	203	172	224	215	89	0	0	215	21	7
12.57722	12	34	38	223	203	172	224	215	89	0	0	215	20	9
12.57861	12	34	43	223	203	172	224	215	89	0	0	215	20	11
12.58	12	34	48	223	203	172	224	215	89	0	0	215	20	14
12.58139	12	34	53	223	203	172	224	215	89	0	0	215	19	15
12.58278	12	34	58	223	203	172	224	215	89	0	0	215	19	18
12.58417	12	35	3	223	203	172	224	215	89	0	0	215	19	20
12.58556	12	35	8	223	204	172	224	215	89	0	0	215	19	22
12.58694	12	35	13	223	204	174	224	215	89	0	0	215	18	24
12.58833	12	35	18	223	204	174	224	213	89	0	0	215	18	26
12.58972	12	35	23	223	204	174	224	213	89	0	0	215	18	26
12.59111	12	35	28	223	204	174	224	216	87	0	0	189	19	25
12.5925	12	35	33	250	204	174	252	71	72	0	0	74	19	22
12.59389	12	35	38	261	211	179	258	71	67	0	0	74	19	19
12.59528	12	35	43	267	225	187	265	62	64	0	0	67	20	15
12.59667	12	35	48	273	231	192	272	61	63	0	0	60	20	12
12.59806	12	35	53	273	236	198	277	64	61	0	0	60	20	9
12.59944	12	35	58	273	236	198	277	61	61	0	0	60	21	7
12.60083	12	36	3	273	243	198	277	60	60	0	0	60	21	3
12.60222	12	36	8	273	243	204	277	60	60	0	0	60	21	1
12.60361	12	36	13	273	249	204	277	63	60	0	0	60	21	1
12.605	12	36	18	273	249	204	277	60	60	0	0	60	21	1
12.60639	12	36	23	279	249	204	277	58	59	0	0	60	22	1
12.60806	12	36	29	279	254	209	277	57	59	0	0	54	22	1
12.60944	12	36	34	279	254	209	277	63	59	0	0	63	22	1
12.61083	12	36	39	279	254	209	277	57	59	0	0	57	22	1
12.61222	12	36	44	279	254	209	277	66	59	0	0	64	22	1
12.61361	12	36	49	279	254	209	277	63	59	0	0	64	22	1
12.615	12	36	54	279	254	209	283	63	59	0	0	64	22	1
12.61639	12	36	59	279	254	209	283	58	59	0	0	58	22	1
12.61778	12	37	4	279	254	209	283	62	59	0	0	58	22	1
12.61917	12	37	9	279	254	209	283	62	59	0	0	58	22	0
12.62056	12	37	14	279	254	209	283	63	59	0	0	65	22	0
12.62194	12	37	19	279	254	209	283	59	59	0	0	59	22	0
12.62333	12	37	24	280	254	209	283	59	59	0	0	59	22	0
12.62472	12	37	29	280	256	212	283	56	58	0	0	59	22	0
12.62611	12	37	34	280	256	212	283	56	58	0	0	59	22	0
12.6275	12	37	39	280	256	212	283	62	58	0	0	59	22	0
12.62889	12	37	44	280	256	212	283	65	58	0	0	63	22	0

Flow meter calibration data.

12.63028	12	37	49	280	256	212	283	62	58	0	0	58	22	0
12.63167	12	37	54	280	256	212	284	63	58	0	0	62	22	0
12.63306	12	37	59	280	256	212	284	59	58	0	0	62	22	0
12.63444	12	38	4	280	256	212	284	59	58	0	0	56	22	0
12.63583	12	38	9	280	256	212	284	63	58	0	0	63	22	0
12.63722	12	38	14	280	256	212	284	59	58	0	0	63	22	0
12.63861	12	38	19	280	256	212	284	64	58	0	0	63	22	0
12.64	12	38	24	279	256	212	284	64	58	0	0	63	21	3
12.64139	12	38	29	279	256	212	284	58	58	0	0	57	21	5
12.64278	12	38	34	279	256	212	284	59	58	0	0	57	21	7
12.64417	12	38	39	279	256	212	284	59	58	0	0	57	20	9
12.64556	12	38	44	279	256	212	284	59	58	0	0	57	20	12
12.64694	12	38	49	279	256	212	284	63	58	0	0	63	20	14
12.64833	12	38	54	279	256	212	282	58	58	0	0	57	19	17
12.64972	12	38	59	279	256	212	282	58	58	0	0	62	19	19
12.65111	12	39	4	279	256	212	282	58	58	0	0	62	19	22
12.6525	12	39	9	279	256	212	282	58	58	0	0	57	18	24
12.65389	12	39	14	279	256	212	282	58	58	0	0	57	18	26
12.65528	12	39	19	279	256	212	282	60	58	0	0	57	18	26
12.65667	12	39	24	280	256	212	282	60	58	0	0	57	18	26
12.65806	12	39	29	280	256	211	282	60	58	0	0	57	19	25
12.65944	12	39	34	280	255	211	282	60	57	0	0	57	19	22
12.66083	12	39	39	280	255	211	282	56	57	0	0	53	19	19
12.66222	12	39	44	280	255	211	282	59	57	0	0	59	20	15
12.66333	12	39	48	280	255	211	282	62	57	0	0	59	20	12
12.66472	12	39	53	280	255	211	281	67	57	0	0	67	21	8
12.66611	12	39	58	280	255	211	281	64	57	0	0	67	21	5
12.6675	12	40	3	280	255	211	281	56	57	0	0	60	21	1
12.66889	12	40	8	280	255	211	281	56	57	0	0	56	21	1
12.67028	12	40	13	280	255	211	281	60	57	0	0	62	22	1
12.67167	12	40	18	280	255	211	281	65	57	0	0	62	22	1
12.67306	12	40	23	280	255	211	281	61	57	0	0	62	22	1
12.67444	12	40	28	280	255	212	281	62	57	0	0	62	22	1
12.67611	12	40	34	280	256	212	281	61	58	0	0	62	22	1
12.6775	12	40	39	280	256	212	281	61	58	0	0	62	22	1
12.67889	12	40	44	280	256	212	281	64	58	0	0	62	22	1
12.68028	12	40	49	280	256	212	281	60	58	0	0	62	22	1
12.68167	12	40	54	280	256	212	281	63	58	0	0	62	22	1
12.68306	12	40	59	280	256	212	281	60	58	0	0	62	22	1
12.68444	12	41	4	280	256	212	281	67	58	0	0	62	22	1
12.68583	12	41	9	280	256	212	281	63	58	0	0	63	22	0
12.68722	12	41	14	280	256	212	281	58	58	0	0	63	22	0
12.68861	12	41	19	280	256	212	281	61	58	0	0	63	22	0
12.69	41	24	279	256	212	281	58	58	0	0	63	22	0	
12.69139	12	41	29	279	256	214	281	63	58	0	0	63	22	0
12.69278	12	41	34	279	257	214	281	63	58	0	0	63	22	0
12.69417	12	41	39	279	257	214	281	64	58	0	0	63	21	0
12.69556	12	41	44	279	257	214	281	61	58	0	0	63	21	2
12.69694	12	41	49	279	257	214	281	61	58	0	0	63	21	6
12.69833	12	41	54	279	257	214	283	65	58	0	0	63	20	7
12.69944	12	41	58	279	257	214	283	60	58	0	0	63	20	10
12.70083	12	42	3	279	257	214	283	60	58	0	0	63	20	11
12.70222	12	42	8	279	257	214	283	60	58	0	0	63	19	15
12.70361	12	42	13	279	257	214	283	60	58	0	0	61	19	17
12.705	12	42	18	279	257	214	283	60	58	0	0	61	19	19
12.70639	12	42	23	279	257	214	283	58	58	0	0	61	18	22
12.70778	12	42	28	279	257	214	283	58	58	0	0	61	18	24
12.70917	12	42	33	279	256	214	283	54	57	0	0	55	18	27
12.71056	12	42	38	279	256	214	283	61	57	0	0	61	18	28
12.71194	12	42	43	279	256	214	283	63	57	0	0	61	18	26
12.71333	12	42	48	279	256	214	283	59	57	0	0	61	18	28
12.71472	12	42	53	279	256	214	280	58	57	0	0	61	18	29
12.71611	12	42	58	279	256	214	280	58	57	0	0	61	18	30
12.7175	12	43	3	279	256	214	280	61	57	0	0	61	18	30
12.71889	12	43	8	279	256	214	280	59	57	0	0	61	18	31
12.72028	12	43	13	279	256	214	280	63	57	0	0	61	18	32
12.72167	12	43	18	279	256	214	280	59	57	0	0	61	18	32
12.72306	12	43	23	279	256	214	280	62	57	0	0	61	18	32
12.72444	12	43	28	279	256	216	280	59	57	0	0	55	18	32
12.72583	12	43	33	279	256	216	280	59	57	0	0	55	18	32
12.72722	12	43	38	279	256	216	280	57	57	0	0	55	18	32
12.72861	12	43	43	279	256	216	280	56	57	0	0	62	18	32
12.73	43	48	279	256	216	280	61	57	0	0	60	18	32	
12.73139	12	43	53	279	256	216	278	60	57	0	0	60	18	32
12.73278	12	43	58	279	256	216	284	65	57	0	0	65	18	28
12.73417	12	44	3	279	256	216	284	61	57	0	0	57	19	24
12.73556	12	44	8	279	256	216	284	60	57	0	0	57	19	20
12.73694	12	44	13	279	256	216	284	62	57	0	0	63	20	17
12.73833	12	44	18	279	256	216	284	64	57	0	0	63	20	12

Flow meter calibration data.

12.73972	12	44	23	280	256	216	284	57	57	0	0	57	20	10
12.74111	12	44	28	280	256	215	284	57	57	0	0	57	21	6
12.7425	12	44	33	280	258	215	284	60	57	0	0	57	21	3
12.74389	12	44	38	280	258	215	278	60	57	0	0	57	21	1
12.74528	12	44	43	280	258	215	278	60	57	0	0	63	21	1
12.74667	12	44	48	280	258	215	278	58	57	0	0	63	22	1
12.74806	12	44	53	280	258	215	278	62	57	0	0	61	22	1
12.74944	12	44	58	280	258	215	284	62	57	0	0	61	22	1
12.75083	12	45	3	280	258	215	284	56	57	0	0	54	22	1
12.75222	12	45	8	280	258	215	284	56	57	0	0	54	22	1
12.75361	12	45	13	280	258	215	284	63	57	0	0	63	22	1
12.755	12	45	18	280	258	215	284	62	57	0	0	63	22	1
12.75667	12	45	24	280	258	215	284	62	57	0	0	63	22	1
12.75806	12	45	29	280	257	215	284	59	58	0	0	57	22	1
12.75944	12	45	34	280	257	215	284	62	58	0	0	57	22	1
12.76083	12	45	39	280	257	215	284	59	58	0	0	57	22	1
12.76222	12	45	44	280	257	215	284	59	58	0	0	57	22	1
12.76361	12	45	49	280	257	215	284	67	58	0	0	66	22	1
12.765	12	45	54	280	257	215	284	64	58	0	0	66	22	1
12.76639	12	45	59	280	257	215	283	60	58	0	0	58	22	1
12.76778	12	46	4	280	257	215	283	60	58	0	0	58	22	1
12.76917	12	46	9	280	257	215	283	59	58	0	0	58	22	1
12.77056	12	46	14	280	257	215	283	59	58	0	0	58	22	1
12.77194	12	46	19	280	257	215	283	66	58	0	0	66	22	1
12.77333	12	46	24	281	257	215	283	66	58	0	0	66	22	1
12.77472	12	46	29	281	257	215	283	70	58	0	0	66	22	1
12.77611	12	46	34	281	257	215	283	66	58	0	0	66	22	1
12.7775	12	46	39	281	257	215	283	62	58	0	0	60	22	1
12.77889	12	46	44	281	257	215	283	65	58	0	0	60	22	1
12.78028	12	46	49	281	257	215	283	61	58	0	0	60	22	1
12.78167	12	46	54	281	257	215	283	64	58	0	0	60	22	1
12.78306	12	46	59	281	257	215	280	64	58	0	0	60	22	1
12.78444	12	47	4	281	257	215	280	60	58	0	0	60	22	1
12.78583	12	47	9	281	257	215	280	65	58	0	0	60	22	1
12.78722	12	47	14	281	257	215	280	62	58	0	0	60	22	1
12.78861	12	47	19	281	257	215	280	58	58	0	0	60	22	1
12.79	12	47	24	283	257	215	280	63	58	0	0	67	22	1
12.79139	12	47	29	283	257	216	280	61	58	0	0	61	22	1
12.79278	12	47	34	283	257	216	280	62	58	0	0	61	22	1
12.79417	12	47	39	283	257	216	280	62	58	0	0	61	22	1
12.79556	12	47	44	283	257	216	280	58	58	0	0	61	22	1
12.79694	12	47	49	283	257	216	280	62	58	0	0	61	22	1
12.79833	12	47	54	283	257	216	280	58	58	0	0	61	22	1
12.79972	12	47	59	283	257	216	280	58	58	0	0	61	22	1
12.80111	12	48	4	283	257	216	280	61	58	0	0	61	22	1
12.8025	12	48	9	283	257	216	280	66	58	0	0	68	22	1
12.80389	12	48	14	283	257	216	280	63	58	0	0	60	22	1
12.80528	12	48	19	283	257	216	280	59	58	0	0	60	22	1
12.80667	12	48	24	281	257	216	280	62	58	0	0	60	22	1
12.80806	12	48	29	281	257	215	280	61	58	0	0	60	22	1
12.80917	12	48	33	281	257	215	280	59	58	0	0	59	22	1
12.81056	12	48	38	281	257	215	280	63	58	0	0	59	22	1
12.81194	12	48	43	281	257	3	280	60	58	0	0	59	22	1
12.81333	12	48	48	281	257	3	280	63	58	0	0	59	22	1
12.81472	12	48	53	281	257	3	280	57	58	0	0	59	22	1
12.81611	12	48	58	281	257	40	281	64	58	0	0	59	22	1
12.8175	12	49	3	281	257	17	281	60	58	0	0	65	22	1
12.81889	12	49	8	281	257	214	281	64	58	0	0	65	22	1
12.82028	12	49	13	281	257	214	281	64	58	0	0	65	22	1
12.82167	12	49	18	281	257	214	281	61	58	0	0	59	22	1
12.82306	12	49	23	280	257	214	281	58	58	0	0	59	22	1
12.82444	12	49	281	280	257	214	281	61	58	0	0	59	22	1
12.82583	12	49	33	280	259	214	281	61	58	0	0	59	22	1
12.82722	12	49	38	280	259	214	281	61	58	0	0	59	22	1
12.82861	12	49	43	280	259	214	281	61	58	0	0	57	22	1
12.83	12	49	48	280	259	214	281	60	58	0	0	60	22	1
12.83139	12	49	53	280	259	214	281	55	58	0	0	54	22	1
12.83278	12	49	58	280	259	214	280	58	58	0	0	60	22	1
12.83417	12	50	3	280	259	214	280	61	58	0	0	61	22	1
12.83556	12	50	8	280	259	213	280	61	58	0	0	61	22	1
12.83694	12	50	13	280	259	213	280	65	58	0	0	66	22	1
12.83833	12	50	18	280	259	213	280	62	58	0	0	58	22	1
12.83972	12	50	23	280	259	213	280	58	58	0	0	58	22	1
12.84111	12	50	28	280	259	213	280	69	58	0	0	63	22	1
12.8425	12	50	33	260	257	213	261	111	73	0	0	115	22	1
12.84389	12	50	38	234	234	196	233	119	88	0	0	122	22	1

Panel Temperature Data During Freezing

CRIT-Net 99 POINT DATA FILE		TEST-DATE: Tue Jun 4 1994 10:27:11 am		TEST-TIME		FT1730		FT1800		FT1860		FT1920		FT1980		FT2040		FT2100		FT2160		FT220		FT2260		FT230		FT2360		FT2420		FT2480		FT2540		FT2600		FT2660		FT2720		FT2780		FT2840		FT2900		FT2960		FT2980		FT2986		FT2992		FT2998		FT3004		FT3010		FT3016		FT3022		FT3028		FT3034		FT3040		FT3046		FT3052		FT3058		FT3064		FT3070		FT3076		FT3082		FT3088		FT3094		FT3100		FT3106		FT3112		FT3118		FT3124		FT3130		FT3136		FT3142		FT3148		FT3154		FT3160		FT3166		FT3172		FT3178		FT3184		FT3190		FT3196		FT3202		FT3208		FT3214		FT3220		FT3226		FT3232		FT3238		FT3244		FT3250		FT3256		FT3262		FT3268		FT3274		FT3280		FT3286		FT3292		FT3298		FT3304		FT3310		FT3316		FT3322		FT3328		FT3334		FT3340		FT3346		FT3352		FT3358		FT3364		FT3370		FT3376		FT3382		FT3388		FT3394		FT3400		FT3406		FT3412		FT3418		FT3424		FT3430		FT3436		FT3442		FT3448		FT3454		FT3460		FT3466		FT3472		FT3478		FT3484		FT3490		FT3496		FT3502		FT3508		FT3514		FT3520		FT3526		FT3532		FT3538		FT3544		FT3550		FT3556		FT3562		FT3568		FT3574		FT3580		FT3586		FT3592		FT3598		FT3604		FT3610		FT3616		FT3622		FT3628		FT3634		FT3640		FT3646		FT3652		FT3658		FT3664		FT3670		FT3676		FT3682		FT3688		FT3694		FT3700		FT3706		FT3712		FT3718		FT3724		FT3730		FT3736		FT3742		FT3748		FT3754		FT3760		FT3766		FT3772		FT3778		FT3784		FT3790		FT3796		FT3802		FT3808		FT3814		FT3820		FT3826		FT3832		FT3838		FT3844		FT3850		FT3856		FT3862		FT3868		FT3874		FT3880		FT3886		FT3892		FT3898		FT3904		FT3910		FT3916		FT3922		FT3928		FT3934		FT3940		FT3946		FT3952		FT3958		FT3964		FT3970		FT3976		FT3982		FT3988		FT3994		FT3998		FT4004		FT4010		FT4016		FT4022		FT4028		FT4034		FT4040		FT4046		FT4052		FT4058		FT4064		FT4070		FT4076		FT4082		FT4088		FT4094		FT4098		FT4104		FT4110		FT4116		FT4122		FT4128		FT4134		FT4140		FT4146		FT4152		FT4158		FT4164		FT4170		FT4176		FT4182		FT4188		FT4194		FT4198		FT4204		FT4210		FT4216		FT4222		FT4228		FT4234		FT4240		FT4246		FT4252		FT4258		FT4264		FT4270		FT4276		FT4282		FT4288		FT4294		FT4298		FT4304		FT4310		FT4316		FT4322		FT4328		FT4334		FT4340		FT4346		FT4352		FT4358		FT4364		FT4370		FT4376		FT4382		FT4388		FT4394		FT4398		FT4404		FT4410		FT4416		FT4422		FT4428		FT4434		FT4440		FT4446		FT4452		FT4458		FT4464		FT4470		FT4476		FT4482		FT4488		FT4494		FT4498		FT4504		FT4510		FT4516		FT4522		FT4528		FT4534		FT4540		FT4546		FT4552		FT4558		FT4564		FT4570		FT4576		FT4582		FT4588		FT4594		FT4598		FT4604		FT4610		FT4616		FT4622		FT4628		FT4634		FT4640		FT4646		FT4652		FT4658		FT4664		FT4670		FT4676		FT4682		FT4688		FT4694		FT4698		FT4704		FT4710		FT4716		FT4722		FT4728		FT4734		FT4740		FT4746		FT4752		FT4758		FT4764		FT4770		FT4776		FT4782		FT4788		FT4794		FT4798		FT4804		FT4810		FT4816		FT4822		FT4828		FT4834		FT4840		FT4846		FT4852		FT4858		FT4864		FT4870		FT4876		FT4882		FT4888		FT4894		FT4898		FT4904		FT4910		FT4916		FT4922		FT4928		FT4934		FT4940		FT4946		FT4952		FT4958		FT4964		FT4970		FT4976		FT4982		FT4988		FT4994		FT4998		FT5004		FT5010		FT5016		FT5022		FT5028		FT5034		FT5040		FT5046		FT5052		FT5058		FT5064		FT5070		FT5076		FT5082		FT5088		FT5094		FT5098		FT5104		FT5110		FT5116		FT5122		FT5128		FT5134		FT5140		FT5146		FT5152		FT5158		FT5164		FT5170		FT5176		FT5182		FT5188		FT5194		FT5198		FT5204		FT5210		FT5216		FT5222		FT5228		FT5234		FT5240		FT5246		FT5252		FT5258		FT5264		FT5270		FT5276		FT5282		FT5288		FT5294		FT5298		FT5304		FT5310		FT5316		FT5322		FT5328		FT5334		FT5340		FT5346		FT5352		FT5358		FT5364		FT5370		FT5376		FT5382		FT5388		FT5394		FT5398		FT5404		FT5410		FT5416		FT5422		FT5428		FT5434		FT5440		FT5446		FT5452		FT5458		FT5464		FT5470		FT5476		FT5482		FT5488		FT5494		FT5498		FT5504		FT5510		FT5516		FT5522		FT5528		FT5534		FT5540		FT5546		FT5552		FT5558		FT5564		FT5570		FT5576		FT5582		FT5588		FT5594		FT5598		FT5604		FT5610		FT5616		FT5622		FT5628		FT5634		FT5640		FT5646		FT5652		FT5658		FT5664		FT5670		FT5676		FT5682		FT5688		FT5694		FT5698		FT5704		FT5710		FT5716		FT5722		FT5728		FT5734		FT5740		FT5746		FT5752		FT5758		FT5764		FT5770		FT5776		FT5782		FT5788		FT5794		FT5798		FT5804		FT5810		FT5816		FT5822		FT5828		FT5834		FT5840		FT5846		FT5852		FT5858		FT5864		FT5870		FT5876		FT5882		FT5888		FT5894		FT5898		FT5904		FT5910		FT5916		FT5922		FT5928		FT5934		FT5940		FT5946		FT5952		FT5958		FT5964		FT5970		FT5976		FT5982		FT5988		FT5994		FT5998		FT6004		FT6010		FT6016		FT6022		FT6028		FT6034		FT6040		FT6046		FT6052		FT6058		FT6064		FT6070		FT6076		FT6082		FT6088		FT6094		FT6098		FT6104		FT6110		FT6116		FT6122		FT6128		FT6134		FT6140		FT6146		FT6152		FT6158		FT6164		FT6170		FT6176		FT6182		FT6188		FT6194		FT6198		FT6204		FT6210		FT6216		FT6222		FT6228		FT6234		FT6240		FT6246		FT6252		FT6258		FT6264		FT6270		FT6276		FT6282		FT6288		FT6294		FT6298		FT6304		FT6310		FT6316		FT6322		FT6328		FT6334		FT6340		FT6346		FT6352		FT6358		FT6364		FT6370		FT6376		FT6382		FT6388		FT6394		FT6398		FT6404		FT6410		FT6416		FT6422		FT6428		FT6434		FT6440		FT6446		FT6452		FT6458		FT6464		FT6470		FT6476		FT6482		FT6488		FT6494		FT6498		FT6504		FT6510		FT6516		FT6522		FT6528		FT6534		FT6540		FT6546		FT6552		FT6558		FT6564		FT6570		FT6576		FT6582		FT6588		FT6594		FT6598		FT6604		FT6610		FT6616		FT6622		FT6628		FT6634		FT6640		FT6646		FT6652		FT6658		FT6664		FT6670		FT6676		FT6682		FT6688		FT6694		FT6698		FT6704		FT6710		FT6716		FT6722		FT6728		FT6734		FT6740		FT6746		FT6752		FT6758		FT6764		FT6770		FT6776		FT6782		FT6788		FT6794		FT6798		FT6804		FT6810		FT6816		FT6822		FT6828		FT6834		FT6840		FT6846		FT6852		FT6858		FT6864		FT6870		FT6876		FT6882		FT6888		FT6894		FT6898		FT6904		FT6910		FT6916		FT6922		FT6928		FT6934		FT6940		FT6946		FT6952		FT6958		FT6964		FT6970		FT6976		FT6982		FT6988		FT6994		FT6998		FT7004		FT7010		FT7016		FT7022		FT7028		FT7034		FT7040		FT7046		FT7052		FT7058		FT7064		FT7070		FT7076		FT7082		FT7088		FT7094		FT7098		FT7104		FT7110		FT7116		FT7122		FT7128		FT7134		FT7140		FT7146		FT7152		FT7158		FT7164		FT7170		FT7176		FT7182		FT7188		FT7194		FT7198		FT7204		FT7210		FT7216		FT7222		FT7228		FT7234		FT7240		FT7246		FT7252		FT7258		FT7264		FT7270		FT7276		FT7282		FT7288		FT7294		FT7298		FT7304		FT7310		FT7316		FT7322		FT7328		FT7334		FT7340		FT7346		FT7352		FT7358		FT7364		FT7370		FT7376		FT7382		FT7388		FT7394		FT7398		FT7404		FT7410		FT7416		FT7422		FT7428		FT7434		FT7440		FT7446		FT7452		FT7458		FT7464		FT7470		FT7476		FT7482		FT7488		FT7494		FT7498		FT7504		FT7510		FT7516		FT7522		FT7528		FT7534		FT7540		FT7546		FT7552		FT7558		FT7564		FT7570		FT7576		FT7582		FT7588		FT7594		FT7598		FT7604		FT7610		FT7616		FT7622		FT7628		FT7634		FT7640		FT7646		FT7652		FT7658		FT7664		FT7670		FT7676		FT7682		FT7688		FT7694		FT7698		FT7704		FT7710		FT7716		FT7722		FT7728		FT7734		FT7740		FT7746		FT7752		FT7758		FT7764		FT7770		FT7776		FT7782		FT7788		FT7794		FT7798		FT7804		FT7810		FT7816		FT7822		FT7828		FT7834		FT7840		FT7846		FT7852		FT7858		FT7864		FT7870		FT7876		FT7882		FT7888		FT7894		FT7898		FT7904		FT7910		FT7916		FT7922		FT7928		FT7934		FT7940		FT7946		FT7952		FT7958</th	

Panel Temperature Data During Freezing

Time	Time	Time	TEW1	TEW2	TEW3	TEW4	TEW5	TEW6	TEW7	TEW8	TEW9	TEW10	TEW11	TEW12	TEW13	TEW14	TEW15	TEW16	TEW17	TEW18	TEW19	TEW20	TEW21	TEW22	TEW23	TEW24	TEW25	TEW26	TEW27	TEW28	TEW29	TEW30
hour	min	sec	DEG F	DEG F	DEG F	DEG F	DEG F	DEG F	DEG F	DEG F	DEG F	DEG F	DEG F	DEG F	DEG F	DEG F	DEG F	DEG F	DEG F	DEG F	DEG F	DEG F	DEG F	DEG F	DEG F	DEG F	DEG F	DEG F	DEG F	DEG F	DEG F	
13	11	48	308	207	342	206	350	207	343	207	343	207	345	207	345	207	345	207	345	207	345	207	345	207	345	207	345	207	345	207	345	
13	12	31	308	207	341	206	349	207	341	206	349	207	348	207	341	207	349	207	347	207	349	207	347	207	349	207	349	207	349	207	349	
13	12	49	307	206	351	205	340	207	340	205	341	206	345	207	346	207	345	207	346	207	345	207	346	207	345	207	346	207	345	207	346	
13	12	33	306	205	339	204	341	203	311	203	346	202	345	203	321	204	344	202	345	203	346	202	345	203	346	202	345	203	346	202	345	
13	12	48	305	204	349	203	340	205	339	203	347	202	340	203	336	204	341	202	340	203	347	202	340	203	347	202	340	203	347	202	340	
13	13	31	305	202	346	201	335	202	346	201	335	201	347	200	346	201	347	200	346	201	347	200	346	201	347	200	346	201	347	200	346	
13	13	49	303	201	344	200	334	201	343	200	334	201	342	200	333	201	343	200	334	201	342	200	333	201	343	200	334	201	342	200	333	
13	14	31	302	200	343	199	333	201	343	199	333	201	342	198	332	200	343	199	332	200	342	198	332	200	343	199	332	200	342	198	332	
13	14	48	301	200	342	199	332	200	342	199	332	200	341	198	331	200	342	199	331	200	340	198	331	200	341	199	331	200	340	198	331	
13	14	33	300	200	340	199	330	200	340	199	330	200	339	198	330	200	340	199	330	200	339	198	330	200	340	199	330	200	339	198	330	
13	14	49	299	198	338	197	329	198	338	197	329	198	337	197	329	198	338	197	329	198	337	197	329	198	338	197	329	198	338	197	329	
13	15	34	298	197	336	196	328	197	336	196	328	197	335	196	327	197	336	196	328	197	335	196	327	197	336	196	328	197	335	196	327	
13	15	49	296	196	334	195	326	197	334	195	326	196	333	195	325	196	334	195	326	196	333	195	325	196	334	195	326	196	333	195	325	
13	16	4	296	194	333	193	325	194	333	193	325	194	332	193	324	194	333	193	325	194	332	193	324	194	333	193	325	194	332	193	324	
13	16	49	295	193	332	192	324	193	332	192	324	193	331	192	323	193	332	192	324	193	331	192	323	193	332	192	324	193	331	192	323	
13	16	34	294	192	331	191	323	192	331	191	323	192	330	191	322	193	331	190	323	191	330	190	322	193	331	190	323	191	330	190	322	
13	16	49	293	191	330	190	322	191	330	190	322	191	329	190	321	191	330	189	320	190	329	189	321	190	330	189	320	190	329	189	321	
13	17	4	293	190	329	189	321	190	329	189	321	190	328	189	320	190	329	189	320	189	328	189	320	190	329	189	320	190	328	189	320	
13	17	33	291	189	327	188	319	189	327	188	319	189	326	188	318	189	327	188	319	189	326	188	318	189	327	188	319	189	326	188	318	
13	17	48	290	188	326	187	318	188	326	187	318	188	325	187	317	188	326	187	318	188	325	187	317	188	326	187	318	188	325	187	317	
13	18	3	289	187	325	186	316	187	325	186	316	187	324	186	315	187	325	186	316	187	324	186	315	187	325	186	316	187	324	186	315	
13	18	48	288	186	324	185	315	186	324	185	315	186	323	185	314	186	324	185	315	186	323	185	314	186	324	185	315	186	323	185	314	
13	18	33	287	185	323	184	314	185	323	184	314	185	322	184	313	185	323	184	314	185	322	184	313	185	323	184	314	185	322	184	313	
13	18	48	286	184	322	183	313	184	322	183	313	184	321	183	312	184	322	183	313	184	321	183	312	184	322	183	313	184	321	183	312	
13	19	3	286	183	321	182	312	183	321	182	312	183	320	182	311	183	321	182	312	183	320	182	311	183	321	182	312	183	320	182	311	
13	19	48	285	182	320	181	311	182	320	181	311	182	319	181	310	182	320	181	311	182	319	181	310	182	320	181	311	182	319	181	310	
13	19	33	284	181	319	180	310	181	319	180	310	181	309	180	309	181	319	180	310	181	309	180	309	181	319	180	310	181	309	180	309	
13	19	48	283	180	318	179	309	180	318	179	309	180	317	179	308	180	318	179	309	180	317	179	308	180	318	179	309	180	317	179	308	
13	20	34	282	179	317	178	308	179	317	178	308	179	307	178	307	179	317	178	308	179	307	178	307	179	317	178	308	179	307	178	307	
13	20	49	281	178	316	177	307	178	316	177	307	178	306	177	306	178	316	177	307	178	306	177	306	178	316	177	307	178	306	177	306	
13	21	4	280	177	315	176	306	177	315	176	306	177	305	176	305	177	315	176	306	177	305	176	305	177	315	176	306	177	305	176	305	
13	21	49	279	176	314	175	305	176	314	175	305	176	304	175	304	176	314	175	305	176	304	175	304	176	314	175	305	176	304	175	304	
13	21	31	278	175	313	174	304	175	313	174	304	175	303	174	303	175	313	174	304	175	303	174	303	175	313	174	304	175	303	174	303	
13	21	48	277	174	312	173	303	174	312	173	303	174	302	173	302	174	312	173	303	174	302	173	302	174	312	173	303	174	302	173	302	
13	22	3	277	173	311	172	302	173	311	172	302	173	301	172	301	173	311	172	302	173	301	172	301	173	311	172	302	173	301	172	301	
13	22	49	276	172	310	171	301	172	310	171	301	172	300	171	300	172	310	171	301	172	300	171	300	172	310	171	301	172	300	171	300	
13	22	31	275	171	309	170	299	171	309	170	299	171	298	170	298	171	309	170	299	171	298	170	299	171	309	170	299	171	298	170	299	
13	22	48	274	170	308	169	298	170	308	169	298	170	297	169	297	170	308	169	298	170	297	169	298	170	308	169	298	170	297	169	298	
13	23	3	273	169</td																												

Panel Temperature Data During Freezing

Time hour	Time min	TEW1 Time sec	TEW17	TEW16	TEW15	TEW14	TEW13	TEW12	TEW11	TEW10	TEW9	TEW8	TEW7	TEW6	TEW5	TEW4	TEW3	TEW2	TEW1	TEW19	TEWLH20	TEWLH21	TEBL70	TEBL90		
			DEG F	DEG F	DEG F	DEG F																				
13	29	48	259	283	307	280	160	307	276	270	279	279	282	221	275	276	265	292	275	275	275	275	275	499	519	
13	29	48	256	286	307	282	163	296	276	269	273	278	273	281	220	274	275	265	293	272	273	272	273	272	499	519
13	30	3	255	285	305	281	162	295	278	261	274	278	278	277	219	274	275	263	292	272	274	273	274	272	499	518
13	30	34	255	285	305	281	162	291	278	260	273	278	278	277	218	273	274	263	292	271	272	273	274	272	499	518
13	30	48	254	284	304	279	161	290	279	260	273	278	278	276	218	272	273	265	291	271	272	273	274	272	499	518
13	31	4	254	283	303	277	162	290	279	261	273	278	278	275	217	271	272	265	291	271	272	273	274	272	499	518
13	31	49	253	283	302	276	163	290	278	260	273	277	277	275	217	271	272	265	290	271	272	273	274	272	499	518
13	31	34	253	282	301	276	163	289	277	261	273	276	276	275	216	269	270	265	289	271	272	273	274	272	499	518
13	31	49	252	282	301	275	164	288	276	260	273	275	275	274	215	268	269	265	288	270	271	272	273	272	499	518
13	32	4	252	282	300	275	163	289	276	261	273	275	275	274	214	267	268	265	289	270	271	272	273	272	499	518
13	32	19	252	282	300	274	163	289	275	260	273	275	275	274	213	266	267	264	290	270	271	272	273	272	499	518
13	32	34	250	280	299	273	163	288	274	260	273	275	275	274	212	265	266	263	289	270	271	272	273	272	499	518
13	32	49	250	280	299	274	163	288	274	260	273	275	275	274	211	264	265	263	289	270	271	272	273	272	499	518
13	33	4	250	280	299	273	162	287	273	260	272	274	274	273	211	263	264	262	288	270	271	272	273	272	499	518
13	33	19	249	278	297	273	162	287	273	260	272	274	274	273	210	262	263	261	287	270	271	272	273	272	499	518
13	33	33	249	278	296	273	162	286	272	260	271	273	273	272	210	261	262	260	286	269	270	271	272	272	499	518
13	33	48	249	277	295	272	162	286	271	260	271	273	273	272	210	260	261	258	285	268	269	270	271	272	499	518
13	34	3	248	277	294	271	162	285	270	259	270	271	271	270	209	259	260	256	284	267	268	269	270	271	499	518
13	34	19	248	277	294	270	161	285	270	259	269	271	271	270	209	258	259	255	284	266	267	268	269	270	499	518
13	34	34	248	276	293	269	161	284	269	258	268	269	269	268	208	257	258	254	283	266	267	268	269	270	499	518
13	34	48	248	276	293	268	161	284	269	258	268	269	269	268	207	257	258	254	283	265	266	267	268	269	499	518
13	35	3	245	275	292	268	161	283	268	257	267	268	268	267	206	256	257	253	282	264	265	266	267	268	499	518
13	35	18	245	275	292	268	160	283	268	257	267	268	268	267	205	255	256	252	281	263	264	265	266	267	499	518
13	35	33	244	275	291	267	160	282	267	256	266	267	267	266	204	255	256	252	280	262	263	264	265	266	499	518
13	35	48	244	274	290	267	160	281	266	255	265	266	266	265	203	254	255	251	279	261	262	263	264	265	499	518
13	36	3	244	273	289	266	159	280	266	254	265	266	265	264	202	253	254	250	278	260	261	262	263	264	499	518
13	36	19	244	273	289	266	159	280	265	254	265	266	265	264	201	252	253	249	277	259	260	261	262	263	499	518
13	36	34	244	273	289	266	159	280	265	254	265	266	265	264	200	251	252	249	276	258	259	260	261	262	499	518
13	36	49	244	273	289	266	159	280	265	254	265	266	265	264	199	250	251	249	275	257	258	259	260	261	499	518
13	37	19	243	273	288	265	159	279	264	253	264	265	265	264	198	249	250	247	274	256	257	258	259	260	499	518
13	37	34	243	273	288	265	159	279	264	253	264	265	265	264	197	248	249	246	273	255	256	257	258	259	499	518
13	37	49	243	273	288	265	159	279	264	253	264	265	265	264	196	248	249	246	273	254	255	256	257	258	499	518
13	38	4	243	273	288	264	158	278	263	252	263	264	264	263	195	247	248	245	272	253	254	255	256	257	499	518
13	38	19	243	273	288	264	158	278	263	252	263	264	264	263	194	247	248	245	272	253	254	255	256	257	499	518
13	38	34	243	273	288	264	158	278	263	252	263	264	264	263	193	247	248	245	271	252	253	254	255	256	499	518
13	38	49	243	273	288	264	158	278	263	252	263	264	264	263	192	247	248	245	271	252	253	254	255	256	499	518
13	39	3	242	272	287	263	157	277	262	251	262	263	263	262	191	246	247	244	270	251	252	253	254	255	499	518
13	39	19	242	272	287	263	157	277	262	251	262	263	263	262	190	245	246	243	269	250	251	252	253	254	499	518
13	39	34	242	272	287	263	157	277	262	251	262	263	263	262	189	244	245	242	268	249	250	251	252	253	499	518
13	39	49	242	272	287	263	157	277	262	251	262	263	263	262	188	244	245	242	268	248	249	250	251	252	499	518
13	39	3	241	271	286	262	157	276	261	250	261	262	262	261	187	243	244	241	267	247	248	249	250	251	499	518
13	39	19	241	271	286	262	157	276	261	250	261	262	262	261	186	243	244	241	267	246	247	248	249	250	499	518
13	39	34	241	271	286	262	157	276	261	250	261	262	262	261	185	243	244	241	266	245	246	247	248	249	499	518
13	39	49	241	271	286	262	157	276	261	250	261	262	262	261	184	243	244	241	266	244	245	246	247	248	499	518
13	39	3	240	270	285	261	156	275	260	249	260	259	259	258	183	242	243	240	265	243	244	245	246	247	499	518
13	39	19	240	270	285	261	156	275	260	249	260	259	259	258	182	242	243	240	265	242	243	244	245	246	499	518
13	39	34	240	270	285	261	156	275	260	249	260	259	259	258	181	242	243	240	265	241	242	243	244	245	499	518
13	39	49	240	270	285	261	156	275	260	249	260	259	259	25												

Checkvalve Cycling Data

CRTF NET-90 99 POINT DATA FILE										
Time	Time	Time		FT720	PF-001	FT730	FT800	PT710	PP-001	PT720
hour	min	sec		Lt/min	Lt/min	Lt/min	Lt/min	PSIG	PSIG	PSIG
7	40	3		0	56	4	0	-2	-2	-1
7	40	18		0	68	4	0	-2	-2	-1
7	40	33		0	67	3	0	-2	-2	-1
7	40	48		0	61	3	0	-2	-2	-1
7	46	3		0	58	5	0	-2	-2	-1
7	46	6		0	58	5	0	-2	-2	-1
7	46	10		0	58	5	0	-2	-2	-1
7	46	13		0	58	5	0	-2	-2	-1
7	46	16		0	58	5	0	-2	-2	-1
7	46	19		0	58	5	0	-2	-2	-1
7	46	22		0	60	5	0	-2	-2	-1
7	46	25		0	55	5	0	-2	-2	-1
7	46	28		0	69	5	0	-2	-2	-1
7	46	31		0	62	5	0	-2	-2	-1
7	46	34		0	56	5	0	-2	-2	-1
7	46	38		0	56	5	0	-2	-2	-1
7	46	41		0	61	5	0	-2	-2	-1
7	46	44		0	61	5	0	-2	-2	-1
7	46	47		0	61	5	0	-2	-2	-1
7	46	50		0	61	5	0	-2	-2	-1
7	46	53		0	61	1	0	-2	-2	-1
7	46	56		0	68	1	0	-2	-2	-1
7	46	59		0	59	1	0	-2	-2	-1
7	47	2		0	59	1	0	-2	-2	-1
7	47	6		0	66	7	0	-2	-2	-1
7	47	9		0	66	1	0	-2	-2	-1
7	47	12		0	66	1	0	-2	-2	-1
7	47	15		0	66	1	0	-2	-2	-1
7	47	18		0	55	8	0	-2	-2	-1
7	47	21		0	69	2	0	-2	-2	-1
7	47	34		0	76	6	0	-2	-2	-1
7	47	49		0	64	5	0	-2	-2	-1
7	48	4		0	68	5	0	-2	-2	-1
7	48	19		0	58	5	0	-2	-2	-1
7	48	34		0	71	5	0	-2	-2	-1
7	48	49		0	68	1	0	-2	-2	-1
7	49	4		0	53	7	0	-2	-2	-1
7	49	19		0	50	7	0	-2	-2	-1
7	49	34		0	61	2	0	-2	-2	-1
7	49	49		0	56	2	0	-2	-2	-1
7	50	4		0	56	2	0	-2	-2	-1
7	50	18		0	56	2	0	-2	-2	-1
7	50	33		0	56	7	0	-2	-2	-1
7	50	48		0	51	2	0	-2	-2	-1
7	51	3		0	50	1	0	-2	-2	-1
7	51	18		0	50	8	0	-2	-2	-1
7	51	33		0	45	7	0	-2	-2	-1
7	51	48		0	45	0	0	-2	-2	-1
7	52	3		0	51	2	0	-2	-2	-1
7	52	18		0	51	2	0	-2	-2	-1
7	52	33		0	56	7	0	-2	-2	-1
7	52	48		0	56	7	0	-2	-2	-1
7	53	3		0	56	5	0	-2	-2	-1
7	53	19		0	51	5	0	-2	-2	-1
7	53	34		0	55	5	0	-2	-2	-1
7	53	49		0	52	5	0	-2	-2	-1
7	54	4		0	52	1	0	-2	-2	-1
7	54	19	-1	0	52	5	0	-2	-2	-1
7	54	34	-1	0	52	5	0	-2	-2	-1
7	54	49	-1	0	50	5	0	-2	-2	-1
7	55	4	-1	0	50	5	0	-2	-2	-1
7	55	19	0	55	1	0	-2	-2	-1	
7	55	33	214	322	2	0	106	83	-1	
7	55	49	320	309	2	0	111	103	-1	
7	56	3	320	303	2	0	110	103	-1	
7	56	18	392	367	225	0	46	33	0	
7	56	33	403	385	192	0	62	49	2	
7	56	48	397	379	186	0	64	50	4	
7	57	3	392	378	173	0	66	52	6	

Checkvalve Cycling Data

Time hour	Time min	Time sec	FT720 L/min	PF-001 L/min	FT730 L/min	FT800 L/min	PT710 PSIG	PP-001 PSIG	PT720 PSIG
7	57	18	386	361	162	0	68	53	10
7	57	33	386	373	148	0	71	57	14
7	57	48	387	302	5	0	68	55	15
7	58	3	387	289	5	0	68	55	15
7	58	18	387	336	5	0	68	55	15
7	58	34	387	352	5	0	68	55	15
7	58	49	74	335	77	0	-3	16	13
7	59	4	4	-4	4	0	-6	31	10
7	59	19	4	-4	4	0	-6	31	9
7	59	34	4	-4	4	0	-6	30	9
7	59	49	4	-4	4	0	-6	30	8
8	0	4	0	-5	0	0	-6	30	8
8	0	19	0	-5	1	0	-6	30	8
8	0	33	0	-5	6	0	-6	30	7
8	0	48	0	-5	6	0	-6	30	7
8	1	3	0	-5	1	0	-6	30	6
8	1	18	0	-5	2	0	-6	30	6
8	1	33	0	-5	7	0	-6	30	6
8	1	48	0	-5	7	0	-6	30	5
8	2	3	0	-5	1	0	-6	30	5
8	2	18	0	-5	0	0	-6	30	5
8	2	33	0	-5	0	0	-6	30	4
8	2	48	0	-5	1	0	-6	29	4
8	3	3	0	-5	11	0	-6	29	4
8	3	18	0	-5	11	0	-6	29	4
8	3	34	0	-5	0	0	-6	29	3
8	3	49	0	-5	6	0	-6	28	3
8	4	4	0	-5	7	0	-6	28	3
8	4	19	0	-5	1	0	-6	28	3
8	4	34	0	-5	7	0	-6	28	2
8	4	49	0	-5	7	0	-6	28	2
8	5	4	0	-5	11	0	-6	28	2
8	5	19	0	-5	1	0	-6	28	2
8	5	33	0	-5	0	0	-6	28	2
8	5	48	0	-5	0	0	-6	27	1
8	6	3	3	-5	6	0	-6	5	0
8	6	18	399	-5	221	0	56	49	0
8	6	33	399	388	188	0	63	51	2
8	6	48	393	359	183	0	64	51	5
8	7	3	393	366	171	0	66	53	8
8	7	18	387	367	159	0	69	55	12
8	7	33	380	358	30	0	67	55	16
8	7	48	387	361	4	0	68	55	15
8	8	4	387	382	4	0	68	55	15
8	8	19	387	382	4	0	68	55	15
8	8	34	387	347	4	0	68	55	15
8	8	49	387	320	6	0	68	55	15
8	9	4	387	359	5	0	68	55	15
8	9	19	387	371	5	0	68	55	15
8	9	34	387	309	5	0	68	55	15
8	9	49	386	361	5	0	68	55	15
8	10	4	386	352	6	0	68	55	15
8	10	19	386	370	6	0	68	55	15
8	10	34	386	352	2	0	68	55	15
8	10	49	386	361	11	0	68	55	15
8	11	4	386	364	11	0	68	55	15
8	11	19	386	349	11	0	68	55	15
8	11	33	386	355	11	0	68	54	15
8	11	48	386	384	11	0	68	54	15
8	12	3	386	383	0	0	68	54	15
8	12	18	386	381	21	0	68	54	15
8	12	33	386	373	61	0	68	55	15
8	12	48	387	352	11	0	68	55	15
8	13	3	387	411	11	0	68	55	15
8	13	18	387	399	11	0	68	55	15
8	13	33	387	360	11	0	68	55	15
8	13	48	386	401	0	0	68	55	15
8	14	4	386	359	0	0	68	55	15
8	14	19	386	355	21	0	68	55	15
8	14	34	386	385	11	0	68	55	15
8	14	49	386	383	21	0	68	55	15

Checkvalve Cycling Data

Time hour	Time min	Time sec	FT720 Lt/min	PF-001 Lt/min	FT730 Lt/min	FT800 Lt/min	PT710 PSIG	PP-001 PSIG	PT720 PSIG
8	15	4	386	362	6	0	68	55	15
8	15	19	386	390	2	0	68	55	15
8	15	34	387	378	2	0	68	55	15
8	15	49	387	383	5	0	68	55	15
8	16	4	387	370	0	0	68	55	15
8	16	19	387	398	1	0	68	55	15
8	16	33	387	349	1	0	68	55	15
8	16	48	388	351	1	0	68	55	15
8	17	3	388	353	1	0	68	55	15
8	17	18	388	364	1	0	68	55	15
8	17	33	388	364	1	0	68	55	15
8	17	48	387	360	2	0	68	55	15
8	18	3	387	352	2	0	68	55	15
8	18	18	387	358	1	0	68	55	15
8	18	33	387	325	1	0	68	55	15
8	18	48	387	360	1	0	68	55	15
8	19	4	387	378	1	0	68	55	15
8	19	19	387	342	1	0	68	55	15
8	19	34	388	340	7	0	68	55	15
8	19	49	388	342	7	0	68	55	15
8	20	4	388	365	6	0	68	55	15
8	20	19	388	314	7	0	68	55	15
8	20	34	388	322	1	0	68	54	15
8	20	49	388	385	2	0	68	54	15
8	21	4	388	364	2	0	68	54	15
8	21	19	388	356	2	0	68	54	15
8	21	34	388	386	1	0	68	55	15
8	21	48	387	372	7	0	68	55	15
8	22	3	387	359	1	0	68	55	15
8	22	18	387	398	2	0	68	55	15
8	22	33	387	354	1	0	68	55	15
8	22	48	386	357	6	0	68	55	15
8	23	3	386	378	1	0	68	55	15
8	23	18	386	359	1	0	68	55	15
8	23	33	386	335	2	0	68	55	15
8	23	48	388	366	2	0	68	55	15
8	24	3	388	382	0	0	68	55	15
8	24	18	388	337	2	0	68	55	15
8	24	34	388	348	2	0	68	55	15
8	24	49	388	383	2	0	68	55	15
8	25	4	388	350	2	0	68	55	15
8	25	19	388	354	2	0	68	55	15
8	25	34	388	325	0	0	68	55	15
8	25	49	387	371	2	0	68	55	15
8	26	4	387	374	2	0	68	55	15
8	26	19	387	403	1	0	68	55	15
8	26	34	386	362	1	0	68	55	15
8	26	49	386	376	1	0	68	55	15
8	27	4	386	402	2	0	68	55	15
8	27	19	386	354	1	0	68	55	15
8	27	33	386	367	2	0	68	55	15
8	27	48	387	366	5	0	68	55	15
8	28	3	387	379	5	0	68	55	15
8	28	18	387	335	5	0	68	55	15
8	28	33	387	375	5	0	68	54	15
8	28	48	387	337	8	0	68	54	15
8	29	3	387	361	2	0	68	54	15
8	29	18	387	303	2	0	68	54	15
8	29	33	387	371	2	0	68	55	15
8	29	48	388	338	0	0	68	55	15
8	30	4	388	375	7	0	68	55	15
8	30	19	388	401	1	0	68	53	15
8	30	34	389	357	7	0	68	53	15
8	30	49	389	363	2	0	68	53	15
8	31	4	389	379	6	0	68	43	15
8	31	19	1	-3	4	0	-6	38	17
8	31	34	1	-3	4	0	-6	38	16
8	31	49	1	-3	4	0	-6	38	14
8	32	3	1	-3	4	0	-6	36	14
8	32	18	0	-5	6	0	-6	36	13
8	32	33	0	-5	7	0	-6	36	12

Checkvalve Cycling Data

Time hour	Time min	Time sec	FT720 L/min	PF-001 L/min	FT730 L/min	FT800 L/min	PT710 PSIG	PP-001 PSIG	PT720 PSIG
8	32	48	0	-5	2	0	-6	36	11
8	33	3	0	-5	6	0	-6	35	11
8	33	18	0	-5	7	0	-6	35	10
8	33	33	0	-5	0	0	-6	35	10
8	33	48	0	-5	7	0	-6	35	9
8	34	3	0	-5	1	0	-6	35	9
8	34	18	6	-5	1	0	-6	35	8
8	34	34	6	-5	2	0	-6	35	8
8	34	49	1	-5	7	0	-6	35	7
8	35	4	1	-5	1	0	-6	33	7
8	35	19	6	-5	2	0	-6	33	6
8	35	34	1	-5	2	0	-6	33	6
8	35	49	1	-5	2	0	-6	32	5
8	36	4	6	-5	1	0	-6	32	5
8	36	19	0	-5	1	0	-6	32	5
8	36	34	0	-5	2	0	-6	30	5
8	36	49	0	-5	8	0	-6	30	4
8	37	3	0	-5	0	0	-6	30	4
8	37	18	0	-5	1	0	-6	30	4
8	37	33	0	-5	1	0	-6	29	3
8	37	48	0	-5	0	0	-6	29	3
8	38	3	0	-5	1	0	-6	29	3
8	38	18	0	-5	2	0	-6	29	3
8	38	33	0	-5	2	0	-6	27	2
8	38	48	0	-5	2	0	-6	27	2
8	39	3	0	-5	1	0	-6	27	2
8	39	18	0	-5	2	0	-6	27	2
8	39	34	0	-5	2	0	-6	26	2
8	39	49	19	-5	9	0	-6	19	1
8	40	4	253	-5	203	0	58	50	0
8	40	19	400	358	195	0	62	52	2
8	40	34	394	380	184	0	65	52	5
8	40	49	394	348	172	0	67	52	8
8	41	4	388	355	160	0	69	55	12
8	41	19	382	351	45	0	68	55	16
8	41	34	382	365	7	0	68	55	16
8	41	49	382	365	1	0	68	55	15
8	42	4	388	367	1	0	68	55	15
8	42	19	388	354	2	0	68	55	15
8	42	34	388	364	2	0	68	55	15
8	42	48	388	380	2	0	68	55	15
8	43	3	388	350	2	0	68	55	15
8	43	18	388	373	2	0	68	55	15
8	43	33	388	349	1	0	68	55	15
8	43	48	388	352	2	0	68	55	15
8	44	3	386	355	7	0	68	55	15
8	44	18	386	399	5	0	68	55	15
8	44	33	386	307	0	0	68	55	15
8	44	48	386	356	7	0	68	55	15
8	45	3	387	379	7	0	68	55	15
8	45	19	387	376	7	0	68	55	15
8	45	34	387	386	1	0	68	55	15
8	45	49	387	354	2	0	68	55	15
8	46	4	386	335	2	0	68	55	15
8	46	19	386	393	2	0	68	55	15
8	46	34	386	333	0	0	68	55	15
8	46	49	386	333	1	0	68	55	15
8	47	4	387	344	7	0	68	55	15
8	47	19	387	397	2	0	68	55	15
8	47	33	387	340	0	0	68	55	15
8	47	48	387	366	1	0	68	55	15
8	48	3	385	374	0	0	68	55	15
8	48	18	385	336	2	0	68	55	15
8	48	33	385	353	1	0	68	55	15
8	48	48	385	394	2	0	68	55	15
8	49	3	389	381	4	0	68	55	15
8	49	18	389	343	4	0	68	55	15
8	49	33	389	361	4	0	68	55	15
8	49	48	389	376	4	0	68	55	15
8	50	3	387	355	2	0	68	55	15
8	50	18	387	338	2	0	68	55	15

Checkvalve Cycling Data

Time hour	Time min	Time sec	FT720 Lt/min	PF-001 Lt/min	FT730 Lt/min	FT800 Lt/min	PT710 PSIG	PP-001 PSIG	PT720 PSIG
8	50	34	387	301	2	0	68	55	15
8	50	49	387	386	2	0	68	55	15
8	51	4	386	347	2	0	68	55	15
8	51	19	386	366	1	0	68	55	15
8	51	34	386	303	2	0	68	55	15
8	51	49	386	359	2	0	68	55	15
8	52	4	388	341	7	0	68	55	15
8	52	19	388	347	2	0	68	55	15
8	52	33	388	370	2	0	68	55	15
8	52	48	388	343	1	0	68	55	15
8	53	3	387	369	1	0	68	55	15
8	53	18	387	337	6	0	68	55	15
8	53	33	387	365	2	0	68	55	15
8	53	48	387	378	5	0	68	55	15
8	54	3	389	368	0	0	68	55	15
8	54	18	389	353	2	0	68	55	15
8	54	33	389	343	7	0	68	55	15
8	54	48	389	337	1	0	68	55	15
8	55	4	386	356	1	0	68	55	15
8	55	19	386	372	7	0	68	55	15
8	55	34	386	357	7	0	68	55	15
8	55	49	386	405	6	0	68	55	15
8	56	4	387	368	0	0	68	55	15
8	56	19	387	362	4	0	68	55	15
8	56	34	387	388	4	0	68	55	15
8	56	48	387	377	4	0	68	55	15
8	57	3	386	369	4	0	68	55	15
8	57	18	386	349	0	0	68	55	15
8	57	33	386	376	0	0	68	55	15
8	57	48	386	355	1	0	68	55	15
8	58	3	389	358	2	0	68	55	15
8	58	18	389	408	0	0	68	55	15
8	58	33	389	359	2	0	68	55	15
8	58	48	389	366	0	0	68	55	15
8	59	3	388	365	2	0	68	55	15
8	59	18	388	355	2	0	68	55	15
8	59	33	389	369	7	0	68	55	15
8	59	49	389	331	6	0	68	55	15
9	0	4	389	379	2	0	68	55	15
9	0	19	389	395	1	0	68	55	15
9	0	34	385	354	6	0	68	55	15
9	0	49	385	370	6	0	68	55	15
9	1	4	385	356	7	0	68	55	15
9	1	19	385	367	4	0	68	55	15
9	1	33	388	373	4	0	68	55	15
9	1	48	388	351	4	0	68	55	15
9	2	3	388	396	4	0	68	55	15
9	2	18	388	343	0	0	68	55	15
9	2	33	387	329	1	0	68	55	15
9	2	48	387	365	2	0	67	55	15
9	3	5	387	376	2	0	68	55	15
9	3	18	387	345	2	0	68	55	15
9	3	33	388	373	2	0	68	55	15
9	3	48	388	313	2	0	68	55	15
9	4	3	388	377	7	0	68	55	15
9	4	18	388	384	2	0	68	55	15
9	4	34	386	386	6	0	68	55	15
9	4	49	386	317	1	0	68	55	15
9	5	4	363	365	54	0	70	60	15
9	5	19	1	-3	5	0	-6	38	16
9	5	34	1	-3	5	0	-6	38	15
9	5	49	1	-3	5	0	-6	38	14
9	6	4	1	-3	5	0	-6	36	13
9	6	19	0	-5	0	0	-6	36	12
9	6	33	0	-5	2	0	-6	36	12
9	6	48	0	-5	6	0	-6	36	11
9	7	3	6	-5	0	0	-6	35	11
9	7	18	1	-5	1	0	-6	35	10
9	7	33	7	-5	2	0	-6	35	10
9	7	48	7	-5	8	0	-6	35	9
9	8	3	12	-5	6	0	-6	35	9

Checkvalve Cycling Data

Time hour	Time min	Time sec	FT720 L/min	PF-001 L/min	FT730 L/min	FT800 L/min	PT710 PSIG	PP-001 PSIG	PT720 PSIG
9	8	18	9	-5	0	0	-6	35	8
9	8	33	4	-5	0	0	-6	35	7
9	8	48	4	-5	0	0	-6	35	7
9	9	4	4	-5	0	0	-6	33	6
9	9	19	4	-5	0	0	-6	33	6
9	9	34	4	-5	0	0	-6	33	6
9	9	49	0	-5	1	0	-6	32	5
9	10	4	0	-5	1	0	-6	32	5
9	10	19	0	-5	2	0	-6	32	5
9	10	34	0	-5	2	0	-6	30	4
9	10	49	0	-5	2	0	-6	30	4
9	11	4	0	-5	1	0	-6	30	4
9	11	18	0	-5	7	0	-6	29	4
9	11	34	2	-5	2	0	-6	29	3
9	11	48	2	-5	6	0	-6	29	3
9	12	3	2	-5	6	0	-6	29	3
9	12	18	2	-5	7	0	-6	27	3
9	12	33	0	-5	1	0	-6	27	2
9	12	48	0	-5	1	0	-6	27	2
9	13	3	0	-5	4	0	-6	27	2
9	13	18	0	-5	4	0	-6	26	2
9	13	33	0	-5	4	0	-6	26	2
9	13	48	5	-5	10	0	-6	12	0
9	14	3	396	118	194	0	62	52	1
9	14	18	397	367	189	0	63	52	3
9	14	33	391	363	177	0	65	52	6
9	14	48	391	366	165	0	68	54	10
9	15	3	385	360	153	0	70	57	14
9	15	19	387	355	4	0	68	55	16
9	15	34	387	367	4	0	68	55	15
9	15	49	387	354	41	0	68	55	15
9	16	4	387	367	4	0	68	55	15
9	16	19	385	362	5	0	68	55	15
9	16	34	385	341	0	0	68	55	15
9	16	49	385	406	4	0	68	55	15
9	17	4	385	355	4	0	68	55	15
9	17	18	386	326	4	0	68	55	15
9	17	33	386	365	4	0	68	55	15
9	17	48	386	353	2	0	68	55	15
9	18	3	386	381	2	0	68	55	15
9	18	18	386	324	2	0	68	55	15
9	18	33	386	322	2	0	68	55	15
9	18	48	386	363	5	0	68	55	15
9	19	3	386	352	7	0	68	55	15
9	19	18	386	394	11	0	68	55	15
9	19	33	386	387	7	0	68	55	15
9	19	48	386	345	11	0	68	55	15
9	20	3	386	340	1	0	68	55	15
9	20	19	387	407	1	0	68	55	15
9	20	34	387	386	0	0	68	55	15
9	20	49	387	368	8	0	68	55	15
9	21	4	387	355	2	0	68	55	15
9	21	19	387	363	6	0	68	55	15
9	21	34	387	411	6	0	68	55	15
9	21	49	387	393	0	0	68	55	15
9	22	4	387	348	1	0	68	55	15
9	22	19	387	361	0	0	68	55	15
9	22	34	387	361	1	0	68	55	15
9	22	48	387	359	2	0	68	55	15
9	23	3	387	372	0	0	68	55	15
9	23	18	386	338	8	0	68	55	15
9	23	33	386	365	2	0	68	55	15
9	23	48	386	333	2	0	67	55	15
9	24	3	386	380	6	0	68	55	15
9	24	18	387	308	6	0	68	55	15
9	24	33	387	366	1	0	68	55	15
9	24	48	387	328	1	0	68	55	15
9	25	3	387	391	8	0	68	55	15
9	25	18	388	362	2	0	68	55	15
9	25	34	388	325	1	0	68	55	15
9	25	49	388	349	8	0	67	55	15

Checkvalve Cycling Data

Time hour	Time min	Time sec	FT720 L/min	PF-001 L/min	FT730 L/min	FT800 L/min	PT710 PSIG	PP-001 PSIG	PT720 PSIG
9	26	4	388	336	4	0	68	55	15
9	26	19	387	372	4	0	68	55	15
9	26	34	387	362	4	0	68	55	15
9	26	49	387	392	4	0	68	55	15
9	27	3	387	371	8	0	68	55	15
9	27	18	384	296	1	0	68	55	15
9	27	33	384	320	6	0	68	55	15
9	27	48	384	369	1	0	68	55	15
9	28	3	384	370	2	0	68	55	15
9	28	18	387	372	0	0	68	55	15
9	28	33	387	353	6	0	68	55	15
9	28	48	387	342	7	0	68	55	15
9	29	3	387	354	1	0	68	55	15
9	29	18	388	366	1	0	68	55	15
9	29	33	388	360	1	0	68	55	15
9	29	48	388	374	6	0	68	55	15
9	30	4	388	330	0	0	68	55	15
9	30	19	387	345	2	0	68	55	15
9	30	34	387	380	7	0	67	55	15
9	30	49	387	349	1	0	68	55	15
9	31	4	387	371	1	0	68	55	15
9	31	19	388	385	2	0	68	55	15
9	31	34	388	352	7	0	68	55	15
9	31	49	388	351	0	0	68	55	15
9	32	4	388	325	1	0	68	55	15
9	32	19	387	359	7	0	68	55	15
9	32	34	387	365	2	0	68	55	15
9	32	48	387	354	2	0	68	55	15
9	33	3	387	343	7	0	68	55	15
9	33	18	385	316	2	0	68	55	15
9	33	33	385	344	1	0	68	55	15
9	33	48	385	287	1	0	68	55	15
9	34	3	385	334	1	0	68	55	15
9	34	18	385	352	1	0	67	55	15
9	34	33	385	351	6	0	68	55	15
9	34	48	385	345	7	0	68	55	15
9	35	4	385	334	7	0	68	55	15
9	35	19	386	401	2	0	68	55	15
9	35	34	386	346	6	0	68	55	15
9	35	49	391	361	1	0	68	55	15
9	36	4	385	381	1	0	68	55	15
9	36	19	385	309	1	0	68	55	15
9	36	34	385	392	1	0	68	55	15
9	36	49	385	336	1	0	68	55	15
9	37	4	388	331	1	0	67	55	15
9	37	19	388	368	11	0	68	55	15
9	37	33	388	314	8	0	68	55	15
9	37	48	388	343	8	0	68	55	15
9	38	3	388	361	2	0	68	55	15
9	38	18	388	360	2	0	68	55	15
9	38	35	388	364	6	0	68	55	15
9	38	48	388	372	0	0	68	55	15
9	39	3	377	315	7	0	78	69	15
9	39	18	3	2	3	0	-6	36	15
9	39	33	3	-4	3	0	-6	36	14
9	39	48	3	-4	3	0	-6	36	13
9	40	3	3	-4	3	0	-6	36	12
9	40	19	0	-5	4	0	-6	35	12
9	40	34	0	-5	4	0	-6	35	11
9	40	49	0	-5	4	0	-6	35	11
9	41	4	0	-5	4	0	-6	35	10
9	41	19	0	-5	2	0	-6	35	10
9	41	34	0	-5	2	0	-6	35	9
9	41	49	0	-5	0	0	-6	35	9

Thermal Shock Data for Components

CRTF NET-90 99 POINT DATA FILE				Check	4"	6"
TEST DATE: Tue May 3 1994 8:52:37				valve	flange	flange
Time	Time	Time	FT720	TEPL-5	TEPL-8	TEPL-12
hour	min	sec	Lt/min	DEG F	DEG F	DEG F
8	53	3	0	72	69	92
8	53	18	0	72	69	92
8	53	33	0	72	69	92
8	53	48	0	72	70	92
8	54	3	0	72	70	92
8	54	19	0	72	70	92
8	54	34	0	72	70	92
8	54	49	0	71	68	91
8	55	4	0	71	68	91
8	55	19	0	71	68	91
8	55	34	0	71	68	91
8	55	49	0	72	70	92
8	56	4	0	72	70	92
8	56	18	0	72	70	92
8	56	33	0	72	70	92
8	56	48	0	72	69	92
8	57	3	0	72	69	92
8	57	18	323	72	69	92
8	57	33	355	134	69	92
8	57	48	361	223	80	98
8	58	3	361	279	105	122
8	58	18	361	329	154	145
8	58	33	361	367	191	168
8	58	48	360	391	241	193
8	59	3	360	415	283	228
8	59	18	360	438	320	265
8	59	33	360	451	344	288
8	59	49	360	461	367	311
9	0	4	360	472	390	336
9	0	19	360	484	402	347
9	0	34	360	496	414	372
9	0	49	361	507	425	384
9	1	4	361	507	425	384
9	1	19	361	518	437	395
9	1	34	361	518	448	407
9	1	49	359	530	448	407
9	2	3	359	530	448	418
9	2	18	359	541	461	418
9	2	33	359	541	461	429
9	2	48	359	541	461	429
9	3	3	359	552	472	441
9	3	18	359	552	472	441
9	3	33	359	552	472	441
9	3	48	357	552	472	441
9	4	3	357	561	482	452
9	4	18	357	561	482	452
9	4	33	357	561	482	452
9	4	49	361	561	482	461

Thermal Shock Data for Components

Time hour	Time min	Time sec	FT720 L/min	TEPL-5 DEG F	TEPL-8 DEG F	TEPL-12 DEG F
9	5	4	361	568	492	461
9	5	19	361	568	492	461
9	5	34	361	568	492	461
9	5	49	359	568	492	472
9	6	4	359	572	500	472
9	6	19	359	572	500	472
9	6	34	359	572	500	472
9	6	48	358	572	500	479
9	7	3	358	575	505	479
9	7	18	358	575	505	479
9	7	33	358	575	505	479
9	7	48	358	575	505	488
9	8	3	358	575	512	488
9	8	18	358	578	512	488
9	8	33	358	578	512	488
9	8	48	359	578	512	495
9	9	3	359	578	516	495
9	9	19	359	579	516	495
9	9	34	359	579	516	495
9	9	49	360	579	516	502
9	10	4	360	579	523	502
9	10	19	360	581	523	502
9	10	34	360	581	523	502
9	10	49	359	581	523	507
9	11	3	359	581	526	507
9	11	18	359	581	526	507
9	11	33	359	581	526	507
9	11	48	358	581	526	507
9	12	3	358	581	530	512
9	12	18	358	583	530	512
9	12	33	358	583	530	512
9	12	48	358	583	530	512
9	13	3	358	583	535	518
9	13	19	358	584	535	518
9	13	34	358	584	535	518
9	13	49	358	584	535	518
9	14	4	358	584	537	522
9	14	19	358	584	537	522
9	14	34	358	584	537	522
9	14	49	358	584	537	522
9	15	4	358	584	542	526
9	15	18	358	586	542	526
9	15	33	358	586	542	526
9	15	48	357	586	542	526
9	16	3	357	586	544	530
9	16	18	357	585	544	530
9	16	33	357	585	544	530
9	16	48	357	585	544	530
9	17	3	357	585	548	533
9	17	18	357	586	548	533

Thermal Shock Data for Components

Time hour	Time min	Time sec	FT720 Lt/min	TEPL-5 DEG F	TEPL-8 DEG F	TEPL-12 DEG F
9	17	33	357	586	548	533
9	17	49	358	586	548	533
9	18	4	358	586	551	537
9	18	19	358	587	551	537
9	18	34	358	587	551	537
9	18	49	358	587	551	537
9	19	4	358	587	552	540
9	19	18	358	587	552	540
9	19	33	358	587	552	540
9	19	48	358	587	552	540
9	20	3	358	587	556	543
9	20	18	358	588	556	543
9	20	33	358	588	556	543
9	20	48	359	588	556	543
9	21	4	359	588	557	545
9	21	19	359	588	557	545
9	21	34	359	588	557	545
9	21	49	360	588	557	545
9	22	4	360	588	557	548
9	22	19	360	590	561	548
9	22	34	360	590	561	548
9	22	49	357	590	561	548
9	23	4	357	590	561	550
9	23	19	357	590	562	550
9	23	34	357	590	562	550
9	23	49	357	590	562	550
9	24	3	357	590	562	552
9	24	18	357	591	564	552
9	24	33	357	591	564	552
9	24	48	357	591	564	552
9	25	3	357	591	564	555
9	25	18	357	591	567	555
9	25	33	357	591	567	555
9	25	48	357	591	567	555
9	26	3	357	591	567	556
9	26	19	357	591	567	556
9	26	34	357	591	567	556
9	26	49	357	591	567	556
9	27	4	357	591	567	558
9	27	19	357	591	570	558
9	27	34	357	593	570	558
9	27	48	356	593	570	558
9	28	3	356	593	570	560
9	28	18	356	593	570	560
9	28	33	356	592	570	560
9	28	48	358	592	570	560

Data for Slow Cool Down of Components with Fan Simulating Nightly Cool Down.

					Check	4"flg	6"flg		
			Time	Z	521	522	523	524	525
OCT20,1993	12:28:20	12	28	20	12.5	583	585	585	582
OCT20,1993	12:43:20	12	43	20	12.7	586	588	588	586
OCT20,1993	12:58:20	12	58	20	13.0	592	594	594	591
OCT20,1993	13:13:20	13	13	20	13.2	574	582	579	581
OCT20,1993	13:28:20	13	28	20	13.5	572	566	559	561
OCT20,1993	13:43:20	13	43	20	13.7	584	550	539	543
OCT20,1993	13:58:20	13	58	20	14.0	586	533	519	526
OCT20,1993	14:13:20	14	13	20	14.2	579	518	501	506
OCT20,1993	14:28:20	14	28	20	14.5	589	502	482	487
OCT20,1993	14:43:20	14	43	20	14.7	570	486	462	466
OCT20,1993	14:58:20	14	58	20	15.0	591	469	444	449
OCT20,1993	15:13:20	15	13	20	15.2	567	454	424	432
OCT20,1993	15:28:20	15	28	20	15.5	585	437	406	415
OCT20,1993	15:43:20	15	43	20	15.7	569	423	390	399
OCT20,1993	15:58:20	15	58	20	16.0	575	408	374	384
OCT20,1993	16:13:20	16	13	20	16.2	572	393	358	370
OCT20,1993	16:28:20	16	28	20	16.5	564	378	343	358
OCT20,1993	16:43:20	16	43	20	16.7	575	364	330	345
OCT20,1993	16:58:20	16	58	20	17.0	565	350	317	332
OCT20,1993	17:13:20	17	13	20	17.2	573	339	304	322
OCT20,1993	17:28:20	17	28	20	17.5	554	327	292	311
OCT20,1993	17:43:20	17	43	20	17.7	575	315	282	301
OCT20,1993	17:58:20	17	58	20	18.0	553	304	272	291
OCT20,1993	18:13:20	18	13	20	18.2	572	294	261	282
OCT20,1993	18:28:20	18	28	20	18.5	551	283	252	273
OCT20,1993	18:43:20	18	43	20	18.7	571	273	243	265
OCT20,1993	18:58:20	18	58	20	19.0	549	264	235	256
OCT20,1993	19:13:20	19	13	20	19.2	570	255	227	248
OCT20,1993	19:28:20	19	28	20	19.5	547	247	218	241
OCT20,1993	19:43:20	19	43	20	19.7	569	239	212	234
OCT20,1993	19:58:20	19	58	20	20.0	547	232	205	227
OCT20,1993	20:13:20	20	13	20	20.2	568	224	198	221
OCT20,1993	20:28:20	20	28	20	20.5	546	218	192	215
OCT20,1993	20:43:20	20	43	20	20.7	567	211	186	209
OCT20,1993	20:58:20	20	58	20	21.0	545	205	181	204
OCT20,1993	21:13:20	21	13	20	21.2	565	199	176	199
OCT20,1993	21:28:20	21	28	20	21.5	542	194	171	194
OCT20,1993	21:43:20	21	43	20	21.7	563	188	166	189
OCT20,1993	21:58:20	21	58	20	22.0	547	183	162	185
OCT20,1993	22:13:20	22	13	20	22.2	562	179	157	181
OCT20,1993	22:28:20	22	28	20	22.5	544	174	153	177
OCT20,1993	22:43:20	22	43	20	22.7	567	170	149	172
OCT20,1993	22:58:20	22	58	20	23.0	541	165	144	168
OCT20,1993	23:13:20	23	13	20	23.2	564	162	142	166
OCT20,1993	23:28:20	23	28	20	23.5	538	159	139	162
OCT20,1993	23:43:20	23	43	20	23.7	563	155	135	159
OCT20,1993	23:58:20	23	58	20	24.0	539	151	132	156

Data for Slow Heat Up of Components with Two Heat Trace Circuits.

Time,hr	Heatup With Two Circuits		
	CheckV	4"Flange	6"flange
	TEPL-4	TEPL-8	TEPL-10
0	104.8205	104.8205	104.8205
0.4135	137.351	169.8815	148.1945
0.827	202.412	281.931	238.557
1.2405	245.786	354.221	289.16
1.654	285.5455	401.2095	354.221
2.0675	325.305	433.74	397.595
2.481	383.137	484.343	444.5835
2.8945	379.5225	469.885	448.198
3.308	404.824	502.4155	495.1865
3.7215	415.6675	502.4155	495.1865
4.135	422.8965	506.03	502.4155
4.5485	433.74	516.8735	516.8735
4.962	448.198	527.717	527.717
5.3755	459.0415	538.5605	538.5605
5.789	451.8125	520.488	520.488

Unlimited Distribution

Attn: Tom Tracey
6922 S. Adams Way
Littleton, CO 80122

Bechtel National, Inc.
Attn: William Gould
50 Beale Street
45/4/C27
P.O. Box 193965
San Francisco, CA 94119-3965

Advanced Thermal Systems
Attn: Dave Gorman
7600 East Arapahoe Road, Suite 215
Englewood, CO 80112

Bechtel National, Inc.
Attn: Bruce Kelly
50 Beale Street
45/4/C27
P.O. Box 193965
San Francisco, CA 94119-3965

Advanced Thermal Systems
Attn: Robert Thomas
7600 East Arapahoe Road, Suite 215
Englewood, CO 80112

Bechtel National, Inc.
Attn: Lorne Marjerison
50 Beale Street
45/4/C27
P.O. Box 193965
San Francisco, CA 94119-3965

Arizona Public Service Co.
Attn: Scott McLellan
P.O. Box 53999
MS 1424
Phoenix, AZ 85072-3999

Bechtel National, Inc.
Attn: S. Nickovich
50 Beale Street
50/15 D8
P.O. Box 193965
San Francisco, CA 94119-3965

Arizona State University
Attn: Paul Russell
College of Engineering
Tempe, AZ 85287

Bechtel National, Inc.
Attn: Brock Parsens
50 Beale Street
45/4/C27
P.O. Box 193965
San Francisco, CA 94119-3965

Bechtel Group, Inc.
Attn: Madanjit Singh
50 Beale Street
45/4/C27
P.O. Box 193965
San Francisco, CA 94119-3965

Bechtel National, Inc.
Attn: Alex Zavoico
50 Beale Street
45/4/C27
P.O. Box 193965
San Francisco, CA 94119-3965

Bechtel National, Inc.
Attn: Pat DeLaquil
50 Beale Street
50/15 D8
P.O. Box 193965
San Francisco, CA 94119-3965

Bureau of Reclamation
Attn: Stanley Hightower
Code D-3710
P.O. Box 205007
Denver, CO 80225

California Energy Commission
Attn: Alec Jenkins
Energy Technology Development Div. R&D
Office
1516 9th Street
MS-43
Sacramento, CA 95814-5512

California Polytechnic State University
Attn: William B. Stine
Department of Mechanical Engineering
3801 West Temple Avenue
Pomona, CA 91768-4062

Carrizo Solar Corporation
Attn: Mike Elliston
P.O. Box 10239
1011-C Sawmill Road NW
Albuquerque, NM 87184-0239

Carrizo Solar Corporation
Attn: John Kusianovich
P.O. Box 10239
1011-C Sawmill Road NW
Albuquerque, NM 87184-0239

Central and Southwest Services
Attn: E.L. Gastineau
1616 Woodall Rogers Freeway
MS 7RES
Dallas, TX 75202

Centro Investigaciones Energeticas
Attn: M. Macias
Medioambientales y Technologicas
Instituto de Energias Renovables
Avda. Complutense, 22
28040 Madrid, SPAIN

Centro Investigaciones Energeticas
Attn: M. Romero
Medioambientales y Technologicas
Instituto de Energias Renovables
Avda. Complutense, 22
28040 Madrid, SPAIN

Conservation and Renewable Energy System
Attn: Ben Wolff
6918 N.E. Fourth Plain Blvd., Suite B
Vancouver, WA 98661

DEO Enterprises
Attn: Dave Ochenreider
P.O. Box 2110
Helendale, CA 92342

DLR
Attn: Reiner Buck
Pfaffenwaldring 38-40
7000 Stuttgart 80, GERMANY

Dynatherm Corporation
Attn: D. Wolf
1 Beaver Court
P.O. Box 398
Cockeystown, MD 21030

Electric Power Research Institute
Attn: Doug Morris
P.O. Box 10412
3412 Hillview Avenue
Palo Alto, CA 94303

Electric Power Research Institute
Attn: J. Schaeffer
P.O. Box 10412
3412 Hillview Avenue
Palo Alto, CA 94303

Flachglas Solartechnik GmbH
Attn: M. Geyer
Theodor-Heuss-Ring 1
5000 Koln 1, GERMANY

Florida Solar Energy Center
Attn: Library
300 State Road, Suite 401
Cape Canaveral, FL 32920-4099

Fricker Consulting
Attn: Hans Fricker
Breitestr. 22
CH 8544 Rickenbach, SWITZERLAND

Georgia Power Co.
Attn: W. Rosskist
7 Solar Circle
Shenandoah, GA 30265

Idaho Power
Attn: John Carstensen
P.O. Box 70
Boise, ID 83707

Idaho Power
Attn: Jerry Young
P.O. Box 70
Boise, ID 83707

Institute of Gas Technology
Attn: Library
34245 State Street
Chicago, IL 60616

Dick Holl
1938A Avenida Del Oro
Oceanside, CA 92056

Jet Propulsion Laboratory
Attn: M. Alper
4800 Oak Grove Drive
Pasadena, CA 91109

Kearney & Associates
Attn: David W. Kearney
14022 Condessa Drive
Del Mar, CA 92014

KJC Operating Company
Attn: Gilbert Cohen
41100 Highway 395
Boron, CA 93516

KJC Operating Company

Attn: R. Hollis
41100 Highway 395
Boron, CA 93516

Lawrence Berkeley Laboratory
Attn: Arlon Hunt
University of California
MS 90-2024
One Cyclotron Road
Berkeley, CA 94720

Los Alamos National Laboratory
Attn: M. Merrigan
P.O. Box 1663
MS-E13
Los Alamos, NM 87545

Los Angeles Dept. of Water and Power
Attn: David Anderson
Alternate Energy Systems
111 North Hope Street, Rm. 661A
Los Angeles, CA 90012

Los Angeles Dept. of Water and Power
Attn: Daryl Yonamine
Alternate Energy Systems
111 North Hope Street, Rm. 661A
Los Angeles, CA 90012

McDonnell-Douglas Astronautics Co.
Attn: Bob Drubka
5301 Bolsa Avenue
Huntington Beach, CA 92647-2048

McDonnell-Douglas Astronautics Co.
Attn: J. Rogan
5301 Bolsa Avenue
Huntington Beach, CA 92647

McDonnell-Douglas Astronautics Co.
Attn: D. Steinmeyer (3)
5301 Bolsa Avenue
Huntington Beach, CA 92647

National Renewable Energy Laboratory
Attn: Mark Bohn
1617 Cole Blvd.
Golden, CO 80401-3393

Nevada Power Co.
Attn: Mark Shank
P.O. Box 230
Las Vegas, NV 89151

National Renewable Energy Laboratory
Attn: Gary Jorgensen
1617 Cole Blvd.
Golden, CO 80401-3393

Northern Research & Engineering Corp.
Attn: James B. Kesseli
39 Olympia Avenue
Woburn, MA 01801-2073

National Renewable Energy Laboratory
Attn: A. Lewandowski
1617 Cole Blvd.
Golden, CO 80401-3393

Pacific Gas and Electric Co.
Attn: Chris Haslund (2)
3400 Crow Canyon Road
San Ramon, CA 94583

National Renewable Energy Laboratory
Attn: L.M. Murphy
1617 Cole Blvd.
Golden, CO 80401-3393

Pacific Power
Attn: Stephen Schuck
Park and Elizabeth Streets
GPO Box 5257
Sydney
New South Wales, 2001 AUSTRALIA

National Renewable Energy Laboratory
Attn: Hank Price
1617 Cole Blvd.
Golden, CO 80401-3393

PacifiCorp
Attn: Ian Andrews
Utah Power
1407 West North Temple
Salt Lake City, UT 84140-0001

National Renewable Energy Laboratory
Attn: Tim Wendelin
1617 Cole Blvd.
Golden, CO 80401-3393

Power Kinetics, Inc.
Attn: W.E. Rogers
415 River Street
Troy, NY 12180-2822

National Renewable Energy Laboratory
Attn: Tom Williams
1617 Cole Blvd.
Golden, CO 80401-3393

Renewable Energy Training Institute
Attn: Kevin Porter
122 C St. NW, Suite 520
Washington, DC 20001

Nevada Power Co.
Attn: Doug Bailey
P.O. Box 230
Las Vegas, NV 89151

Research International
Attn: E. Saaski
18706 142nd Avenue, NE
Woodinville, WA 98072

Nevada Power Co.
Attn: Eric Dominguez
P.O. Box 230
Las Vegas, NV 89151

Rockwell International Corp.
Attn: William Bigelow
Energy Technology Engineering Center
P.O. Box 1449
Canoga Park, CA 91304

Rockwell International Corp.
Attn: Tom M. Griffin
P.O. Box 582808
Tulsa, OK 74158

Rockwell International Corp.
Attn: R. LeChevalier
Energy Technology Engineering Center
P.O. Box 1449
Canoga Park, CA 91304

Rockwell International Corp.
Attn: Bob Litwin
Rocketdyne Division
P.O. Box 7922
6633 Canoga Avenue
MS SA70
Canoga Park, CA 91309-7922

Rockwell International Corp.
Attn: Mark Marko
Rocketdyne Division
P.O. Box 7922
6633 Canoga Avenue
MS SA70
Canoga Park, CA 91309-7922

Rockwell International Corp.
Attn: W. Marlatt
Rocketdyne Division
P.O. Box 7922
6633 Canoga Avenue
Canoga Park, CA 91309-7922

Rockwell International Corp.
Attn: Bob Musica
Energy Technology Engineering Center
P.O. Box 1449
Canoga Park, CA 91304

Rockwell International Corp.
Attn: Ron Pauckert
Rocketdyne Division
P.O. Box 7922
6633 Canoga Avenue
MS SA70
Canoga Park, CA 91309-7922

Sacramento Municipal Utility District
Attn: Bud Beebee
Generation Systems Planning
Power Systems Dept.
6201 'S' St.
P.O. Box 15830
Sacramento, CA 95852-1830

Sacramento Municipal Utility District
Attn: Don Osborne
Generation Systems Planning
Power Systems Dept.
6201 'S' St.
P.O. Box 15830
Sacramento, CA 95852-1830

Sacramento Municipal Utility District
Attn: R. Wichert
Generation Systems Planning
Power Systems Dept.
6201 'S' St.
P.O. Box 15830
Sacramento, CA 95852-1830

Salt River Project
Attn: Bob Hess
Research and Development
P.O. Box 52025
Phoenix, AZ 85072-2025

Salt River Project
Attn: Ernie Palomino
Research and Development
P.O. Box 52025
Phoenix, AZ 85072-2025

Schlaich, Bergermann & Partner
Attn: W. Schiel
Hohenzollernstr. 1
D-7000 Stuttgart 1, GERMANY

Science Applications International Corp.
Attn: Kelly Beninga
15000 W. 6th Avenue
Suite 202
Golden, CO 80401

Solar Energy Industries Association
Attn: Scott Sklar
122 C Street., NW
4th Floor
Washington, DC 20001-2109

Science Applications International Corp.
Attn: Bill Bruninga
15000 W. 6th Avenue
Suite 202
Golden, CO 80401

Solar Kinetics, Inc.
Attn: Gus Hutchinson
10635 King William Drive
P.O. Box 540636
Dallas, TX 75354-0636

Science Applications International Corp.
Attn: Barry L. Butler
Room 2043, M/S C2J
10260 Campus Point Dr.
San Diego, CA 92121

Solar Kinetics, Inc.
Attn: D. White
10635 King William Drive
P.O. Box 540636
Dallas, TX 75354-0636

Science Applications International Corp.
Attn: Roger L. Davenport
15000 W. 6th Avenue
Suite 202
Division 448
Golden, CO 80401

South Coast AQMD
Attn: Ranji George
21865 Copley Drive
Diamond Bar, CA 91765

Science Applications International Corp.
Attn: Neil Otto
10260 Campus Point Dr.
Mail Stop 32
San Diego, CA 92121

Southern California Edison Co.
Attn: Amy Brown
P.O. Box 800
2244 Walnut Grove Avenue
Rosemead, CA 91770

Solar Energy Industries Association
Attn: Linda Ladas
122 C Street, NW
4th Floor
Washington, DC 20001-2109

Southern California Edison Co.
Attn: Donald Brundage
P.O. Box 800
2131 Walnut Grove Avenue
Rosemead, CA 91770

Solar Energy Industries Association
Attn: Ken Sheinkopf
122 C Street, NW
4th Floor
Washington, DC 20001-2109

Southern California Edison Co.
Attn: Irving Katter
P.O. Box 800
2244 Walnut Grove Avenue
Rosemead, CA 91770

Southern California Edison Co.
Attn: Chuck Lopez
P.O. Box 800
Rosemead, CA 91770

Southern California Edison Co.
Attn: Hugh Reilly
P.O. Box 800, G01
2244 Walnut Grove Avenue
Rosemead, CA 91770

U.S. Department of Energy
Attn: R. (Bud) Annan (2)
Code EE-13
Forrestal Building
1000 Independence Ave. SW
Washington, DC 20585

Southern California Edison Co.
Attn: Mark Skowronski
P.O. Box 800
2244 Walnut Grove Avenue
Rosemead, CA 91770

U.S. Department of Energy
Attn: Gary Burch (5)
Code EE-132
Forrestal Building
1000 Independence Avenue, SW
Washington, DC 20585

Southern California Edison Co.
Attn: Paul Sutherland
P.O. Box 800
2131 Walnut Grove Avenue
Rosemead, CA 91770

U.S. Department of Energy
Attn: R. Hughey
San Francisco Operations Office
1333 Broadway
Oakland, CA 94612

Southern California Edison Co.
Attn: Roy Takekawa
37000 Santa Fe Road
Daggett, CA 92327

U.S. Department of Energy
Attn: Bob Martin
Golden Field Office
1617 Cole Boulevard
Golden, CO 80401

Sunpower, Inc.
Attn: W. Beale
6 Byard Street
Athens, OH 45701

U.S. Department of Energy
Attn: John Meeker
Golden Field Office
1617 Cole Boulevard
Golden, CO 80401

Technology Properties Limited
Attn: Janet Neal
4010 Moorpark Avenue, Suite 215
San Jose, CA 95117

U.S. Department of Energy
Attn: D.A. Sanchez (2)
Albuquerque Operations Office
P.O. Box 5400
Albuquerque, NM 87115

The Solar Letter
Attn: Allan L. Frank
9124 Bradford Road
Silver Spring, MD 20901-4918

Union of Concerned Scientists
Attn: Donald Aitken
20100 Skyline Boulevard
Woodside, CA 94062

U.S. Department of Energy
Attn: Dan Alpert
2140 L Street, #709
Washington, DC 20037-1530

University of Houston
Attn: James Richardson (2)
Solar Energy Laboratory
4800 Calhoun Road
Houston, TX 77004

University of Houston
Attn: Lorin Vant-Hull (2)
Energy Laboratory 5505
4800 Calhoun Road
Houston, TX 77004

University of Minnesota
Attn: E.A. Fletcher
1111 Church Street, SE
Dept. of Mech. Engr.
Minneapolis, MN 55455

Zomeworks
Attn: Steve Baer
1011A Sawmill Road, NW
Albuquerque, NM 87104

Internal Distribution:

MS 0100 Document Proc. for DOE/OSTI, 7613-2 (2)
MS 0619 G.C. Claycomb, 13416
MS 0619 Technical Publications, 12613
MS 0702 D.E. Arvizu, 6200
MS 0703 R.B. Diver, 6216
MS 0703 L.R. Evans, 6216
MS 0703 S.A. Jones, 6216
MS 0703 G.J. Kolb, 6216
MS 0703 F. Lippke, 6216
MS 0703 T.R. Mancini, 6216
MS 0703 J.E. Pacheco, 6216
MS 0703 M.R. Prairie, 6216
MS 0703 C.E. Tyner, 6216
MS 0704 P.C. Klimas, 6201
MS 0724 D.L. Hartley, 6000
MS 0753 C.P. Cameron, 6218
MS 0753 M.E. Ralph, 6218
MS 0835 R.E. Hogan, Jr., 1513
MS 0835 V.J. Romero, 1513
MS 0835 R.D. Skocypec, 1513
MS 0899 Technical Library, 13414 (5)
MS 0980 G.S. Phipps, 9225
MS 1127 J.M. Chavez, 6215
MS 1127 S.R. Dunkin, 6215
MS 1127 R.M. Edgar, 6215
MS 1127 C.M. Ghanbari, 6215
MS 1127 J.W. Grossman, 6215
MS 1127 R.M. Houser, 6215
MS 1127 D.W. Johnson, 6215
MS 1127 J.J. Kelton, 6215
MS 1127 W.J. Kolb, 6215
MS 1127 Library, 6215 (5)
MS 1127 A.R. Mahoney, 6215
MS 1127 K.S. Rawlinson, 6215
MS 1127 E.E. Rush, 6215
MS 1127 R.K. Tucker, 6215
MS 9018 Central Technical Files, 8523-2